

Multi – Photochromic Systems Based on Azobenzene Units: Towards 2D and 3D Photoresponsive Materials

Inauguraldissertation

zur

Erlangung der Würde eines Doktors der Philosophie

vorgelegt der

Philosophisch-Naturwissenschaftlichen Fakultät

der Universität Basel

von

Jasmin Santoro

aus Italien

Basel, 2019

Originaldokument gespeichert auf dem Dokumentenserver der Universität

Basel edoc.unibas.ch



This work is licensed under a [Creative Commons Attribution - Non commerciale 4.0
Internazionale](https://creativecommons.org/licenses/by-nc/4.0/).

Genehmigt von der Philosophisch-Naturwissenschaftlichen Fakultät
auf Antrag von

Prof. Dr. Marcel Mayor
Prof. Dr. Oliver Wenger

Basel, 26.03.2019

Prof. Dr. Martin Spiess
Dekan

Dedicated to:
My family

Acknowledgements

At first, I would like to express my sincere gratitude to my advisor Prof. Dr. Marcel Mayor for giving me the privilege to be part of his research group, and who introduced me to a very fascinating and intriguing project. Thanks for the trustful and welcoming working atmosphere during the last four years. Your encouragement and optimism have helped me in all the time of research.

I would also like to greatly thank Prof. Dr. Oliver Wenger for agreeing to be my second supervisor and for co-refereeing my thesis and Prof. Dr. Dennis Gillingam for chairing my defence.

Furthermore, I would like to thank Dr. Michal Valášek for his supervision during the entire time of research and writing of this thesis. From him I gained the experience of improving my scientific skills.

My sincere thanks go also to Dr. Pierpaolo Greco from SCRIBA Nanotechnology and Dr. Akimitsu Narita from the Max-Planck Gesellschaft, who gave me the opportunity to join their teams during my secondments. Thanks for your support and motivating scientific discussions during my internship.

A special thank goes to my colleagues Liang Xu and Nico Balzer for the fruitful and stimulating discussions and for the nice time spent together. Thank you for supporting me and for making me smile during the difficulties. To me you are not only labmates, but friends. I also thank my former labmates Dr. Marcin Lindner, Dr. Adam Groczyński, Dr. Alfred Błaszczuk, Dr. Alexandrina Schramm and all the current and former members of Prof. Dr. Marcel Mayor group in Basel. Thanks also to all the friends from the Institute of Nanotechnology.

I am especially grateful to my friends Emanuela, Ovelia, Laura, Giulia and Alessandro, who have always been a major source of support when things would get discouraging and hard. Thank you for always being there for me.

Last but not the least, I would like to thank my family: my mother Maria, my father Giuseppe, my brother Antonio, Irene and the little Giuseppe for encouraging me in all my pursuits and inspiring me to follow my dreams. This journey would not have been possible without you.

TABLE OF CONTENTS

1	INTRODUCTION	9
1.1	Molecular switches	11
1.1.1	Host – guest molecular switches	12
1.1.2	Mechanically interlocked molecular switches	14
1.1.3	Photochromic molecular switches	15
1.2	Azobenzenes	20
1.2.1	Photoisomerism of azobenzene	21
1.2.2	Preparation of azobenzene: synthetic methods	24
1.2.3	Azobenzenes as organic functional materials	32
1.3	Hexa-<i>peri</i>-hexabenzocoronene	36
1.3.1	Physical properties and supramolecular organization	37
1.3.2	Synthetic strategies towards HBC derivatives	41
1.3.3	HBCs as functional materials	45
1.4	Two-dimensional (2D) and three-dimensional (3D) molecular architectures	46
1.4.1	Two-dimensional organic structures based on self-assembly	47
1.4.2	Metal-organic frameworks (MOFs)	49
1.4.3	Covalent organic frameworks (COFs)	51
2	RESULTS AND DISCUSSION	55
2.1	Star-shaped azobenzenes as multi-chromophoric switches	55
2.1.1	Motivation	55
2.1.2	Synthesis of star-shaped azobenzenes	57
2.1.3	Photophysical and photochemical properties	68
2.1.4	Electrochemistry	76
2.1.5	Kinetical study of $E \rightarrow Z$ thermal isomerization	79
2.1.5	Ion mobility – mass spectrometry (IMMS)	84
2.1.6	Study of the molecular self-assembly on graphite surface	88
2.1.7	Photo-responsive metal-organic frameworks (MOFs)	95
2.1.8	Photo-responsive covalent organic frameworks (COFs)	97
2.1.9	Conclusions	105
		7

2.2	Hexa-<i>peri</i>-hexabenzocoronene derivatives bearing azobenzene photoswitches	107
2.2.1	Motivation	107
2.2.2	Synthesis of 6-azo-HBC-01	109
2.2.3	Synthesis of 6-azo-HBC-02	117
2.2.4	Synthesis of 3-azo-HBC	122
2.2.4	Conclusions and outlooks	135
3	GENERAL REMARKS AND CONCLUSIONS	137
4	EXPERIMENTAL PART	143
4.1	General remarks	143
4.2	Synthetic Procedures	145
5	LIST OF ABBREVIATIONS	203
6	REFERENCES	207
7	APPENDIX	216
7.1	<i>Z</i> → <i>E</i> thermal isomerization studies on star-shaped azobenzene 3, 23 and 27	216
7.2	Curriculum Vitae	228

1 Introduction

In 1946, the first electronic general-purpose computer “ENIAC”^[1] (*Electronic Numerical Integrator and Computer*) was projected at the Moore School of Electrical Engineering and fabricated for the University of Pennsylvania. The device was announced as a “Giant Brain” by the press and an entire room was required to accommodate it. Nobody at that time would expect that, in few years, people would have been able to carry a personal computer in their backpacks. In the last half century, technology has been subjected to an impressive evolution making such devices part of our daily lives. The chance to achieve miniaturization has enticed researchers from many fields, as well as the worldwide market demand and the high economic pressure coming from the electronic industry. In 1959, the physicist Richard Feynman introduced the possibility of a new challenge for the scientific community with his visionary and passionate talk “There’s plenty of Room at the Bottom”^[2] given at the *Caltech*. The “bottom-up” approach represents a key strategy for the fabrication of small electronic devices with a moderate expense. In nanotechnology, bottom-up approaches pursue to attain small size (molecular) components whose assembly creates more complex systems.^[3] Molecular Electronics (ME) is the branch of nanotechnology that employs molecules as building blocks for the construction of electronic units. With their nanoscale size, molecules represent the highest reachable level of miniaturization, and thus a keystone for the ultimate goal of shrinking electrical circuits.^[4,5] In the effort to emulate macroscopic devices at the nanoscopic level, Molecular Switches (MS) play an important role in the field of nanoscience. The possibility of tuning physicochemical properties of a molecule or a supramolecular system using an external stimulus is a fascinating tool, which draws the attention of a wide number of researchers across disparate fields of science and technology (chemistry, biology, pharmacology, physics, engineering and materials science).^[6-8]

The research activity within this PhD work focuses on the design, synthesis and characterization of photo-active organic compounds comprising azobenzenes as the photoswitchable unit. The molecules were conceived for the functionalization of graphite substrates to study the supramolecular self-assembly and to investigate changes in physicochemical properties upon irradiation with UV/Vis light.

The research activity presented in this thesis has been developed within the innovative training network (ITN) **iSwitch** (“integrated self – assembled **switch**able systems and materials: towards responsive organic electronics”). The project has been funded by the EU Framework Programme for Research and Innovation *Horizon 2020*, under the Marie Skłodowska-Curie grant agreement No. 642196.

The multidisciplinary research included a close collaboration of scientists with different background. In this thesis, the work is presented from a synthetic chemist's point of view. The present thesis is organized in four chapters. Chapter 1 gives an introduction to molecular switches and their potential applications in molecular devices. Azobenzenes and hexa-*peri*-hexabenzocoronenes are further detailed, focusing on their chemical and physical properties, synthetic methodologies towards their preparation and applications. Subsequently, the assembly of small organic molecules into 2D and 3D extended molecular architectures as promising materials for gas separation and storage, catalysis, drug delivery and semiconducting materials is described.

The main part, which is discussed in Chapter 2 and Chapter 4, deals with the design, synthesis and characterization of photochromic molecules containing switchable azobenzene moieties. The synthesized compounds were designed either for the functionalization of graphite surfaces aiming to the fabrication of novel optically-triggered 2D self-assembled systems, or as photoactive building blocks in photo-responsive 3D metal-organic frameworks (MOFs) and covalent organic frameworks (COFs).

1.1 Molecular switches

Molecular switches are single organic molecules capable of shifting between two or more stable states in a reversible manner. The switching process between the initial and the final state is induced by external stimuli. The nature of the triggering input can be physical (temperature, electrical current, light irradiation)^[9,10] or chemical (pH variation, redox reagents, ions, ligands),^[11] and it leads to structural, electrochemical, optical or mechanical alterations.

Nature offers innumerable examples of complex and sophisticated switchable systems that accomplish fundamental functions in our life. The apparently simple process of visual perception^[12] is actuated by highly complicated mechanisms, which start with the photo-isomerization of a subunit of *Rhodopsin*.

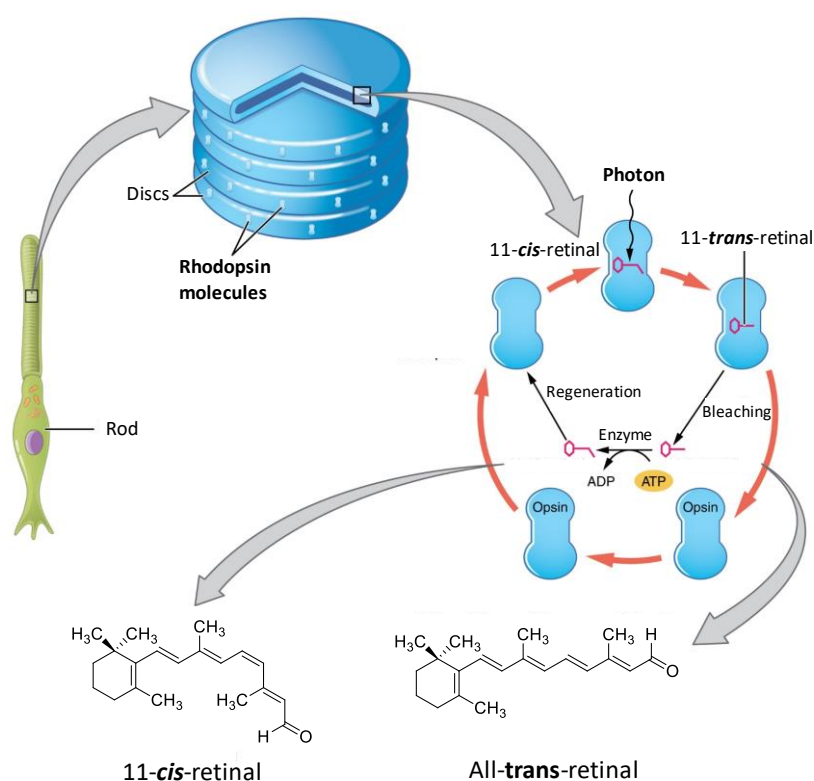


Figure 1. Localization of rhodopsin pigments in the rod photoreceptor cell (left side), photo-isomerization of the 11-*cis*-retinal into all-*trans*-retinal and its regeneration (right side), chemical structures of 11-*cis*-retinal (bottom on the left) and all-*trans*-retinal (bottom on the right).

Inspired by nature, scientists have put many efforts into the development of new smart materials to perform intricate functions of complex systems in many fields of science and technology.

In the recent years, enormous progresses have been observed for molecular switches at the interface between chemistry, physics and material science, aiming to exploit such compounds as trigger elements capable of tuning materials properties.^[3,13,14]

Even though the advancement of chemical synthesis has provided a wide number of molecular switches, the study of their physicochemical properties results more challenging.^[9,15,16] When dissolved

in an appropriate solvent, molecular switches can be easily studied, but their distribution and orientation in solution is completely random. As electrical components in a device^[17], molecules need to be attached to a surface^[18,19] where cooperative processes between molecular units become possible. Once molecules are anchored to a substrate, the characteristics of the entire system (molecule – surface) need to be considered and the intrinsic switching of the single molecule might change. In other words, a molecular switch may lose its switching properties once it is deposited on a substrate, and on the other hand, molecules that are not able to switch could show promising switching properties in the final device (extrinsic switching).^[20]

Despite many hybrid organic-inorganic switches (organometallic compounds),^[21,22] organic molecules represent one of the most charming tools in molecular electronics. A large number of synthetic methodologies are available, which can provide a wide range of compounds with structural flexibility, precisely defined geometry and disparate tunable features (conjugation, dipole moment, solubility, electronic and optical properties, etc.).

Depending on the nature of the external input or the mechanism of the switching event, molecular switches are classified into three types:

- Host-guest molecular switches
- Mechanically interlocked molecular switches
- Photochromic molecular switches

1.1.1 Host – guest molecular switches

According to Cram's host-guest definition,^[23] hosts are defined as the synthetic equivalent of a biological receptor and guests are their complementary counterpart (substrates, inhibitors, co-factors). Generally, hosts are the larger molecule whereas guests are the smaller of the two. Due to the presence of specific binding sites and steric properties that complement the host, guests are selectively recognized. In a host-guest molecular switch, the metastable states of the host exhibit a different affinity for the guest. Hosts are usually macrocycles that welcome the small guest molecules in their cavity. Crown ethers are one of the earliest examples of host-guest structures. In 1978, Desvergne and Bouas-Laurent^[24] synthesized a new crown ether *via* intramolecular photo-dimerization of 9-substituted anthracenes (Figure 2). The bis(anthracene) crown ether molecule complexes cations (e.g. Li^+ ions) forming a host-guest system. The thermal stability of such host-guest system is gained by cation complexation, but host- M^+ complex readily reverts to the open form by competing solvation with a polar solvent (e.g. acetonitrile).

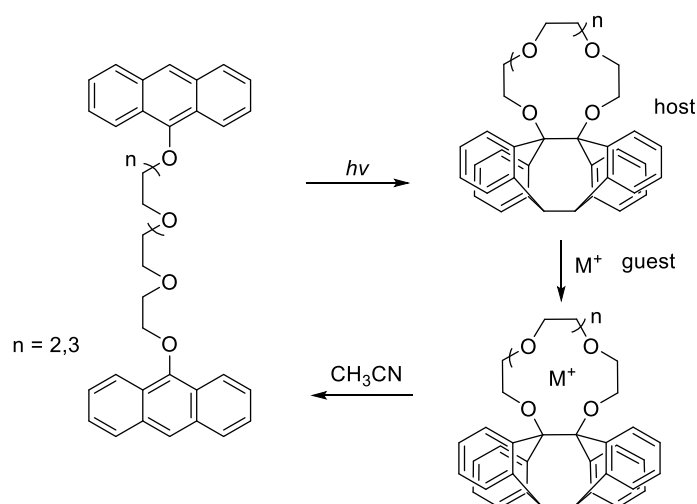


Figure 2. Structure of Desvergne and Bouas-Laurent host-guest system.

Two years later, Shinkai *et al.* proposed a molecular structure analogue to the previous one, but replacing the anthracene units with azobenzene^[25] (Figure 3). The two isomers of the azobenzene-bridged crown ether showed different affinity for cations. Thus, *trans*-azobenzene hosts an ammonium cation and methyl orange salts of Li^+ and Na^+ preferably, whereas its expanded *cis*-isomer bounds methyl orange salts of K^+ and Rb^+ preferably.

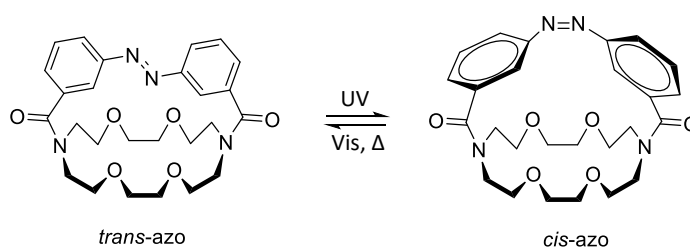


Figure 3. Photo-isomerization of the Shinkai's azobenzene-bridged crown ether.

In the systems showed above, the host entity is an organic molecule, while the guest is an ion. However, macrocyclic structures such as cyclodextrins that accommodate neutral organic molecules are also known.^[26,27] Cyclodextrins (CDs) are cyclic oligosaccharides of D-(+)-glucopyranose units connected by α -(1,4) glucosidic bonds to form a torus like macrocyclic ring. Cyclodextrins are classified as α , β or γ depending on the presence of six, seven or eight glucopyranose units, respectively, and they display differences in molecular weight, cavity size and solubility. Whereas the CDs core is relatively hydrophobic due to the presence of CH_2 groups, the cavity entrances result hydrophilic for the presence of numerous hydroxyl functional groups. This structure allows the formation of host-guest complexes with a very wide range of compounds such as straight or branched aliphatic chains, aldehydes, ketones, organic acids, fatty acids, aromatic compounds, and so forth.^[28,29] One of the popular guest for α -CDs is azobenzene (Figure 4). Being the two azobenzene isomers reversible switchable by means of UV-Vis light irradiation, it is possible to optically control the inclusion or exclusion of this molecule from

the CD cavity. Therefore, the α -CD-azobenzene complex can be employed as a delivery system controlled by light.^[30,31] Such supramolecular systems open new possibilities for molecular recognition and find application as molecular grippers.^[32]

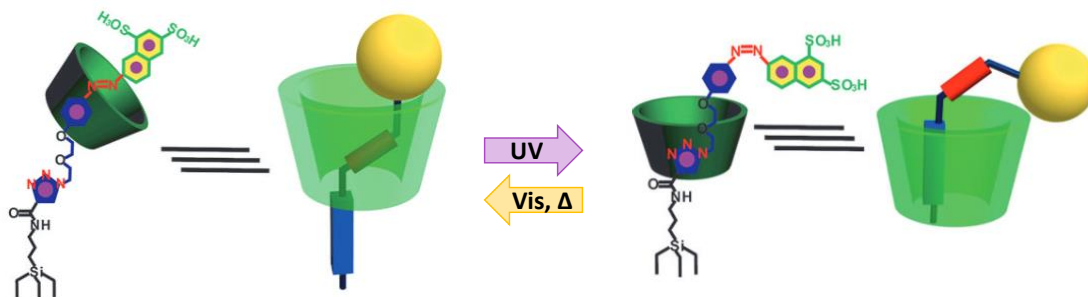


Figure 4. Graphical representation of an α -CD-azobenzene host-guest complex employed as drug-delivery system for the release of curcumin reported by Zhao and co-workers. Image adapted from Ref.^[31]

1.1.2 Mechanically interlocked molecular switches

Mechanically interlocked molecular switches are highly elaborate chemical structures containing a macrocyclic unit. In this class of molecular switches, the switching behaviour between the metastable states is related to the position of the macrocyclic ring. For a better understanding of such intricate structure, it is worth to introduce the concept of “mechanical bonds”. While chemical bonds involve atoms, mechanical bonds are shared between molecular entities (components of the entire structure), such that they cannot be separated without breaking chemical bonds between atoms. Mechanically interlocked molecules (MIMs) are defined as molecules that own mechanical bonds. Catenanes and rotaxanes (Figure 5) are the two main stereotypical MIMs that possess mechanical bonds.^[33]

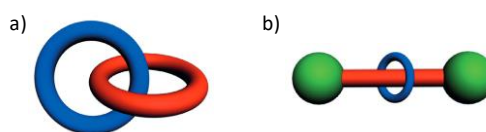


Figure 5. Schematic representation of a) a catenane and b) a rotaxane.

A catenane comprises two or more interlocked macrocycles, whereas a rotaxane contains at least a macrocyclic component with a linear part threaded through the ring and terminated with a bulky unit (stopper), which prevents the unthreading of the linear component. The first realization of switchable molecular shuttles dates back to 1994 when Stoddart (Nobel Prize in Chemistry in 2016) and co-workers^[34] synthesized the rotaxane depicted in Figure 6. The rotaxane comprises a bead (π -electron-accepting tetracationic cyclophane) trapped on a linear thread that contains two π -electron-donating stations (a phenol and a benzidine units) inserted in a polyether chain and terminated with two bulky

stopper groups. This supramolecular structure can be reversibly switched between two states by changing the pH or by electrochemical means. MIMs have aroused the interest of many scientist, providing an incredible variety of noteworthy elaborate structures.^[35–39]

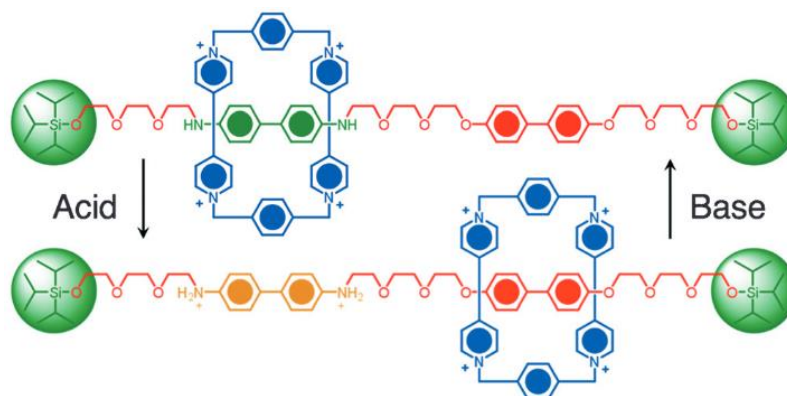


Figure 6. Schematic representation of Stoddart’s switchable molecular shuttle (donor-acceptor [2]rotaxane), whose switching between the two meta stable states is tuned by the pH value.

Mechanically interlocked switches and, more generally, mechanical interlocked molecules need also to be considered as artificially designed and synthesized molecular machines, namely a subgroup of functional molecular systems where an external triggering stimulus causes the mechanical motion of one of the components in the structure.

1.1.3 Photochromic molecular switches

Photochromic switches are organic molecules that behave as sensors for light. In a molecular photochromic switch, the shift between two thermodynamically (meta)stable states is promoted by means of electromagnetic radiation. The distinguished states are characterized by different absorption spectra and usually, the photo-induced change is the result of an intramolecular reaction (photocyclization, *trans-cis* isomerization^[40] or a combination of the two).

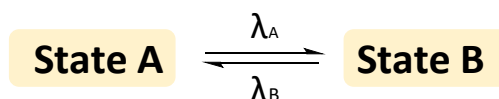


Figure 7. Switching from state A to B by means of irradiation with light.

Light-triggered transformations produce drastic changes in physical properties (emission, absorption, dipole moment, polarizability) of the compound, which are responsible of alterations in macroscopic features such as color, refractive index and so on. Even though the term photochromism was first used in 1950 by Hirshberg^[41] (from Greek “photo” = light and “chromo” = color), describing literally a color change as a consequence of light irradiation, nowadays the definition became wider. Photochromism

represents not only a light-induced color change, but also it offers the possibility to realize optically manipulating systems at the nanoscale level. To date there are many reversible photochromic switches^[42–47] including stilbenes, azobenzenes, overcrowded alkenes, indigoids, diarylethenes, fulgides and spiropyrans. Some of them will be briefly described below, whereas the class of azobenzene will be discussed in more details in Chapter 1.2.

1.1.3.1 Stilbenes

Stilbenes are a broadly studied class of photochromic switches whose photoisomerization is representative of *cis-trans* isomerization reactions.^[48] Stilbene consists of two phenyl rings connected by a C=C double bond. The C=C photo-isomerization generates *E* and *Z*-isomers. However, irradiation of the *cis*-isomer leads to a photocyclization to dihydrophenanthrene **A1**, which is subsequently oxidized in the presence of oxidants (oxygen, I₂) to phenanthrene **A2**, (Figure 8).

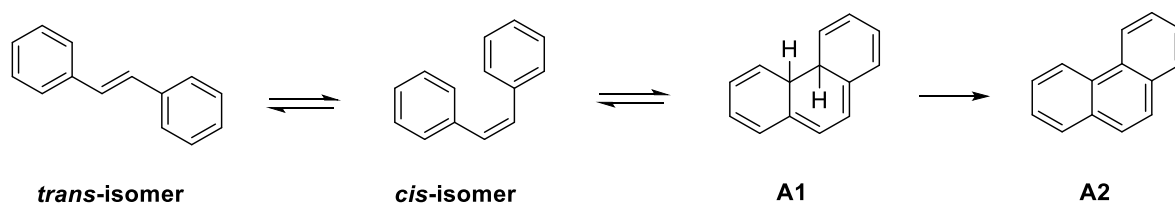


Figure 8. Photoisomerization of stilbene. Its photocyclization to dihydrophenanthrene (**A1**) and subsequent oxidation to phenanthrene (**A2**).

1.1.3.2 Overcrowded alkenes

This class of compounds can be considered as a subgroup of stilbenes where the C=C double bond is sterically hindered *via* the introduction of substituents at the *ortho* position of the stilbene core. Generally, overcrowded alkenes comprise an unsymmetrical upper part (usually based on 2,3-dihydrophenanthrene or 2,3-dihydrocyclopenta[*a*]naphthalene) and a symmetrical lower part based on 9,10-dihydroanthracene or fluorene units, and the region where substituents are closer is known as the *fjord region*. The overcrowding at the double bond region leads to an alteration of the planarity of the molecular structure, thus helical conformation is observed^[42]. Accordingly, right-(*P*) and left-(*M*) handed helicities are distinguishable. After irradiation with UV light, overcrowded alkenes undergo *E*→*Z* isomerization, which will cause an alteration of UV/Vis spectrum as well as the helicity. The *Z*-isomer is strained compared with the *E*-isomer, thus it is thermally unstable, and regresses back to the more stable *E*-form (Figure 9).

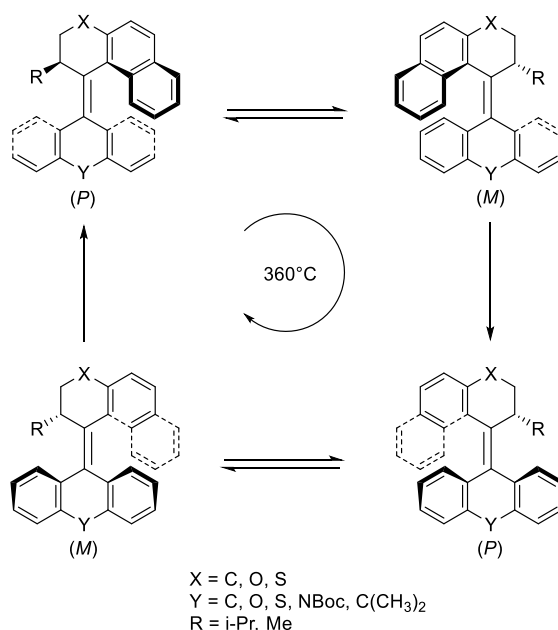


Figure 9. General scheme of overcrowded alkenes photo-isomerization.

1.1.3.3 Spiropyrans

Spiropyrans^[49] have been known since the beginning of the twentieth century. Nevertheless, it was only in the middle of the century when their photoswitchable features were described by Fischer and co-workers.^[50]

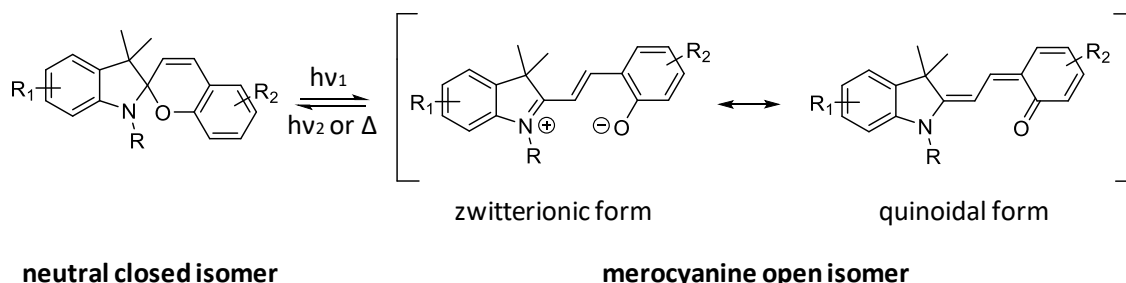


Figure 10. Reversible photo-isomerization of spiropyran compounds.

In the spiropyran family, the photoisomerization (Figure 10) involves the photocleavage of the C-O bond between the spiro-carbon and the pyran-oxygen and the double bond pattern changes resulting in the dearomatization of the adjacent phenyl ring. Whereas the spiropyran closed form is neutral and colorless with the benzopyran and indoline units arranged perpendicularly, the merocyanine open isomer is planar and forms an extended π -conjugated system responsible of its colour, and existing in two resonance structures: a zwitterionic and a quinoidal form. The resulting quinoidal form can exist in either *cis-cis* or *trans-trans* configurations, where *trans* is more stable due to the steric constraints in the *cis* isomer. The hydrophobic closed spiro-isomer can be converted to the remarkably polar open isomer (zwitterionic merocyanine) in a reversible manner. Accordingly, the large difference in polarity

of the two isomers renders spiropyrans promising candidates for controlling surface free energy by light.^[51,52] Koçer and co-workers,^[6] exploited spiropyrans photoswitching to trigger the activity of a mechanosensitive channel of large conductance membrane protein (MscL) to achieve reversibility in channel opening (Figure 11).

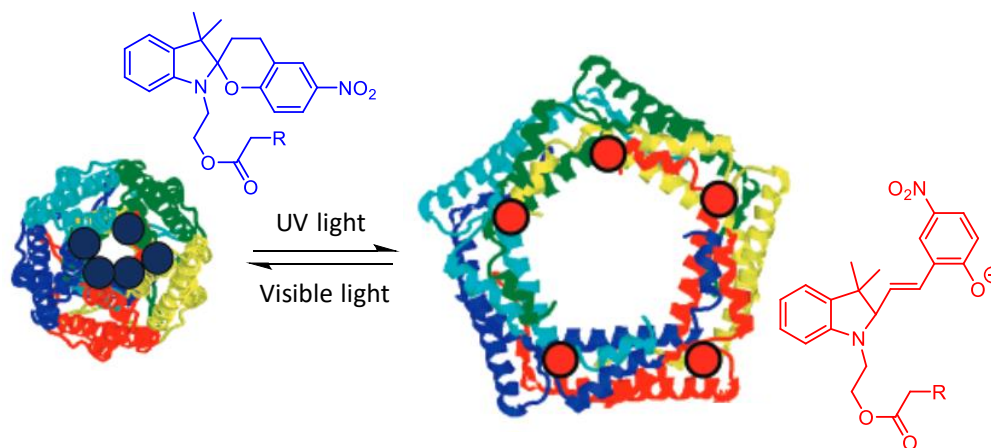


Figure 11. Reversible photo-triggered opening and closing of the large conductance mechanosensitive channel (MscL) using a spiropyran-functionalized protein complex.^[6]

Spiropyrans have been used in different field going from biology to electronics and several examples are reported elsewhere^[53].

1.1.3.4 Dithienylethenes

Analogously to spiropyrans, dithienylethenes (DTEs)^[54] belong to the family of photochromic switchable molecules that undergo photocyclization by means of light irradiation. However, in contrast with spiropyrans chromophores, dithienylethene photoswitches exist in two thermally stable states: a closed form, usually colorless, and an open coloured form (Figure 12). The ring-closed isomer has a more planar structure, resulting in an extended π -conjugation over the entire structure, whereas in the open form π -conjugation is limited at the two halves of the molecule. Hence, the closed form owns better conductance properties with respect to the open one.

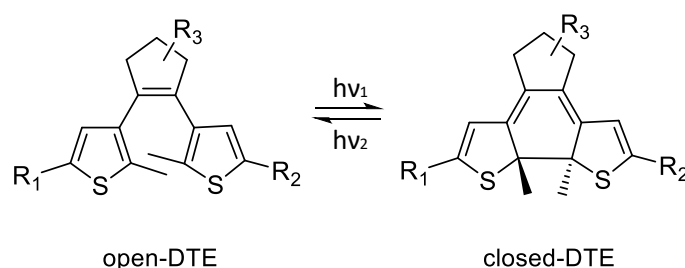


Figure 12. Photoswitching of dithienylethene chromophores. Ring closing of the open-DTE by means of UV irradiation and back isomerization of the closed-DTE upon visible light irradiation.

Depending on the thermal stability of the isomer generated upon light irradiation, photochromic switches are classified in two main groups: T-type and P-type switches. The former type (T-type) comprises all chromophores whose photogenerated isomers are unstable and fade back to their initial form through a thermal back-isomerization, when they are no longer exposed to the light source. In contrast, P-type switches manifest thermal irreversibility and changes colour when irradiated with a specific wavelength range, then remains in this state after removal of the stimulus. It is only when they are subjected to light of a different set of wavelengths that they return to their original colour. DTEs, depending on the type of aryl group,^[55] and fulgides belong to the latter category. Thermal stability of both isomers and fatigue resistance are fundamental features for the application of photochromic molecules to optical memories and switches. Accordingly, since the middle of 80s^[56] these compounds have become broadly studied and used as key elements in functional molecular systems.

1.2 Azobenzenes

Azo compounds are a class of molecules that comprise N=N double bonds (Figure 13). Stating their general structure as $R_1-N=N-R_2$, substituents on the nitrogen atoms can be aliphatic or aromatic units and, in the case of azobenzene, R_1 and R_2 are phenyl rings. According to the IUPAC definition, azo compounds derive from diazene, where both hydrogen atoms are replaced with aryl or alkyl groups.

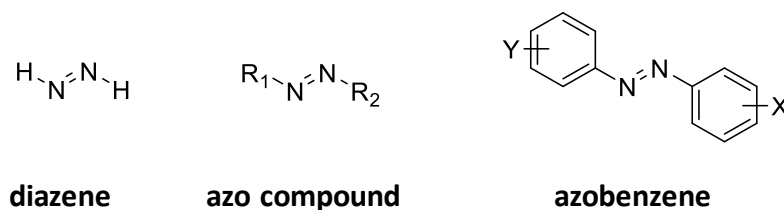


Figure 13. Molecular structures of diazene (left), a general azo compound bearing aliphatic substituents R_1 and R_2 (middle) and azobenzene (right) functionalized with X and Y being alkyl, alkoxy, halogen, hydroxyl, amino or aryl groups.

The first synthesis of azobenzenes dates back to 1834, when the German chemist Mitscherlich^[57] described the preparation of red crystals with the chemical formula $C_{12}H_{10}N_2$. Due to the extended π -delocalization, azobenzenes are stable and coloured species because of the strong absorption of light. Thus, azobenzenes are widely used as dyes (Figure 14) in the textile and pharmaceutical industry, food and drinks colouring, cosmetics, inks and paints.

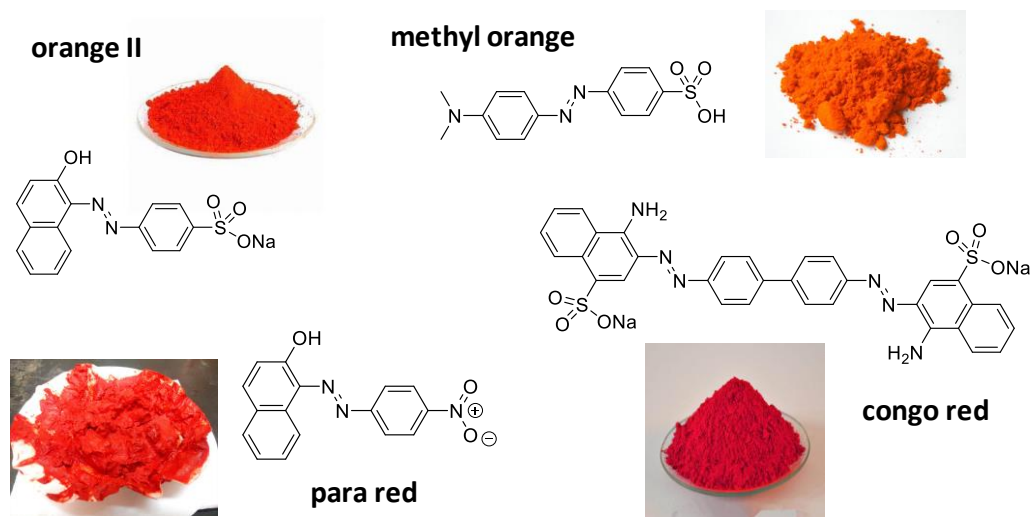


Figure 14. Some examples of textile dyes based on azobenzenes. The substituents affect the electrical properties of the molecule and absorption wavelength resulting in compounds differently coloured from yellow, to orange and red.

Certainly, azobenzenes are more than simple dyes. Their intrinsic capability to photoisomerize into isomers having different structural geometry, conjugation and planarity, length, dipole moment, refractive index and dielectric constant, makes azobenzene extremely appealing candidate for the application in biological systems,^[58] photopharmacology,^[59–61] supramolecular systems,^[62,63] polymer

chemistry,^[64,65] and so on. Furthermore, azobenzenes represent useful scaffolds for the construction of photoactivated molecular sensors,^[25] catalysis,^[66] liquid crystals,^[67] photoresponsive molecular machines^[68] and so forth.

1.2.1 Photoisomerism of azobenzene

Hartley^[69] first discovered the *cis*-isomer of azobenzene in 1937, about a century after the first preparation of this family of chromophores.^[57] Thenceforth, azobenzenes (ABs) draw the attention of many researchers for being promising photo-activated molecular units whose isomerization can lead to conformational and structural changes from nanoscale to macroscale level. As for stilbene, the photochromism of azobenzene is based on the photo-isomerization of the double bond. Simple azobenzene and its more sophisticated derivatives can undergo *trans*↔*cis* (*E*↔*Z*) reversible photoisomerization by means of UV/Vis light irradiation.

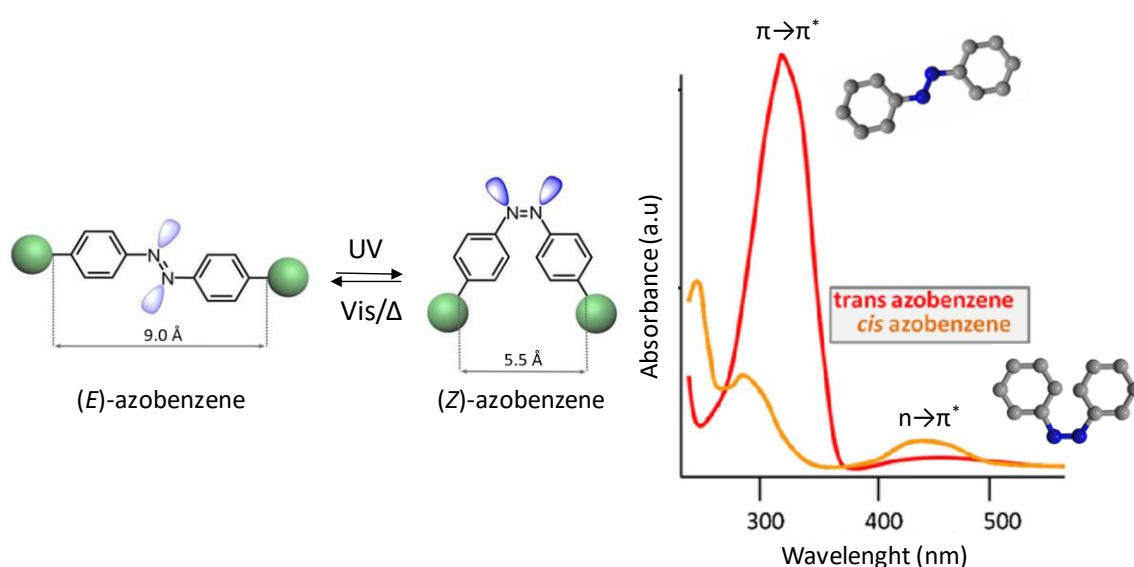


Figure 15. Schematic representation of azobenzene *E* ↔ *Z* photoisomerization (left side) and UV-Vis absorption spectra of *Z* (yellow) and *E* (red) azobenzenes (right side) adapted from Ref.^[70]

The two isomers of azobenzene are characterized by different structural and physical properties (Figure 15). (*E*)-azobenzene presents a planar conjugated structure, while in (*Z*)-azobenzene the structure is distorted with a twist angle of the phenyl rings of 53°. Furthermore, a drastic change of dipole moment is observed in the two forms. Thus, (*Z*)-azobenzene has a dipole moment (μ) of 3.5 Debye, whereas for (*E*)-azobenzene is zero. The conformational *E*→*Z* rearrangement also leads to a decrease in the end-to-end distance of the molecule (9.0 Å and 5.5 Å in the *E* and *Z* form respectively). The interconversion between the two isomers occurs either photochemically (*E*↔*Z*) or thermally (*Z*→*E*) (Figure 15).

Whereas $E \rightarrow Z$ isomerization occurs by means of UV light irradiation, mechanical stress^[71] or electrostatic stimulation,^[10,72] (E)-isomer is recovered by irradiation with visible light or spontaneously in the dark at room temperature, being $\sim 12 \text{ kcal mol}^{-1}$ thermodynamically more stable than the (Z)-form. Considering the absorption spectrum of azobenzenes and related compounds (Figure 15), it becomes clear that two characteristic absorption bands are responsible for the peculiar colours and photochromic behaviour of such molecules. The first one is a significant absorption band corresponding to the $\pi \rightarrow \pi^*$ electronic transition of the azo functionality, observed in the ultraviolet region of the spectrum (350 nm for *trans*-azobenzene and 280 nm for *cis*-azobenzene, roughly). The intensity of the absorption band is much higher for the (E)-form corresponding to the lower planarity of the (Z)-isomer. The second band corresponding to the $n \rightarrow \pi^*$ transition is due to the presence of unshared electron pairs of nitrogen atoms and usually appears in the visible range of the absorption spectrum^[73] (400 nm for (E)-azobenzene and 430 nm for (Z)-azobenzene), actually symmetrically forbidden in the (E)-form. Accordingly, both isomers of azobenzene show overlapped absorption spectra with different intensity of the two transition bands. By irradiating at the $\pi \rightarrow \pi^*$ transition wavelength of azobenzene, $E \leftrightarrow Z$ isomerization in both directions occurs and a photostationary state (PSS) richer of (Z)-azobenzene (about 80% of Z -isomer) is reached; whereas by irradiating at the $n \rightarrow \pi^*$ transition wavelength the *trans*-isomer is generated, and a PSS richer of (E)-azobenzene is observed. A situation of photostationary equilibrium where 100% of E -isomer is present will be reached only thermally, heating the Z -form in the dark. Despite the numerous studies published on azobenzenes, the detailed mechanism of the $Z \leftrightarrow E$ photoisomerization process is still a subject of debate^[74–78]. Additional $n \rightarrow \pi^*$ electronic transition in azobenzene spectra contributes to the difficulties with the evaluation of the mechanism. Whereas the isomerization of stilbene occurs exclusively by rotation (quantum yield equals 1 in $E \leftrightarrow Z$ isomerization in both directions), the sum of quantum yield for azobenzene does not equal 1, suggesting a photoisomerization process that follows different pathways. Figure 16 shows four different mechanisms that have been proposed for azobenzene photoisomerization^[74]: rotation, inversion, concerted inversion and inversion-assisted rotation. No barrier exists along the rotational pathway after excitation into the S_1 state. According to previous computational research, the conical intersection between S_0 and S_1 states exists when the C-N=N-C dihedral angle is $\sim 90^\circ$ and the N=N-C angle is $\sim 140^\circ$. These facts have promoted the acceptance of rotation as the dominant mechanism with concerned inversion occurring under rotation-restricted conditions. The rotational pathway concerns breaking of the N=N π -bond. Accordingly, it allows free rotation around the N-N bond and changes the C-N-N-C dihedral angle, while the N-N-C angle remains fixed at 120° . Contrariwise, in the inversion mechanism the C-N-N-C dihedral angle remains fixed at 0° , but one of the N=N-C angles increases to 180° . One of the N-atoms is thus *sp*-hybridized.

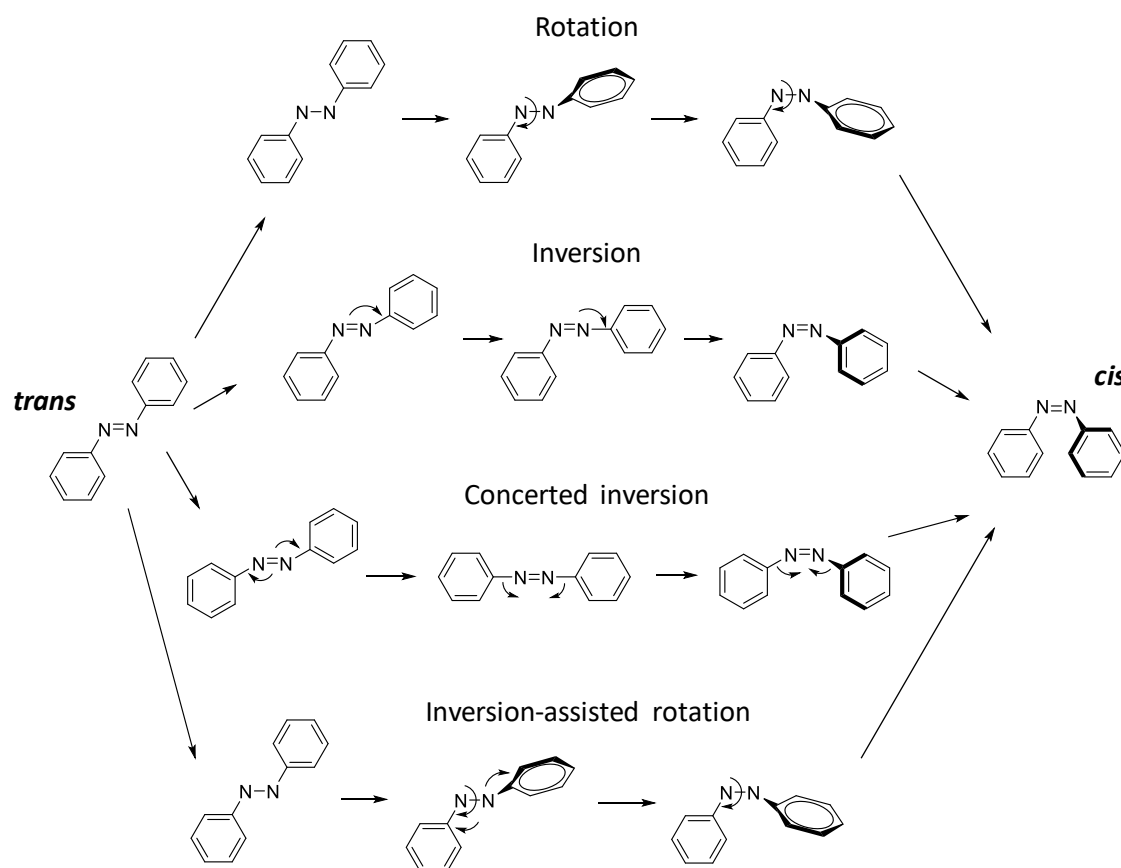


Figure 16. Schematic representation of the four proposed mechanisms for $E \rightarrow Z$ isomerization of azobenzene, adapted from Ref.^[74]

In the case of the concerted inversion pathway, the value of both $N=N-C$ angles increases to 180° , providing a linear transition state. Lastly, inversion-assisted rotation causes both large changes in the $C-N=N-C$ dihedral angle and smaller changes in the $N=N-C$ angles, simultaneously. Relaxation of all aforementioned transition states can generate both (*Z*) and (*E*) isomer, thus the mechanisms describe photoisomerization processes in both directions ($Z \rightarrow E$ and $E \rightarrow Z$). Depending on the external condition and the effect of substitution on the photochromic unit, the photoisomerization process will follow one mechanism rather than another one. It has been seen that parameters such as viscosity and polarity need also to be considered. As already mentioned, immobilization of azobenzene on a solid support costs drastic decrease of isomerization quantum yield. All considerations discussed above are reliable for unsubstituted azobenzene. However, chemical modifications on the azobenzene core cause drastic changes.^[79] By introducing a proper functional group on azobenzene phenyl rings, electronic properties as well as steric hindrance are affected. Consequently, it is possible to vary parameters such as position of the absorption bands, quantum yield, and stability of the *Z*-isomer, as well as changes of the activation energy barrier for the thermal $Z \rightarrow E$ isomerization.

1.2.2 Preparation of azobenzene: synthetic methods

The most used methods for the synthesis of azobenzene are the azo coupling reaction, the Mills and the Wallach reactions. Moreover, in the recent years numerous more efficient methods have been developed due to the increased interest of the scientific community for azobenzene compounds, and several reviews have been published.^[80,81]

1.2.2.1 Azo coupling reaction

The reaction involves aromatic diazonium salts that react with activated electron rich arenes^[82] (Figure 17). Aromatic diazonium compounds are weak electrophiles, therefore the activation of aromatic rings *via* introduction of electron donating groups (-NH₂ or -OH) is essential for the reaction. The actual azo coupling is an electrophilic aromatic substitution where the electrophile is the aryldiazonium ion and the nucleophile is the activated arene. Usually this electrophilic aromatic substitution takes place at the *para* position to the electron donating group of the activated ring, but when that position is already occupied and thus not available, it occurs on the *ortho* position.

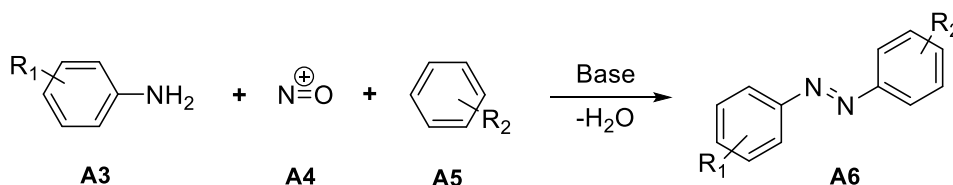


Figure 17. Reaction scheme of the overall azo coupling reaction. R_2 = electron donor group.

The overall azo coupling reaction can be divided into two main steps. The first step is the formation of the diazonium salt (diazotation) from a primary aryl amine (**A3**). The formation of the diazonium cation is usually performed using sodium nitrite in aqueous mineral acidic conditions at low temperature. Acid is necessary to generate *in situ* nitrous acid from NaNO_2 . Protonation followed by H_2O elimination provides the nitrosonium cation $\text{N}^+=\text{O}$ (Figure 17 and 18), which will react with the primary aryl amine. The overall reaction mechanism with detailed diazotation and azo coupling steps is sketched in Figure 18.

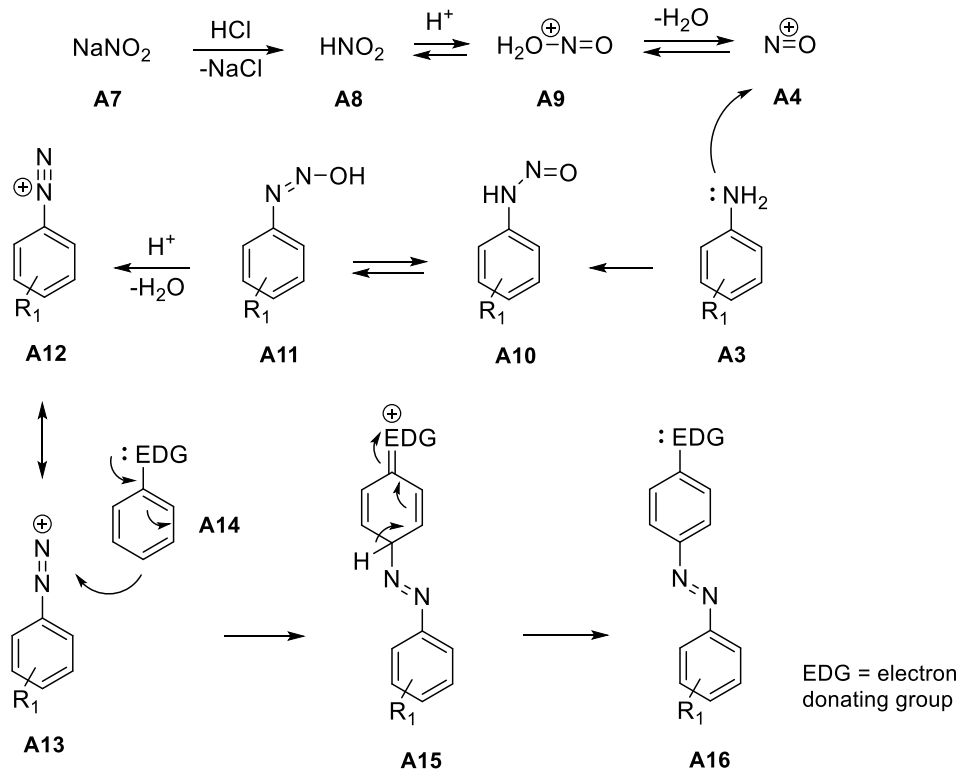


Figure 18. General reaction scheme of azo coupling reaction. Formation of nitrosonium ion (A4), diazotation of a primary aryl amine that provides the diazonium cation (A12) and actual azo coupling, adapted from Ref. [80]

Once nitrosonium ion (nitrosating agent) is formed, an electrophilic nitrosation of the primary aryl amine takes place and provides intermediate A10, which is a tautomeric form of the diazohydroxide A11. Diazonium ion (A12) is formed after protonation of A11 and water elimination, where its structure is stabilized by resonance.^[80] Once the diazonium salt is formed, the accepted mechanism for the azo coupling is an electrophilic aromatic substitution of the activated arene (phenol or aniline) with the electrophilic nitrogen of the diazonium cation (Figure 18). It is worth to mention that reaction conditions and pH play an important role for the reactivity of the starting material as well as for the reaction rate. Accordingly, the coupling of phenols has to be done in a moderate alkaline solution at controlled pH (phenol reacts in the ionized form because the neutral species isn't nucleophilic enough), whereas aryl amines react in weak acid media in order to prevent N-coupling side reaction (without reducing the nucleophilicity of N by protonation). The azo coupling reaction has permitted the synthesis of sophisticated structures such as porphyrins,^[83,84] metacyclophanes^[85] and calixarenes,^[86] which contain azo groups (Figure 19). Azo coupling remains the most used method for the preparation of azo dyes in industry. However, the weak electrophilicity of diazonium ions and the pH dependency of the reaction represent a drawback in many cases, as the amount of activated arenes is limited and the nature of substitution as well as their position has to tolerate the reaction conditions. Moreover, the nature of counterions of the diazonium salts influences their stability.

Accordingly, diazonium chlorides, perchlorates are unstable, decompose explosively at elevated temperatures, while tetrafluoroborates, disulfonimides, hexafluorophosphates and zinc chlorides double salts are more stable and can be stored for a long time.

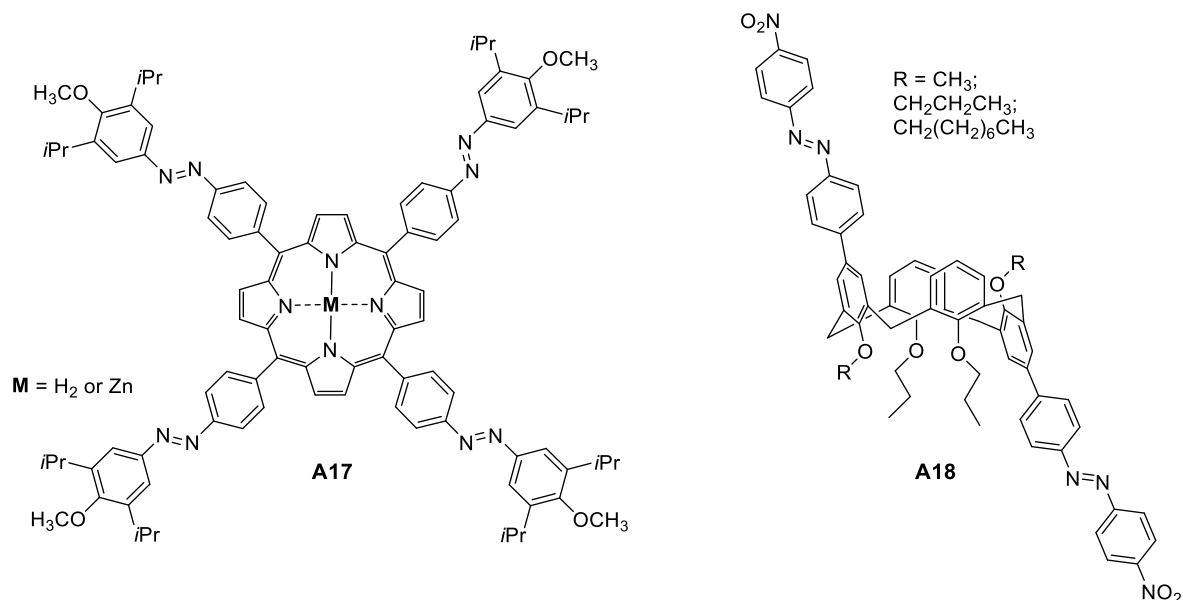


Figure 19. Porphyrin (A17) and calixarene (A18) bearing azo groups introduced by azo coupling reaction. Structures adopted from Ref.^[83,86]

1.2.2.2 Mills reaction

The reaction of an aryl nitroso compound with anilines in glacial acetic acid is known as Mills reaction^[87] (Figure 20) and it provides either symmetric or asymmetric azobenzenes in good yield.^[88]

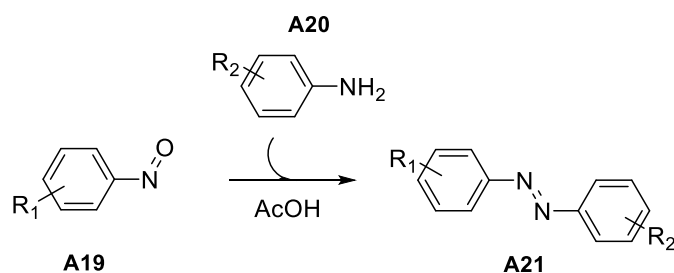


Figure 20. General reaction scheme of Mills reaction to generate asymmetric azobenzene. $R_1 \neq R_2$.

Nitrosobenzene is an organic compound with the formula C_6H_5NO . The first synthesis of nitrosobenzene, performed by Adolf von Baeyer,^[89] dates back to 1874. Since then, a wide number of nitroso derivatives (in which $-NO$ group is directly bounded to a C-atom) have been prepared.^[90] At that time, a curious property of C-nitroso derivatives was observed. In solution, they exhibited colours from blue to emerald green, whereas in the solid state their colour turned to pale yellow-white.

Piloty^[91] first proposed the existence of two distinct forms: a white bimolecular solid and a blue monomolecular form in solution. Many aryl nitroso compounds, indeed, form *cis*- and *trans*- azodioxy dimers (Figure 21).

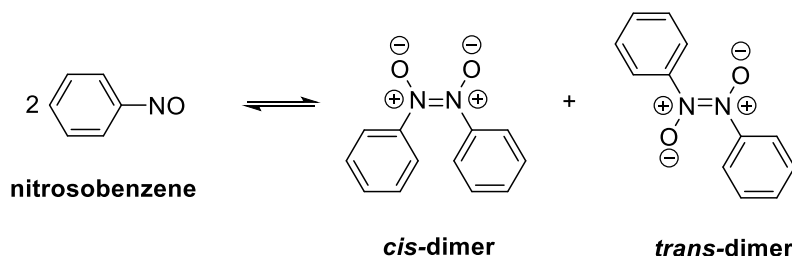


Figure 21. Equilibrium between monomeric and dimeric forms of nitrosobenzene.

Several ways are known for the preparation of nitrosobenzene. Gowecklock and Richter-Addo^[92] reported synthetic strategies for the formation of C-nitroso compounds in an interesting review that dates back to 2004. Nitroso compounds can be obtained by heterogeneous oxidation of their corresponding aromatic hydroxylamine^[88] (Figure 22) with *tert*-butyl hypochlorite (*tert*-BuOCl) or iron(III) chloride (FeCl₃). The oxidation is quite fast and a low temperature (-78°C) is required to prevent overoxidation. Other oxidation procedures involve peracetic acid (CH₃CO₃H), KMnO₄/CH₂O/H₂SO₄, sodium or potassium dichromate and H₂SO₄, *meta*-chloroperbenzoic acid, KMnO₄, diethyl azodicarboxylate, iodine/NaI/NaOAc, silver carbonate, (diacetoxyiodo)benzene, DDQ, performic acid (CH₂O₃) and peroxomonosulfuric acid^[93] (H₂SO₅, *Caro's acid*). Nitroso arenes can also be prepared using tetrabutylammonium cerium (IV) nitrate, pyridinium chlorochromate, potassium ferrate (VI) and phenyl selenic anhydride as oxidizing agents.

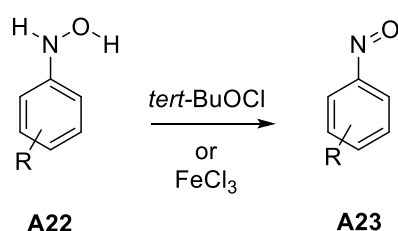


Figure 22. Oxidation of a general aromatic hydroxylamine (A22) to the corresponding aromatic nitrosobenzene (A23) using *tert*-BuOCl or FeCl₃.

Large-scale synthesis of aromatic nitroso compounds is possible if activated anilines are involved. The presence of electron withdrawing substituents in *para* or *meta* position on aniline ring decreases the reaction yield dramatically^[94] and side reactions become more relevant, especially upon prolonged reaction time. One of the possible scenarios is the overoxidation of nitrosobenzenes to nitrobenzenes. When the oxidation step cannot be selectively controlled, the reaction mixture will contain all the possible oxidation products as well as the starting aniline. Consequently, aside from the desired

azobenzene product, formation of azoxybenzene can be observed. The use of two phases heterogeneous systems like Oxone® in H₂O/CH₂Cl₂ (Figure 23) represent a possible way to overcome the side reactions issue.^[94] The biphasic system ensures the separation of the nitrosobenzene (preferably soluble in the organic phase) from the water-soluble arylhydroxylamine intermediates and aniline reactant. The aforementioned biphasic system allows the preparation of nitrosobenzene containing electron withdrawing groups in a quite high yield.^[95]

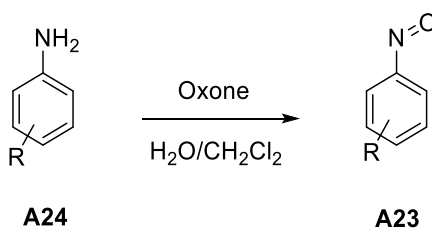


Figure 23. Oxidation of an aniline (**A24**) to the corresponding nitrosobenzene (**A23**) using the Oxone®-biphasic system in H₂O/CH₂Cl₂.

Oxone® and Caroat® are trade names for the triple salt 2KHSO₅·KHSO₄·K₂SO₄. Potassium peroxymonosulfate (KHSO₅) is the potassium salt of the Caro's acid (H₂SO₅). The latter is a very strong oxidizing agent, highly explosive and hard to handle. In contrast, the triple salt Oxone® is a mild oxidizing agent and its higher stability makes this agent one of the best candidates for the preparation of nitrosobenzenes. Yu *et al.*^[95] investigated the oxidation with Oxone® on a broad range of aniline derivatives. The experiments proved that functional groups such as esters, carboxylic acids, nitriles, halides and alkyl groups are well tolerated by the Oxone®-system. Nitrosobenzenes containing hydrophilic substituents are synthesized in lower yield, due to the increased solubility in the water phase. One of the drawbacks of aromatic nitroso compounds is their low stability.^[90] Therefore in many cases, it is better to avoid any further purification, and it is preferable to use the raw unpurified mixture for the next reaction step (Mills reaction). The small presence of side products as impurities (nitrobenzene and azoxybenzene) do not affect the synthesis of the desired azobenzene, and the purification at this step is much easier. The mechanism of the Mills reaction is depicted in Figure 24. The electron lone pair on the aniline nitrogen atom attacks the N=O group and leads to the intermediate **A26**. Intermediate **A26** is in equilibrium with its azohydroxy form (**A27**), and dehydration of the latter provides the final asymmetric azobenzene (**A28**). Depending on the solubility, the coupling can be achieved in glacial acetic acid or a mixture of the acetic acid and dimethyl sulfoxide (DMSO).

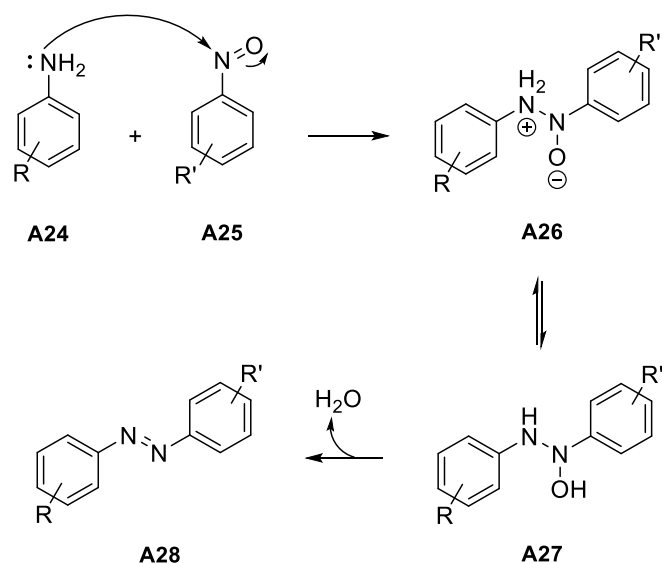


Figure 24. General scheme of Mills reaction mechanism.

Due to the limited side-reactions and to the typically mild reaction conditions, Mills reaction represents an interesting and useful method for the preparation of a wide range of structures, which go from the simple azobenzenes to more complex and sophisticated helical oligomers synthesized by Tie *et al.*^[96]

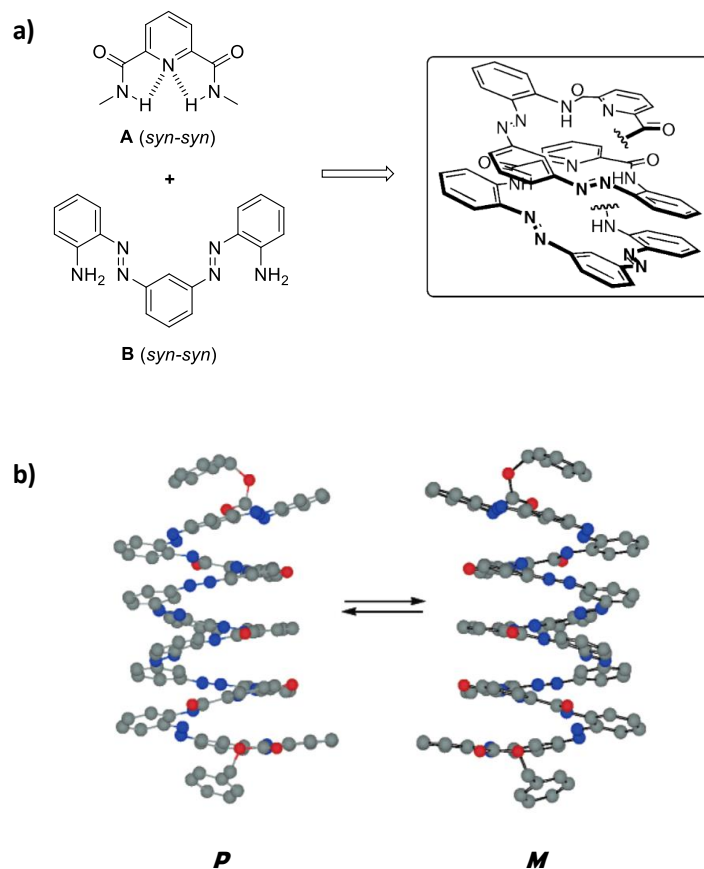


Figure 25. a) the reaction of pyridine-2,6-dicarboxamide (**A**) with 1,3-bis(2-aminophenyldiazenyl)benzene (**B**) provides oligomers with azobenzene linkages; b) helical conformation of the oligomer existing as an interconverting mixture of *M* and *P* helices, adapted with permission from Ref.^[96] Copyright © 2006 American Chemical Society.

1.2.2.3 Wallach transposition

The Wallach rearrangement^[97] involves the conversion of an azoxybenzene into a 4-hydroxy (or sometimes a 2-hydroxy) azobenzene by treatment with strong acids. The general reaction scheme is sketched below (Figure 26).

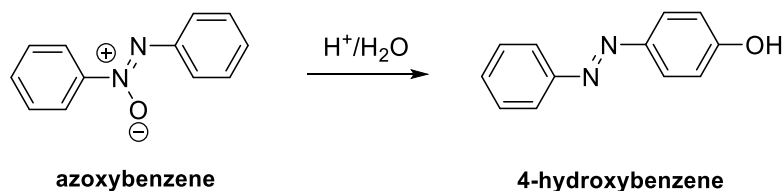


Figure 26. General reaction scheme of the Wallach rearrangement.

The azoxybenzene (Figure 26) is usually generated by reduction of the corresponding nitrobenzene^[98–101] or by oxidation of the aniline. Despite some experimental evidences, the exact reaction mechanism of the Wallach transposition remains not fully understood. Figure 27 shows one of the conceivable mechanisms proposed.

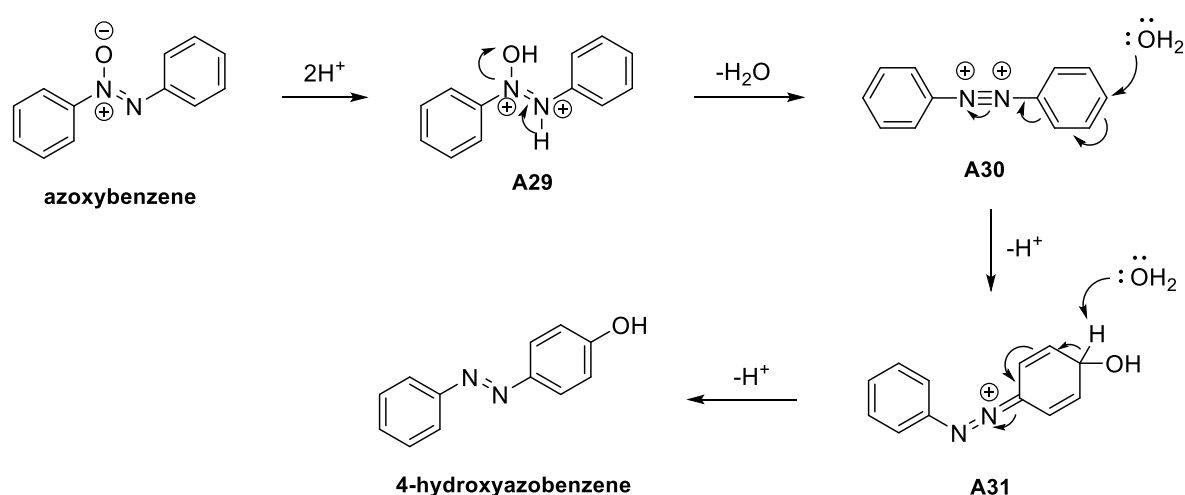


Figure 27. Proposed mechanism for Wallach rearrangement.

The protonation of azoxybenzene with two equivalents of acid generates the intermediate **A29**. The difficult protonation of the oxygen nearby the already cationic nitrogen of azoxybenzene makes the second protonation the rate-determining step of the reaction. Dehydration of **A29** provides a symmetric dicationic intermediate (**A30**). The peculiar structure of the dication **A30** was observed by proton NMR by Olah *et al.*,^[102] in 1972. Subsequently, the conjugated base of the acid acts as nucleophile in a nucleophilic aromatic substitution followed by hydrolysis. Among the available methods for the preparation of azobenzene derivative, it is worth to mention the reductive and oxidative coupling reactions. It is possible to convert aniline to nitrobenzene by oxidation and to reduce nitrobenzene to aniline. Consequently, the oxidation intermediates of aniline and the reduction intermediates of nitrobenzene are the same (hydroxylamine and nitrosobenzene). Figure 28 gives an overview of the

possible intermediates of oxidations and reductions. Most of them were already mentioned as side-products of the reactions described above. Depending on the stability of the intermediates, the strength of the oxidising or reducing agent and the reaction conditions, different products might be obtained. Most of the times, it is difficult to control the reaction process and selectively obtain one of the intermediates. Usually, oxidation and reduction coupling are used to obtain symmetric azo compounds. The use of two different nitro compounds (or two different anilines) as starting materials causes the formation of mixtures of either symmetric or asymmetric products in a statistical manner. Due to the limitations of oxidative and reductive couplings, azo coupling and Mills reaction represent an appealing alternative for the synthesis of asymmetric azobenzenes, and they remain the most used methods.

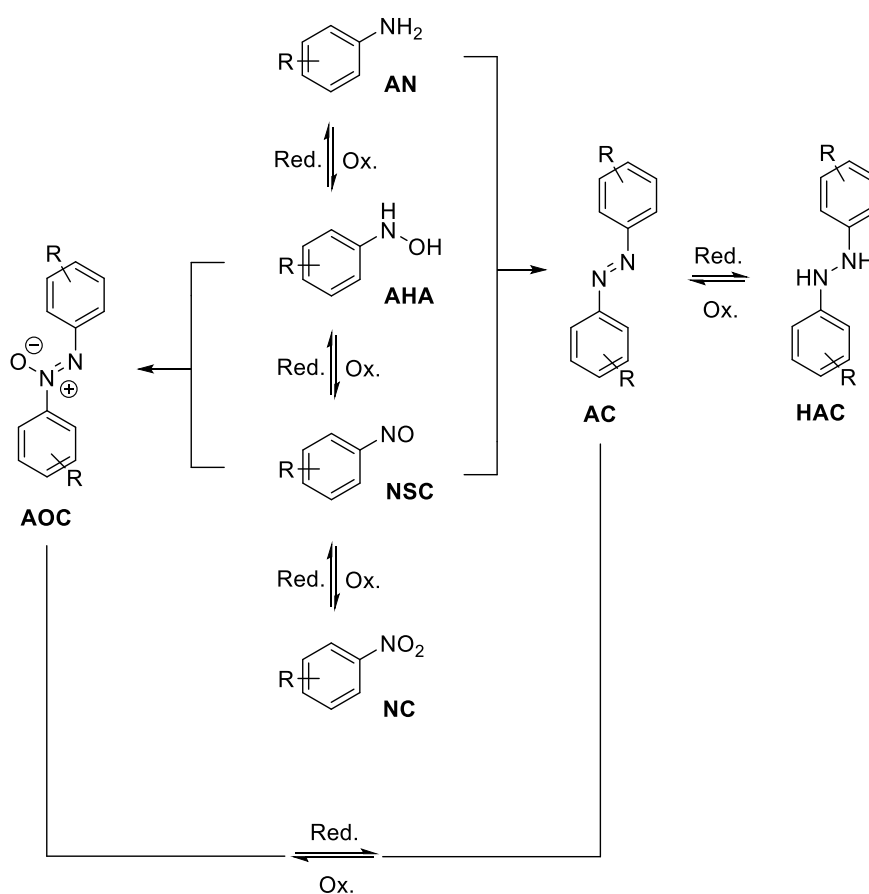


Figure 28. Oxidation and reduction pathways for the hydrogenation of nitrocompounds to anilines and vice versa. AN: aniline, AHA: aromatic hydroxylamine, NSC: nitroso compound, NC: nitro compound, AOC: azoxy compound, AC: azo compound, HAC: hydrazo compound. Scheme adapted from Ref.^[103,104]

An intriguing alternative to the classical methods for the preparation of azobenzenes was introduced by Lim *et al.*^[105] in 2003. Accordingly, Boc-protected hydrazines (Boc = *tert*-butoxycarbonyl) can be converted to Boc-protected diaryl hydrazines by Pd-catalysed coupling reaction with an aryl halide in very high yields. Subsequently, the resulting *N*-Boc diaryl hydrazines undergo oxidation to azobenzenes using NBS/pyridine in dichloromethane at room temperature. The synthetic pathway is

described below (Figure 29). The reaction is suitable for a large number of compounds with a wide range of substituents, both electron withdrawing (EWG) and electron donating (EDG) groups. The presence of bulky substituents in *ortho* or *para* position^[106] to the hydrazine nitrogen might affect the reaction yield.

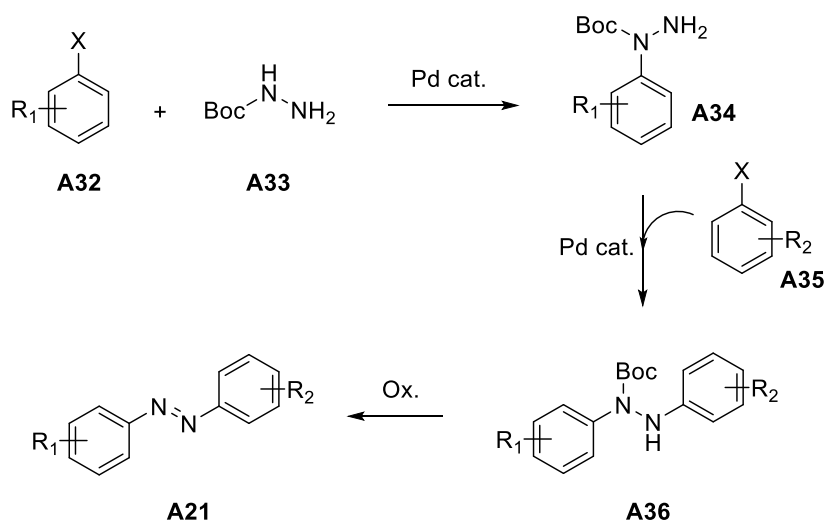


Figure 29. Synthesis of asymmetric azobenzenes via Boc-protected hydrazine intermediate. X: I, Br or OTf.

In addition to the methods described up to now, other “non-classical” strategies towards the preparation of azobenzene can be found in the literature. In this respect, a comprehensive overview is given in the review article published by Merino.^[80]

1.2.3 Azobenzenes as organic functional materials

The possibility of synthesizing azobenzene-based molecular structures for the fabrication of light-triggered functional materials has enticed scientist from different research fields.^[107] As early as 1980, Shinkai *et al.*^[25] reported one of the first examples of azobenzene-based molecular actuator, which later on would be defined as molecular tweezer. Inspired by sophisticated molecular machines that exist in nature, a wide range of artificial molecular machines based on azobenzene photoswitching has been synthesized. In 2008, our group reported the synthesis of a rigid and fully conjugated azobenzene that is able to form highly packed self-assembled monolayers (SAMs) on gold surface Au(111).^[108] The system showed cooperative isomerization of adjacent azo-molecules, which provided both an optoelectronic switch and an optomechanical cargo-lifter (Figure 30).

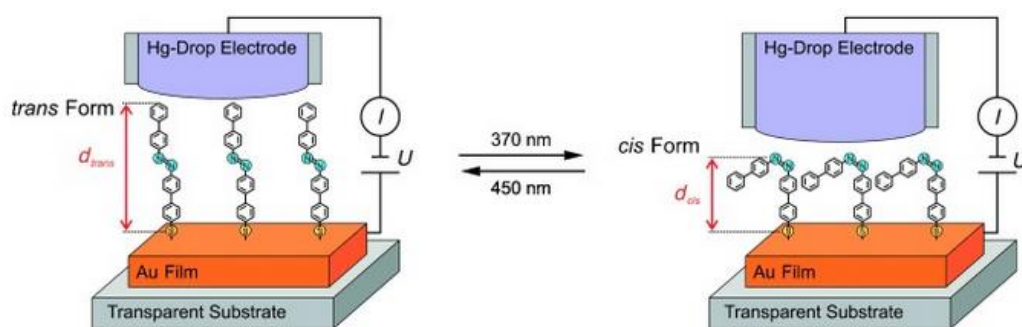


Figure 30. SAM_{AZO} immobilized between a gold surface and a Hg drop electrode. The photoisomerization causes variation of the distance between the electrodes, providing thus an optoelectronic switch and an optomechanical cargo lifter. Figure adopted from Ref.^[108]

Moreover, azobenzene was introduced in rotaxane structures to realize molecular machines, which can execute molecular movements. Dawson *et al.* synthesized a molecular shuttle comprising azobenzene units with collective extension and contraction effects, as molecular artificial muscle.^[109] Subsequently, Credi and co-workers^[110] achieved directionally controlled molecular motion with the realization of a pseudorotaxane containing an azobenzene moiety in the non-symmetric molecular axle. Going from small molecules to bigger structures, azobenzene photoisomerization has been exploited for photocontrolling the activity of biomolecules.^[111] Furthermore, azobenzene-based photoswitches have been used for the functionalization of nanoparticles (NPs) of different nature to tune their properties by means of light irradiation.^[112,113] Usually, azobenzene photoisomerization is used to induce NPs to aggregate or disaggregate in a reversible manner. Klajn *et al.* reported an interesting study on light-driven dynamic self-assembling nanoflasks of different gold NPs functionalized with azobenzenes.^[114] Due to the different dipole moment of azobenzene isomers, *trans-cis* photoisomerization led to a strong dipole-dipole attractive interaction between NPs decorated with azobenzene (Figure 31).

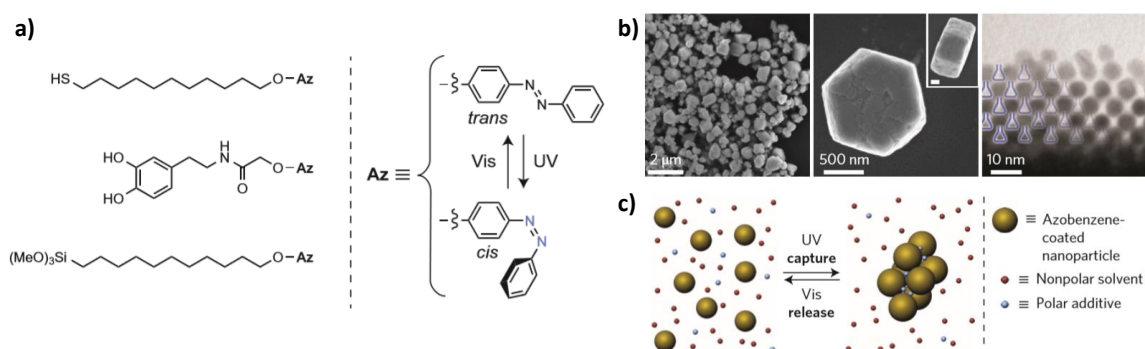


Figure 31. a) molecular structure of azobenzenes used for the functionalization of gold NPs; b) electron micrographs (at different magnification) of colloidal crystals obtained by exposing 6 nm Au-1 to UV light (scale bar in the inset, 200 nm); c) schematic illustration of reversible trapping of dipole molecules during light-induced self-assembly of NPs decorated with azobenzene. Figure adapted from Ref.^[114]

Among the numerous applications of azobenzene, the use of photochromism in nanoelectronics is particularly noteworthy. Although the important progresses achieved for fabrication techniques

developed for conventional silicon-based electronics, limit of miniaturization has been reached. Molecular electronics represent a promising approach for the realization of nanoscale architectures that can be used as functional units in electronics. The introduction of photo-responsive molecules in a device offers the opportunity to generate small-size devices, which respond to a remote light stimulus. Taking advantage of intrinsic properties of a molecule it is possible to achieve charge transport through the single molecule by embedding the latter between two electrodes in an electrode-molecule-electrode structure known as molecular junction. Photoswitchable conductance of molecular junctions is observed when a photochromic molecule is placed between two planar surfaces (electrodes).^[7] Azobenzene photochromism has been studied for the implementation in organic field-effect transistors (OFETs). In OFETs, the charge transport in a semiconducting material can be modulated by electrical gating. More interestingly, the integration of photoresponsive molecules in OFETs enables multifunctionality in the device, which can respond to different stimuli simultaneously. In this regard, photochromic molecules can be mixed into channel layers as dopant or they can be layered between the electrode and the electroactive material to convey bifunctionality to OFETs. Samorì and co-workers developed a bifunctional OFET by introducing an azobenzene self-assembled monolayer (SAM_{AZO}) between the semiconductor and the gold electrode (Figure 32).^[115] In such device, it is possible to reversibly modulate the charge injection at the interfaces by means of UV/Vis light irradiation, thus both electrically and optically gate the source-drain current through the channel.

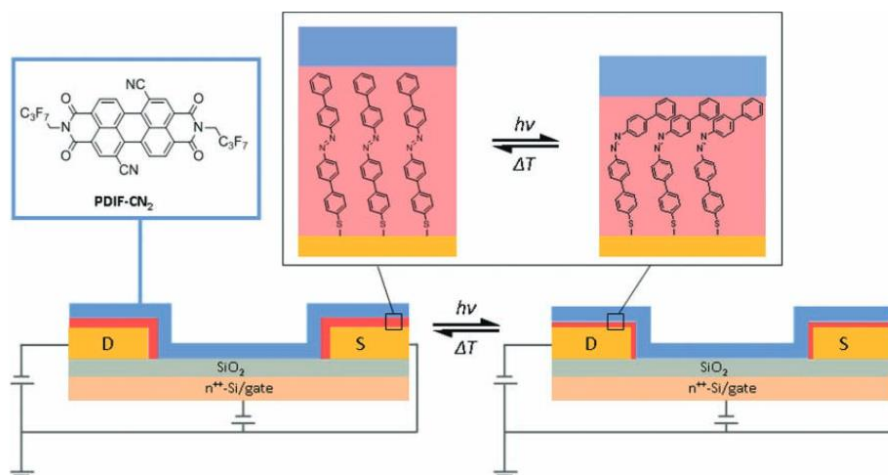


Figure 32. Schematic representation of the bifunctional OFET developed by Samorì and co-workers showing the reversible *trans-cis* isomerization that takes place at the interface between the semiconductor and the electrode decorated with azobenzenes. Adopted from Ref.^[115]

More recently, the attention of an increasing number of chemists has been captured by extended porous 3D metal-organic frameworks (MOFs) as promising materials for application in gas storage, catalysis, drug delivery, separation/purification, etc.^[116] As one of their main features is the high surface area

into the pores, the introduction of photochromic units in MOF architectures represent an appealing way to generate smart light-triggered systems capable to host or release guests present in their cavities upon irradiation at a specific wavelength. Murase *et al.* reported a coordination cage containing azobenzene as pendant photochromic unit in the cavities (Figure 33a).^[117] When azobenzene is in its (*E*)-form, hydrophobic molecules such as pyrene and 1-pyrenecarboxaldehyde are captured into the cage cavity. Irradiation with UV light induces *trans* to *cis* isomerization. As a result, the interior of the cavity becomes less hydrophobic and guest molecules are released. Based on the same principle, Park *et al.* synthesized a light-responsive MOF containing azobenzene pendants into the organic building blocks (Figure 33b).^[118] Studies on CO₂ uptake upon UV/Vis light irradiation showed significant decrease of CO₂ adsorption after *trans*→*cis* isomerization. Hill and co-workers first reported structural transformations of MOFs upon light irradiation.^[119] The researchers synthesized a photoswitchable triply interpenetrated MOF by introducing two different photochromic linkers, *trans*-1,2-bis(4-pyridyl)-ethylene (4,4'-BPE) and 4,4'-azodicarboxylate (AzDC), into the organic backbone Figure 33c). As a result, light-driven framework isomerization strongly affects the pore dimensions, thus light-dependent uptake and release of CO₂ was observed.

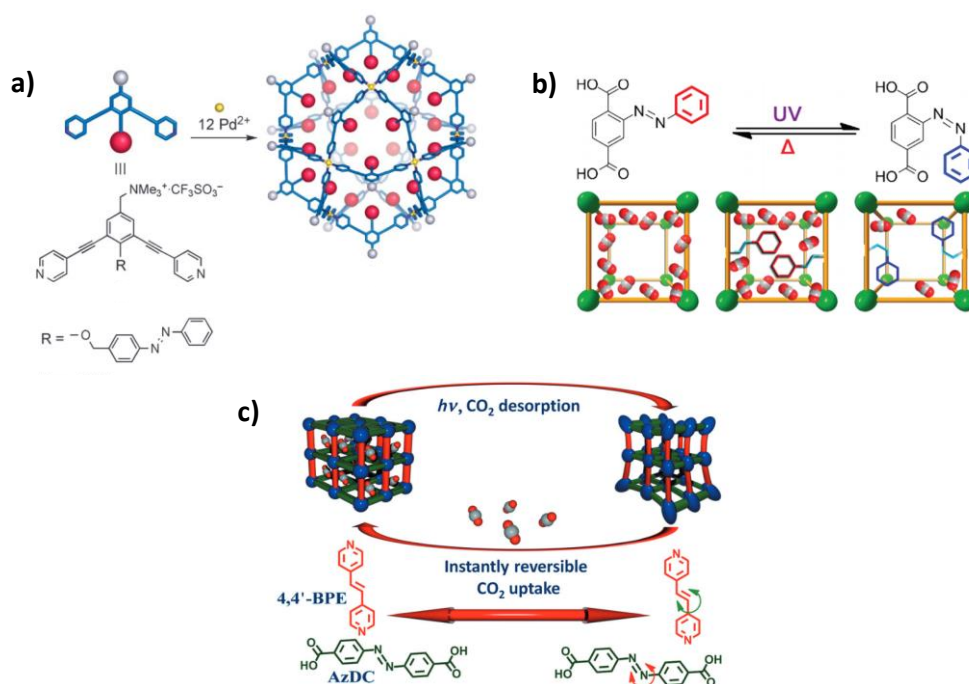


Figure 33. Examples of metal-organic structures including photo-switchable azobenzene units. a) metal-organic cage containing azobenzene pendants for the recognition of hydrophobic molecules;^[117] b) MOF based on organic building blocks exposing photochromic azobenzene units in the cavities for photo-driven uptake and release of CO₂, adapted from Ref.^[118] Copyright © 2012 American Chemical Society; c) photo-responsive MOF containing photoswitchable azobenzene directly in the metal-organic backbone to change pore dimension by light irradiation.^[119]

1.3 Hexa-*peri*-hexabenzocoronene

Polycyclic aromatic hydrocarbons (PAHs) are organic compounds comprising only carbon and hydrogen atoms. They contain fused aromatic rings consisting of all- sp^2 carbon centres, thus they can be considered as two-dimensional segments of graphite. The simplest structure in the family of PAHs is naphthalene, containing two aromatic rings, followed by anthracene and phenanthrene having three fused benzene rings (Figure 34).

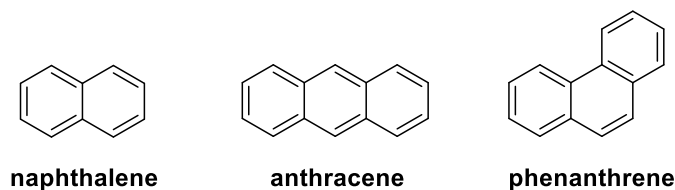


Figure 34. Molecular structures of the simplest PAHs.

In last decades, the attention for polycyclic aromatic hydrocarbons from the scientific community has increased because of chemical and physical features that render these materials appealing candidates as functional units in organic electronics. The interest for such compounds comes mainly from their unique extended sp^2 -network, which enables electron delocalization all over the structure. PAHs show strong intermolecular associations due to the π - π interaction between the aromatic cores that makes them excellent candidates as semiconductors in OFETs, batteries, sensors and solar cells.^[120–122] Despite the wide presence in residues of domestic and natural combustion of coal and wood, and as environmental contaminants, PAHs with specific structural parameters can be obtained only synthetically.^[122,123] Depending on the structure of the PAH, carcinogenic effects^[124,125] can be developed. Among the numerous compounds belonging to the family of PAHs, disk-like PAHs like triphenylene and hexa-*peri*-hexabenzocoronene (HBC) are noteworthy.^[126] Hexa-*peri*-hexabenzocoronene (HBC) is a discotic PAH with chemical formula $C_{42}H_{18}$ containing 42 sp^2 carbons (Figure 35). Due to its D_{6h} symmetry and extended π -system, HBC is considered as a “super-benzene”. With its size exceeding 1 nm, it can be considered as the smallest possible nanographene (NG). Its peculiar disc shape allows the formation of columnar structures by means of π - π stacking.



Figure 35. 3D structure of hexa-*peri*-hexabenzocoronene (HBC).

The strong intermolecular forces make HBC a highly stable and insoluble material that can be processed by vacuum deposition. The introduction of flexible aliphatic chains onto the aromatic core of HBC gives the opportunity to increase its solubility and to control the thermal behaviour of this material. As a result, functionalized HBCs become well soluble in common organic solvents.

1.3.1 Physical properties and supramolecular organization

The molecular structure, size and shape of PAHs influence their physical features, stability and molecular organization. Depending on the way how the aromatic rings are fused, linearly (*cata*-fused) or angularly (*peri*-fused), it is possible to get an extended range of molecules with different physicochemical properties^[127] and packing arrangements.^[128] Various packing motifs are observed because of differences in carbon to hydrogen atom ratios. As a result, C-H $\cdots\pi$ interactions are dominant in molecules with low C/H ratios, whereas in molecules with high C/H ratios (as in the case of HBC) π - π interactions are dominant. As already mentioned, strong π - π stacking of HBC in the solid-state is responsible for its poor solubility. The introduction of flexible aliphatic chains on the HBC core represent a brilliant way to overcome this issue. The enormous progress in synthetic methodology has permitted the preparation of a wide range of functionalized HBC derivatives, and the variety of substituents available allows fine-tuning of solubility, molecular aggregation in solution, morphology and melting temperature.^[129]

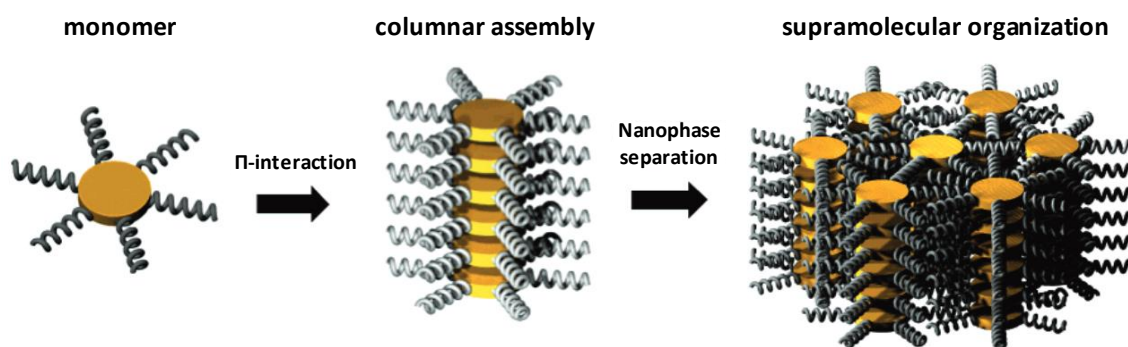


Figure 36. Schematic representation of the molecular organization during the solidification of alkyl-HBC from the solution or isotropic phase. Image adapted from Ref.^[122] Copyright © 2007 American Chemical Society.

Figure 36 shows a schematic representation of the organization process that takes place during the solidification of an alkyl-substituted HBC, from the solution or isotropic phase. Due to the strong π - π intermolecular interactions, monomeric species of alkyl-functionalized HBCs often self-assemble into columns that form supramolecular columnar systems. By increasing the concentration and/or decreasing the temperature, the length of the columns increases considerably, resulting in the solidification of the material. At this stage, a nanophase separation between the highly ordered rigid aromatic cores and the flexible and disordered aliphatic chains is observed.

The columnar aggregates, so-called “discotics”, arrange into a two-dimensional array,^[130] where columns become closer one to another and alkyl chains fill the intercolumnar spaces. The high flexibility of the aliphatic chains increases the disorder of the system and, additionally, the heterogeneity of the two phases that causes changes of the thermal properties of such materials (Figure 37).^[122,131]

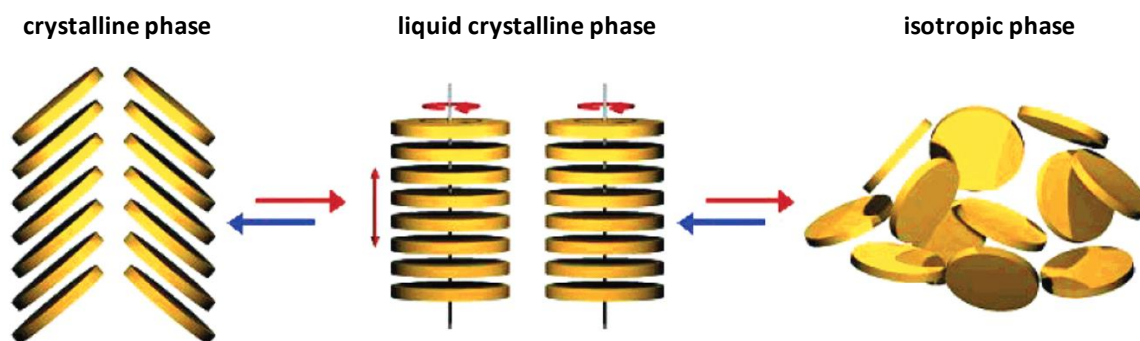


Figure 37. Schematic illustration of the thermal behaviour of alkyl-substituted PAHs. Image adapted from Ref.^[122]

Copyright © 2007 American Chemical Society.

Whereas non-substituted PAHs do not reveal any thermal phase behaviour, alkyl-substituted derivatives show different (meso)phases upon heating, depending on the length and bulkiness of the lateral. Generally, three main phases, characterized by different degree of supramolecular order and dynamics, are observed. In the crystalline phase, the high stacking order within the columnar structures reduces molecular mobility. In this phase, the rigid aromatic cores are tilted with respect to the columnar axis and the alkyl chains are frozen in the periphery. In the liquid crystalline phase (not present in the non-substituted PAHs), the dynamic increases with the temperature. The increased motion of the system leads to lateral and longitudinal fluctuations and to the rotation of the HBC core around the columnar axis. Moving to the isotropic phase, the columnar structures break, generating an amorphous melt where monomeric species are randomly organized into aggregates. The discotic liquid crystalline phase of different alkyl-substituted derivatives has been extensively studied using a combination of techniques such as differential scanning calorimetry (DSC), polarized optical microscopy (POM), solid-state NMR spectroscopy and two-dimensional wide-angle X-ray diffraction (2D-WAXD). A crucial issue for the improvement of charge transport through the supramolecular columnar structures and for their further implementation in organic electronics is the columnar stability. Müllen and co-workers synthesized asymmetrical HBCs bearing carboxylic groups^[132] at the alkyl chain termini, with the aim of taking advantage of hydrogen-bond interaction^[133] for the stabilization of the entire assembly. The capability to control the macroscopic order of HBC derivatives by the choice of solvents, solubilizing alkyl chains and temperature is a fundamental requirement to use these materials as organic thin films in electronic devices. Due to the very high local charge carrier mobility, HBCs became very charming compounds for electronics.

For the actual fabrication of the device, it is fundamental to understand how the molecules are organized in solution and if the supramolecular architecture is maintained during the deposition on a surface. Depending on the deposition method, HBC columnar aggregates can be organized on surface in two different arrangements (Figure 38).

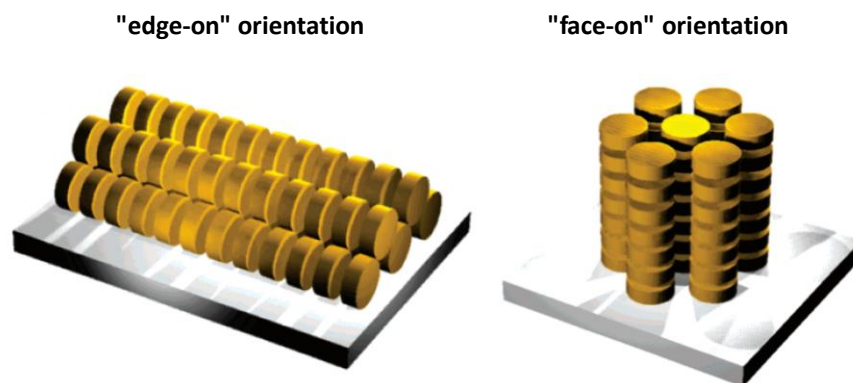


Figure 38. Schematic illustration of the two different types of supramolecular arrangements on surface: “edge-on” orientation (on the left), where the columnar axis is parallel to the surface, and “face-on” orientation (on the right), where the columnar axis is orientated perpendicularly to the substrate. Image adopted from Ref.^[122] Copyright © 2007 American Chemical Society.

In the “edge-on” organization, the molecules are assembled into columnar supramolecular aggregates whose axis is orientated parallelly to the surface. This type of arrangement is desirable for OFETs, where the charge carriers flow through the columnar axis from the source electrode to the drain electrode under controlled voltage. On the other hand, in the “face-on” arrangement the discotic molecules have the columnar axis perpendicular to the substrate. This type of organization is particularly useful for photovoltaic devices, where the fast charge transport between the top and the bottom electrodes can be thus achieved in a short time. Usually, “edge-on” arrangements are preferred for HBC derivatives. However, it is possible to change the molecular aggregation on the substrate by introducing different substituents on the HBC core.^[134] Another parameter that influences the macroscopic order of the aggregates is the technique used for the deposition on the surface. “Face-on” arrangements were obtained with amphiphilic HBCs functionalized with branched hydrophilic chains using Langmuir-Blodgett (LB) technique.^[135] An interesting methodology employed for the preparation of thin films with a high macroscopic order from solution is the “zone-casting” technique. Using this technique, it was possible to form highly ordered “edge-on” organized surface layers of **HBC-C12** (Figure 39).^[136] This technique allows the deposition of the solution of the organic material onto a moving support by a nozzle. In this condition, a concentration gradient between the nozzle and the support is formed. As soon as the critical concentration is reached, nucleation of the material from the solution onto the moving support takes place and thin films of the compound are observed.

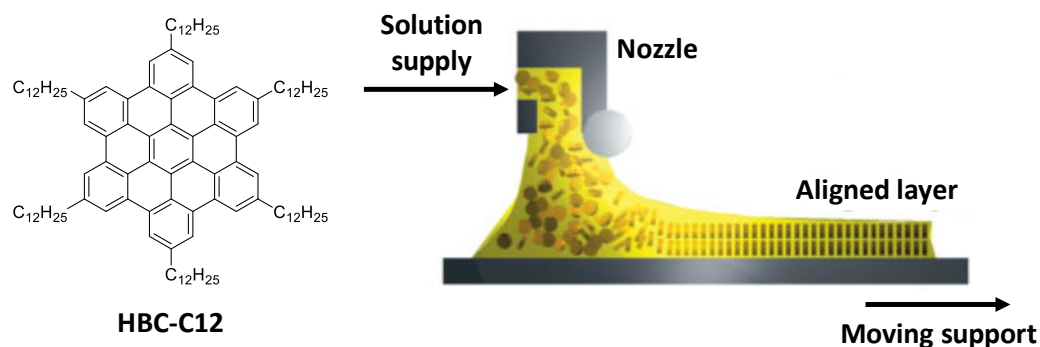


Figure 39. Schematic representation of “zone-cast” technique used for **HBC-C12**. Image adapted from Ref.^[136]

In the case of HBC derivatives, the “zone-casting” technique is particularly efficient due to the strong π - π interactions between the aromatic cores, which determine the formation of big-size pre-aggregates already in the solution before the deposition. The characteristic uniaxial orientation of columnar structure on the substrate was proved by several analytical methods. Highly packed columnar structures parallelly orientated with respect to the deposition direction were observed by atomic force microscopy in tapping mode (TM-AFM).^[137] High-resolution transmission electron microscopy (HR-TEM)^[136] showed a perfect orientation of the material, which suggests extended supramolecular “edge-on” aggregates. Furthermore, additional structural information were obtained by grazing incidence X-ray diffraction^[138] on the “zone-cast” thin layers of hexa(*n*-dodecyl)-substituted HBC. These molecules result assembled in a “herringbone” structure that reminds the packing of unsubstituted HBC, where the aromatic discs are perpendicular to the surface (rotated by approximately 39°) and the long alkyl chains result in an order interdigitated state.

1.3.2 Synthetic strategies towards HBC derivatives

Since the first synthesis of HBC, which was published by Clar and co-workers^[139] in 1958, several synthetic procedures have been proposed for the preparation of PAHs with a well-defined structure.^[122] Clar's synthetic approach towards HBC started with the bromination of 2:3-7:8-dibenzo-*peri*-naphthalene in benzene affording a deep brown precipitate, which was subsequently converted into the tetrabenzoperopyrene upon heating at 153 °C. HBC was finally obtained upon heating tertabenzoperopyrene at 481 °C. Besides the harsh reaction conditions, one of the limitations of Clar's approach is the low reaction yield. In the last decade, Müllen and co-workers have developed a novel protocol towards the synthesis of HBC derivatives (Figure 40).^[122,140]

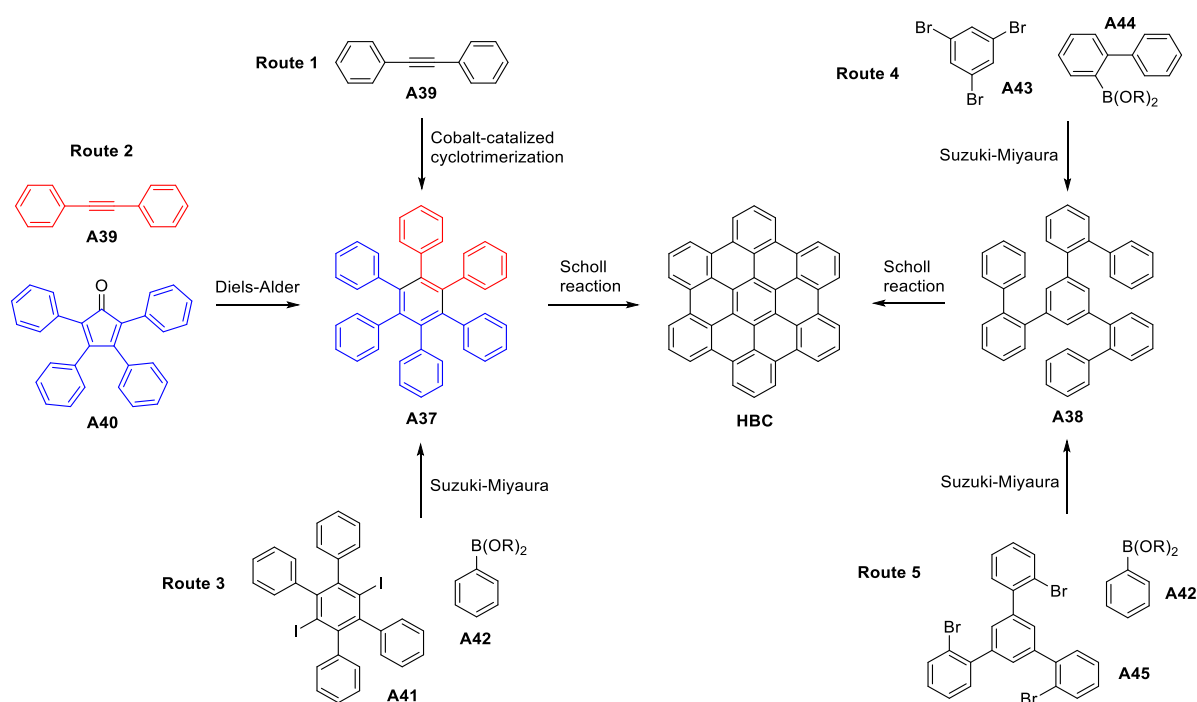


Figure 40. Schematic representation of different synthetic routes towards the HBC derivatives. Functional groups on HBC core are omitted for clarity. Scheme adapted from Ref.^[140]

In 1995, alkyl-functionalized HBCs were prepared in a high yield using mild reaction conditions. The alkyl-substituted hexaphenylbenzene **A37** (Figure 40) was converted into the corresponding HBC by Scholl reaction using Cu(II) and Al(III) salts as oxidizing agent and Lewis acid,^[141,142] respectively. The HBC core can be synthesized *via* different synthetic routes, which are shown in Figure 40. The oxidative coupling of both precursors, hexaphenylbenzene **A37** and 1,3,5-tris(2'-biphenyl)benzene **A38**, provides the desired hexa-*peri*-hexabenzocoronene. Hexaphenylbenzene **A37** can be prepared by cobalt-catalysed cyclotrimerization^[143] of 1,2-diphenylethyne **A39** (Route 1, Figure 40) or, as reported more recently by Xue *et al.*,^[144] using nickel catalyst. This approach was also found to be useful for the synthesis of C3-symmetric HBCs^[145] from asymmetric 1,2-diphenylethyne. In this case, two different regioisomers were obtained and easily separated before the cyclodehydrogenation step.

Diels-Alder [4+2] cycloaddition allowed regiocontrol of functional groups on the HBC core.^[146,147] The reaction between 1,2-diphenylethyne **A39** and cyclopentadienone **A40** (Route 2, Figure 40) gives a carbonyl-bridge intermediate that provides the desired hexaphenylbenzene **A37** after carbon monoxide (CO) elimination. Another way to obtain precursor **A37** is *via* Suzuki-Miyaura cross-coupling reaction^[148] (mechanism depicted in Figure 41) of 1,4-diiodo-2,3,5,6-tetraarylbenzene **A41** with phenylboronic acid or ester **A42** (Route 3, Figure 40).

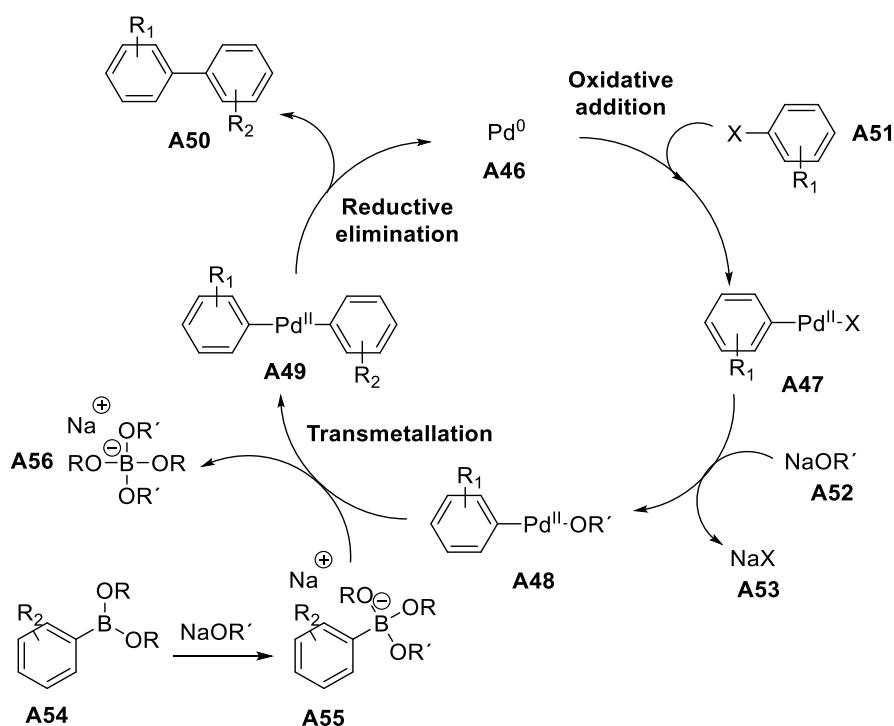


Figure 41. General mechanism of Suzuki-Miyaura cross-coupling reaction.

Suzuki-Miyaura reaction is one of the most used procedures for the C-C bond formation. This synthetic procedure was first reported by Suzuki^[149,150] (Nobel Prize Laureate in 2010) in 1979, and it involves the reaction between an aryl or vinyl halide with aryl or vinyl-boronic derivatives using a Pd^0 catalyst. The Suzuki cycle begins with the oxidative addition aryl halide **A51** to palladium complex **A46** to give organopalladium compound **A47**. In the presence of base **A52** (Figure 41), **A47** is converted to a nucleophilic palladium complex **A48** that, subsequently, reacts with the more reactive arylboronic compound **A55**. The transmetallation step generates a new organopalladium complex **A49**, which undergoes reductive elimination to afford the coupling product **A50** and regenerated Pd^0 complex (**A46**). Suzuki-Miyaura reaction can be also used for the preparation of 1,3,5-tris(2'-biphenyl)benzene **A38** either from 1,3,5-tribromobenzene **A43** and biphenylboronic acid or ester **A44** (Route 4, Figure 40) or from phenylboronic ester **A42** and 1,3,5-tris(2-bromophenyl)benzene **A45** (Route 5, Figure 40).^[151] Despite the huge progress of synthetic methods towards preparation of well-defined PAHs and HBC derivatives, Scholl reaction remains the most prevalent method.

Scholl reaction is defined as an oxidative coupling reaction between two aryl compounds in the presence of a Lewis acid. In 1910, Ronald Scholl^[152] reported the intramolecular oxidative coupling of dibenzo[*a,o*]perylene-7,16-dione, which was converted to the π -extended phenanthron[1,10,9,8-*opqra*]perylene-7,14-dione in the presence of an excess of anhydrous AlCl₃ by heating at 140-145 °C for 45 minutes. In the last few decades, chemists have developed a large number of alternative procedures^[122,153,154] to avoid harsh reaction conditions of Scholl's protocol and thus eliminate the side products. A noteworthy contribution has been given by Müllen and co-workers.^[155] As early as 1995, they overcame the aforementioned issue using AlCl₃/Cu(OTf)₂ in CS₂, lowering thus the reaction temperature to room temperature (RT). Most recent methods employed for the preparation of HBC derivatives involve the use of FeCl₃/CH₃NO₂ mixture,^[146,156] which provides HBCs in almost quantitative yield. Iron chloride acts as a Lewis acid and oxidizing agent. Alternative methodologies adopt MoCl₅^[157,158] or dichlorodicyano-*para*-benzoquinone (DDQ) in the presence of an acid (usually trifluoromethanesulfonic acid, CF₃SO₃H).^[159–161] One of the limitations of Scholl cyclodehydrogenation is the regioselectivity for the C-C bond formation. Furthermore, substituents (electron-withdrawing or electron-donating) on the aromatic core affect reaction rate and hinder the planarization reaction.^[162] This issue can be addressed by using suitable spacers or additional groups that counterbalance the electrical effect. Lateral chlorination and polymerization are typical side-reactions observed in the HBC synthesis *via* oxidative Scholl coupling. However, they can be efficiently reduced by passing a constant flow of inert gas through the reaction mixture for the entire reaction time. The gas flow removes gaseous HCl that is formed during the reaction.

The mechanism of Scholl reaction is still object of debate and several reviews have been reported.^[153,158,163] Two mechanisms have been proposed, namely through the arenium ion and the radical cation intermediates (Figure 42). In the arenium ion mechanism (Pathway A, Figure 42), the aryl compound (**A37**) forms an electrophilic σ complex **A37(i)** after protonation (shown as H⁺ in Figure 45 for clarity reasons, but it could also be a complex with a Lewis acid). The neighbouring nucleophilic aromatic ring attacks the electrophilic arenium ion **A37(i)** and a new C-C bond is formed. Species **A37(ii)** is converted to intermediate **A37(iii)** that provides the condensed product **A37(vii)** by hydrogen elimination during the oxidation step.

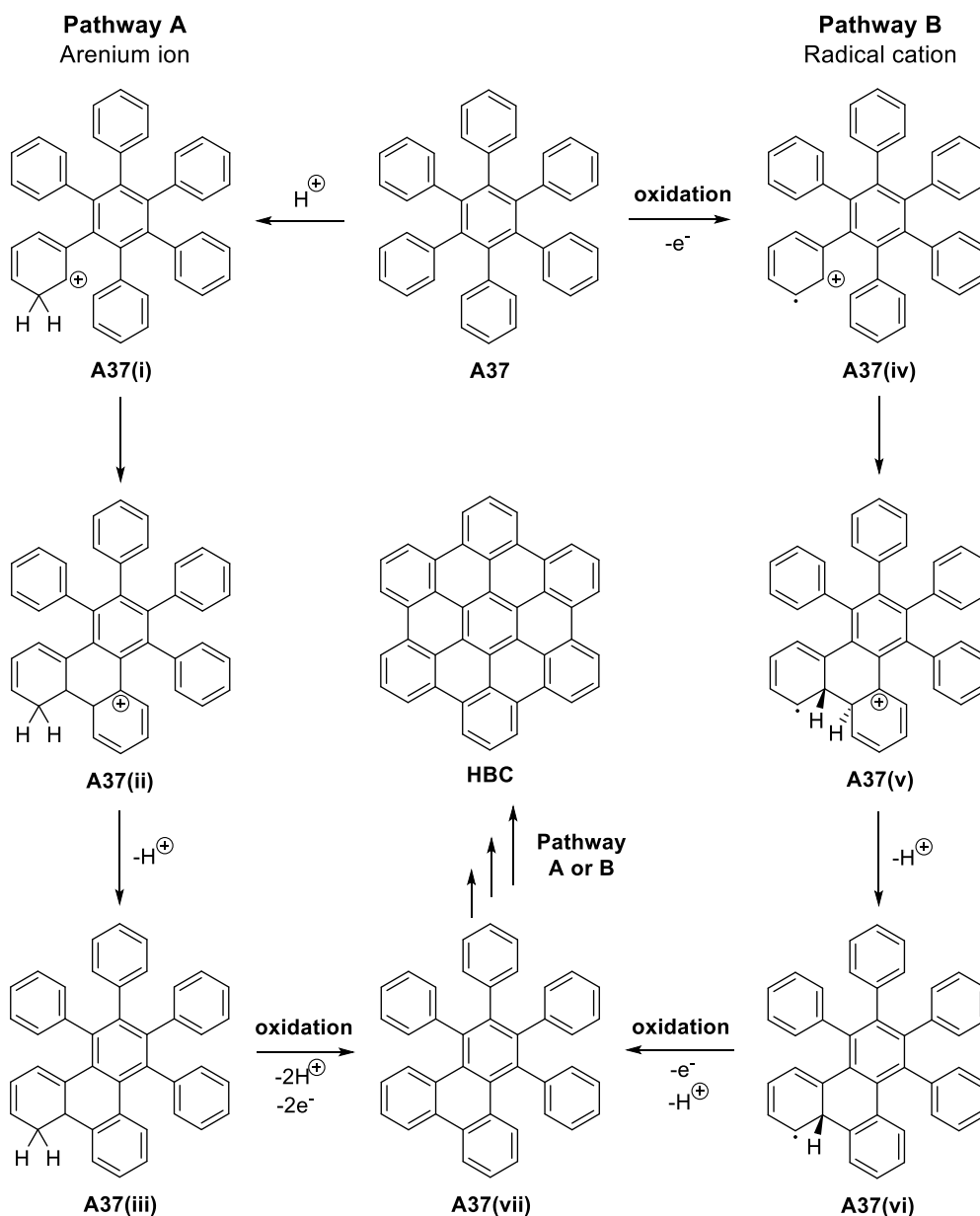


Figure 42. Two proposed mechanism of Scholl reaction: *via* arenium ion (Pathway A) and *via* radical cation (Pathway B). Scheme adapted from Ref. ^[140,153]

In the second mechanism proposed (Pathway B, Figure 42), one-electron oxidation of **A37** induces the formation of radical cation **A37(iv)**. Subsequently, electrophilic substitution of the latter by a second arene provides intermediate **A37(v)**. Deprotonation of **A37(v)** and following oxidation regenerate the aromatic system, finally giving condensed product **A37(vii)**. The reaction can be repeated several times, until the complete condensed product, namely HBC, is formed. Discrimination between the two proposed mechanisms is not a trivial issue. Both mechanisms are supported by experimental data that prove the reliability of the study. ^[161,164,165]

1.3.3 HBCs as functional materials

The strong intermolecular interactions exhibited by HBC and most of its derivatives lead to extended self-assembled structures characterized by long-range order. Hence, this is the main feature exploited in HBC-based functional materials. HBC derivatives are promising materials for lithium-ion batteries. Keil *et al.* reported the high levels of lithium and sodium storage in HBC films.^[166] In a most recent work, Mukai *et al.* investigated the electrochemical behaviour of HBC and hexafluoro-HBC (6F-HBC) in non-aqueous lithium cell medium.^[167] Interestingly, their study showed discharge capacity of 460 and 1230 mAh/g for HBC and 6F-HBC, respectively, suggesting their potential application as negative electrodes in lithium-ion batteries. Certainly, the main application of HBC derivatives remains as semiconducting materials for organic electronics. The columnar structure of HBC shows an intrinsic charge mobility value of $1.1 \text{ cm}^2/\text{Vs}$.^[168] This feature makes such materials extremely good candidates for OFETs^[136,169] and organic photovoltaics (OPVs).^[170–172]

1.4 Two-dimensional (2D) and three-dimensional (3D) molecular architectures

The elegant assembly of small organic and/or inorganic units into extended, well-structured architectures, achieved through either weak (non-covalent) or strong (covalent) interactions, has been witness of huge progresses in the last few decades. Connecting molecular building blocks in order to create porous crystalline structures has given rise to metal-organic frameworks (MOFs)^[173] and covalent organic frameworks (COFs).^[174] Whereas organic synthesis allows the preparation of sophisticated molecular structures through step-by-step reactions, the synthesis of well-defined porous materials exploits one-step reactions, where all the bonds within the 2D or 3D structure are formed simultaneously. The resulting porous material are completely insoluble thus, the synthetic procedure needs to be precisely planned.

The class of two-dimensional (2D) nanomaterials^[175] comprises nanomaterials with a sheet-like structure. These materials own atomic or molecular level thickness and extended lateral size, usually larger than 100 nm or even up to few micrometres.^[176] Since 2004, when Novoselov *et al.* first reported graphene exfoliation from graphite using Scotch tape,^[177] the interest for ultrathin 2D materials dramatically increased, although they have been known for several decades. The 2D feature is exclusive and provides access to unpredicted chemical, physical and electronic properties originating from electron confinement in two dimensions.^[178,179] Recently, organic 2D materials containing a network of repeated organic units, arranged in two orthogonal directions, have drawn the attention of many scientists. Their advantages arise from high molecular diversity (infinite different compounds can be synthesized), reduced weight, intrinsic flexibility and high tunability, which make these 2D nanomaterials as novel potential functional units in devices^[180,181] with tailored properties such as charge-injection,^[182] storage^[183] and charge transport.^[184] Organic molecules assemble into extended structures by means of covalent bonds or non-covalent interactions. The difference consists in the robustness and stability of the resulting structure, which affects their possible applications.

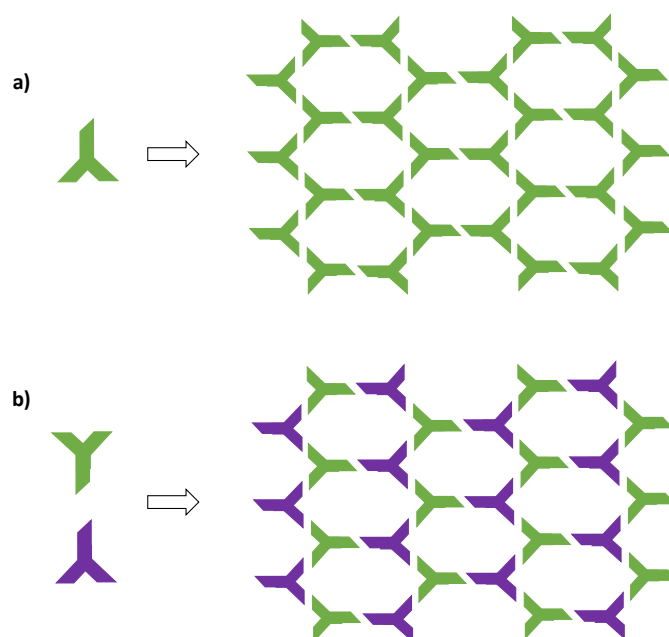


Figure 43. Schematic representation of self-assembled 2D polymers. a) *homo*-polymer generated by means of self-assembly of one molecular species; b) *hetero*-polymer comprising two different organic building blocks.

Depending on the number of organic molecules (monomers or building blocks) involved in the 2D structure, *homo*- and *hetero*-polymers can be formed. 2D *homo*-polymers comprise only one molecular species, which bears the functional group required for the self-assembly. On the other hand, 2D *hetero*-polymers contain two or more molecular species as organic building blocks, thus the supramolecular organization derives from the interaction between the functional groups exposed on different molecules. Figure 43 shows a schematic illustration of *homo*- (a) and *hetero*-polymers (b).

1.4.1 Two-dimensional organic structures based on self-assembly

Supramolecular self-assembly of organic molecules into extended two-dimensional systems is an appealing way to fabricate highly ordered nanostructured materials that allow tuning surface properties for their implementation in organic devices. 2D supramolecular structures based on non-covalent interactions inspired the synthesis of rigid organic building blocks bearing specific functionalities to coordinate their organization into highly ordered architectures. Several 2D supramolecular polymers have been synthesized and studies of their self-assembly on surfaces provided a wide range of organized systems.^[185,186] The capability to control the supramolecular packing at molecular level is a crucial feature for molecular-engineering. Design and synthesis of tailor-made organic building blocks, with a specific molecular structure, allow predictions of the final supramolecular organization. Despite the single molecular structure, supramolecular engineering at surfaces relies on the knowledge of the non-covalent intermolecular interactions that take place, namely van der Waals (vdW), metal-ligand and hydrogen-bonding interactions. Van der Waals (vdW) forces, named from J.D van der Waals,^[187] are weak distance-dependent atomic or molecular interactions. This type of interaction is involved at

first in the absorption of the molecules on surfaces. Due to an inert character and relatively high stability in air, atomically flat surfaces commonly used for investigations at the solid-liquid interface are Au(111), highly oriented pyrolytic graphite (HOPG) and MoS₂. Once molecules are attached on the surface, the nature and directionality of the intermolecular interaction affect the crystallization process at the solid-liquid interface. The introduction of long aliphatic chains in the molecular structure increases the 2D self-assembly stability and allows the formation of crystalline patterns by interdigitation.^[188] Exploiting this strategy, De Feyter and co-workers^[189] realized the first example of a four-components 2D crystal (Figure 44).

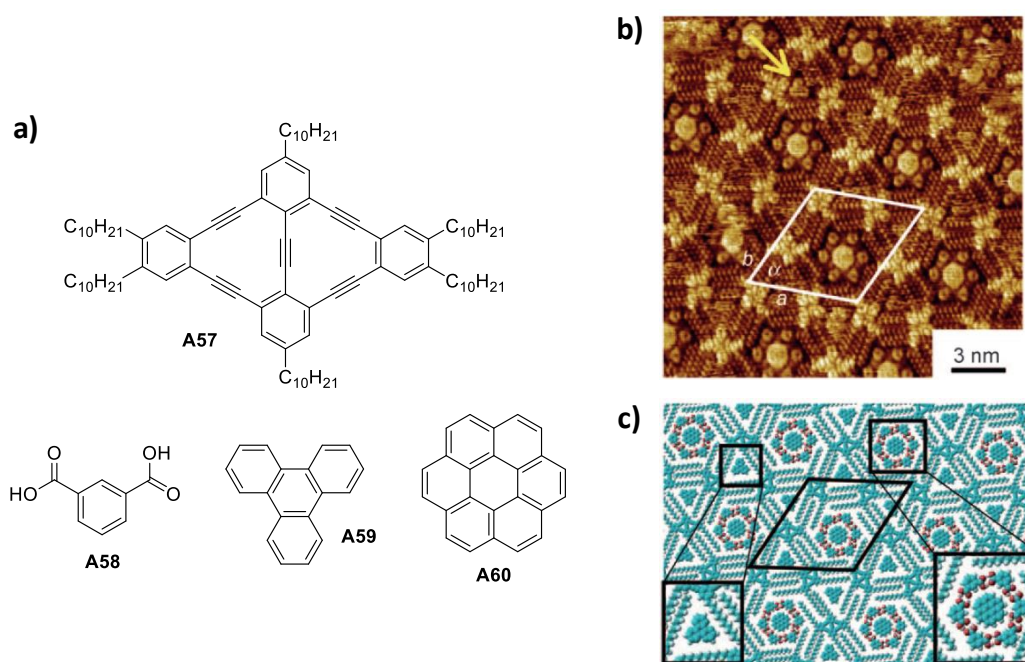


Figure 44. a) Chemical structures of the molecules contained in the four-components 2D crystal: rhombing-shaped fused dehydrobenzo[12]annulene with decyl chains (**A57**), isophthalic acid (**A58**), triphenylene (**A59**) and coronene (**A60**); b) STM image of a mixture of **A57**, **A58**, **A59** and **A60**; c) supposed network model showing the triangular and hexagonal arrangements. Image adapted from Ref.^[189]

Hydrogen-bond is a non-covalent, attractive intramolecular or intermolecular interaction between a proton-donor (X–H) and a proton acceptor (Y).^[190] Depending on the type of donor and acceptor, H-bonds can be weak, moderate or strong. Whereas for weak and moderate hydrogen-bond the strength varies from 1-4 to 4-15 kcal mol⁻¹, respectively,^[191] for strong H-bonds the energy ranges from 15 to 40 kcal mol⁻¹.^[192,193] This type of interaction is extremely peculiar because it combines fundamental features such as directionality, reversibility, specificity and cooperativity.^[133,194,195] In the case of H-bonding interactions, is worth to consider the molecular environment, which can completely change the molecular architecture.^[196] Hydrogen-bonding interaction between two carboxylic acids^[197] is one of the most widely used strategies to control the 2D organization of supramolecular systems. Heckl and co-workers^[198] reported the self-assembly of benzene-1,3,5-tricarboxylic acid (trimesic acid,

TMA) in honeycomb and flower structures (Figure 45) on graphite surface by means of H-bonds between carboxylic groups on adjacent molecules.

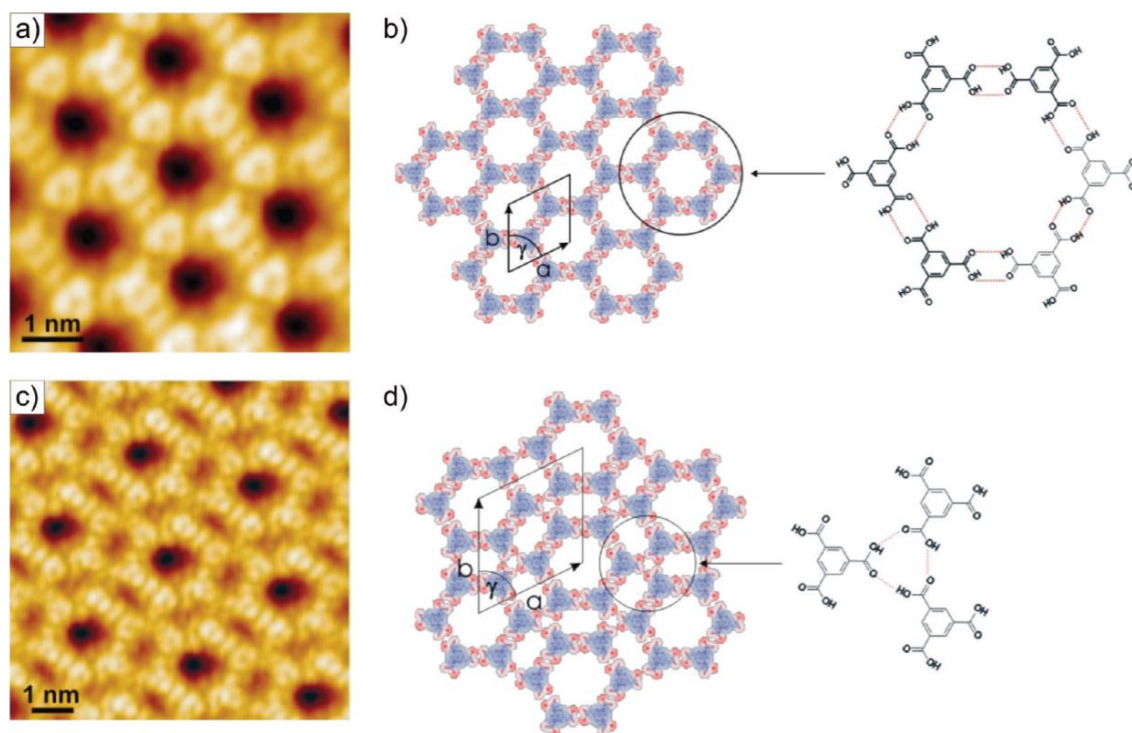


Figure 45. Supramolecular organization of trimesic acid (TMA) on graphite surface in highly ordered honeycomb (a,b) and flower (c,d) structure. In both structures, TMA molecules are adsorbed planar to the surface, and the overall structure is stabilized by means of H-bonds between adjacent carboxylic groups. Figure adopted from Ref.^[198]

1.4.2 Metal-organic frameworks (MOFs)

Metal-ligand interactions between an organic molecules and a transition metal ion have been widely used in different research fields.^[199,200] Exploiting this type of interaction, Schryver and co-workers^[201] reported the STM study of *in situ* complexation of palladium acetate, Pd(OAc)₂, by a monolayer of bipyridine derivative **A61** (Figure 46) at a graphite/liquid interface to form a well-defined monolayer. Metal-organic frameworks (MOFs) consist of metal ions or clusters coordinated to organic electron donor ligands (linkers) to form well-ordered and stable crystalline structures. A wide range of organic ligands is available, and their nature affects structure and properties of the obtained material such as its porosity, thermal and chemical stability.

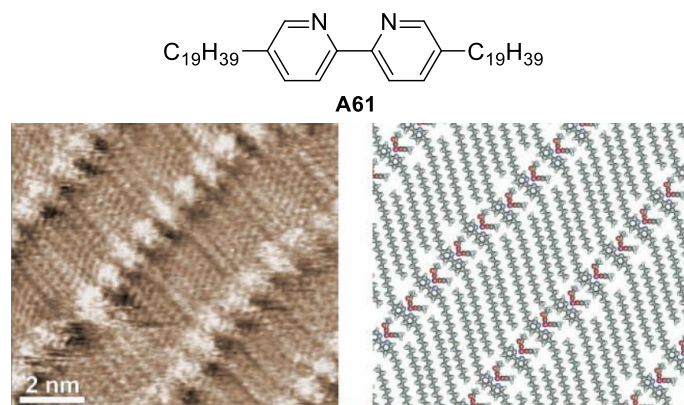


Figure 46. Metal-ligand complex packed at interface. Image adapted from Ref.^[201]

More interestingly, it is as well possible to modify these structures by post-synthetic modification (PSM).^[202–204] MOFs are produced mainly by hydrothermal or solvothermal techniques, where the crystalline extended structure is obtained through slow crystal growth from a hot solution (reaction performed in an oven). As early as 1997, Kitagawa and co-workers^[205] first reported the synthesis of a 3D MOF that exhibited gas sorption properties at room temperature. Two years later, MOF-5^[206] and HKUST-1^[207] (Figure 47) were synthesized and used as highly stable porous structures for gas storage, which are still the most studied MOFs.

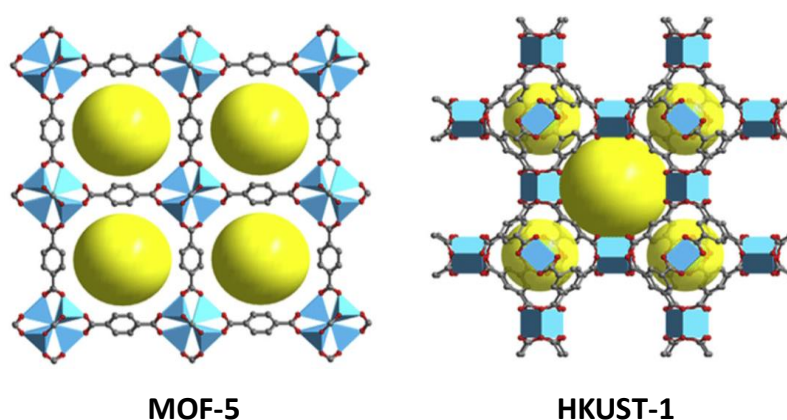


Figure 47. Schematic representation of 3D structure of MOF-5 (left) reported by Yaghi and co-workers and HKUST-1 (right) reported by Williams and co-workers. Image adapted from Ref.^[206,207]

Despite the progresses achieved within the synthesis of MOFs, the control of the pore size and crystallinity remains fundamental features for their applications. MOFs are appealing candidates for smart membranes, catalytic coatings, sensors and drug delivering structures.^[116,208]

1.4.3 Covalent organic frameworks (COFs)

Even though the development of synthetic methodologies has allowed the preparation of extended self-assembled structures, the important issue of their low stability (due to the nature of non-covalent interactions) needs to be addressed. Therefore, 2D and 3D architectures based on covalent bonds were developed for the synthesis of conducting materials owing a higher robustness.^[209,210] Such stable structures based on covalent bonds are commonly called covalent organic frameworks (COFs)^[211] and comprise small organic building blocks (monomers), which are organized into well-ordered structures thorough a chemical reaction between the organic units. The overall structure resulting from the covalent interaction between monomers is a porous structure, where the pores size can be tuned by using different organic molecules. Due to their extended porosity, high surface area and robustness, covalent organic frameworks draw the attention of many scientist as promising materials for gas storage^[212], catalysis^[213] and as semiconducting and photo-conducting materials.^[214,215] Although extended covalent frameworks exist in nature, any analogous structure was synthesized until 2005, when Yaghi and co-workers^[216] first reported the synthesis of a 2D covalent organic framework based on boroxine units by utilizing the principles of dynamic covalent chemistry.^[217,218]

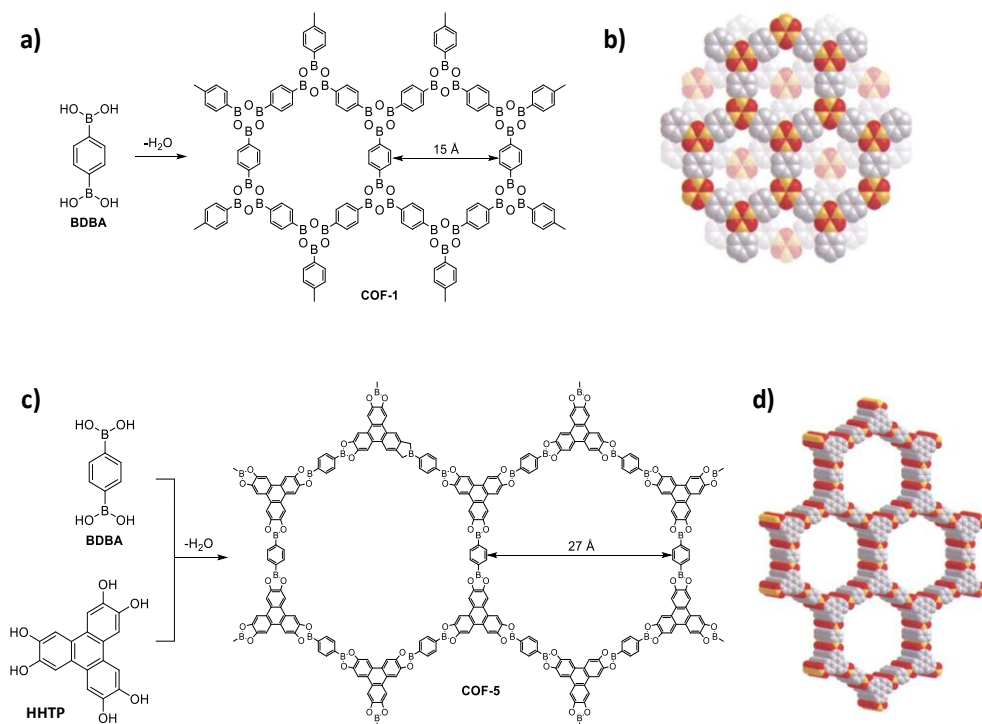


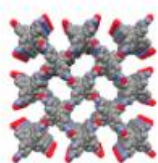
Figure 48. Crystalline COFs reported by Yaghi and co-workers. a) COF-1 synthesis through condensation of benzene-1,4-diboronic acid (BDDBA); c) COF-5 synthesis through condensation reaction between BDDBA and 2,3,6,7,10,11-hexahydroxytriphenylene (HHTP); b) and c) structural representation of COF-1 and COF-5 based on powder diffraction and modelling. Image adapted from Ref.^[216]

Their material was the first crystalline COF obtained, and it was based on condensation between benzene-1,4-diboronic acid (BDBA) and 2,3,6,7,10,11-hexahydroxytriphenylene (HHTP) (Figure 48). Based on Yaghi's structures, numerous 2D COFs have been synthesized by including different organic units.^[219,220] Interestingly, COFs sheets comprising aromatic units can further assemble through π - π interactions forming aligned layered structures.^[221] In 2007, Yaghi and co-workers also pioneered the first 3D COF.^[222] The 3D architecture was achieved by condensation reaction of tetrahedral tetra(4-dihydroxyborylphenyl)methane (TBPM) or tetra(4-dihydroxyborylphenyl)silane (TBPS) units, as well as by its co-condensation with triangular 2,3,6,7,10,11-hexahydroxytriphenylene (HHTP) unit. It is worth to mention that during the high dimension covalent bond formation different structures (with different free energy) can be formed. Consequently, direct crystallization of COFs is almost impossible to obtain. This issue can be addressed by reversible dynamic bonding between the units. Dynamic covalent chemistry (DCvC) relies on the reversible formation and breaking of covalent bonding within the molecules.^[217,218] Reversibility in bond formation allows error corrections and self-healing during the crystallization process. Therefore, if an undesired bond is formed, the system can correct it by to promote the thermodynamically more stable crystalline structure. Most recently, Wuest and co-workers^[223] reported the synthesis of crystalline 3D COFs exploiting the polymerization of nitroso compounds, performed at room temperature. Organic chemistry offers an extremely large amount of reactions that occur between molecules bearing different functional groups. As a result, a wide range of COFs based on various covalent bonds, have been reported in the last decade.^[224–235] Figure 49 gives an overview of the organic reactions used for the preparation of COFs.

To summarize, the function of extended ordered structures such as MOFs and COFs arises from their porosity and stability. Hence, the possibility of synthesizing crystalline porous materials with internal cavities having uniform diameter and high surface area, make these materials extremely appealing for gas adsorption and storage applications, catalysis, drug delivery, separation/purification, and as semiconducting and photo-conducting materials. Although few examples of photo-triggered MOFs comprising azobenzenes pending in the cavities^[118] or integrated in the skeleton^[119] of the material have been reported, the development of stimuli-responsive COFs hasn't been accomplished yet.

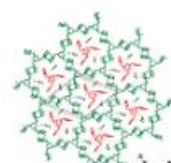
a) Low strength covalent bonds

Dimerization of nitroso



NPN-1

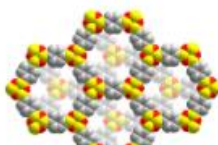
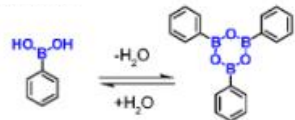
Dimerization of anthracene



2 DP

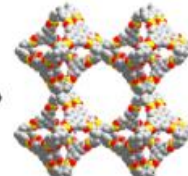
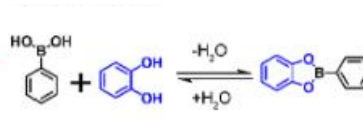
b) Robust covalent bonds

Boroxine



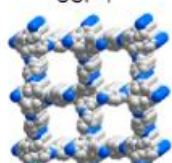
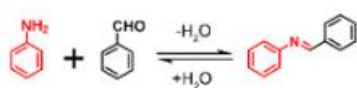
COF-1

Boronate ester



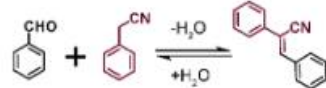
COF-108

Schiff base reaction



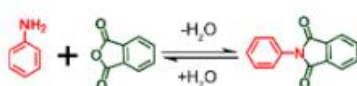
COF-300

Knoevenagel reaction



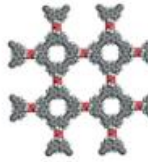
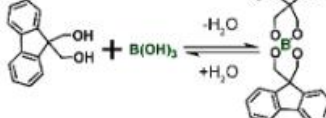
sp²c-COF

Imide formation



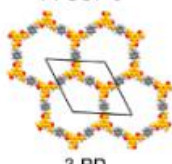
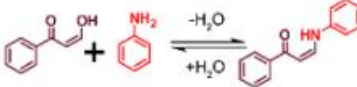
PI-COF-5

Spiroborate formation



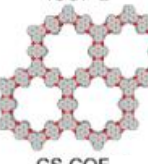
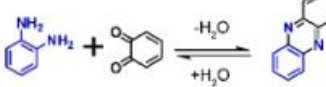
ICOF-2

Michael addition reaction



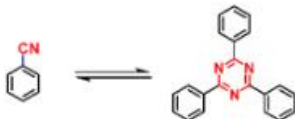
3 PD

Phenazine formation



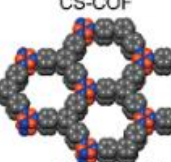
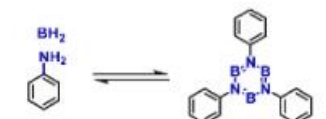
CS-COF

Triazine formation



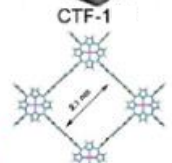
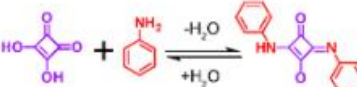
CTF-1

Borazine formation



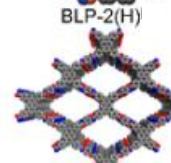
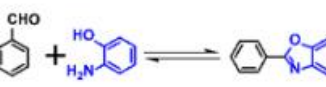
BLP-2(H)

Squaraine



CuP-SQ COF

Benzoxazole formation



LZU-192

Figure 49. a) and b) Different types of reactions used for COF constructions: dimerization of nitroso,^[223] dimerization of anthracene,^[224] boroxine,^[216] boronate ester,^[225] Schiff base reaction,^[226] Knoevenagel reaction,^[227] imide formation,^[228] spiroborate formation,^[229] Michael addition reaction,^[230] phenazine formation,^[231] triazine formation,^[232] borazine formation,^[233] squaraine,^[234] and benzoxazole formation.^[235] Figure adapted from Ref.^[211] Copyright © 2019 American Chemical Society.

2 Results and discussion

2.1 Star-shaped azobenzenes as multi-chromophoric switches¹

This chapter is focused on the design, synthesis and characterization of a series of star-shaped azobenzenes containing up to three photoswitchable “molecular arms” mounted on a rigid benzene core. The compounds were proposed as multi-chromophoric building blocks for the construction of photo-responsive 2D and 3D materials, as well as for the investigation of their supramolecular self-assembly at the solid-liquid interface on graphite (HOPG) surface and photoisomerism. The molecular geometry is bestowed by the introduction of the three switchable (or non-switchable) branches on a benzene ring in the *meta* position reciprocally, and the self-organization on surface is driven both by hydrogen-bonding between the COOH termini and van der Waals interactions. Multi-photochromism of tris(azobenzene) **3** was investigated in solution and on surface at the solid-liquid interface,^[236] and compared with its analogous **10**, **23**, **27** derivatives, as well as with **35** and 4-(phenylazo)benzoic acid **79** used as model compounds (Figure 50).

2.1.1 Motivation

The reversible $E \leftrightarrow Z$ isomerization of azobenzene is responsible of large structural and physical changes that have been widely used to modify chemical systems by means of light irradiation. Upon irradiation, azobenzene undergoes a significant geometrical change, from the extended and flat (*E*)-isomer to the contracted and non-flat (*Z*)-isomer, which makes this chromophore an optimal candidate as a molecular-scale actuator. The introduction of multiple azobenzene units on a rigid molecular scaffold enables amplification of the structural alterations associated with the azobenzene switching.^[238,239] However, the structure of the scaffold and the position where the switchable units are introduced need to be considered for the photoisomerization efficiency. While, the substitution at *para* position on a benzene ring increases the electronic conjugation and this decreases the photoreactivity of azobenzene, the substitution in the *meta* position reduces the electronic coupling between the switchable arms. Electronic decoupling within the structure is fundamental to preserve the photochromism of the system.^[240,241] A few examples of molecular systems comprising more than one photochromic unit are reported in literature.^[242–244]

¹ Large parts of this section have been published.^[236,237]

Among them, star-shaped derivatives with chromophores connected to non-planar^[245] or planar^[242,244] cores have been synthesized. Although the photoisomerization of the individual photochromic unit has been characterized in solution, up to date the presence of multiple isomeric states in self-assembled networks on surface has not been reported.

The possibility of studying 2D self-assembled architectures on graphite (HOPG) substrates by scanning tunnelling microscope (STM) has enhanced research into supramolecular chemistry on surface. STM allows detailed visualization of molecular structures and their supramolecular organization *via* non-covalent interactions such as hydrogen bonding and van der Waals (vdW) forces. Among self-assembled systems, loosely packed structures result particularly interesting as host-guest systems. Their periodic arrangement of voids generates a porous and extended architecture capable of incorporating small molecular species in its cavities. Therefore, C₃-symmetrical aromatic molecules became widely studied as rigid organic ligands in large-scale 2D and 3D structures such as metal-organic frameworks and covalent organic frameworks. Benzene-1,3,5-tricarboxylic acid (trimesic acid, TMA) is one of the most investigated C₃-symmetrical organic ligands. The presence of three carboxylic groups introduced on a benzene ring in *meta* position reciprocally, enables the formation of hexagonal honeycomb structure *via* intermolecular hydrogen-bonding between the COOH termini.^[246] Nevertheless, studies on its larger homologues showed different supramolecular networks suggesting that multiple factors influence the self-assembly.^[247,248] The resulting supramolecular system arises thus from the balance between anisotropic intermolecular interaction, such as hydrogen bonds, isotropic vdW forces and solvent contribution (at the solid-liquid interface, the 2D crystalline assemblies are in thermodynamic equilibrium with the supernatant solution). Our star-shaped derivatives were proposed as a new class of C₃-symmetrical aromatic systems with photoresponsive properties. In this thesis the design, synthesis and characterization of a series of star-shaped molecules bearing up to three azobenzene switchable units and their non-switchable homologous, utilized as reference compounds, is presented.

The photochromic behaviour in solution and on graphite surface, as well as the supramolecular self-organization in hydrogen-bonded networks on graphite were investigated. All the studies were performed in a close collaboration with our partners at the Université de Strasbourg – UdS (Prof. P. Samorì and Dr. A. Galanti) and at the Université de Mons – UMONS (Prof. J. Cornil, Dr. V. Diez-Cabanes and Dr. A. Minoia).

2.1.2 Synthesis of star-shaped azobenzenes

Photoresponsive materials are a highly appealing field of research. Once embedded on a surface or incorporated as photoactive units in an extended system, they enable the transduction of an effect from the molecular level to a macroscopic one. Among photochromic molecules, azobenzene is one of the most studied photoswitches. Its $E \leftrightarrow Z$ photoisomerization is a fast, reversible and well-known process and it induces extended geometrical and physical changes that can be exploited for the implementation of light-driven materials. Azobenzene chromophores can be used as organic building blocks in large-scale architectures to generate optically triggered 2D and 3D materials with application in gas storage, drug-delivery, separation/purification and electronics. Most interestingly, the introduction of more than one photochromic unit on a molecular scaffold gives the opportunity to amplify the structural and physical alterations resulting from the photoisomerization. Therefore, more photochromic states are observed in the system, because of the existence of more than two isomeric forms.

This chapter is mainly focused on the design, synthesis and characterization of a series of star-shaped azobenzene derivatives bearing up to three switchable “molecular arms” within the same molecular backbone. The molecular structure and geometry were adopted taking into account previous research developed in this field.^[240–242,244,245] All our star-shaped derivatives comprise an aromatic benzene ring as rigid molecular scaffold, which bears one, two or three or switchable azobenzene molecular branches, as well as corresponding non-switchable tolanes. The photochromic and/or non-photochromic units are introduced in the position 1,3,5 on the central benzene. Such a substitution results in the arms being reciprocally in *meta* position, thus reducing the conjugation within the multi-chromophoric system.^[240,241] Furthermore, carboxylic groups (-COOH) were introduced as the termini to enable supramolecular self-assembly into hydrogen-bonded networks. The star-shaped photoswitches tris(azobenzene) **3**, bis(azobenzene) **27** and mono(azobenzene) **23** were designed *ad hoc* to include structural features such as conformational rigidity given by the aromatic benzene core, peculiar geometry dictated by the 1,3,5 substitution, azobenzene moieties that bestow photoactivity to the system and carboxylic functions for the self-organization *via* hydrogen-bonding. On the other hand, the synthesized derivative **35** and the non-switchable homologous **10**, as well as the commercial available 4-(phenylazo)benzoic acid **79** were used as reference compounds for the interpretation of the results.

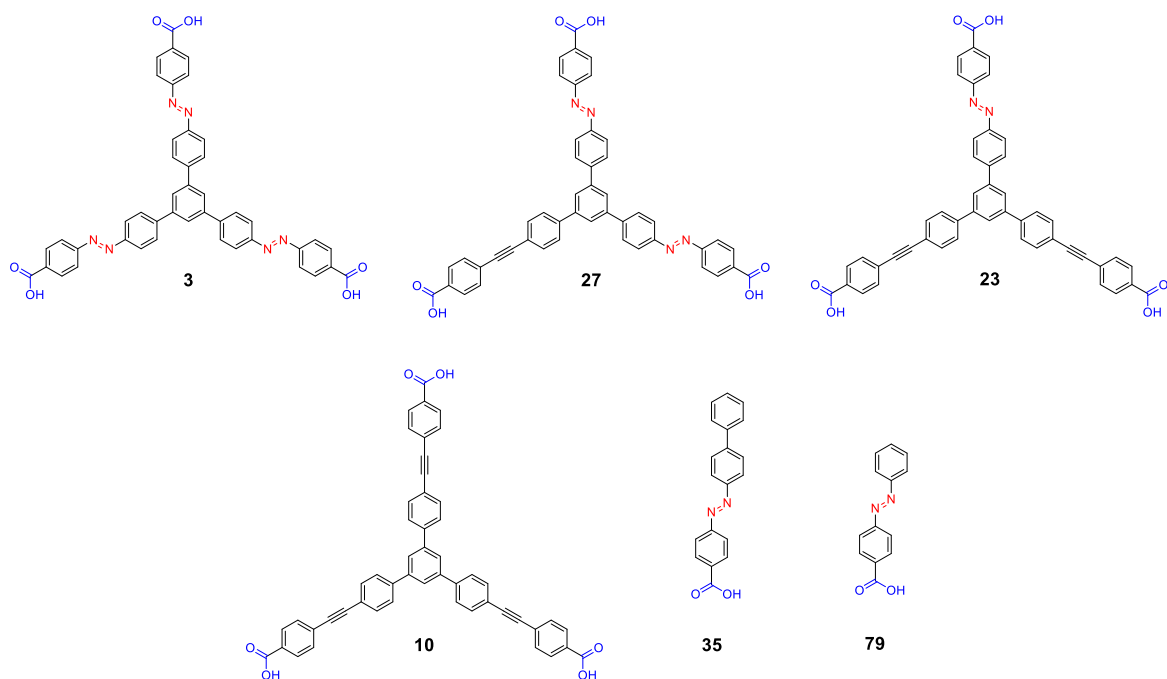


Figure 50. Chemical structures of the star-shaped photoswitchable and non-photoswitchable compounds described within this chapter, namely tris(azobenzene) **3**, bis(azobenzene) **27**, mono(azobenzene) **23**, derivative **35**, 4-(phenylazo)benzoic acid **79** and the non-photoresponsive derivative **10**.

Star-shaped tris(azobenzene) **3** comprises three photoswitchable 4'-[(4''-carboxyphenyl)diazenyl]phenyl- "arms" mounted onto a benzene ring in the position 1,3,5.

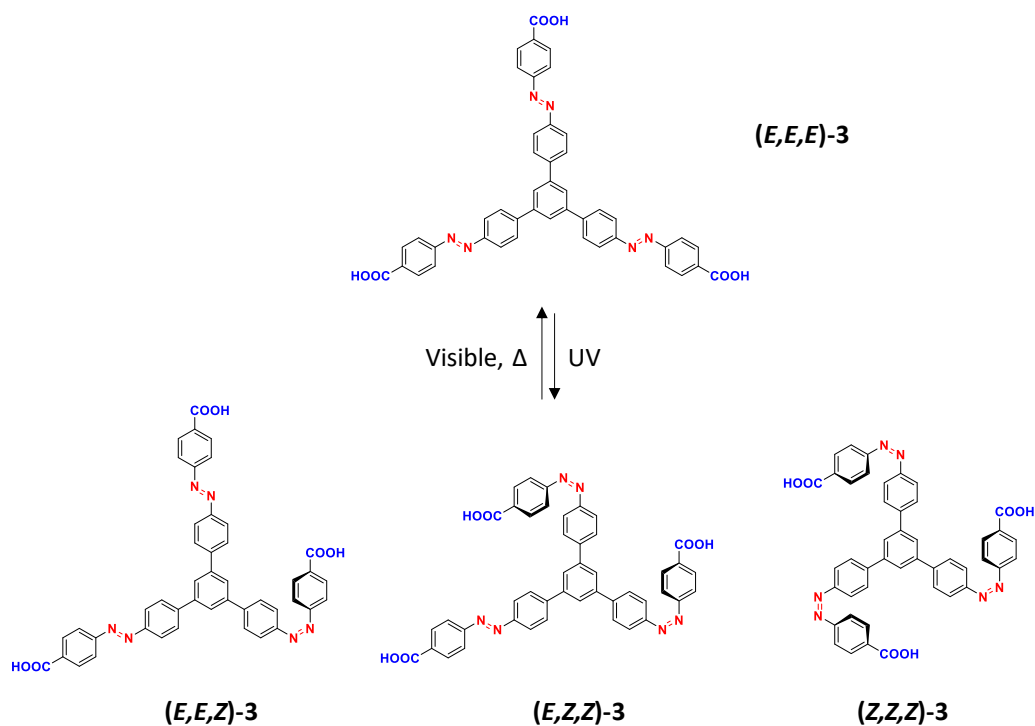


Figure 51. Schematic representation of the photoisomerization of tris(azobenzene) **3**.

The presence of three photoswitches on the aromatic benzene core provides four isomers upon irradiation with UV/Vis light (Figure 51). Upon $E \rightarrow Z$ isomerization, the extended and planar (E,E,E)-**3** is gradually converted into the more compact and non-planar (Z,Z,Z)-isomer. Because of their structural rigidity, the four isomers show different shapes. The process is photo-controlled, and the structures can be recovered in a reversible manner in solution. The synthetic strategy used towards the preparation of star-shaped tris(azobenzene) (E,E,E)-**3** is outlined below (Figure 52).

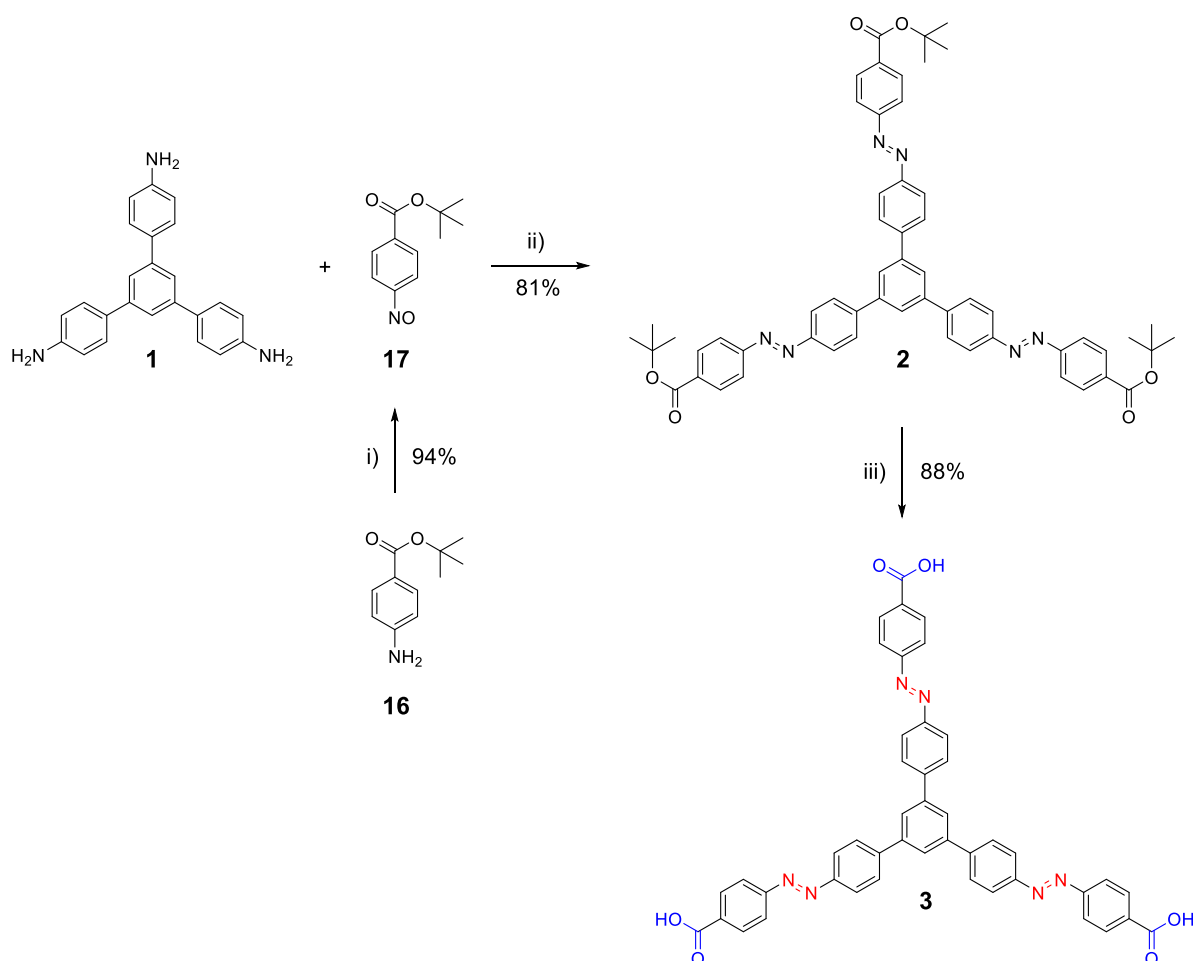


Figure 52. Synthetic strategy towards (E,E,E)-**3**. Reagents and conditions: (i) Oxone®, CH_2Cl_2 , H_2O ; (ii), AcOH, RT; (iii) TFA, CH_2Cl_2 , RT.

The synthesis of star-shaped tris(azobenzene) (E,E,E)-**3** starts with the oxidation of *tert*-butyl-4-aminobenzoate (**16**) in a biphasic solvent mixture of dichloromethane and water with Oxone®. Oxone®, a trade name for the triple salt $2\text{KHSO}_5 \cdot \text{KHSO}_4 \cdot \text{K}_2\text{SO}_4$, is a mild oxidizing agent. An aqueous solution of Oxone® was added to a solution of *tert*-butyl-4-aminobenzoate (**16**) in CH_2Cl_2 and the biphasic system was stirred at room temperature for 16 hours. Due to the low stability of nitroso compounds, after work up the greenish crude was used without further purification for the next reaction step. *tert*-Butyl ester **2** was assembled *via* Mills reaction between nitroso derivative **17** and compound **1**. Thus, *tert*-butyl-4-nitrosobenzoate (**17**) was dissolved in glacial acetic acid and then 1,3,5-tris(4'-

aminophenyl)benzene (**1**) was added to the green solution. The reaction mixture was stirred at room temperature for 20 hours under argon atmosphere until an orange precipitate was formed. The precipitate corresponds to the azobenzene *tert*-butyl ester (**2**), which is insoluble in acetic acid, while the unreacted excess of *tert*-butyl-4-nitrosobenzoate (**17**) remains in the solution. Filtration of the precipitate provided the desired product 1,3,5-tris(4'-{[4''-(*tert*-butoxycarbonyl)phenyl]diazenyl}phenyl)benzene (**2**) without further purification. The introduction of a protecting group such as *tert*-butyl ester is required for a solubility reason. *tert*-Butyl ester **2** was dissolved in dichloromethane and then trifluoroacetic acid (TFA) was added to the solution. The reaction mixture was stirred at room temperature for 16 hours. Subsequent hydrolysis of *tert*-butyl ester (**2**) in acidic conditions leads to the formation of an orange precipitate, which corresponds to tris(azobenzene) **3**, completely insoluble in dichloromethane and most of organic solvents. Thus, the desired pure product (**3**) was isolated *via* filtration in 88% yield.

The synthetic strategy adopted for the preparation of derivatives **23** and **27** bearing one and two azobenzene switchable molecular arms respectively was accomplished *via* Suzuki-Miyaura cross-coupling reaction between the non-photoresponsive ethyn-1,2-diyl building block (**15**) and the photoresponsive azobenzene building blocks (**21** and **25**).

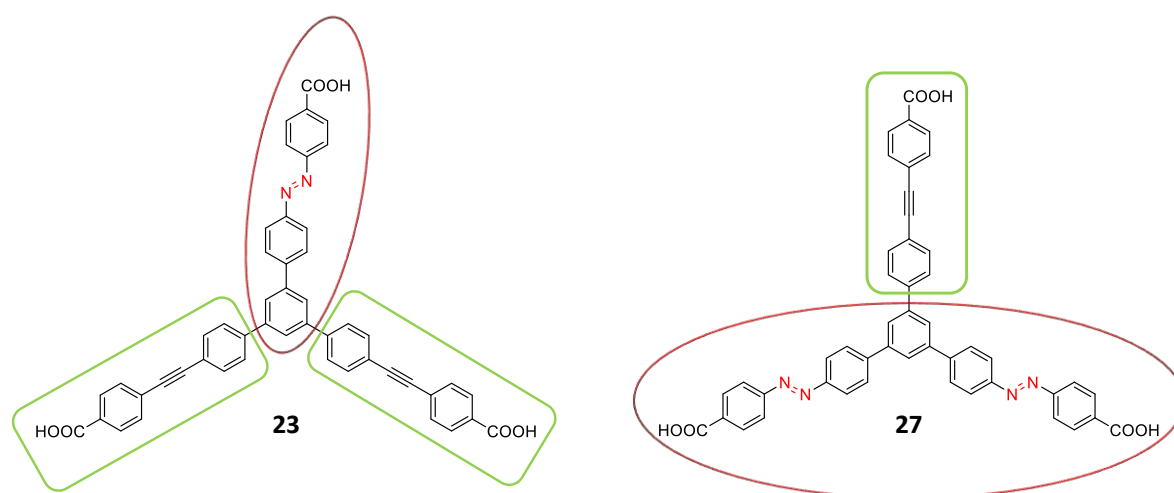


Figure 53. Molecular structures of azobenzene derivatives **23** and **27**. Their preparation is based on the assembly of two building blocks separately synthesized, namely a non-photoswitchable ethyn-1,2-diyl building unit (green square) and a photoswitchable azobenzene unit (red circle).

The synthesis of the non-switchable tolane unit (**15**) is outlined in Figure 54. It begins with the esterification of 4-iodobenzoic acid (**4**) into the corresponding *tert*-butyl ester **5**. As aforementioned for tris(azobenzene) **3**, the protecting group is fundamental to maintain solubility. Carboxylic acids are characterized by very low solubility in common organic solvents; thus the introduction of solubilizing alkyl esters is required. The esterification reaction was performed following two different literature procedures. The first method (Method A), reported by Wang *et al.*,^[249] involves the preparation of the

4-iodobenzoyl chloride intermediate. 4-Iodobenzoic acid (**4**) was dissolved in an excess of thionyl chloride (SOCl_2) and then few drops of *N,N*-dimethylformamide (DMF) were added to the solution. The reaction mixture was refluxed under argon atmosphere for 30 min. During this time, 4-iodobenzoic acid was converted to the more reactive 4-iodobenzoyl chloride intermediate and the unreacted SOCl_2 was removed by distillation. Subsequently, 4-iodobenzoyl chloride was dissolved in anhydrous dichloromethane and a solution of *tert*-BuOK in anhydrous tetrahydrofuran (THF) was slowly added via a cannula. After work up, the desired *tert*-butyl-4-iodobenzoate (**5**) was isolated as a yellow oil in 62% yield. In order to improve the reaction yield, a second method (Method B), reported by Ma and Xia,^[250] was adopted for the preparation of compound **5**. 4-Iodobenzoic acid **4** was reacted with di-*tert*-butyl-dicarbonate (Boc_2O) and 4-dimethylaminopyridine in *tert*-butyl alcohol (*tert*-BuOH). After work up, the desired *tert*-butyl-4-iodobenzoate **5** was isolated as a yellow oil in 97% yield.

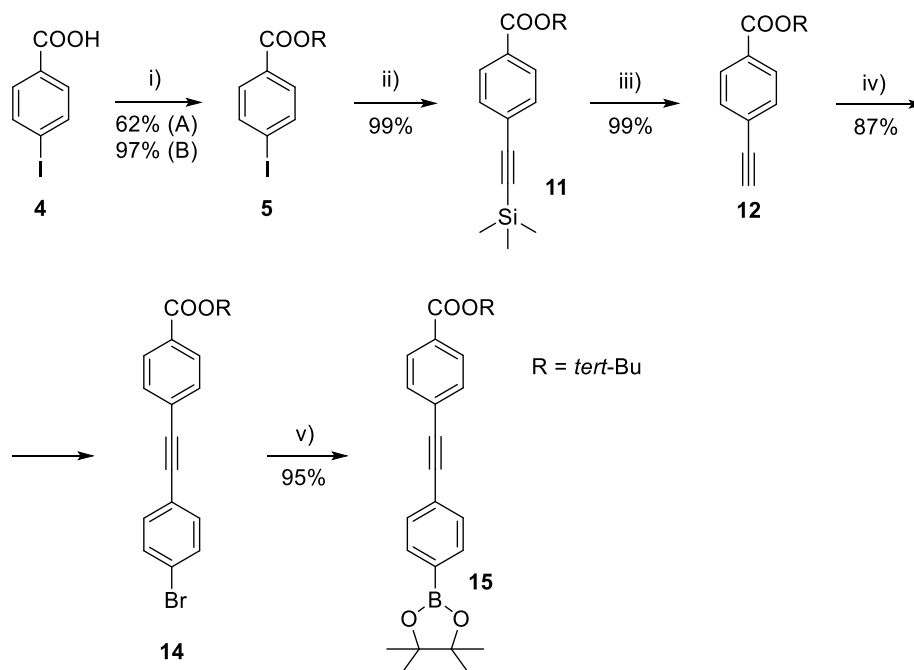


Figure 54. Synthetic strategy towards the non-photoresponsive ethyn-1,2-diyl building block (**15**). Reagents and conditions: i) 1. SOCl_2 , 70 °C; 2. *tert*-BuOK, THF, RT (Method A); DMAP, Boc_2O , *tert*-BuOH, 40 °C (Method B); ii) trimethylsilylacetylene, $\text{Pd}(\text{PPh}_3)_2\text{Cl}_2$, CuI, Et_3N , RT; iii) Cs_2CO_3 , *tert*-BuOH, 45 °C; iv) 1-bromo-4-iodobenzene (**13**), $\text{Pd}(\text{PPh}_3)_2\text{Cl}_2$, CuI, Et_3N , 0 °C; v) bis(pinacolato)diboron, AcOK, $\text{Pd}(\text{dppf})\text{Cl}_2$, dioxane, 90 °C.

tert-Butyl-4-iodobenzoate (**5**) was coupled with an excess of trimethylsilylacetylene *via* Sonogashira cross-coupling reaction. Since iodine is a good leaving group and it does not need high temperature to be substituted, the reaction can be performed at room temperature using triethylamine (Et_3N) as a solvent and a base to provide trimethylsilyl protected derivative **11** in quantitative yield. The subsequent cleavage of the TMS group was done under basic conditions. *tert*-Butyl-4-[(trimethylsilyl)ethynyl]benzoate (**11**) was dissolved in *tert*-butyl alcohol, and then an excess of Cs_2CO_3 was added. At the beginning, the cleavage reaction was performed in methanol providing

methyl-4-ethynylbenzoate side-product (**78**) as main product (Figure 55). Thus, in order to prevent transesterification, *tert*-butyl alcohol was used as solvent yielding compound **12** quantitatively.

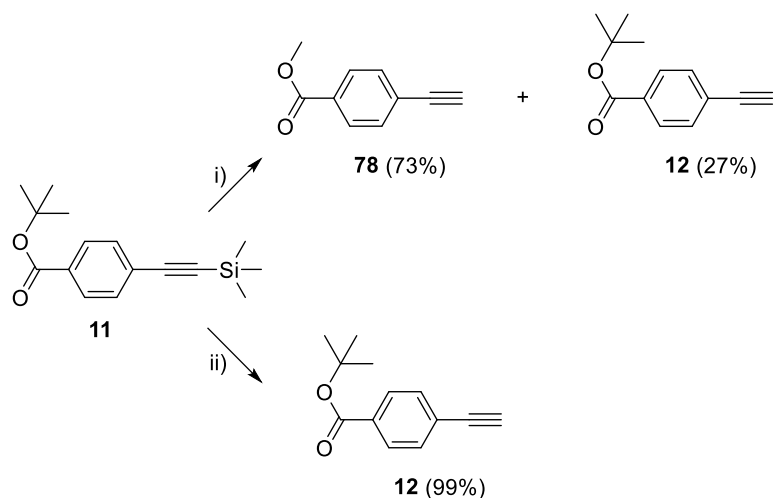


Figure 55. Synthetic strategies towards *tert*-butyl-4-ethynylbenzoate (**12**). In this reaction step, the choice of the solvent is fundamental to prevent transesterification side reaction. Reagents and conditions: i) K_2CO_3 , MeOH, RT; ii) Cs_2CO_3 , *tert*-BuOH, 45 °C.

Tolane derivative **14** was obtained *via* Sonogashira cross-coupling reaction between *tert*-butyl-4-ethynylbenzoate (**12**) and 1-bromo-4-iodobenzene in 87% yield. The reaction was performed in an ice bath at 0 °C to maintain regioselectivity to iodine atom. Subsequently, Miyaura borylation reaction of compound **14** with bis(pinacolato)diboron was performed to afford the non-photoresponsive ethyn-1,2-diyl building block (**15**) in almost quantitative yield.

The synthetic pathway for the preparation of the photoresponsive azobenzene building block **21** is outlined in Figure 56. 4-Amino-3',5'-dibromobiphenyl (**20**) was obtained *via* Suzuki-Miyaura cross-coupling reaction between 1,3,5-tribromobenzene (**18**) and 4-aminophenylboronic acid pinacol ester (**19**) in toluene. In order to obtain the mono(amino) derivative **20**, a slight excess of pinacol boronic ester **19** was used, providing the desired product as a yellow solid in 43% yield. Finally, azobenzene derivative **21** was synthesized *via* Mills reaction between amine **20** and an excess of *tert*-butyl-4-nitrosobenzoate (**17**) in 70% yield.

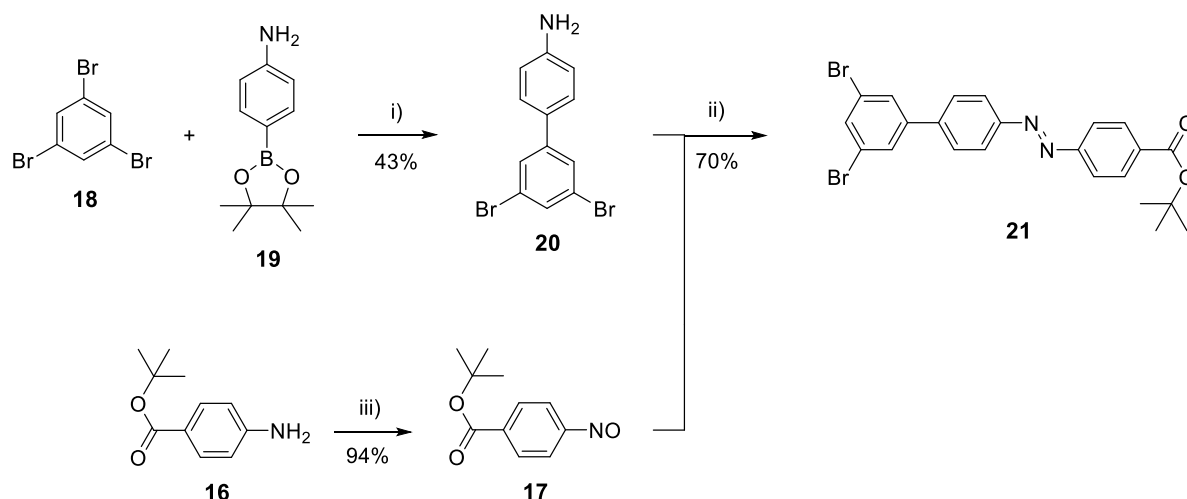


Figure 56. Synthetic strategy towards the photoresponsive azobenzene building block **21**. Reagents and conditions: i) $\text{Pd}(\text{PPh}_3)_4$, K_2CO_3 , H_2O , toluene, 95°C ; ii) AcOH , RT, iii) Oxone®, CH_2Cl_2 , H_2O , RT.

The synthesis of star-shaped mono(azobenzene) **23** is depicted in Figure 57. Star-shaped (mono)azobenzene *tert*-butyl ester (**22**) was assembled *via* Suzuki-Miyaura cross-coupling between the non-photoresponsive unit **15** and the photoresponsive mono(azobenzene) building block **21**. The reaction was performed using K_3PO_4 as a mild base in dioxane affording derivative **22** in 82% yield. The coupling reaction is very fast, and the reaction process was constantly monitored by TLC to prevent the hydrolysis of *tert*-butyl protecting groups. Final acid-catalysed hydrolysis of *tert*-butyl ester derivative **22** was performed to obtain the target molecule **23** in 97% yield. *tert*-Butyl ester **22** was dissolved in dichloromethane and then trifluoroacetic acid was added to the solution. Slow formation of an orange precipitate was observed. The precipitate corresponds to the desired product (**23**), which is completely insoluble in dichloromethane due to the presence of three carboxylic groups.

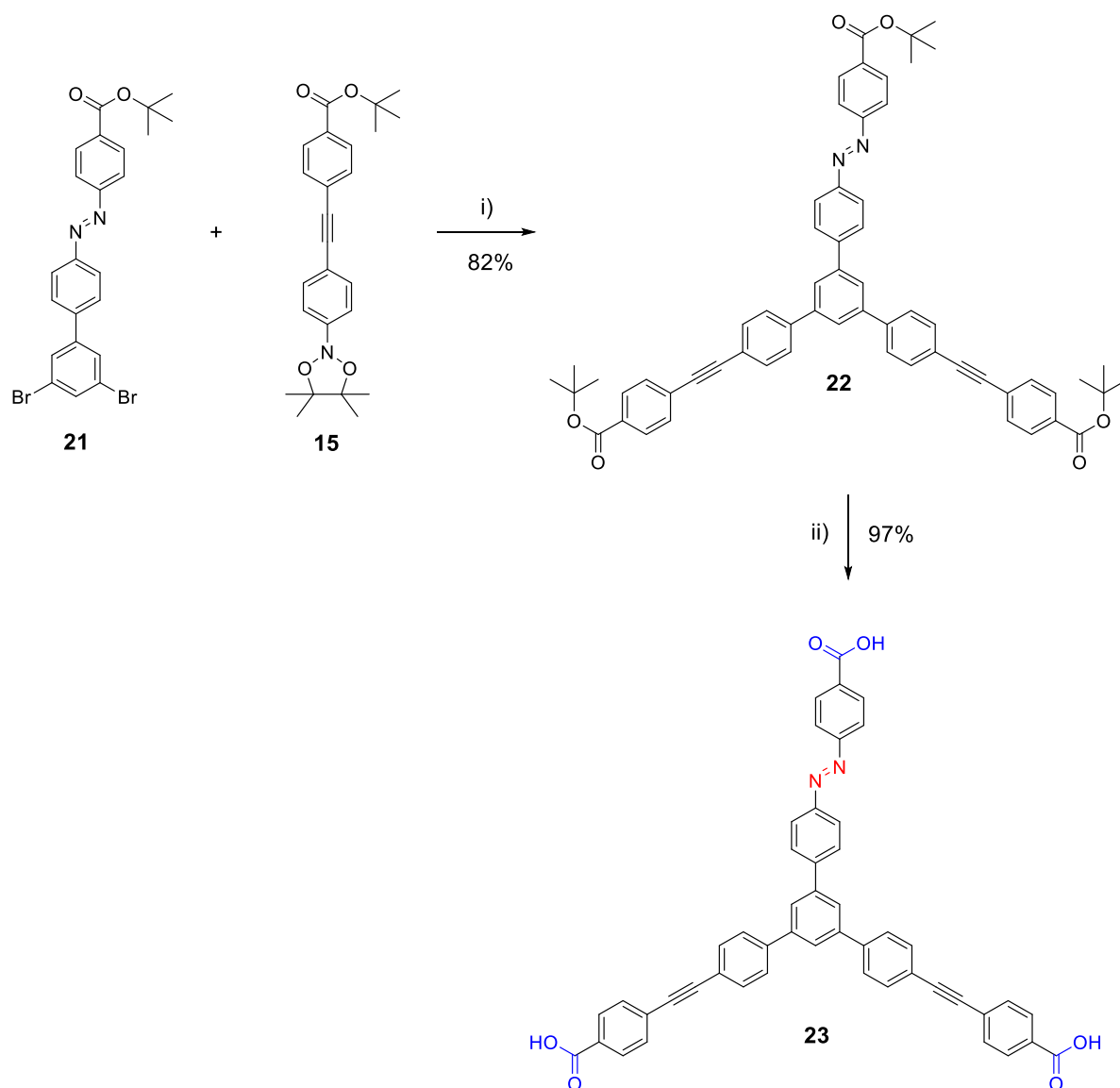


Figure 57. Synthetic strategy used for the preparation of star-shaped mono(azobenzene) **23**. Reagents and conditions: i) Pd(dppf)Cl₂, K₃PO₄, H₂O, dioxane, 90 °C; ii) CH₂Cl₂, TFA, RT.

The synthetic pathway used for the preparation of star-shaped bis(azobenzene) **27** is based on the same strategy employed for mono(azobenzene) star-shaped derivative **23**. Both molecules contain switchable and non-switchable molecular arms in different ratio and their synthesis involves the assembly of the two main building blocks *via* Suzuki-Miyaura cross-coupling reaction. Whereas mono(azobenzene) **23** comprises a single photoresponsive branch (photochromic building block **21**), bis(azobenzene) **27** consists of two photochromic units (photoresponsive building block **25**) and one non-photoresponsive ethynyl-1,2-diyl building block (**15**).

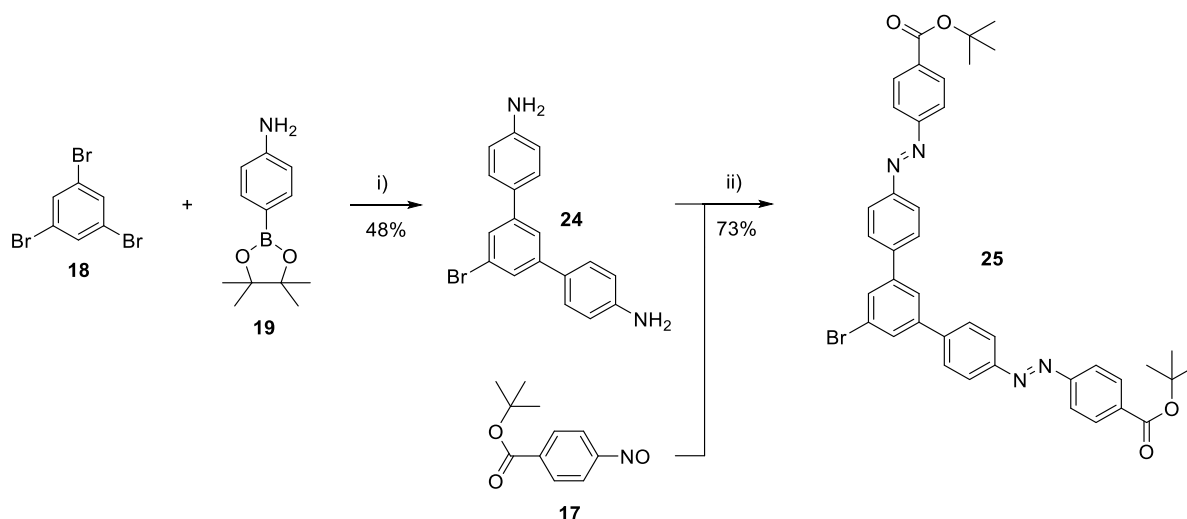


Figure 58. Synthetic pathway for the preparation of bis(azobenzene) photo-switchable building block (**25**). Reagents and conditions: i) $\text{Pd(PPh}_3)_4$, K_2CO_3 , H_2O , toluene, $90\text{ }^\circ\text{C}$; ii) AcOH , RT.

The synthesis of bis(azobenzene) photoresponsive building block (**25**) (Figure 58) starts with the Suzuki-Miyaura cross-coupling reaction between 1,3,5-tribromobenzene (**18**) and 4-aminophenylboronic acid pinacol ester (**19**) in toluene. This time, a larger excess of compound **19** was used (2.5 equivalents) in order to induce the formation of the di-amino derivative **24**. Derivative **24** was isolated as a dark yellow solid in 48% yield. Subsequently, photoresponsive building block **25** was obtained *via* Mills reaction between compound **24** and nitroso derivative **17**, which was freshly prepared. The reaction was performed under the standard Mills conditions affording derivative **25** in 73% yield.

Finally, start-shaped bis(azobenzene) *tert*-butyl ester (**26**) was assembled *via* Suzuki-Miyaura cross-coupling of the photoresponsive building block **25** with the non-photoresponsive building block **15** (Figure 59). As previously mentioned for derivative **22**, K_3PO_4 was employed as a mild base to prevent the cleavage of the *tert*-butyl protecting groups, and the reaction progress was constantly monitored by TLC. The reaction afforded the desired bis(azobenzene) **26** as an orange solid in 83% yield. Finally, the cleavage of *tert*-butyl protecting groups was performed under acidic conditions, using trifluoroacetic acid yielding the target molecule **27** almost quantitatively.

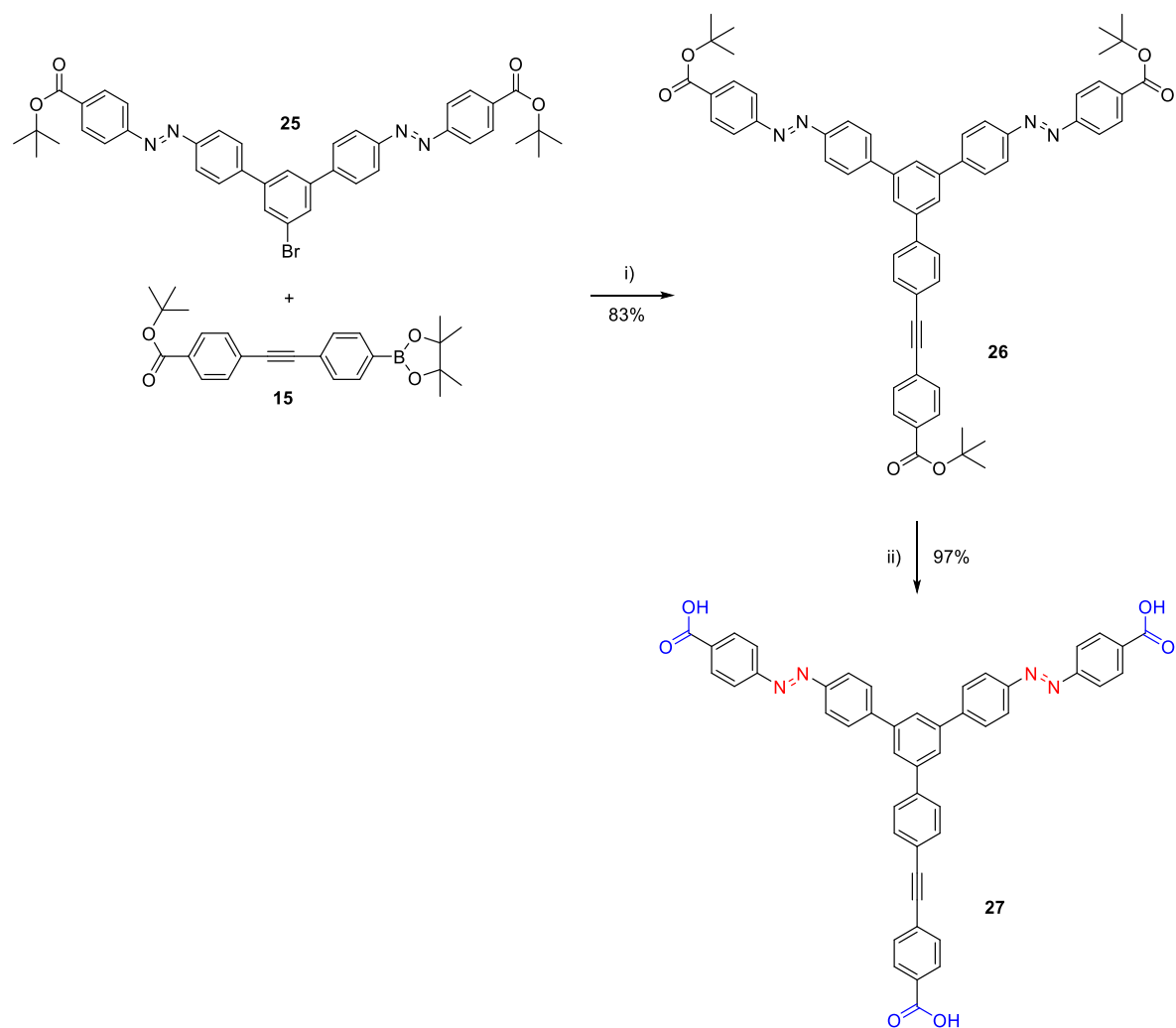


Figure 59. Synthetic strategy used for the preparation of star-shaped bis(azobenzene) **27**. Reagents and conditions: i) Pd(dppf)Cl₂, K₃PO₄, H₂O, dioxane, 90 °C; ii) CH₂Cl₂, TFA, RT.

Star-shaped derivative **10** was designed and synthesized as a reference compound for investigating the self-assembly of star-shaped tris(azobenzene) **3**. Molecule **10** consists of three non-photoresponsive ethynyl-1,2-diyl molecular arms, which are introduced in the position 1,3,5 of a benzene ring to bestow the typical star-shape geometry. The synthetic strategy towards 1,3,5-tris-{4[4''-(carboxyphenyl)ethynyl]phenyl}benzene (**10**) is outlined in Figure 60. Our synthetic approach is based on the assembly of two building blocks **5** and **8** via a Sonogashira type reaction.

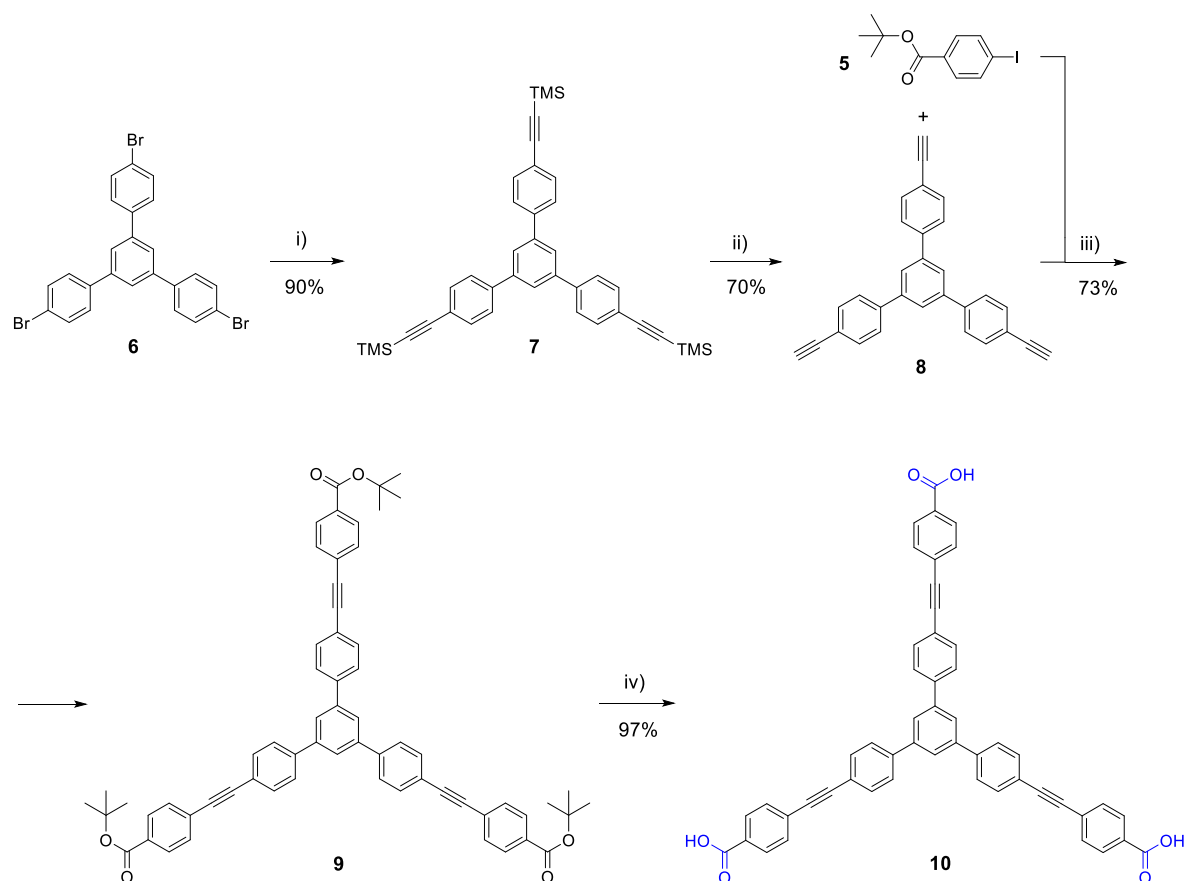


Figure 60. Synthetic strategy towards non-photoresponsive star-shaped derivative **10**. Reagents and conditions: i) ethynyltrimethylsilane, Pd(PPh₃)₂Cl₂, CuI, Et₃N, 65 °C; ii) K₂CO₃, MeOH, THF, RT; iii) Pd(PPh₃)₂Cl₂, CuI, Et₃N, RT; iv) TFA, CH₂Cl₂, RT.

The synthesis of star-shaped molecule **10** begins with a Sonogashira cross-coupling reaction between 1,3,5-tris(4-bromophenyl)benzene (**6**) and trimethylsilylacetylene in large excess. The cross-coupling reaction was performed using triethylamine as a base and solvent in presence of a palladium-catalyst at 65 °C. This temperature is required for the substitution of bromine, which is less reactive than iodine. After standard work up, the desired product **7** was obtained in 90% yield. Compound **7** was then converted to the building block **8** via deprotection of trimethylsilyl groups in basic conditions with K₂CO₃ in a solvent mixture of methanol and tetrahydrofuran in 70% yield. With both building blocks in hands, namely 1,3,5-tris[4'-(ethynyl)phenyl]benzene (**8**) and *tert*-butyl-4-iodobenzoate (**5**) previously prepared 4-iodobenzoic acid (**4**), 1,3,5-tris{4'-(*tert*-butoxycarbonyl)phenylethynyl}phenyl]benzene (**9**) was assembled via Sonogashira cross-coupling reaction. Final hydrolysis of *tert*-butyl ester protecting groups under acidic conditions afforded target molecule **10** as a white solid in 97% yield.

Azobenzene derivative **35** was designed and synthesized as a reference compound employed during the studies of the photochromic behavior of star-shaped azobenzenes **3**, **23** and **27**. The synthetic strategy used for its preparation is displayed below (Figure 61).

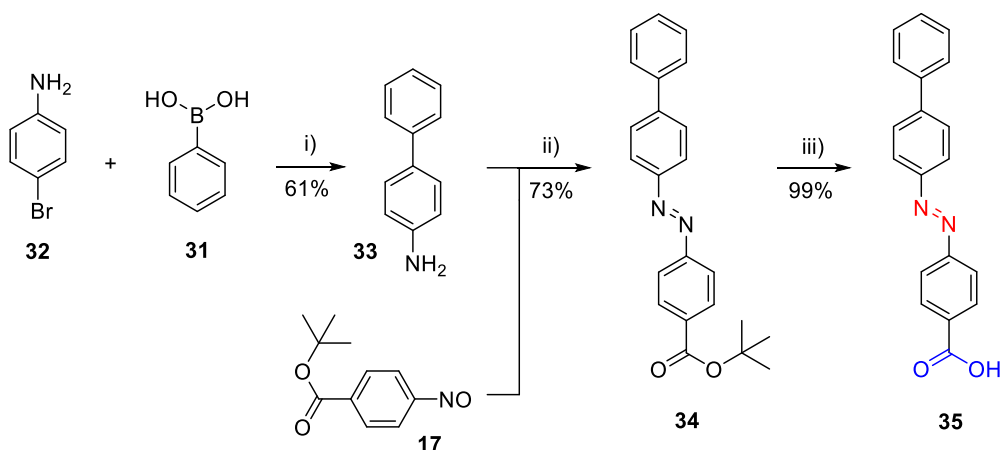


Figure 61. Synthetic strategy towards azobenzene derivative **35**. i) $\text{Pd}(\text{PPh}_3)_4$, K_2CO_3 , H_2O , dioxane, 90°C ; ii) AcOH , RT; iii) CH_2Cl_2 , TFA, RT.

The synthesis of derivative **35** starts with the preparation of 4-aminobiphenyl (**33**) *via* Suzuki-Miyaura reaction using a modified literature procedure reported by Kandathil *et al.*^[251] The cross-coupling reaction between phenylboronic acid (**31**) and 4-bromoaniline (**32**) was performed in dioxane affording derivative **33** in 61% yield. Subsequently, *tert*-butyl ester **34** was obtained *via* Mills reaction of 4-aminobiphenyl (**33**) with *tert*-butyl 4-nitrosobenzoate (**17**), which was freshly prepared, in 73% yield. Finally, acid-catalysed hydrolysis of *tert*-butyl ester **34** with trifluoroacetic acid in dichloromethane provided the desired product (**35**) as an orange solid in almost quantitative yield.

2.1.3 Photophysical and photochemical properties²

The photophysical properties of our photoresponsive derivatives tris(azobenzene) **3**, mono(azobenzene) **23**, bis(azobenzene) **27**, azobenzene **35** and 4-(phenylazo)benzoic acid **79** and their switching in solution have been investigated by absorption spectroscopy. UV/Vis absorption spectra were measured at room temperature with a Jasco V650 spectrophotometer in optical quartz Suprasil Hellma cuvettes (1.0 cm light path) using spectroscopy grade solvents purchased from Merck. Ultraviolet and visible light irradiation was performed with ThorLabs optical fibre-coupled LEDs: for UV light $\lambda_{\text{max}} = 367$ nm, FWHM = 9 nm and for Vis light $\lambda_{\text{max}} = 454$ nm, FWHM = 20 nm. Thorough stirring of the solution, in a closed spectrophotometric cell, was provided during the irradiation experiments using a miniaturized cuvette stirrer (IKA). Photoisomerization in solution of azobenzene

² The experiments have been performed in the group of Prof. P. Samorì at the Institut de Science et d'Ingénierie Supramoléculaires (I.S.I.S.) in Strasbourg, by Dr. A. Galanti, whom are greatly acknowledged.

derivatives **3**, **23**, **27**, **35** and **79** was investigated by absorption spectroscopy in dimethyl sulfoxide (DMSO) (for **3**, **23** and **27** $c = 2.0 \times 10^{-5}$ M, **35** $c = 6.0 \times 10^{-5}$ M, **79** $c = 7.8 \times 10^{-5}$ M) with a slight base excess (NaOH in H₂O, 6.0 eq. for **3**, **23** and **27**, and 2.0 eq. for **35** and **79**). The base was added to ensure the complete solubilisation of the compounds, according to preliminary experiments made on azobenzene **3**. The $E \rightarrow Z$ isomerization quantum yields (LED $\lambda_{\text{irr}} = 367$ nm) were calculated monitoring the decrease of the maximum $\pi-\pi^*$ absorption band of the (*E*)-isomer starting from a non-irradiated solution of the compound. On the other hand, the $Z \rightarrow E$ isomerization quantum yields (LED $\lambda_{\text{irr}} = 454$ nm) were determined monitoring the increase of the maximum $\pi-\pi^*$ absorption band of the (*E*)-isomer starting from the UV photostationary state (PSS). The quantum yields were determined at low conversion by extrapolation at $t = 0$ and taking into account the fraction of light transmitted at the irradiation wavelength. The error estimated is $\pm 10\%$. Furthermore, the UV-induced quantum yield for the $E \rightarrow Z$ isomerization of azobenzene compounds was measured in acetonitrile (CH₃CN) solution in the same experimental conditions to further validate our procedure, and it resulted equal to the values reported in literature ($\Phi \sim 0.14$).

Qualitative absorption spectra of star-shaped azobenzene derivatives **3**, **23** and **27** were measured via high performance liquid chromatography (HPLC) separation (*Accela HPLC*, reverse phase C₁₈ Hypersil GOLD column, 50 x 2.1 mm, 1.9 μm – *Thermo Fischer Scientific*). The elution was done with solvent gradient of 5 – 95% CH₃CN / 95 – 5% H₂O with 0.1% TFA (pH ~ 2) injecting the pre-irradiated DMSO solution of azobenzene to the UV PSS. The separation of all isomers was performed monitoring their UV-Vis absorption spectra using the photodiode array detector, in a range of 200 – 650 nm wavelength. The qualitative absorption spectra obtained for the isomers of compound **3**, **23** and **27** were normalized at their isosbestic point wavelength, which was determined by UV-Vis absorption spectroscopy of the mixture.

UV-Vis absorption spectra were measured for all-(*E*) derivatives tris(azobenzene) **3**, bis(azobenzene) **27**, mono(azobenzene) **23**, derivative **35**, 4-(phenylazo)benzoic acid **79**, and for the non-photoresponsive derivative **10** (Figure 62). UV/Vis absorption spectra of star-shaped azobenzene derivatives **3**, **23** and **27** show the two characteristic absorption bands of azobenzene chromophores. The first absorption band, at higher energy, is related to the $\pi-\pi^*$ transition and the second one, at lower energy, is related to the $n-\pi^*$ transition. All star-shaped derivative **3**, **23** and **27** exhibit maximum absorption at *ca.* 370 nm for the $\pi-\pi^*$ and at *ca.* 455 nm for the $n-\pi^*$.

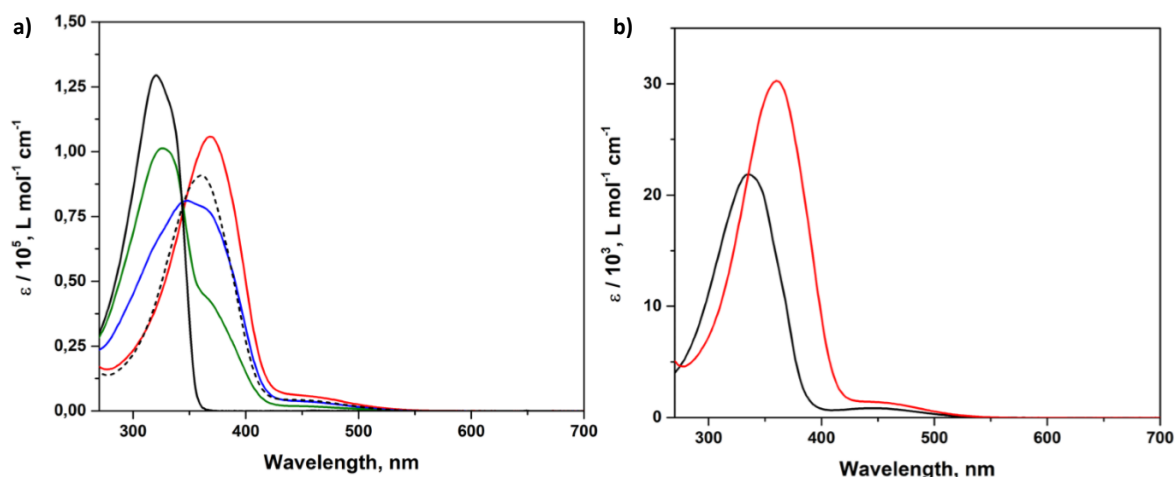


Figure 62. UV/Vis spectra of derivatives **3**, **10**, **23**, **27**, **35** and **79** (in DMSO with slight base excess), without irradiating. a) Comparative absorption spectra of (*E,E,E*)-**3** (full red line), (*E,E*)-**27** (full blue line), (*E*)-**23** (full green line), **10** (full black line), (*E*)-**35** (black dashed line). b) Comparative absorption spectra of (*E*)-**35** (full red line) and (*E*)-**79** (full black line).

Compared with the linear azobenzene **35**, the $\pi\text{-}\pi^*$ transition band results slightly shifted of *ca.* 10 nm (bathochromic shift). Furthermore, a moderate broadening of the bands suggests the presence of a partial conjugation within the system (**3**, **23** and **27**) despite the *meta* substitution. Due to the presence of the 4-(phenylethynyl)-1,1'-biphenyl (PE) chromophoric unit, an additional absorption band in the UV region of the spectrum (*ca.* 320 nm) is observed for mono(azobenzene) **23** and bis(azobenzene) **27**. Despite the existence of a partial conjugation between the switchable arms of **3**, **23** and **27**, ϵ values (Table 1) of the most intense transition of azobenzene and PE units enlighten that the transitions are localized on each chromophoric molecular arm. Moreover, the maxima transitions observed for start-shaped molecule **3**, **23** and **27** remain almost constant. As previously mentioned, azobenzene **35** shows a $\pi\text{-}\pi^*$ transition absorption band at *ca.* 360 nm. This value results largely red-shifted if compared to the one observed for azobenzene (*ca.* 315 nm) and for 4-(phenylazo)benzoic acid **79** (*ca.* 335 nm). Thus, it suggests that the bathochromic effect is related to the additional phenyl ring located in the *para* position with respect to the azobenzene moiety, rather than to the introduction of the azo chromophore in the π -extended **3**, **23** and **27** systems.

	λ_{\max} all-(<i>E</i>) isomer [nm] ($\epsilon / 10^3$ [L mol ⁻¹ cm ⁻¹])			$\Phi_{E \rightarrow Z} (\times 10^2)^a$		$\Phi_{Z \rightarrow E} (\times 10^2)^b$		UV – PSS composition [%] ^c	Vis – PSS composition [%] ^c
	π - π^* PE	π - π^* Azo	n - π^* Azo	Overall ^d	Single Azo ^e	Overall ^d	Single Azo ^e		
3	-	370 (110)	455 (5.7)	3.3	8.8	28	77	55 (Z,Z,Z) 27 (E,Z,Z) 13 (E,E,Z) 5 (E,E,E)	9 (Z,Z,Z) 17 (E,Z,Z) 30 (E,E,Z) 44 (E,E,E)
27	320 (65)	370 (77)	455 (3.7)	4.5	9.5	47	98	61 (Z,Z) 29 (E,Z) 10 (E,E)	13 (Z,Z) 32 (E,Z) 55 (E,E)
23	320 (100)	370 (42)	455 (1.8)	9.1		100		73 (Z) 27 (E)	32 (Z) 68 (E)
10	320 (130)	-	-	-		-			
35	-	360 (30)	455 (1.4)	9.6		88		~ 99 (Z) 1 (E)	
79	-	335 (21)	450 (0.8)	11		70			

^aUV π - π^* irradiation, $\lambda_{\text{irr}} = 367$ nm (FWHM = 9 nm). ^bVis n - π^* irradiation, $\lambda_{\text{irr}} = 454$ nm (FWHM = 20 nm).

^cDetermined by HPLC-MS. ^dOverall isomerisation quantum yield, calculated using the ϵ of the compounds.

^eIsomerisation quantum yield of the single chromophore unit, calculated using the ϵ of mono(azobenzene) compound 4.

Table 1. Photochemical characterization of compounds **3**, **10**, **23**, **27**, **35** and **79** in DMSO (with a slight excess of NaOH) at 298 K.

The photoisomerization of our azobenzene derivatives (**3**, **23**, **27**, **35** and **79**) was investigated *via* UV ($\lambda_{\max} = 367$ nm) and Vis ($\lambda_{\max} = 451$ nm) light irradiation. Upon UV irradiation, their solution in DMSO (with a slight base excess) showed a progressive decrease of the absorption band related with the π - π^* transition together with an increase of the n - π^* transition band (Figure 63 and 64), which are the typical spectral variation observed for $E \rightarrow Z$ azobenzene photoisomerization.

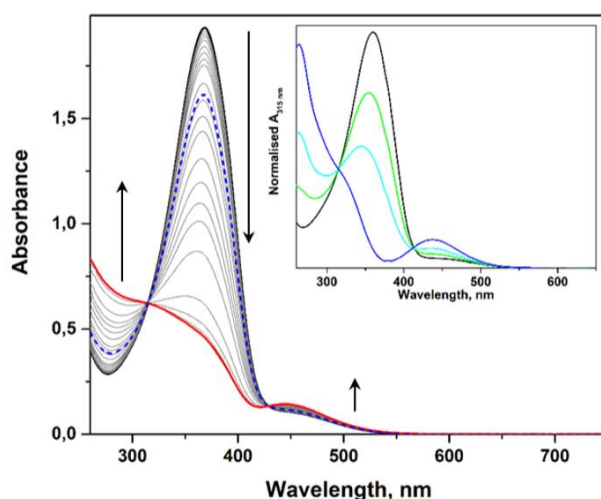


Figure 63. UV-Vis spectral variation of star-shaped tris(azobenzene) **3** upon UV irradiation: *full black line* for the non-irradiated solution, *full red line* for UV PSS and *blue dotted line* for Vis PSS. Inset, absorption spectra of the single isomers of **3** recorded by HPLC separation: *black line* (E,E,E)-**3**, *green line* (E,E,Z)-**3**, *light blue line* (E,Z,Z)-**3** and *dark blue line* (Z,Z,Z)-**3**.

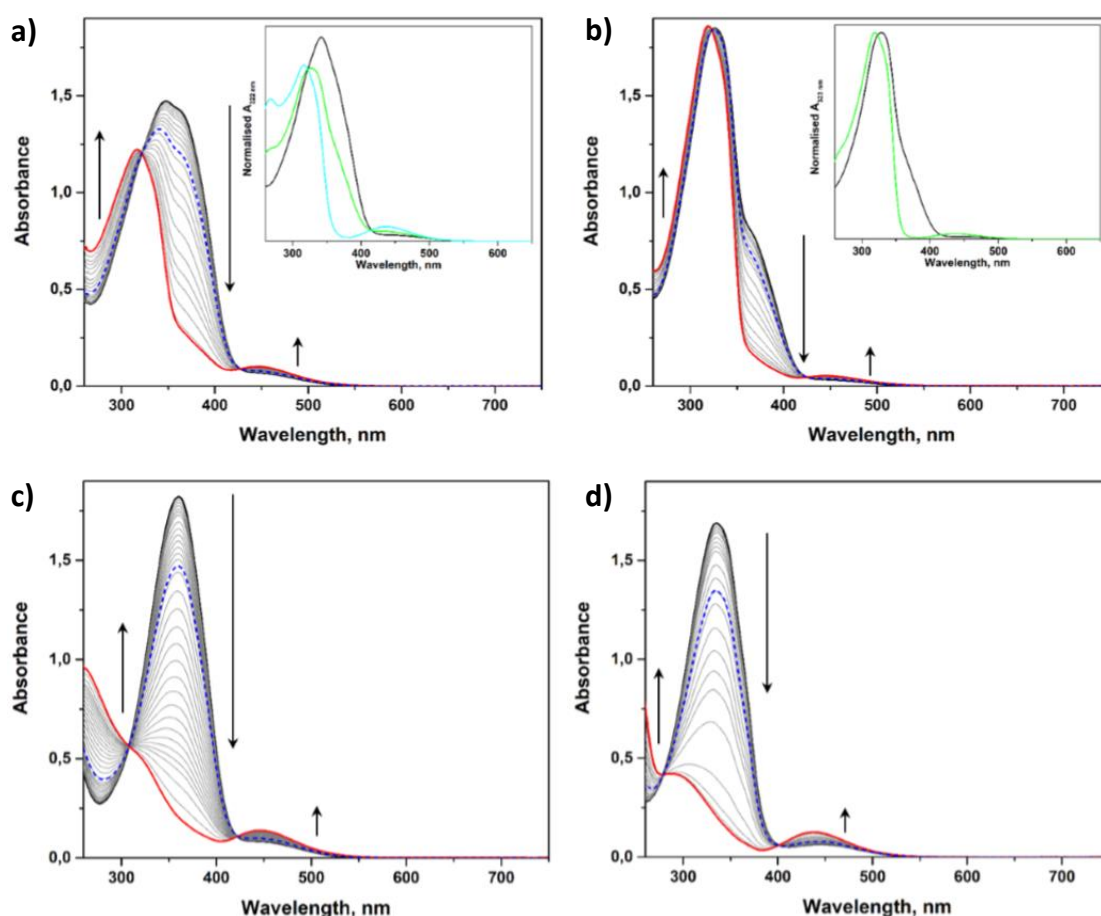


Figure 64. UV-Vis spectral variation of derivatives **23**, **27**, **35** and **79** upon UV irradiation: *full black line* for the non-irradiated solution, *full red line* for UV PSS and *blue dotted line* for Vis PSS. a) star-shaped bis(azobenzene) **27**, inset: *black line* (*E,E*)-**27**, *green line* (*E,Z*)-**27**, *light blue line* (*Z,Z*)-**27**; b) star-shaped mono(azobenzene) **23**, inset: *black line* (*E*)-**23**, *green line* (*Z*)-**23**; c) azobenzene **35**; d) 4-(phenylazo)benzoic acid **79**.

The decrease of (*E*)-isomers concentration is accompanied by a consequent increase of the (*Z*)-isomers concentration until the photostationary state is reached (UV – PSS). Performing the back isomerization *via* Vis light irradiation, the initial absorption spectra recorded for the all (*E*)-isomers were recovered only partially reaching another photostationary state (Vis – PSS). On the other hand, complete recovery was obtained only by storing the irradiated solution in the dark for several days. The presence of clear isosbestic points all over both *E* → *Z* and *Z* → *E*, especially for star-shaped tris(azobenzene) **3** and bis(azobenzene) **27**, confirms the absence of inter-chromophore interactions. Due to the different molecular dipole moment between the *E* and *Z* isomers of azobenzene, it was possible to characterize the composition of UV – and Vis – PSS by means of HPLC and all the isomers of derivatives **3**, **23** and **27** were isolated. The qualitative absorption spectra obtained for all the isomeric forms of azobenzenes **3**, **27** and **23** separated by HPLC are depicted in Figure 63 (inset) and Figure 64 (a-b, insets). The spectra were obtained with the photodiode array spectrophotometer integrated in the HPLC setup and were normalized at the isosbestic point measured by UV-Vis (315 nm for compound **3**, 321 nm for compound **27** and 322 nm for compound **23**).

The qualitative absorption spectra obtained result comparable with the simulated spectra by TD-DFT (Figure 65, calculation performed by Dr. V. Diez-Cabanes, Université de Mons).

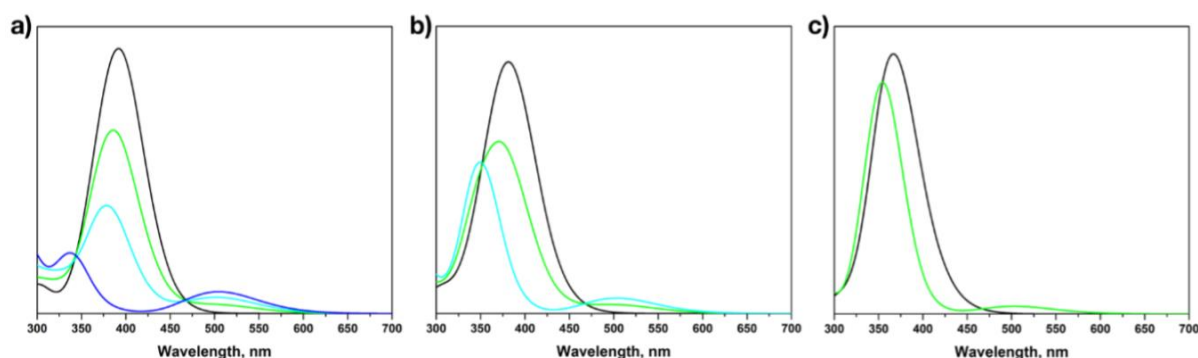


Figure 65. UV-Vis absorption spectra of azobenzenes **3**, **23** and **27** calculated by TD-DFT. a) Tris(azobenzene) **3**, black line for (E,E,E)-**3**, green line for (E,E,Z)-**3**, light blue line for (E,Z,Z)-**3** and dark blue line for (Z,Z,Z)-**3**. b) Bis(azobenzene) **27**, black line for (E,E)-**27**, green line (E,Z)-**27** and light blue line for (Z,Z)-**27**. c) Mono(azobenzene) **23**, black line for (E)-**23** and green line for (Z)-**23**.

The quantification of the photostationary states composition was accomplished using an HPLC-MS set-up (Table 1, Figure 66-67). The mass spectrometer used for the detection employed an electrospray ionization (ESI) source and the measurements were performed in negative mode, in order to detect the signal of the anions generated after deprotonation of the carboxylic groups present in molecules **3**, **23**, **27** and **35**.

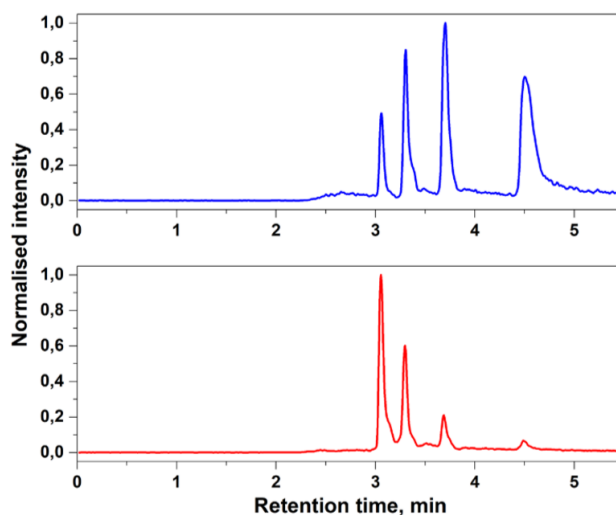


Figure 66. Isomeric composition of UV – PSS (red line) and Vis – PSS (blue line) for tris(azobenzene) **3** obtained by HPLC-MS. Chromatograms integrated at $[M-H]^+$ $m/z = 749.2$. Peak at 3 min 5 s retention time corresponds to (Z,Z,Z)-**3**, 3 min 20 s (Z,Z,E)-**3**, 3 min 40 s (Z,E,E)-**3** and 4 min 30 s (E,E,E)-**3**.

For both tris(azobenzene) **3** and bis(azobenzene) **27** a (Z)-rich UV – PSS of 95% and 90% overall Z content for **3** and **27** respectively was reached, while for mono(azobenzene) **23** the UV – PSS contains *ca.* 70% of (Z)-isomer. On the other hand, upon UV irradiation of the linear azobenzene **35** the isomerization was quantitative with *ca.* 90% of (Z)-isomer.

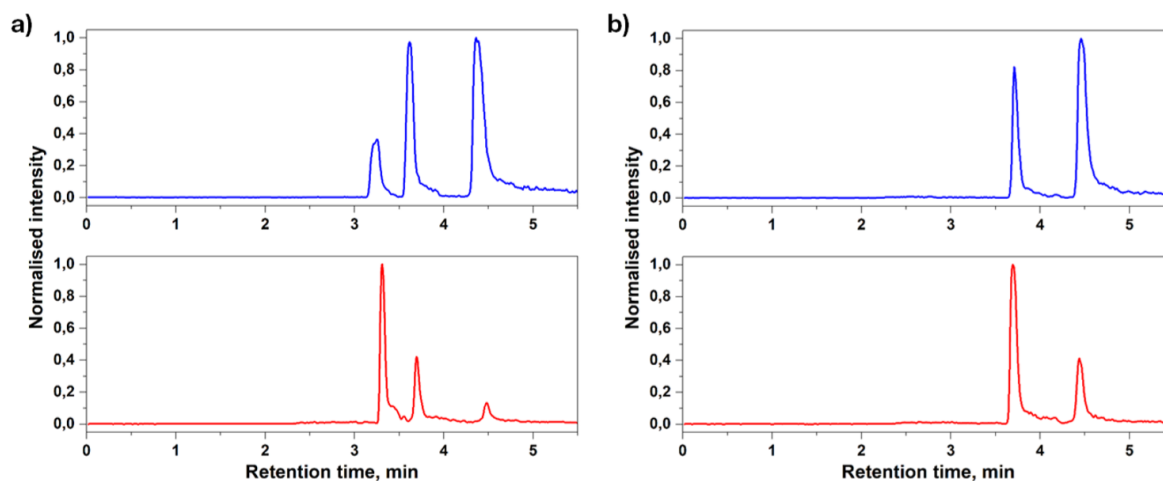


Figure 67. Isomeric composition of UV – PSS (red line) and Vis – PSS (blue line) determined by HPLC-MS. a) Bis(azobenzene) **27**, chromatograms integrated at $[M-H^+]$ $m/z = 745.2$. Peak at 3min 20 s retention time corresponds to (Z,Z)-**27**, 3 min 40 s (Z,E)-**27**, 4 min 30 s (Z,Z)-**27**. b) Mono(azobenzene) **23**, chromatograms integrated at $[M-H^+]$ $m/z = 741.2$. Peak at 3min 40 s retention time corresponds to (Z)-**23**, 4 min 30 s (E)-**23**.

The isomerization quantum yields (Φ) were employed to evaluate the $E \rightarrow Z$ and $Z \rightarrow E$ photoreaction efficiency. The variation in concentration of the all-(E)-isomer over the irradiation time by UV-Vis absorption spectroscopy was used to determine the photoisomerization quantum yields. The quantum yield values indicated as *overall* Φ in Table 1 were calculated using the ϵ of each azobenzene derivative, thus they refer to all the azobenzene units within each molecular scaffold. On the other hand, the *single Azo* Φ values were calculated using the ϵ of the mono(azobenzene) **23** “molecular-arm” and give a comparative estimation over the isomerization quantum yield of the single photochrome.^[252] Hence, ϵ of a different compound was used to calculate the photoreaction quantum yields and this procedure was particularly suitable for star-shaped derivatives **3**, **27** and **23** following the additivity of the ϵ values of each photochrome (Table 1). However, it is possible to obtain similar results by dividing the ϵ of the azobenzene chromophore by the number of azobenzene units contained in each molecule (for instance, dividing by three and by two the ϵ values of azobenzene **3** and **27** respectively). Since it is known that the conjugation within the molecule dramatically decreases the photoreaction efficiency,^[240] *single Azo* Φ values of star-shaped azobenzenes **3**, **23** and **27** were compared to the values calculated for linear azobenzene derivatives. The simple azobenzene shows $E \rightarrow Z$ isomerization quantum yield (Φ) of *ca.* 0.14 – 0.15 in polar solvents ($\lambda_{irr} = 345$ nm).^[240,253] For 4-(phenylazo)benzoic acid **79** the value is slightly lower ($\Phi \approx 0.11$), and it might be due to the presence of the electron-withdrawing carboxylic group that is in the *para* position to the chromophore.^[252]

The introduction of an additional phenyl ring in derivative **35** induces an almost negligible decrease of isomerization efficiency ($\Phi \approx 0.10$). Interestingly, mono(azobenzene) **23** shows $\Phi \approx 0.09$ and both bis(azobenzene) **27** and tris(azobenzene) **3** exhibit the same *single Azo* Φ value. On the other hand, quantum yields values resulted even higher than simple azobenzene ($\Phi \approx 0.63$, $\lambda_{\text{irr}} = 436 \text{ nm}$)^[254] for the $Z \rightarrow E$ back isomerization. The results obtained demonstrate that the introduction of multiple azobenzene chromophores into aromatic and partially π -conjugated rigid scaffold such as tris(azobenzene) **3**, bis(azobenzene) **27** and mono(azobenzene) **23** does not affect drastically the photoreactivity of the system. According to literature, the electronic disconnection within the structure is further ensured by the *meta* substitution pattern of the chromophores on the benzene ring in our series of star-shaped azobenzenes. Furthermore, a test over ten photoswitching cycles was performed to demonstrate the photochemical robustness of tris(azobenzene) **3** (Figure 68) and a very slight degeneration of its photochromic activity was observed.

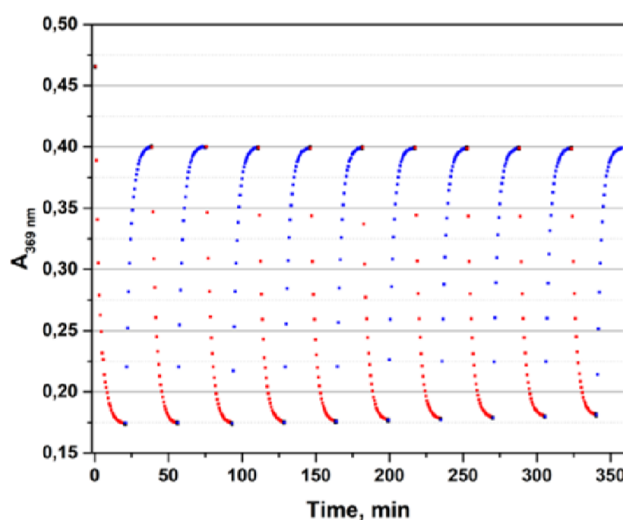


Figure 68. UV – Vis spectral variation of tris(azobenzene) **3** upon multiple irradiation cycles. Plot of the absorbance variation over time observed at λ_{max} for π - π^* transition band of **3** (DMSO solution, $c = 5.0 \times 10^{-6} \text{ M}$) upon irradiation with UV light (*red squares*, $P_d \approx 1.5 \text{ mW cm}^{-2}$) and Vis light (*blue squares*, $P_d \approx 1.5 \text{ mW cm}^{-2}$).

2.1.4 Electrochemistry³

The redox properties of azobenzene have been widely studied, and a general agreement on the mechanism of its electrochemical reduction in aprotic media such as *N,N*-dimethylformamide (DMF) consisting of two consecutive one-electron processes has been reported.^[255,256] The well-known redox behaviour of azobenzene allowed to successfully employ cyclic voltammetry to obtain a qualitative insight into the π -conjugation of our multi-azobenzene systems by focussing on their first reduction. However, the presence of carboxylic groups at the azobenzene termini, which are not inert from the electrochemical point of view, complicated the interpretation of the experimental data obtained. It is known that the carboxylic substituents, indeed, undergo reduction in the potential range of our interest.^[257] Nevertheless, taking into account that the redox potential for the reduction of aromatic hydrocarbons occurs at more negative values than the range observed during our experiments, we assume that it is possible to safely exclude the reduction of the aromatic backbone of derivatives **3**, **10**, **23**, **27** and **35** to happen in the potential range used during the experiments.

Herein, the electrochemical properties of tris(azobenzene) **3**, bis(azobenzene) **27**, mono(azobenzene) **23**, non-switchable derivative **10**, linear azobenzenes **35** and **79** have been investigated, using azobenzene as reference, in anhydrous DMF (purchased from *Sigma Aldrich*) using tetra-*n*-butylammonium hexafluorophosphate ($c = 0.1$ M, from *Fluka*) as supporting electrolyte in a comparative fashion by means of cyclic voltammetry (CV) and differential pulse voltammetry (DPV) (Figure 69-71). All the potentials reported in the present work are referred to the ferrocene redox potential (Fc, *Sigma Aldrich*), which was added to the solution as internal standard ($c = 0.25$ mM). A conventional three-electrodes cell with a silver wire as the pseudoreference electrode, a 2 mm platinum disk working electrode and a platinum wire counter electrode (*CH Instruments*) were used for the experiments. Voltammetric experiments were performed using a *PGSTAT204* potentiostat/galvanostat controlled with *NOVA* software (Metrohm). All the experiments were performed at room temperature (RT). In all cases, the cyclic voltammograms of aforementioned compounds ($c = 1$ mM) exhibit a peculiar behaviour, which was assigned to the subsequent reduction of the carboxylic function and the diazene moiety (when present). To better clarify the complicate process, DPV was employed. This technique allows to distinguish the multiple processes that take place in such narrow potential range and to estimate more precisely the redox potential of sluggish electrode reactions that show broad peaks in cyclic voltammetry. All the potential reported in this work have been determined at the peaks of DPV experiments.

³ The experiments have been performed in the group of Prof. P. Samorì at the Institut de Science et d'Ingénierie Supramoléculaires (I.S.I.S.) in Strasbourg, by Dr. A. Galanti, whom are greatly acknowledged.

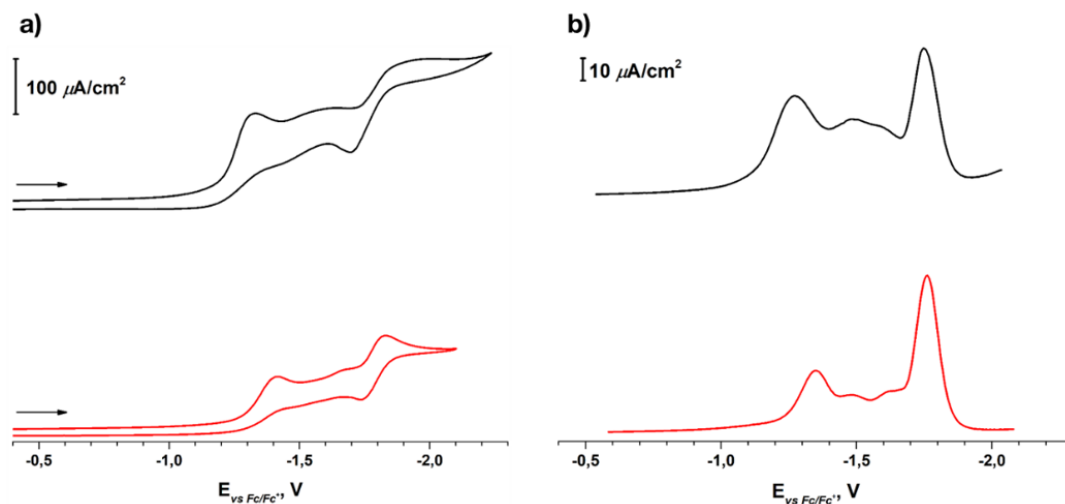


Figure 69. Electrochemical experiments performed on tris(azobenzene) **3** (black line) and linear azobenzene **35** (red line) derivatives, $c = 1$ mM in Ar-purged anhydrous DMF, in presence of $n\text{Bu}_4\text{NPF}_6$ ($c = 0.1$ M). a) Cyclic voltammetry (CV), scan speed: 50 mV s^{-1} ; b) Differential pulse voltammetry (DPV), pulse amplitude: 25 mV , scan speed: 10 mV s^{-1} , modulation time: 50 ms .

The results obtained for derivatives **3**, **10**, **23**, **27** and **35** were compared with 4-(phenylazo)benzoic acid **79** and azobenzene voltammograms (Figure 71) in the same experimental conditions to correctly assign the redox processes observed.

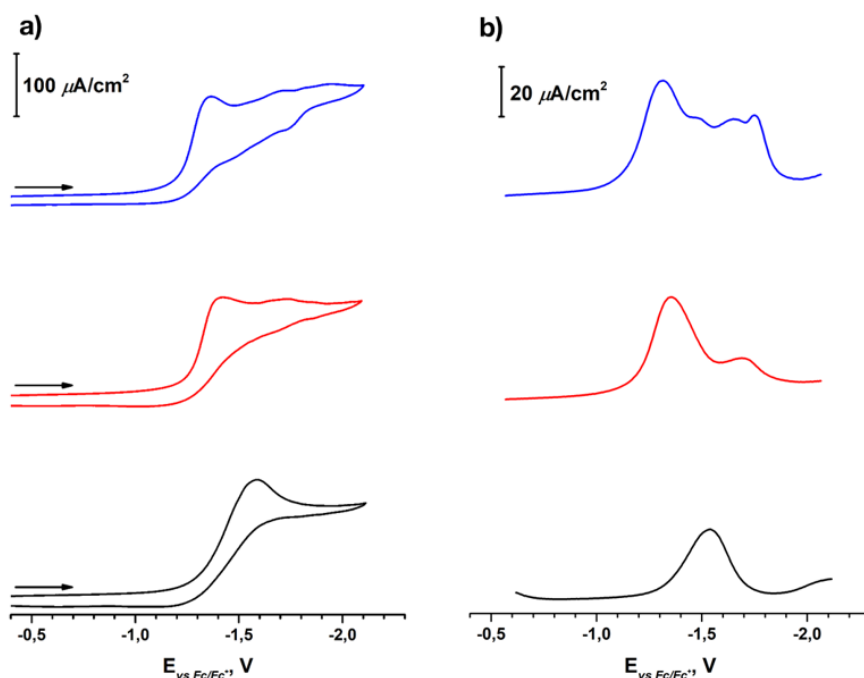


Figure 70. Electrochemical experiments on star-shaped bis(azobenzene) **27** (blue line), mono(azobenzene) **23** (red line) and the non-photochromic **10** (black line) derivatives, $c = 1$ mM in Ar-purged anhydrous DMF, in presence of $n\text{Bu}_4\text{NPF}_6$ ($c = 0.1$ M). a) Cyclic voltammetry, scan speed: 50 mV/s . b) Differential pulse voltammetry, pulse amplitude: 25 mV ; scan rate: 10 mV/s ; modulation time: 50 ms .

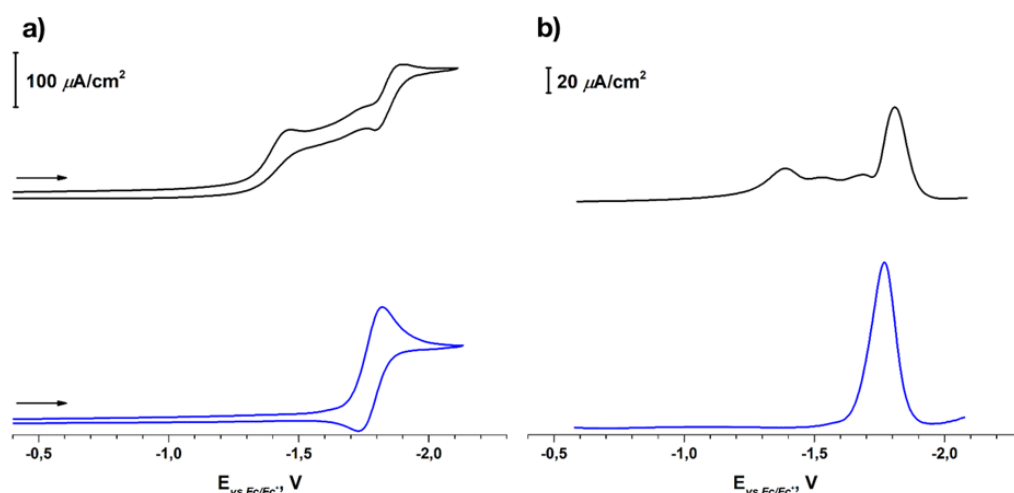


Figure 71. Electrochemical experiments on reference compounds 4-(phenylazo)benzoic acid **79** (black line) and azobenzene (blue line), $c = 1$ mM in Ar-purged anhydrous DMF, in presence of $n\text{Bu}_4\text{NPF}_6$ ($c = 0.1$ M). a) Cyclic voltammetry, scan speed: 50 mV/s. b) Differential pulse voltammetry, pulse amplitude: 25 mV; scan rate: 10 mV/s; modulation time: 50 ms.

Cyclic voltammograms of derivatives **3**, **10**, **23**, **27**, **35** and **79** show a first irreversible wave with a cathodic peak located between -1.3 and -1.5 V. For tris(azobenzene) **3** and the linear azobenzenes **35** and **79**, a second quasi-reversible process was observed at a spacing of *ca.* -0.4 V from the first wave. In between these two peaks, additional broad signals related to the redox behaviour of the carboxylic units appeared, and thus were not considered for our investigations. According to the literature, azobenzene displays a quasi-reversible reduction peak at -1.77 V with a spacing between the cathodic and the anodic peaks (ΔE_p) of 70 mV. Azobenzene voltammogram was compared to the results obtained for azobenzene **79**, which differs from the former for the presence of a carboxylic group on one phenyl ring. Interestingly, the voltammogram of **79** presents two main reduction events: the first irreversible process at higher potential and a quasi-reversible reduction at -1.81 V ($\Delta E_p = 70$ mV from CV). Hence, the first irreversible reduction event was assigned to the reduction of the carboxylic moiety, whereas the second quasi-reversible process was ascribed to the azobenzene unit reduction. This hypothesis was further confirmed electrochemical behaviour of the non-photoresponsive star-shaped derivative **10**, which only displays the irreversible process at *ca.* -1.5 V relative to the reduction of the carboxylic groups. Azobenzene **35** showed analogous behaviour to azobenzene **79** with the reduction of the azobenzene moiety occurring at -1.76 V ($\Delta E_p = 80$ mV from CV). The lower reduction energy observed for **35** is coherent with the extension of the π -conjugation core and the slight broadening indicates a slight lower reversibility. Particularly interesting was found the electrochemical behaviour of tris(azobenzene) **3**, which was substantially analogous to **35** and **79** except for its broader character (Figure 69, $\Delta E_p > 150$ mV from CV). Furthermore, DPV shows only one peak for the reduction of the azobenzene unit at -1.75 V, and this potential value is comparable to the one observed for linear azobenzene **35**. This evidence together with the absence of any splitting in the electrochemical process further confirms the electronic decoupling between the photochromic

azobenzene units in our star-shaped series. For bis(azobenzene) **27** and mono(azobenzene) **23** star-shaped compounds broad CV curves were observed and in which the redox behaviour of the azobenzene units is shadowed by the irreversible reduction of the carboxylic groups (Figure 70). However, DPV technique allowed the identification of the reduction peaks of the azobenzene moiety on bis(azobenzene) **27** at -1.75 V, which is a potential value analogous to the values observed for **3** and **35**.

2.1.5 Kinetical study of $E \rightarrow Z$ thermal isomerization⁴

The $Z \rightarrow E$ thermal isomerization of tris(azobenzene) **3**, bis(azobenzene) **27**, mono(azobenzene) **23** and azobenzene **35** was monitored by HPLC in order to determine the ratios of each isomeric form starting from the UV – PSS over time. The linear azobenzene **35** was employed as reference compound. A Shimadzu LC-20AD HPLC set-up equipped with a photodiode array UV/Vis detector (Shimadzu SPD-M20A VP, $\lambda = 200 - 600$ nm), a column oven Shimadzu CTO-20AC and a reverse phase column BDS HUPERSIL C18 (5 μ m, 250 x 3 mm) Thermo Scientific were used for the experiments. The elution was performed with solvent gradients of 70 – 90% CH₃CN (+ 0.1% v/v formic acid, HCOOH) / 30 – 10% H₂O (+ 0.1% v/v HCOOH). Irradiation of the samples at 365 nm was performed on a Polychrome V device. All solutions were prepared and measured under air saturated conditions. For each azobenzene derivative, a solution in CH₃CN/DMSO was prepared. The sample was stirred and irradiated at 365 nm for 30 min with an 8 W UV lamp, filtered by a monochromator with a spectral transmission band of 2 nm. Thereafter, the isomer distribution over time was monitored upon periodical injection of the solution (10 μ L aliquots) into the HPLC kept at four different temperature (25, 30, 35 and 40 °C).

After irradiating at 365 nm azobenzenes **3**, **23**, **27** and **35** for 30 min, their $Z \rightarrow E$ thermal isomerization reaction was monitored by HPLC at four different temperatures (25, 30, 35 and 40 °C). All four isomers for **3** ((Z,Z,Z)-**3**, (E,Z,Z)-**3**, (E,E,Z)-**3**, (E,E,E)-**3**), all three isomers for **27** ((Z,Z)-**27**, (E,Z)-**27**, (E,E)-**27**) and two isomers for **23** ((Z)-**23**, (E)-**23**) and **35** ((Z)-**35**, (E)-**35**) were observed. Ratios of all isomers were determined integrating the chromatograms of **3**, **23** and **27** at the wavelength of their isosbestic points measured by UV-Vis absorption spectroscopy of the mixture. (Z,Z,Z)-Tris(azobenzene) **3** was converted to (E,E,E)-**3** via (Z,Z,E)-**3** and (Z,E,E)-**3** by thermal isomerization and the transformation was monitored by HPLC (Figure 72). The evolution curves are in agreement with an exponential decay of the first-order for (Z,Z,Z)-**3** and with an exponential decay of the second-order for the (E,Z,Z), (E,E,Z) and (E,E,E) isomers.^[258] The experimental data nicely fit also for bis(azobenzene) **27**, mono(azobenzene) **23** and linear azobenzene **35** (Figure 73-75).

⁴ Experiments performed by R. Mannancherry, Prof. M. Mayor group (Basel Universität), whom is greatly acknowledged.

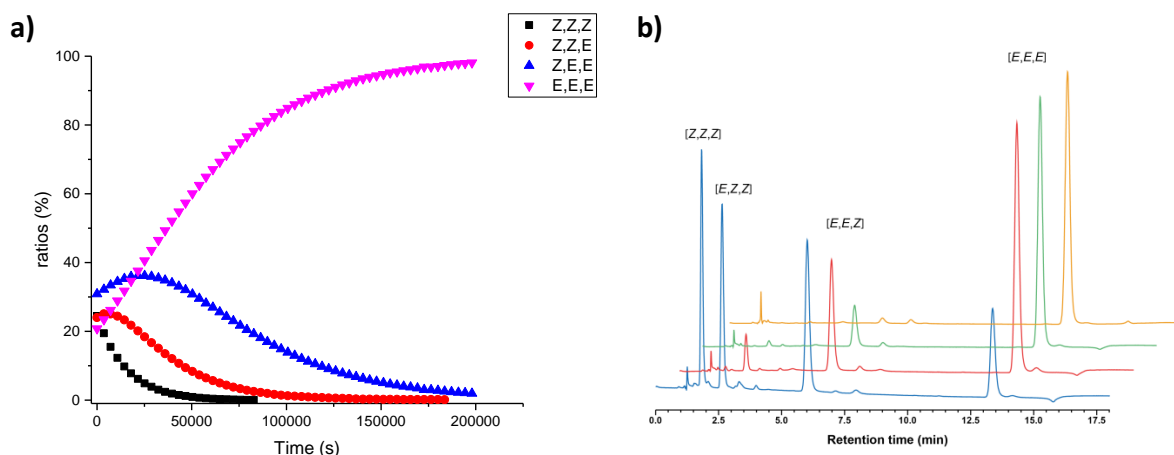


Figure 72. a) Time profile at 40 °C for the thermal $Z \rightarrow E$ isomerization of **3** starting from the UV – PSS obtained upon irradiation at 365 nm, monitored by HPLC integrating the UV absorption at 290 nm (isosbestic point): (Z,Z,Z)-**3** (black squares), (E,Z,Z)-**3** (red dots), (E,E,Z)-**3** (blue triangles), (E,E,E)-**3** (pink triangles). b) Chromatograms of **3** recorded upon heating at 40 °C: blue line recorded after 30 min irradiation (PSS), the red line recorded after 17 h, the green line recorded after 29 h, the orange line recorded after 55 h.

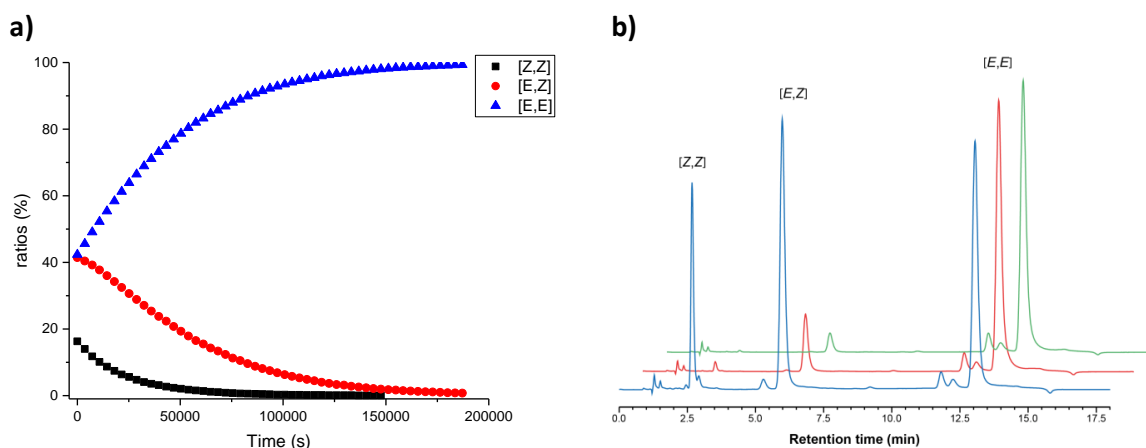


Figure 73. a) Time profile at 40 °C for the thermal $Z \rightarrow E$ isomerization of **27** starting from the UV – PSS obtained upon irradiation at 365 nm, monitored by HPLC integrating the UV absorption at 280 nm (isosbestic point): (Z,Z)-**27** (black squares), (E,Z)-**27** (red dots), (E,E)-**27** (blue triangles). b) Chromatograms of **27** recorded upon heating at 40 °C: blue line recorded after 30 min irradiation (PSS), the red line recorded after 17 h, the green line recorded after 29 h.

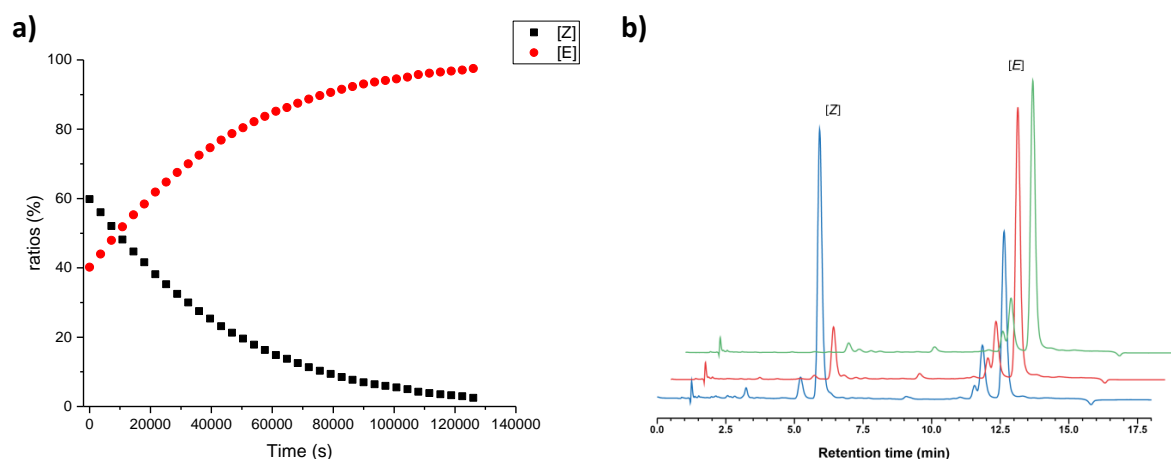


Figure 74. a) Time profile at 40 °C for the thermal $Z \rightarrow E$ isomerization of **23** starting from the UV – PSS obtained upon irradiation at 365 nm, monitored by HPLC integrating the UV absorption at 265 nm (isosbestic point): (Z)-**23** (black squares), (E)-**23** (red dots). b) Chromatograms of **23** recorded upon heating at 40 °C: blue line recorded after 30 min irradiation (PSS), the red line recorded after 17 h, the green line recorded after 36 h.

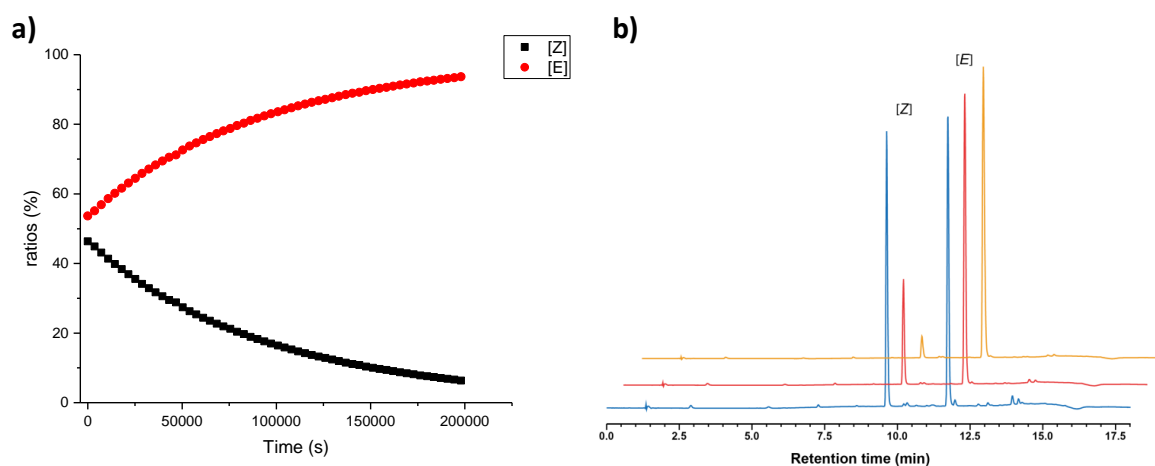
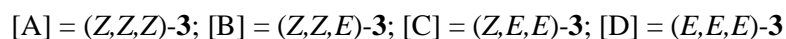


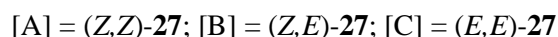
Figure 75. a) Time profile at 40 °C for the thermal $Z \rightarrow E$ isomerization of **35** starting from the UV – PSS obtained upon irradiation at 365 nm, monitored by HPLC integrating the UV absorption at 285 nm (isosbestic point): (Z)-**35** (black squares), (E)-**35** (red dots). b) Chromatograms of **35** recorded upon heating at 40 °C: blue line recorded after 30 min irradiation (PSS), the red line recorded after 17 h, the orange line recorded after 55 h.

Compounds comprising multiple azobenzene moieties undergo back isomerization from the all-(*Z*) to the all-(*E*) isomer *via* the mixed intermediate isomeric forms. The isomerization could be treated as a consecutive and irreversible reaction that involves one first-order reaction and subsequent second-order reactions.^[258]

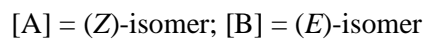
For star-shaped tris(azobenzene) **3**:



For star-shaped bis(azobenzene) **27**:



For star-shaped mono(azobenzene) **23** and azobenzene **35**:



The first isomerization process $[A] \rightarrow [B]$ can be described as a first-order reaction (Equation 2.2), whereas the subsequent isomerizations $[B] \rightarrow [C]$ and $[C] \rightarrow [D]$ can be described as second-order reactions (Equation 2.3 and 2.4).



$$[A] = [A]_0 e^{-k_1 t} \quad (2.2)$$

$$[B] = \frac{[A]_0 k_1}{k_2 - k_1} [e^{-k_1 t} - e^{-k_2 t}] + [B]_0 e^{-k_2 t} \quad (2.3)$$

$$[C] = [A]_0 k_1 k_2 \left[\frac{e^{-k_1 t}}{(k_2 - k_1)(k_3 - k_1)} - \frac{e^{-k_2 t}}{(k_2 - k_1)(k_3 - k_2)} + \frac{e^{-k_3 t}}{(k_3 - k_1)(k_3 - k_2)} \right] + \frac{[B]_0 k_2}{k_3 - k_2} [e^{-k_2 t} - e^{-k_3 t}] + [C]_0 e^{-k_3 t} \quad (2.4)$$

Where k_1 , k_2 and k_3 are the isomerization rates, $[A]_0$, $[B]_0$, $[C]_0$ and $[D]_0$ are the initial concentrations, and t is the time. Free Gibbs energy of isomerization $\Delta G_{n(T)}^\ddagger$ was calculated from the $k_{n=1,2,3}$ values by rearranging the Eyring equation:

$$\Delta G_{n(T)}^\ddagger = -RT \ln \left(\frac{h k_n}{k_B T} \right) \quad (2.5)$$

Where k_n is the obtained kinetic rate constant, k_B is the Boltzmann constant ($k_B = 1.380662 \times 10^{-23} \text{ J K}^{-1}$), h the Planck's constant ($h = 6.626176 \times 10^{-34} \text{ J s}$), R the universal gas constant ($R = 8.31446 \text{ J K}^{-1} \text{ mol}^{-1}$) and T the temperature. Furthermore, using the Eyring equation:

$$k_n = \frac{k_B T}{h} e^{-\frac{\Delta G_n^\ddagger}{RT}} \quad (2.6)$$

And substituting ΔG_n^\ddagger with

$$\Delta G_{n(T)}^\ddagger = \Delta H_n^\ddagger - T\Delta S_n^\ddagger \quad (2.7)$$

Gives:

$$k_n = \frac{k_B T}{h} e^{\frac{-\Delta H_n^\ddagger + T\Delta S_n^\ddagger}{RT}} \quad (2.8)$$

Which can be brought to a linear form:

$$\ln\left(\frac{k_n}{T}\right) = -\left(\frac{\Delta H_n^\ddagger}{R}\right)\left(\frac{1}{T}\right) + \frac{\Delta S_n^\ddagger}{R} + \ln\left(\frac{k_B}{h}\right) \quad (2.9)$$

This equation states that plotting $\ln\left(\frac{k_n}{T}\right)$ vs. $\frac{1}{T}$ yield a straight line with slope $= -\left(\frac{\Delta H_n^\ddagger}{R}\right)$ and an intersect of $= \frac{\Delta S_n^\ddagger}{R} + \ln\left(\frac{k_B}{h}\right)$.

Finally, with the Arrhenius equation $k_n = Ae^{-\frac{E_{an}}{RT}}$ it is possible to plot $\ln(k_n)$ against $\frac{1}{T}$ to get the activation energy:

$$\ln(k_n) = -\left(\frac{E_{an}}{R}\right)\left(\frac{1}{T}\right) + \ln(A) \quad (2.10)$$

Detailed experimental data can be found in Appendix I. Thanks to such evidences, we were able to demonstrate that for our star-shaped tris(azobenzene) **3** the thermal back isomerization follows the expected pseudo first-order cascade reaction: $(Z,Z,Z)\text{-}\mathbf{3} \rightarrow (E,Z,Z)\text{-}\mathbf{3} \rightarrow (E,E,Z)\text{-}\mathbf{3} \rightarrow (E,E,E)\text{-}\mathbf{3}$, and bis(azobenzene) **27**: $(Z,Z)\text{-}\mathbf{27} \rightarrow (E,Z)\text{-}\mathbf{27} \rightarrow (E,E)\text{-}\mathbf{27}$ shows analogous behaviour. Furthermore, it is worth considering the statistical character of the first isomerization reaction, since the first isomerization can take place on the three equivalent azobenzene units for molecule **3** and on two equivalents azobenzene units for molecule **27**. In our specific case, the normalized rate constant $|k_1|$ for the $(Z,Z,Z)\text{-}\mathbf{3} \rightarrow (E,Z,Z)\text{-}\mathbf{3}$ isomerization reaction was divided by three, while the normalized rate constant $|k_2|$ for $(E,Z,Z)\text{-}\mathbf{3} \rightarrow (E,E,Z)\text{-}\mathbf{3}$ and $(Z,Z)\text{-}\mathbf{27} \rightarrow (E,Z)\text{-}\mathbf{27}$ isomerizations was divided by two. Moreover, the $Z \rightarrow E$ thermal isomerization constants result analogous for tris(azobenzene) **3** and bis(azobenzene) **27** confirming that the azobenzene chromophores do not influence one another, being thus electrochemically and geometrically decoupled. Analysis of the activation energy parameters for the $Z \rightarrow E$ thermal isomerization obtained under dark show that for multi(azobenzene) **3** and **27** the azobenzene units exhibit the same kinetic behaviour, whereas for star-shaped mono(azobenzene) **23** a small negligible decrease of the free activation energy is observed. On the other hand, for reference azobenzene **35** the thermal back isomerization results slightly faster, compared to the star shaped derivatives. It is also interesting to note the weak lowering effect on the activation energy by the carboxylic group. The latter is indeed a mild electron-withdrawing groups if compared to stronger electron accepting groups such as nitro ($-\text{NO}_2$) or cyano ($-\text{CN}$), which are known to significantly decrease the thermal isomerization activation energy.^[259]

2.1.5 Ion mobility – mass spectrometry (IMMS)⁵

Ion mobility – mass spectrometry (IMMS) was employed to study the shape alterations resulting from the $E \rightarrow Z$ isomerization of star-shaped azobenzene **3**. A hybrid quadrupole (Q) – traveling wave (T-wave) ion mobility (TWIMMS)-time-of-flight (TOF) mass spectrometer (*Synapt G2-Si, Waters, U.K.*) equipped with an electrospray ionization (ESI) source (negative mode) was used for the measurements. The solution containing the sample were injected in the instrument by either direct infusion or by using an HPLC set-up. The latter was employed in order to separate the isomers of **3** before the analysis. The ion-source conditions were capillary voltage 3.1 kV, sampling cone 40 V, source offset 80 V, source temperature 150 °C and desolvation temperature 300 °C. The same mass spectrometer was used to record ESI full-scan mass spectra and to perform the ion mobility experiments. Traps and transfer cell were saturated with argon, while the IMMS cell was filled with nitrogen. A small RF-cell filled with helium was placed between the traps and the IMMS cell. Energy-resolved collisional activation

⁵ Experiments performed by Dr. A. Galanti (Université de Strasbourg) in collaboration with Q. Duez, Dr. J. De Winter, Prof. P. Gerbaux (Université de Mons), whom are greatly acknowledged.

experiments were executed on the single isomers of **3**, after selecting them *via* HPLC. The ion selected with a specific mass were subjected to collisions with higher kinetic energies in the trap cell and then separated and detected by IMMS. The collisional energies (CE) employed in the trap were low to avoid a collision-induced fragmentation of the ions.

The structure of our star-shaped tris(azobenzene) **3**, bis(azobenzene) **27** and mono(azobenzene) **23** was specifically designed to amplify the geometrical alteration within the molecule upon irradiation. As previously mentioned, three azobenzene chromophoric units were introduced on a rigid aromatic scaffold in *meta* position reciprocally, to ensure geometrical and electrical decoupling as well as to increase the shape variation *via* UV/Vis light irradiation. Ion mobility – mass spectrometry (IMMS), namely the coupling between ion mobility spectrometry (IMS) and mass spectrometry (MS), was employed to distinguish the molecular configurations of the different isomeric forms of **3**, **23** and **27**. Thanks to this technique, it was possible to resolve mixture of different isomers on the basis of their different collisional cross-section (CCS), which is affected by the ions geometry.^[260] The generated ions flow under the influence of an electric field and are subjected to collisions with a buffer gas. The ion drift time across the mobility cell is directly related to the probability of collisions with the gas and, thus, to the CCS of the ions. However, for IMMS experiments ionized species are required. Hence, deprotonation of the carboxylic terminal groups on the chromophoric arms of star-shaped derivatives **3**, **23** and **27** was accomplished upon Electrospray Ionization (ESI) in negative mode to obtain the anionic species. The mass spectra of **3**, **23** and **27** recorded upon ESI show intense signals, with the highest intensity peak corresponding to the mono-deprotonated species: $[3-H^+]^-$ $m/z = 749.2$, $[27-H^+]^-$ $m/z = 745.2$ and $[23-H^+]^-$ $m/z = 741.2$ (Figure 76).

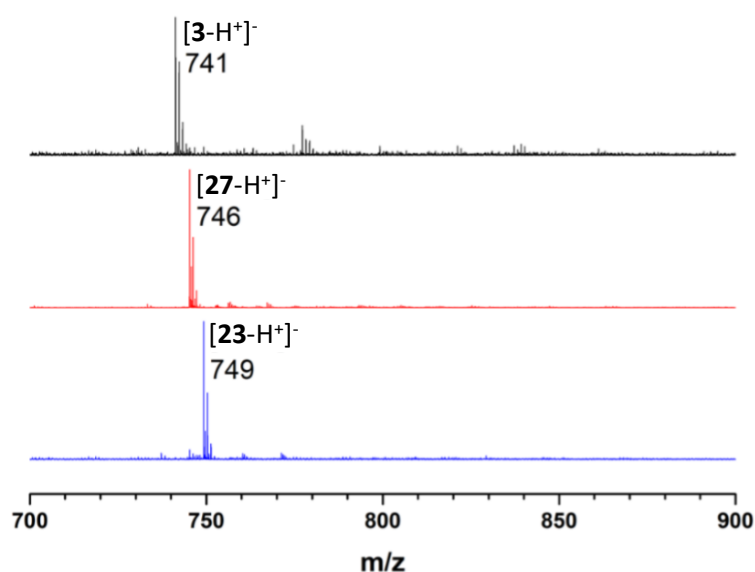


Figure 76. ESI – MS (negative mode) spectra of solutions ($c = 10^{-5}$ M, in THF) of tris(azobenzene) **3** (bottom, *blue spectrum*), bis(azobenzene) **27** (middle, *red spectrum*) and mono(azobenzene) **23** (top, *black spectrum*).

The IMMS investigation was focused only on the singly charged ions, although multiply charged anions were detected. When subjected to IMMS, singly charged anions such as $[3-H^+]^-$, $[27-H^+]^-$ and $[23-H^+]^-$, from non-irradiated solutions, are characterized by single Arrival Time Distribution (ATD) that is associated to the all-(*E*) isomers. On the other hand, the measurements of the UV-irradiated solutions (UV – PSS) showed the presence of additional ATD signals at lower drift times (Figure 77), thus enlightening that for the UV-generated forms (more compact) the CCS are lower than for the extended all-(*E*) configurations. Furthermore, it is interesting to point out that for each star-shaped derivative the number of ATD signals detected for the irradiated solutions corresponds to the number of all possible isomeric forms, namely four for **3**, three for **27** and two for **23**. Subsequently, the ATD values were used to calculate the experimental CCS. Collision cross-section values further confirm the big shape variation resulting from the *E* → *Z* isomerization, and the most representative example is tris(azobenzene) **3** whose CCS dramatically decreases from 269 Å to 187 Å passing from the extended all-(*E*) to the compact all-(*Z*) form (Table 2).

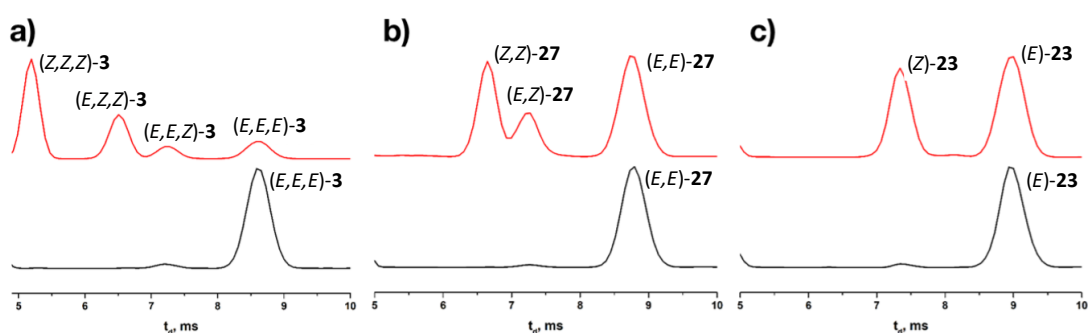


Figure 77. Ion mobility – mass spectrometry (IMMS) experiments on star-shaped azobenzenes **3**, **27** and **23** upon UV light irradiation in solution. Arrival time distributions (ATD) measured for: a) tris(azobenzene) **3**, b) bis(azobenzene) **27** and c) mono(azobenzene) **23**. Black line chromatogram for non-irradiated solutions and red line chromatogram for UV – PSS.

IMMS was also performed on linear azobenzene **35** as reference experiment. Interestingly, the analysis of the UV-irradiated solution did not show the presence of new peaks in the IMMS chromatogram, suggesting that the shape variation associated with the *E* → *Z* isomerization of **35** is moderate if compared to the one observed for the star-shaped derivatives, and it is not detectable with this technique. The photoisomerization of tris(azobenzene) **3** was also monitored in real-time by IMMS, upon on-line irradiation of a DMSO solution of **3**, which was continuously injected in the ESI source (Figure 78). The analysis of ATDs shows the gradual formation of the isomers of **3** confirmed by the presence of additional peaks related to (E,E,Z)-**3**, (E,Z,Z)-**3** and (Z,Z,Z)-**3** in the IMMS chromatogram, until the UV – PSS is reached. The integration of the peaks obtained at the UV – PSS provided the isomeric ratios of all isomers (63% (Z,Z,Z)-**3**, 30% (E,Z,Z)-**3**, 3% (E,E,Z)-**3** and 4% (E,E,E)-**3**), which were subsequently compared to the previous results obtained by HPLC-MS (Table 1).

	CCS (Å ²)		CCS (Å ²)		CCS (Å ²)
(E,E,E)- 3	269	(E,E)- 27	273	(E)- 23	277
(E,E,Z)- 3	237	(E,Z)- 27	239	(Z)- 23	241
(E,Z,Z)- 3	220	(Z,Z)- 27	224		
(Z,Z,Z)- 3	187				

Table 2. Experimental collisional cross-section (CCS) values of the different isomeric forms of azobenzene **3**, **27** and **23** determined by IMMS.

The comparison showed the mobility diagrams overestimate the ratio of the all-(Z) isomer with respect to the (E,E,Z)-**3**, and this discrepancy arises from the fact that for IMMS analysis only the singly charged ions were monitored, whereas they are mixed with other different charged states for the HPLC measurements.

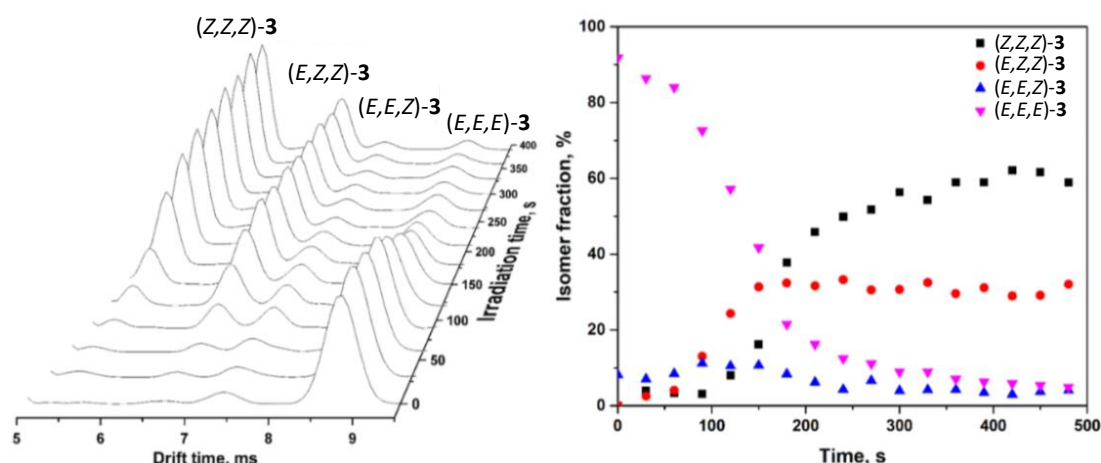


Figure 78. Photoisomerization of **3** monitored by IMMS. A solution of **3** was UV-irradiated upon continuous IMMS separation. *Left*: temporal evolution of the IMMS traces. *Right*: isomeric fractions over time, calculated by IMMS peaks integration.

In-flight $Z \rightarrow E$ isomerization of **3** induced by collisional activation before the ion separation by ion mobility was also investigated.^[260] For the separation of the ions before their injection in the mass spectrometer, an HPLC set-up was used. (Z,Z,Z)-**3** previously isolated by HPLC was then ionized upon ESI (negative mode) and the molecular anions ($[\mathbf{3}-\text{H}^+]^-$ with m/z 749.2) can be mass-selected with the quadrupole mass selector. Thus, the ions undergo collisional heating (collisional activation) in the trap cell prior to the ion mobility separation, by slowly increasing their kinetics energy (Figure 79).

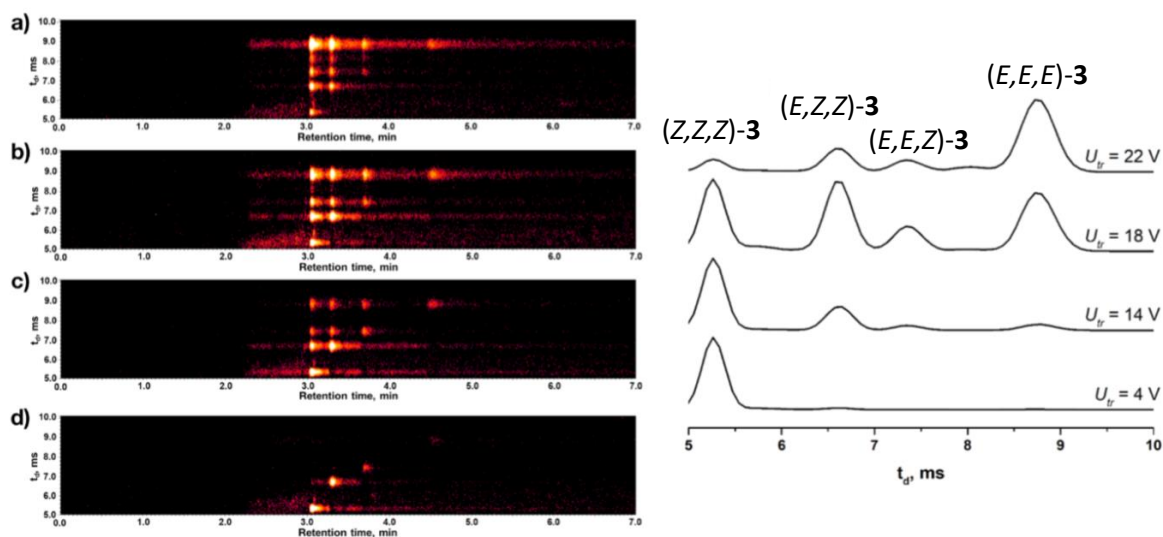


Figure 79. $Z \rightarrow E$ isomerization of **3** induced by collision. *Left:* 2D IMMS/HPLC traces of azobenzene **3** irradiated with UV light (UV – PSS) in DMSO at different collision energies (U_{ir}). Chromatograms integrated at $[M-H]^+$ $m/z = 749.2$. Peak at 3 min 5 s retention time corresponds to (Z,Z,Z)-**3**, 3 min 20 s (E,Z,Z)-**3**, 3 min 40 s (E,E,Z)-**3**, 4 min 30 s (E,E,E)-**3**. a) Traces recorded at $U_{ir} = 2$ V, b) traces recorded at $U_{ir} = 18$ V, c) traces recorded at $U_{ir} = 14$ V, d) traces recorded at $U_{ir} = 4$ V showing the occurrence of $Z \rightarrow E$ isomerization. *Right:* ion mobility traces plotted for the HPLC chromatographic peak at 3 min 5 s corresponding to (Z,Z,Z)-**3**.

At the lowest voltage (U_{ir}) used, only the signature of (Z,Z,Z)-**3** was detected by IMMS, confirming thus the successful isolation of the all-(Z) isomer by HPLC and that no isomerization occurs in this conditions. Subsequently, by increasing the voltage, new signals corresponding to the (E,Z,Z)-**3**, (E,E,Z)-**3** and (E,E,E)-**3** appear. The experiment shows that it is possible to induce $Z \rightarrow E$ isomerization of azobenzene by collisional activation, in analogous fashion as heating, generating the most thermally stable all-(E) form.

2.1.6 Study of the molecular self-assembly on graphite surface⁶

The investigation on the self-assembly was performed by Scanning Tunnelling Microscopy (STM) at room temperature and ambient pressure, using freshly cleaved highly ordered pyrolytic graphite (HOPG) as substrate. A *Veeco Multimode III (Bruker)* equipped with an STM head and a 1 μm -range piezoelectric scanner (*A-Piezo, Veeco*) working in constant mode was used for the experiments. The STM tips were mechanically cut from a Pt/Ir (80:20) wire (0.25 mm diameter, *Goodfellow*). The study was performed at the solid-liquid interface between HOPG and a supernatant solution of the compound in 1-heptanoic acid (purchased from *Sigma Aldrich*), by applying 4 μL of the latter on the substrate, after checking the integrity of substrate and tip by visualizing the graphite lattice. The raw STM data

⁶ Experiments performed by Dr. A. Galanti, Prof. P. Samorì (Université de Strasbourg), whom are greatly acknowledged.

were processed with a dedicated image processing software (SPIP, Image Metrology). The images obtained were corrected from drift by calibration with the underlying graphite lattice. Unit cell parameters were acquired by Fourier analysis. The experiments at the solid-liquid interface were performed at an initial concentration of 10 μM of (*E,E,E*)-**3** (before irradiation) and compound **10** in 1-heptanoic acid, freshly prepared by a THF mother solution. This concentration was found to be the optimal value. Indeed, the use of less concentrated solution did not lead to the observation of ordered structures, while increasing the concentration fuzzy contrast was obtained, most likely due to the formation of additional disordered layers on the crystalline (*E,E,E*)-**3** monolayer. Several attempts were also done using fatty acids with different chain length such as solvents such as 1-octanoic or 1-nonanoic acid, but they did not lead to different crystalline structures of (*E,E,E*)-**3**.^[246]

The peculiar structure of tris(azobenzene) **3** was proposed for the study of its self-assembly on graphite (HOPG) surface. The multi-chromophoric molecule contains three photoswitchable “arms” based on azobenzene that are directly attached to an aromatic benzene ring (rigid molecular scaffold) in position 1,3,5 to ensure geometrical and electrical decoupling. The introduction of carboxylic groups (-COOH) at the azobenzene termini was conceived for the formation of highly ordered honeycomb self-assembled structures on graphite surface based on hydrogen-bonding.^[246] STM experiments on tris(azobenzene) **3** at the solid-liquid interface showed that the compound forms highly ordered monolayers, which exhibit peculiar light response. On the other hand, the self-assembly of non-photoresponsive derivative **10** was investigated by STM as blank experiment, in order to prove the role of the isomerization of **3** in the alteration of the surface assembly. At first, the self-assembly of (*E,E,E*)-**3** in the dark at the solid-liquid interface between HOPG and its solution in 1-heptanoic acid was investigated. STM images recorded *in situ* reveal a tightly packed 2D crystalline lamellar structure consisting of (*E,E,E*)-**3** organized in a zig-zag fashion (Figure 80). The structure observed shows a unit cell ($a = 4.1 \pm 0.2 \text{ nm}$, $b = 3.0 \pm 0.3 \text{ nm}$, $\alpha = 41 \pm 5^\circ$ with an area $A = 8.7 \pm 0.3 \text{ nm}^2$) containing two molecules, and the crystalline packing is characterized by absence of polymorphism. The expected “honeycomb network” hydrogen-bonded pattern is totally absent, and it does not surprise. Due to its large dimensions, the rigid aromatic core of tris(azobenzene) **3** prefers to form densely packed structures.^[248] The more tightly packed crystal gives an higher adsorption energy contribution compared to the “ideal” honeycomb structure. Thus, the driving force of the self-assembly is the molecule-substrate adsorption energy per unit area, which yields the tightest assembly rather than the hydrogen-bonding motif.^[248]

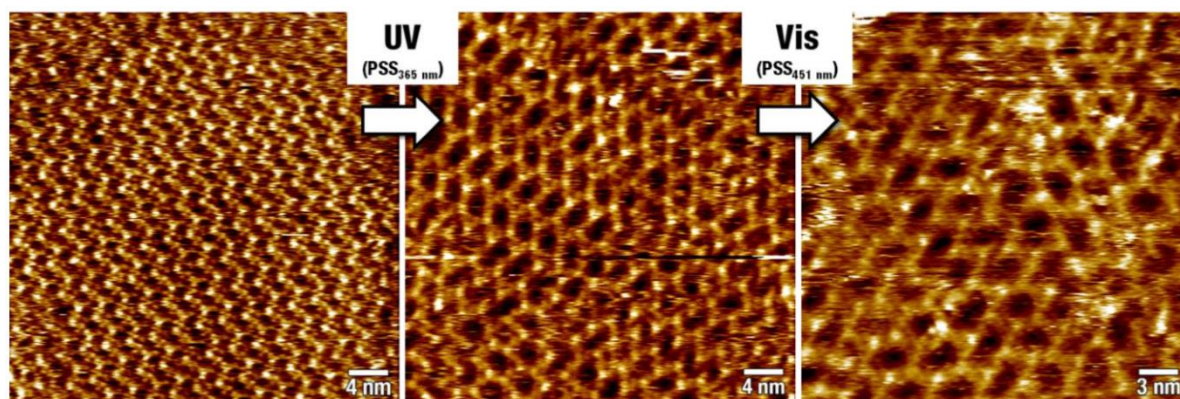


Figure 80. STM images of tris(azobenzene) **3** recorded at the interface between HOPG substrate and its solution (10 μM in 1-heptanoic acid). *Left*: no light irradiation (average tunnelling current $I_T = 30$ pA, tip bias voltage $V_T = +800$ mV). *Middle*: *in situ* UV ($\lambda_{\text{max}} = 365$ nm) light irradiation ($I_T = 30$ pA, $V_T = +800$ mV). *Right*: subsequent *in situ* Vis ($\lambda_{\text{max}} = 451$ nm) light irradiation ($I_T = 20$ pA, $V_T = +800$ mV).

Upon *in situ* irradiation of the (*E,E,E*)-**3** solution with UV light, a disruption of the order of packing is observed together with a loss of crystallinity. This alteration indicates the progressive decrease of concentration of the all-(*E*) isomer of **3** in the solution. The gradual destruction of the initial ordered packing does not surprise. Indeed, the non-planarity associated with the (*Z*)-isomers of azobenzene is responsible of a lower stability when absorbed on a surface if compared with the planar (*E*)-isomers.^[261,262] Interestingly, it was possible to visualize different domains of tris(azobenzene) **3** exhibiting a periodical assembly (Figure 80), which were addressed to domains composed by (*E,Z,Z*)-**3** and (*E,E,Z*)-**3**.

As blank experiment, the non-photoswitchable derivative **10** was also investigated by STM in the same conditions of tris(azobenzene) **3**. Compound **10** may be considered as a non-photoresponsive analogous of **3**, since it is characterized by the same geometry of (*E,E,E*)-**3**, but bearing three 1,2-diphenylethyne non-photoactive branches instead of the azobenzene chromophores. The self-assembly observed for **10** is characterized by the same symmetry displayed by (*E,E,E*)-**3** (Figure 81), with a unit cell ($a = 4.2 \pm 0.2$ nm, $b = 2.9 \pm 0.1$ nm, $\alpha = 46 \pm 1^\circ$ with an area $A = 8.8 \pm 0.4$ nm²) containing two molecules. The *in situ* irradiation of the solution of **10** with both UV and Vis light did not lead to any alteration of the crystalline ordered packing (Figure 82), thus confirming that the alterations observed for (*E,E,E*)-**3** are due to the photoisomerization of the azobenzene units. Whereas ordered domains of both isomeric forms (*E,E,Z*)-**3** and (*E,Z,Z*)-**3** were observed by means of STM, it was not possible to envision (*Z,Z,Z*)-**3** isomer. In fact, when all the three azobenzene units are in the *Z* form, the molecule results completely compact and non-planar, thus surface desorption occurs and does not allow the visualization of the isomer.

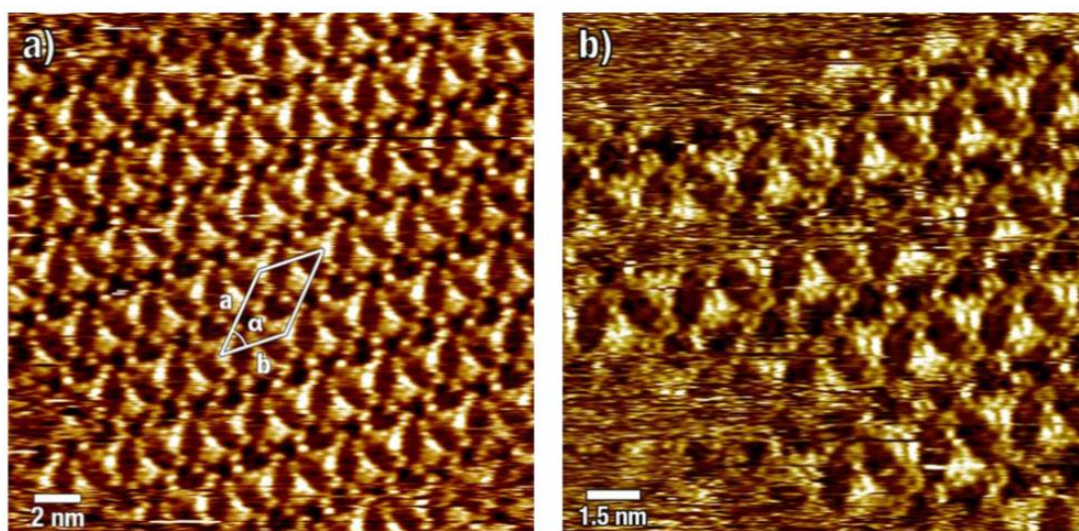


Figure 81. STM images of non-photoresponsive derivative **10** at the solid-liquid interface between HOPG and a solution of **10** ($c = 10 \mu\text{M}$ in 1-heptanoic acid). a) $I_T = 20 \text{ pA}$, $V_T = +800 \text{ mV}$; b) 20 pA , $V_T = +800 \text{ mV}$. Images recorded without irradiation.

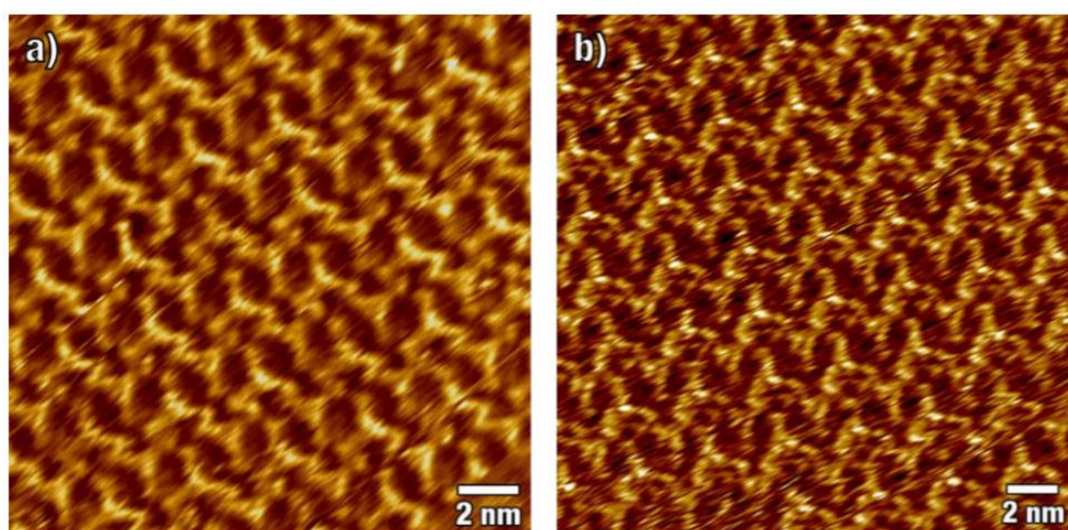


Figure 82. STM images of **10** at the solid-liquid interface between HOPG and a solution of **10** ($c = 10 \mu\text{M}$ in 1-heptanoic acid). a) STM image of **10** obtained after 15 min *in situ* UV irradiation ($I_T = 20 \text{ pA}$, $V_T = +800 \text{ mV}$); b) STM image of **10** obtained after subsequent *in situ* irradiation with Vis light for 15 min ($I_T = 20 \text{ pA}$, $V_T = +800 \text{ mV}$).

Our experimental data were further confirmed by means of Molecular Dynamics (MD) simulations⁷ (Figure 83). The results obtained by MD simulation, indeed, match very well with the values obtained by STM experiments and corroborate the validity of the model used for the interpretation of the self-assembled domains.

⁷ MD simulations were performed by Dr. V. Diez-Cabanes, Dr. A. Minoia, Prof. J. Cornil (Université de Mons), whom are greatly acknowledged.

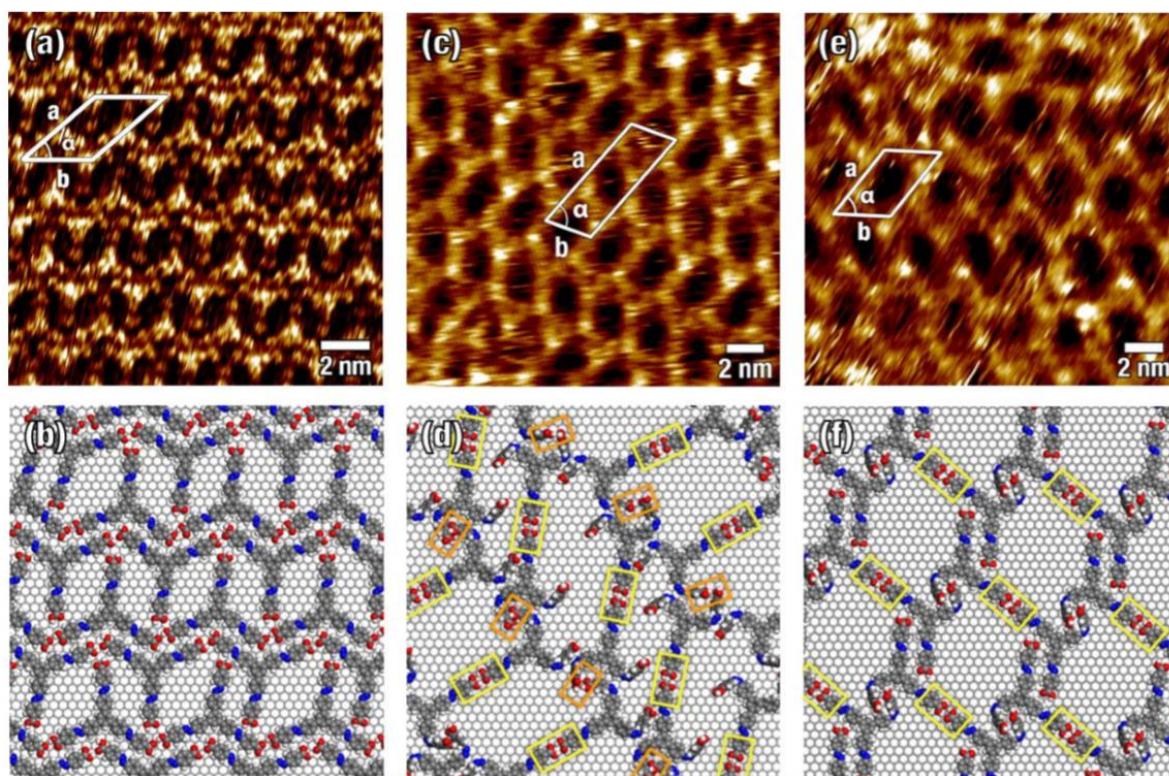


Figure 83. High resolution STM images of ordered domains of: (a) (*E,E,E*)-**3**, (c) (*E,Z,Z*)-**3** and (e) (*E,E,Z*)-**3** self-assembled at the solid-liquid interface between HOPG and a solution of **3** ($c = 10 \mu\text{M}$ in 1-heptanoic acid). Supramolecular packing models obtained by MM/MD simulations for: (b) (*E,E,E*)-**3**, (d) (*E,Z,Z*)-**3** and (f) (*E,E,Z*)-**3**. The *yellow rectangles* indicate the formation of hydrogen-bonded carboxylic acid dimers between the (*E*)-arms, while the *orange rectangles* indicate the formation of hydrogen-bonded carboxylic acid dimers between the (*Z*)-arms. Tunnelling parameters: (a) $I_T = 40 \text{ pA}$, $V_T = +800 \text{ mV}$, (c) $I_T = 30 \text{ pA}$, $V_T = +800 \text{ mV}$, (e) $I_T = 20 \text{ pA}$, $V_T = +800 \text{ mV}$.

For (*E,E,E*)-**3** the estimated unit cell parameters are: $a = 4.3 \text{ nm}$, $b = 2.8 \text{ nm}$, $\alpha = 41^\circ$ with two molecules per unit cell (Figure 83a), thus perfectly in agreement with the experimental values. On the other hand, for (*E,Z,Z*)-**3** the estimated unit cell has the following parameters: $a = 7.6 \text{ nm}$, $b = 2.7 \text{ nm}$, $\alpha = 69^\circ$ with an area $A = 20 \text{ nm}^2$ containing two molecules (Figure 83c), and for (*E,E,Z*)-**3** the parameters for unit cell are: $a = 4.0 \text{ nm}$, $b = 3.3 \text{ nm}$, $\alpha = 55^\circ$ with an area $A = 11 \text{ nm}^2$ each containing two molecules (Figure 83e). Both (*E,Z,Z*)-**3** and (*E,E,Z*)-**3** assemblies display different parameters compared to the all-(*E*) **3** and **10** and also lower stability of the packing evidenced by the smaller size of ordered domains. Furthermore, the formation of (*Z*)-isomers causes a decrease of crystallinity associated to the (*E,E,E*)-**3** assembly, because the non-planarity of (*Z*)-azobenzene units is responsible of less favourable molecule-substrate interactions with respect to the (*E*)-form. Nevertheless, the loss of interactions with the substrate is balanced by the occurrence of hydrogen-bonding interactions between the carboxylic groups placed at the azobenzene termini, as evidenced by the larger spacing between rows of (*E,Z,Z*)-**3** and (*E,E,Z*)-**3**, nicely corroborated by MM/MD simulations. In order to correctly explain the experimental data obtained for (*E,Z,Z*)-**3** and (*E,E,Z*)-**3**, the simulation over multiple different assemblies was performed (Table 3, Figure 84).

		a [nm]	b [nm]	α [°]	A [nm ²]	N	H-bonds	E_{ads} [kcal/mol]	BE [kcal/mol]
(E,E,E)-3	experimental	(4.1 ± 0.2)	(3.0 ± 0.3)	(41 ± 5)	(8.7 ± 0.7)	2			
	theoretical	4.3	2.8	41	8.0		2	-101.91	-6.83
(E,Z,Z)-3	experimental	(4.2 ± 0.2)	(2.9 ± 0.1)	(46 ± 1)	(8.8 ± 0.4)	2			
	experimental	(7.6)	(2.7)	(69)	(20)				
	I	8.1	3.7	61	26	4	1.5	-80.50	-6.63
	II	7.6	2.8	74	20		2	-78.84	-10.13
	III	7.8	3.3	56	21		2.5	-78.59	-8.63
(E,E,Z)-3	experimental	(4.0)	(3.3)	(55)	(11)				
	I	3.8	3.3	56	11	2	1	-90.38	-8.87
	II	4	3.8	55	13		2	-89.96	-6.36
	III	5.5	3.2	50	13		2	-90.59	-7.83

Table 3. Experimental and simulated unit cell parameters for tris(azobenzene) **3** and non-photoresponsive derivative **10**, and estimated thermodynamic quantities.

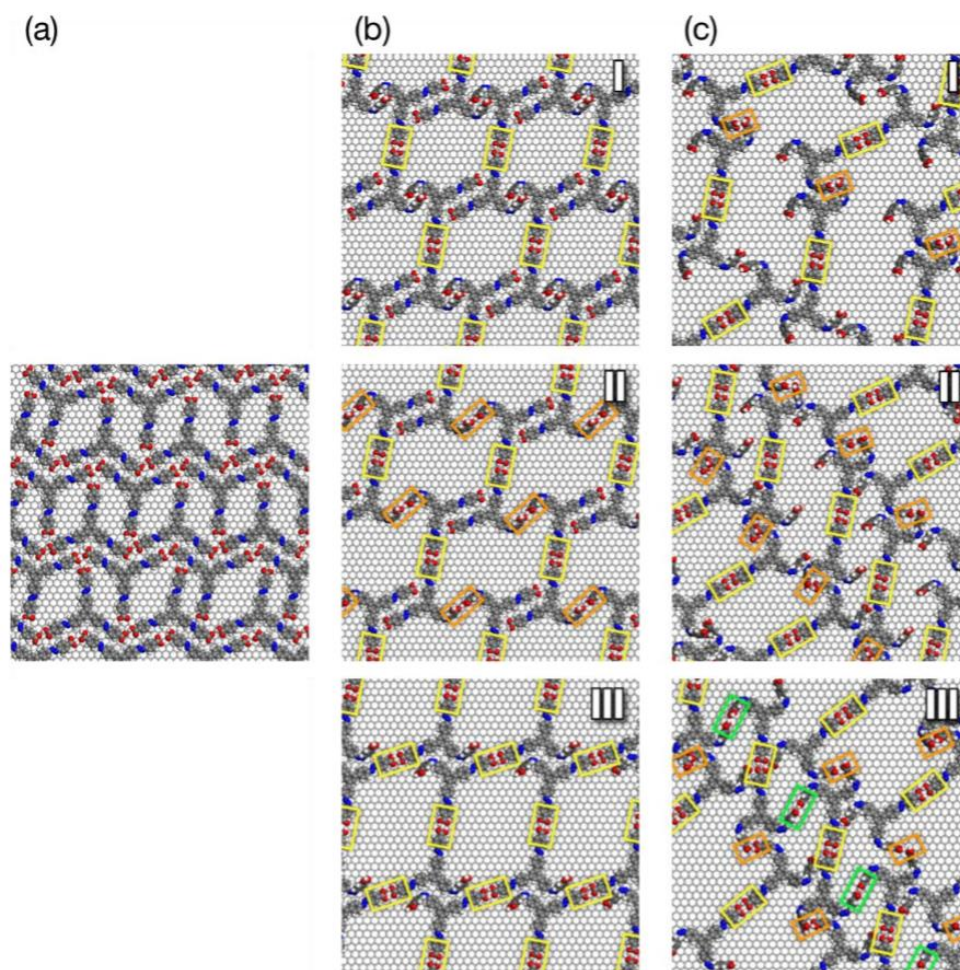


Figure 84. (a) Top view of the (E,E,E)-**3** MD simulated self-assembly. (b) Top view of the (E,E,Z)-**3** MD simulated self-assembly models: model I (top), model II (middle), model III (bottom). (c) Top view of the (E,Z,Z)-**3** MD simulated self-assembly models: model I (top), model II (middle), model III (bottom). The yellow rectangles evidence the (E)-H-bonds, the orange rectangles represent the (Z)-H-bonds that connect the vertical and horizontal rows and the green rectangles represent the (Z)-H-bonds that connect molecules of the horizontal rows.

The two parameters computed are the adsorption energy (E_{ads}) and the binding energy (BE), which give an indication of the strength of the molecule-substrate and intermolecular interactions respectively (Table 3). The structural packing of (*E,Z,Z*)-**3** and (*E,E,Z*)-**3** arises from a lower E_{ads} with respect to (*E,E,E*)-**3**, because of the decrease of π - π and van der Waals interactions between the non-planar molecules in the (*Z*)-form and the graphite substrate. This evidence also explains the absence of (*Z,Z,Z*)-**3** self-assembly in the experimental data. On the other hand, (*E,Z,Z*)-**3** and (*E,E,Z*)-**3** display higher BE values that arise from the formation of strong intermolecular H-bonds between the carboxylic groups, which stabilize the H-bonded network. Consequently, the planarity within the (*E,E,E*)-**3** structure gives rise to a completely opposite behaviour of E_{ads} and BE values. The experimental data together with the MM/MD simulation results indicate that the self-assembly of C_3 -symmetrical large aromatic carboxylic acids such as **3** and **10** arise from the balance between intermolecular and molecule-substrate interactions, the former dominating the self-assembly of (*Z*)-azobenzenes and the latter dominating the organization of (*E*)-azobenzenes. STM studies at the solid-air interface of **3** (Figure 85) were also performed to investigate the photoisomerization on the basal plane of the surface and to exclude any interference of the supernatant solution on the process.

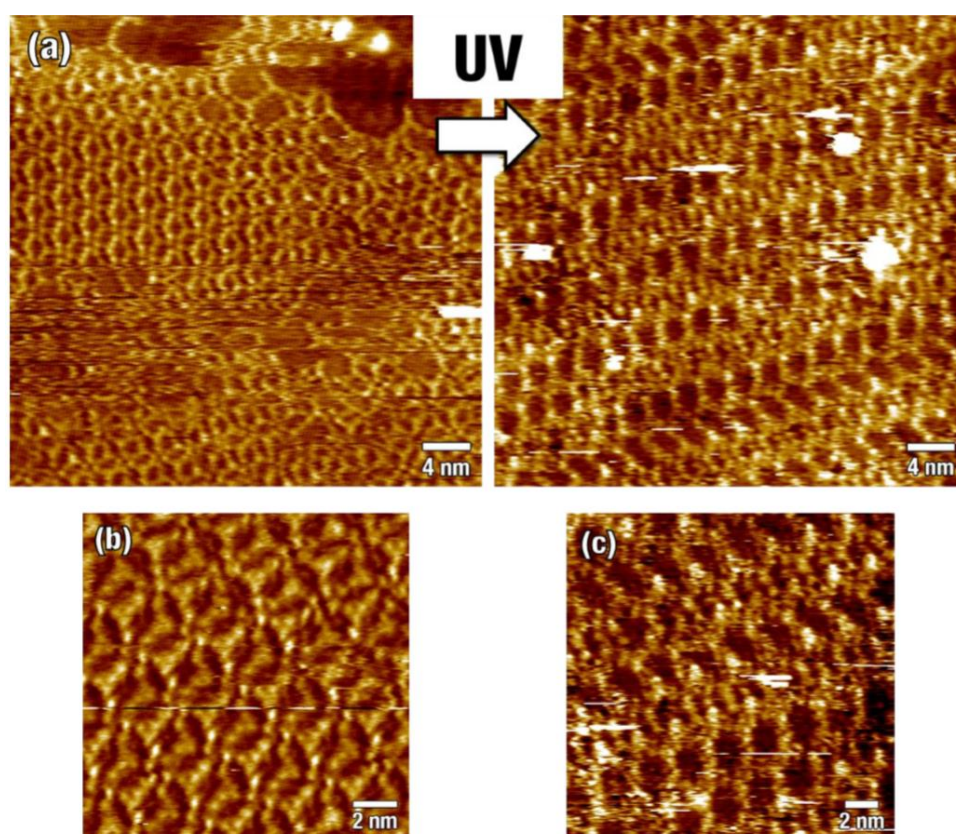


Figure 85. STM images of **3** at the solid-air interface. (a) *Left panel*, no irradiation ($I_T = 20$ pA, $V_T = +700$ mV); *right panel*, after 30 min *in situ* UV irradiation ($\lambda_{max} = 367$ nm, $I_T = 20$ pA, $V_T = +700$ mV). (b) Magnification of (*E,E,E*)-**3** before irradiation. (c) Magnification of **3** after 30 min *in situ* UV irradiation.

(*E,E,E*)-**3** was thus physisorbed on the HOPG surface and its photoisomerization upon *in situ* irradiation was studied. A non-irradiated solution of (*E,E,E*)-**3** (10 μ M in THF) was deposited in a freshly cleaved HOPG substrate and, subsequently, the excess of the solution and the solvent were removed by spinning on a spin-coater. The high affinity of all-(*E*)-tris(azobenzene) **3** for the substrate allowed the formation of molecular adsorbates characterized by small crystalline regions surrounded by non-coated regions. Interestingly, the unit cell parameters obtained by STM at the solid-liquid (Figure 80) and solid-air (Figure 85) interfaces found for (*E,E,E*)-**3** are similar. Furthermore, upon *in situ* UV irradiation, an evident alteration of the packing was observed as a result of the azobenzene photoisomerization. It is worth to mention that the absence of supernatant solution does not allow the desorption of the (*Z*)-isomers from the graphite substrate, thus the inter-row spacing variation observed upon *in situ* UV irradiation is most evident consequence of the *E* \rightarrow *Z* photoisomerization. The morphology of the patterns observed in this case is different from the one obtained with the solid-liquid interface experiments. The isomerized molecules, indeed, are not capable of surface desorption in this case, and consequently they cannot arrange in ordered crystalline domains containing one isomeric form.

2.1.7 Photo-responsive metal-organic frameworks (MOFs)

The molecular structure of tris(azobenzene) **3** was conceived not only for its self-assembly into a 2D photo-responsive system on surface, but also as organic ligand for the construction of photoactive 3D architectures such as metal-organic frameworks (MOFs). C_3 -symmetrical rigid molecular scaffold have been employed as organic ligands in highly porous metal-organic framework with different pore size and surface areas.^[263] The presence of carboxylic groups on the azobenzene termini may allow the organization into three-dimensional highly ordered architectures through the formation of a strong metal-oxygen (M-O bond, M = Ti(IV), V(III), Cr(II), Mn(II), Fe(III), Co(II), Ni(II), Cu(II), Zn(II), Zr(IV), Ln(III), Al(III), Mg(II)) covalent bond between the inorganic and the organic units. In MOF chemistry, the crystallinity of the material is crucial, and it has been accomplished by slowing down the formation of the metal-oxygen bond in order to permit self-correction of the structure during the formation of the covalent bond. The deprotonation of the organic acid ($-\text{COO}^-$) is required for the MOF formation and for the metal-oxygen bond. Moreover, the rate at which the deprotonation occurs is a crucial factor to control the crystallization process. MOFs are formed almost exclusively by hydrothermal or solvothermal techniques, where crystals grow slowly from a hot solution. Usually, *N,N*-dimethylformamide (DMF), *N,N*-dimethylacetamide (DMA) and *N*-methyl-2-pyrrolidone (NMP) are used as a solvent and a base source for MOF formation. Since they are heated during the process, they act as a source of basic amines, which gradually deprotonate the organic acid and induce the formation of the covalent bond between the metal ion and the organic ligand.

One of the main goals of MOF chemistry is to obtain a crystalline structure. Therefore, other methods employing water or modulators have been reported.^[264–267] Some of our attempts towards the preparation of photo-switchable metal-organic frameworks are summarized in Table 4. Numerous trials have been performed under different conditions, changing the solvent or employing mixture of solvents, controlling the temperature of the process and the time of heating and/or cooling, using different salts as metal sources and adding monocarboxylic acids (formic acid, acetic acid) as modulators.

Ligand	Metal source	Equivalents of metal source	Solvents	Temperature	Heating time
10	Zn(NO ₃) ₂ ·6H ₂ O	16	DMF/NMP, 1:1 v/v	85 °C	72 h
10	Zn(NO ₃) ₂ ·6H ₂ O	5	DEF/NMP, 1:1 v/v	85 °C	72 h
10	Zn(NO ₃) ₂ ·6H ₂ O	16	DMF/NMP, 1:1 v/v	100 °C	96 h
10	Zn(NO ₃) ₂ ·6H ₂ O	7	DEF	100 °C	96 h
10	Zn(NO ₃) ₂ ·6H ₂ O	7	DEF	70 °C	96 h
10	Zn(NO ₃) ₂ ·6H ₂ O	17	DMF/NMP, 1:1 v/v	70 °C	96 h
10	Zn(NO ₃) ₂ ·6H ₂ O	16	DMF/NMP, 1:1 v/v	85 °C	96 h
10	Zn(NO ₃) ₂ ·6H ₂ O	20	DMF/MeOH/H ₂ O, 2:1:1, v/v	85 °C	72 h
10	Zn(NO ₃) ₂ ·6H ₂ O	15	DMF/MeOH/H ₂ O, 2:1:1, v/v	85 °C	72 h
10	Zn(NO ₃) ₂ ·6H ₂ O	6	CH ₃ CN/DMF/AcOH, 2:2:1	85 °C	96 h
10	Zn(OAc) ₂	16	DMF/NMP, 1:1 v/v	85 °C	72 h
10	Zn(OAc) ₂	8	DEF/MeOH/H ₂ O, 4:1:1 v/v	85 °C	72 h
10	Zn(OAc) ₂	9	DEF/MeOH/H ₂ O/AcOH, 4:1:1:1, v/v	85 °C	96 h
10	Zn(OAc) ₂	3	DMF/H ₂ O/AcOH, 3:1:2, v/v	85 °C	96 h
10	Zn(OAc) ₂	11	DMF/NMP/H ₂ O/AcOH, 2:2:1:1, v/v	85 °C	96 h
10	Zn(OAc) ₂	10	DEF	85 °C	96 h
3	Cu(NO ₃) ₂ ·3H ₂ O	6	DEF/NMP, 1:1 v/v	85 °C	48 h
3	Zn(NO ₃)·6H ₂ O	12	DEF	85 °C	24 h
3	Zn(OAc) ₂	8	DEF	85 °C	24 h
3	Cu(OAc) ₂	11	DEF	85 °C	24 h
3	Zn(NO ₃)·6H ₂ O	3	DEF/HNO ₃ , 3:0.1 v/v	85 °C	48 h
3	Cu(NO ₃) ₂ ·3H ₂ O	3	DEF/HNO ₃ , 3:0.1 v/v	85 °C	48 h
3	Zn(NO ₃) ₂ ·6H ₂ O	3	DEF	100 °C	48 h
3	Zn(AcO) ₂	3	DEF/AcOH, 3:0.2 v/v	100 °C	48 h
3	ZrCl ₄	1.15	DME/AcOH, 4:0.4 v/v	100 °C	48 h

Table 4. Attempts towards the preparation of MOFs containing tris(azobenzene) **3** or non-switchable derivative **10** as an organic ligand.

However, all our attempts provided non-crystalline materials. We addressed this issue to the flexibility of tris(azobenzene) **3**, which contains three photo-switchable azobenzene units. Same experiments have also been performed with the more rigid non-photoresponsive derivative **10**. Nonetheless, these experiments provided only amorphous materials. Moreover, nitrogen-adsorption measurements confirmed the absence of porosity of the amorphous materials obtained.

2.1.8 Photo-responsive covalent organic frameworks (COFs)

The difficulties faced during the preparation of MOFs containing the star-shaped tris(azobenzene) **3** as an organic ligand brought our attention to an alternative approach. Since any crystalline material was obtained *via* the typical solvothermal method used for MOF preparation, we decided to induce the formation of the 3D photoactive structure by means of covalent bonds generation. For this purpose, a new star-shaped tris(CN-azobenzene) **30** was synthesized. The molecular structure of **30** (Figure 86) may be considered analogous to molecule **3**, which contains a central benzene ring as a scaffold on which three photochromic azobenzene units are introduced in the position *meta* reciprocally. In contrast to tris(azobenzene) **3**, tris(CN-azobenzene) **30** bears a nitrile group ($-C\equiv N$) as the azobenzene termini, which results fundamental for the formation of a triazine-based covalent organic framework (COF) *via* cyclotrimerization.^[219,222,268]

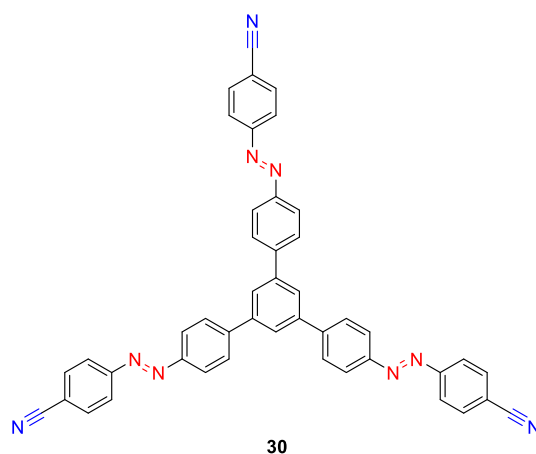


Figure 86. Molecular structure of (*E,E,E*)-star-shaped tris(CN-azobenzene) **30**. Three photochromic molecular “arms” are introduced in the position 1,3,5 on a benzene ring. The presence of a nitrile group ($-C\equiv N$) at the azobenzene termini allows the formation of a triazine heterocycle *via* cyclotrimerization.

The synthetic approach towards star-shaped tris(CN-azobenzene) **30** is based on the assembly of two building blocks, namely the central 1,3,5-tris(4-aminophenyl)benzene (**1**) and the 4-nitrosobenzonitrile (**29**) (Figure 87). The two steps sequence towards the target molecule **30** started from 4-aminobenzonitrile **28**, which was converted into the corresponding nitroso derivative **29** (first building

block) *via* oxidation with an aqueous solution of Oxone® in 95% yield. With the 4-nitrosobenzonitrile in hands, it was possible to form azobenzene **30** *via* Mills reaction.

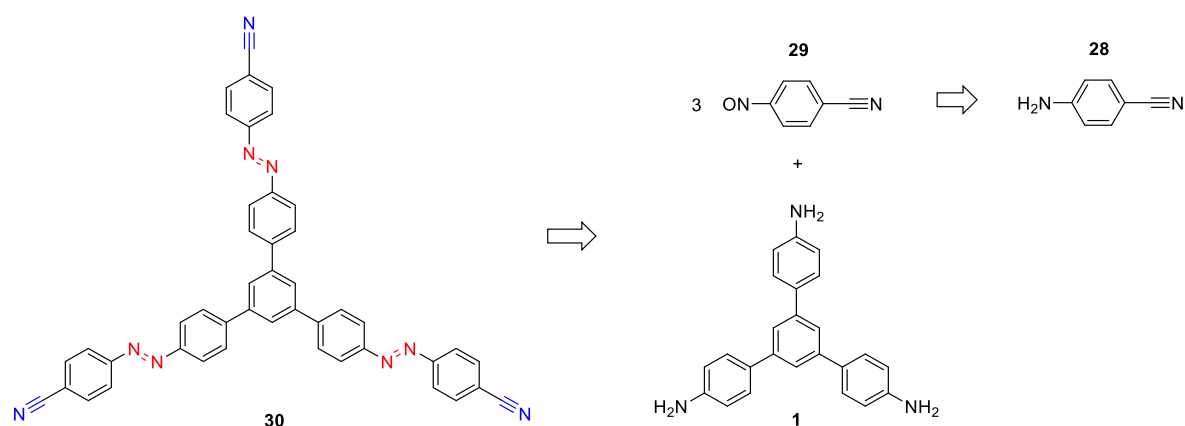


Figure 87. Retrosynthetic analysis to the target molecule **30** based on the assembly of two building blocks 1,3,5-tris(4-aminophenyl)benzene (**1**) and 4-nitrosobenzonitrile (**29**).

The reaction between 4-nitrosobenzonitrile **29** and 1,3,5-tris(4-aminophenyl)benzene **1** under standard Mills conditions (Figure 88) provided the precipitation of the desired product **30**, which was filtered off and copiously washed with acetic acid, then dried under vacuum to afford the target molecule **30** as an orange solid in quantitative yield.

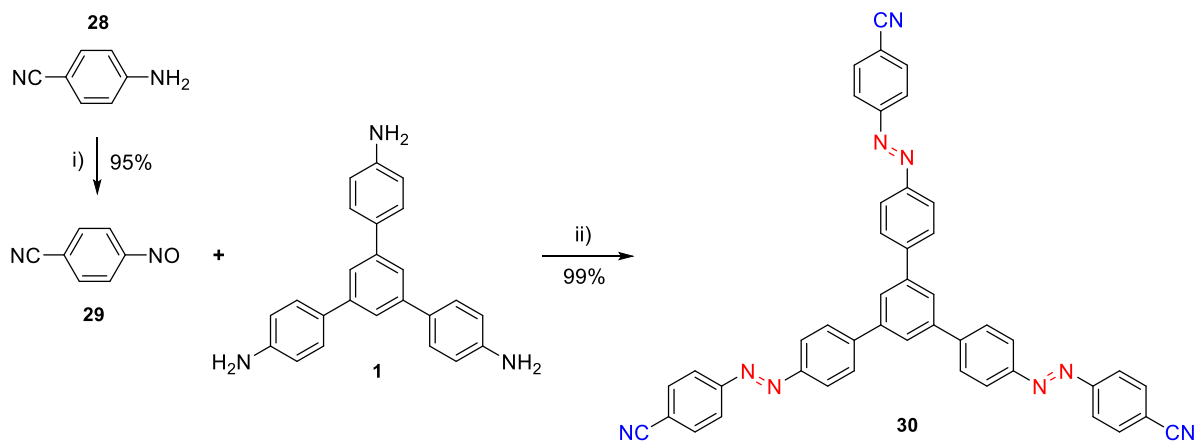


Figure 88. Synthetic strategy towards star-shaped tris(CN-azobenzene) **30**. Reagents and conditions: i) Oxone®, H₂O, CH₂Cl₂, RT; ii) AcOH, RT.

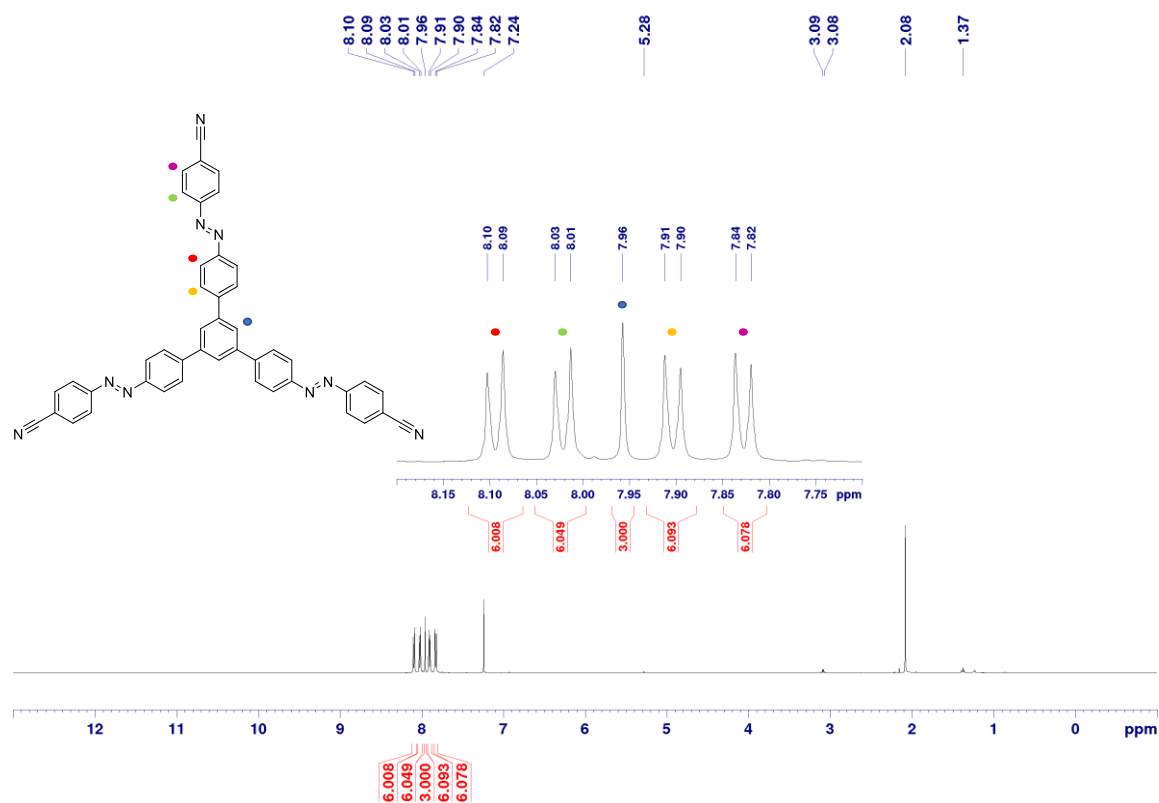


Figure 89. ¹H NMR spectrum (500 MHz) of star-shaped tris(azobenzene)-CN **30**, measured in deuterated chloroform (CDCl₃).

Tris(azobenzene)-CN **30** is a promising candidate as a photoresponsive building block in photo-switchable covalent organic frameworks based on triazine.^[269] In our experiments we used tris(CN-azobenzene) **30** as only ligand containing photoactive motifs, without the addition of any second building block for the formation of the COF structure. Our first attempts towards triazine-based COF preparation were performed following the typical procedures reported in literature.^[232,270] After checking its stability at high temperature, star-shaped derivative **30** and a large excess of anhydrous ZnCl₂ were loaded into a quartz tube, and then the tube was saturated with argon and flame-sealed under vacuum (Figure 91). Subsequently, the mixture was heated up to 400 °C in a ceramic oven for 30 hours. Under these conditions, the molten zinc chloride (m.p. = 290 °C) acts as a solvent and a catalyst in the ionothermal reaction, and aromatic nitriles show good solubility in this ionic melt due to strong Lewis acid – base interactions. Furthermore, ZnCl₂ was found to be a good catalyst for the cyclotrimerization reaction (Figure 90), and at this temperature allows a sufficient reversibility of the bond formation (self-healing character).

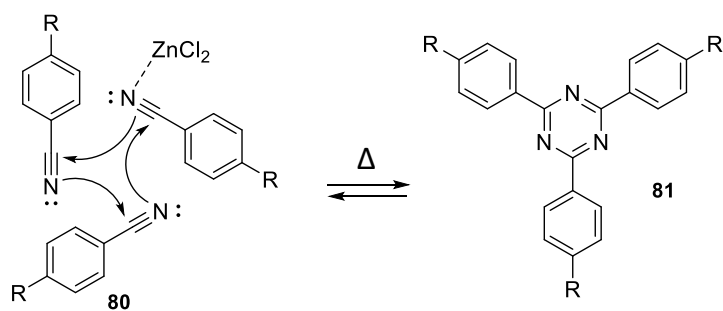


Figure 90. General mechanism of aromatic nitriles cyclotrimerization reaction catalysed by molten ZnCl_2 at high temperature.

After 30 hours of heating, the crude suspension (black solid) was cooled down to room temperature spontaneously. The black solid was poured into water and stirred for 18 hours. Subsequently, the crude product was filtered off, copiously washed with H_2O , poured in HCl (1.0 M aqueous solution) and stirred for 2 hours, then filtered again, washed with HCl (1.0 M aq. sol.), H_2O and dried under vacuum at $120\text{ }^\circ\text{C}$ for 48 hours.

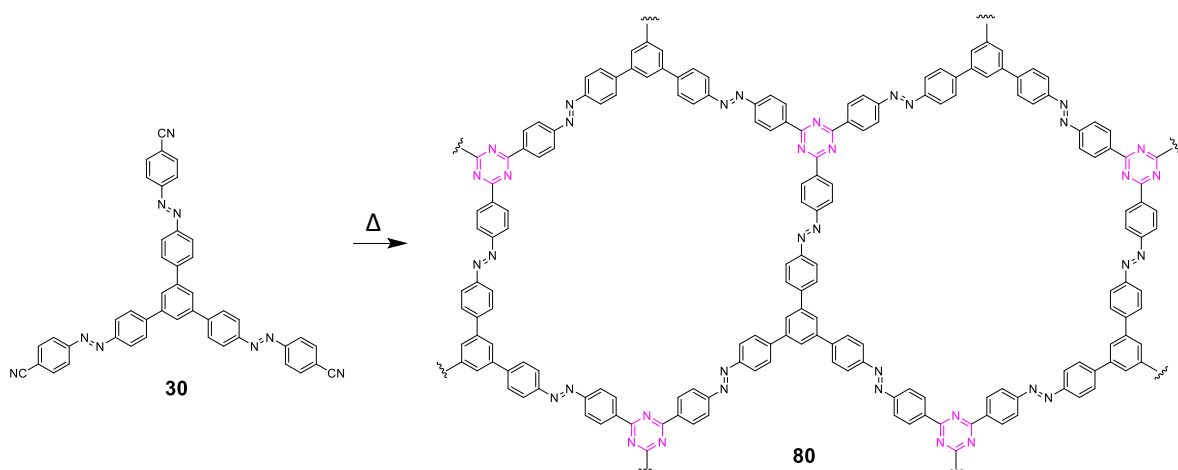


Figure 91. Synthetic strategy towards triazine-based COF-80 by heating up to $400\text{ }^\circ\text{C}$ of a mixture of tris(CN-azobenzene) **30** with an excess of ZnCl_2 in a ceramic oven for 30 h.

The rather harsh condition required for the preparation of triazine-based COFs *via* solvothermal reaction might cost partial carbonization of the material at such high temperature. On the other hand, porous materials can be also prepared under milder conditions, at moderate temperature, using Brønsted acids.^[268] Recently, Thomas and co-workers reported a two-steps synthesis of triazine-based covalent organic frameworks using trifluoromethanesulfonic acid (TfOH) in chloroform for the preparation of a pre-COF (partially polymerized) and subsequent heating of the obtained material with ZnCl_2 above $500\text{ }^\circ\text{C}$.^[271,272] Using Thomas procedure, we performed the synthesis of a photoswitchable triazine-based COF comprising star-shaped azobenzene **30**. Our first attempt (*Method A*) was performed using chloroform as a solvent and TfOH as acid-catalyst for the cyclotrimerization. An excess of trifluoromethanesulfonic acid (3.0 eq.) was diluted with anhydrous CHCl_3 at $0\text{ }^\circ\text{C}$ in an ice-bath. Subsequently, a solution of tris(CN-azobenzene) **30** in CHCl_3 was added dropwise to the acid

solution. The reaction mixture was stirred at 0 °C for 2 hours, then heated up to 40 °C and stirred under argon atmosphere for 60 hours. During the reaction time, a purple precipitate was formed, which after work-up became dark orange. The obtained solid was filtrated, copiously washed with H₂O, EtOH, acetone and CHCl₃, dried under vacuum at 120 °C for 12 hours to provide COF-77-A as dark orange solid in 40 % yield. All the washing fraction obtained were coloured in orange, suggesting the presence of small oligomers based on azobenzene units. One of the drawbacks faced with *Method A* is the relatively low solubility of tris(CN-azobenzene) **30** in chloroform. Therefore, in our second approach (*Method B*) the reaction was performed in 1,1,2,2-tetrachloroethane (C₂H₂Cl₄) as a solvent. Although only the different solvent has been employed, COF-77-B was isolated as dark purple spheres in quantitative yield.

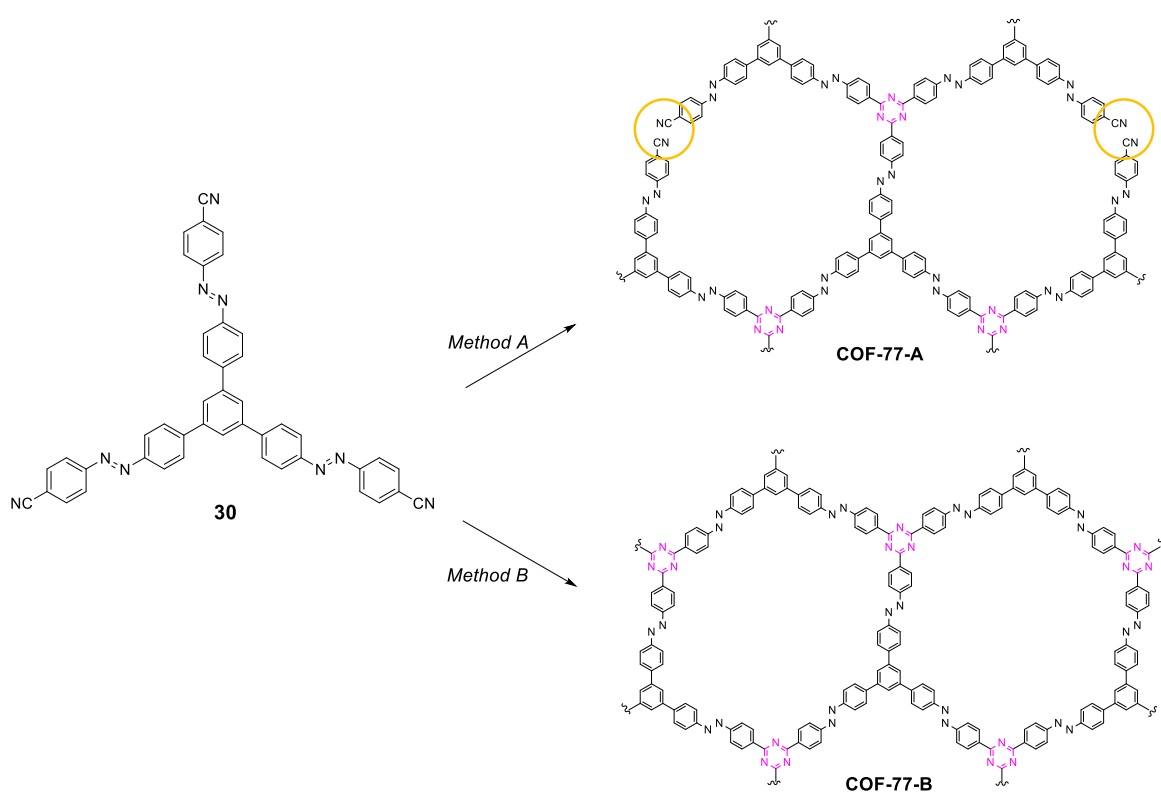


Figure 92. Cyclotrimerization of nitriles performed under mild reaction conditions at low temperature using chloroform (*Method A*) or 1,1,2,2-tetrachloroethane (*Method B*) as a solvent. Reagents and conditions: TfOH, CHCl₃ (C₂H₂Cl₄), 40 °C.

Identification and analysis of triazine-based COFs

All triazine-based covalent organic frameworks synthesized (COF-80, COF-77-A and COF-77-B) resulted insoluble in common organic solvents including chloroform, dichloromethane, DMF, acetone, ethanol or DMSO. Powder X-ray diffraction (PXRD) was measured to confirm the nature of the synthesized materials, but none of the COFs displayed feature of crystallinity. The reason may be related to the polymerization rate, which is rather fast and does not allow self-correction during the polymerization providing thus a structurally disordered material. The insoluble materials were also analyzed by FTIR in order to detect the typical vibration bands of triazine-based compounds ($1560\text{--}1520\text{ cm}^{-1}$, $1480\text{--}1350\text{ cm}^{-1}$ and $860\text{--}736\text{ cm}^{-1}$). The FTIR spectra obtained are depicted in Figure 93.

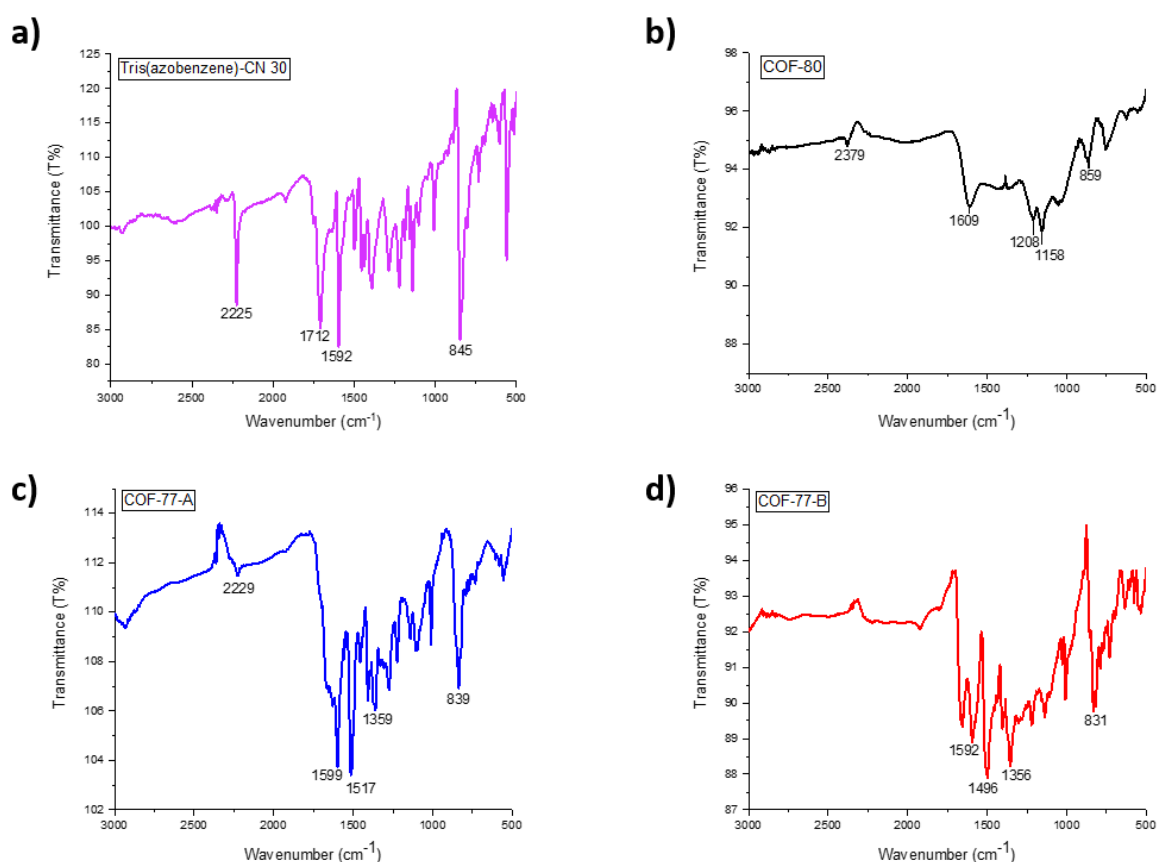


Figure 93. FTIR spectra of triazine-based COFs. a) FTIR spectrum of tris(azobenzene)-CN **30**; b) FTIR spectrum of COF-**80** prepared by solvothermal reaction; c) FTIR spectrum of COF-**77-A** prepared using TfOH in CHCl_3 as solvent (*Method A*); d) FTIR spectrum of COF-**77-B** prepared using TfOH in $\text{C}_2\text{H}_2\text{Cl}_4$ as solvent (*Method B*).

Although the FTIR spectrum of COF-**80** (Figure 93b) does not show the characteristic band at *ca.* 2225 cm^{-1} for nitrile derivatives (Figure 93a), the expected bands at *ca.* 1535 and 1315 cm^{-1} indicative of aromatic C–N stretching vibrations in the triazine units are not clearly distinguishable. Indeed, for COF-**80** the overall spectrum looks broadened probably due to the carbonization of the material.

On the other hand, in FTIR spectra of COF-77-A and COF-77-B the strong characteristic carbonitrile stretching vibration band around 2225 cm^{-1} disappeared or decreased significantly after the reaction. Furthermore, the appearance of the peaks at $1560 - 1520\text{ cm}^{-1}$, $1480 - 1350\text{ cm}^{-1}$ and $860 - 736\text{ cm}^{-1}$ demonstrates the formation of the triazine ring. Porosity parameters of COF-80, COF-77-A and COF-77-B were studied by means of N_2 adsorption – desorption measurements at 77 K (Figure 94-95)⁸. Before the measurements, the samples were dried overnight at $120\text{ }^\circ\text{C}$ to get rid of residual solvents/gases trapped in the pores. Prior to the measurements the samples were degassed for 3 hours at 423 K. Specific surface area and porosity of the materials were analyzed with the Brunauer-Emmett-Teller (BET) method.^[273] Physisorption isotherms were collected on a *Micromeritics ASAP 2020* instrument by applying nitrogen gas at liquid nitrogen temperature. Pore size distributions were calculated by applying a non-linear Density Functional Theory (NL-DFT) model.

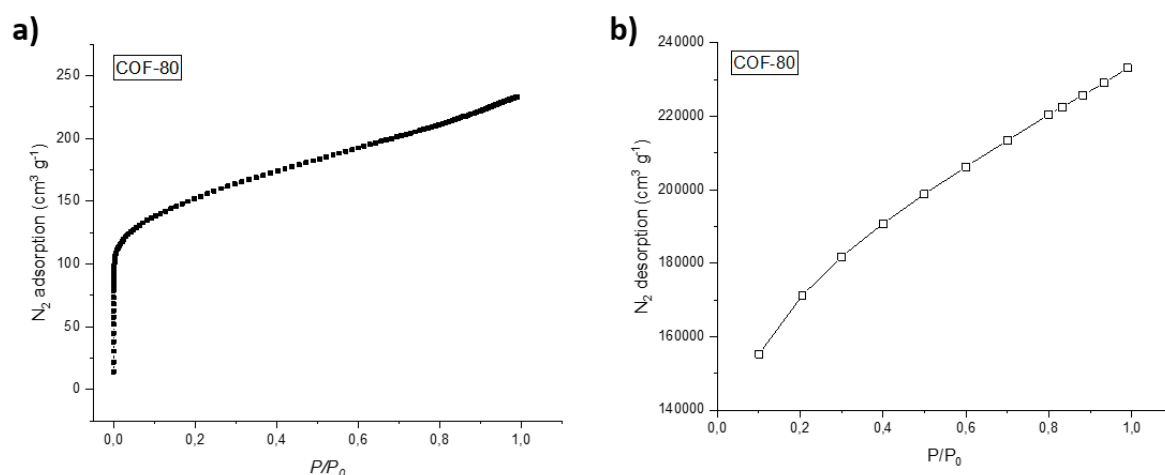


Figure 94. Nitrogen adsorption-desorption isotherms of COF-80 prepared *via* solvothermal reaction at $400\text{ }^\circ\text{C}$ using ZnCl_2 as Lewis acid catalyst for the cyclotrimerization. a) N_2 adsorption isotherm of COF-80; b) N_2 desorption isotherm of COF-80.

Adsorption is the adhesion of atoms, ions or molecules from a gas, liquid or dissolved solid to a surface. This process is studied through the adsorption isotherms, which are generally accepted to be six types according to their shape.^[274] The nitrogen adsorption isotherm of COF-80 (Figure 94a) showed a steep rise in N_2 uptake in the low relative pressure region ($P/P_0 < 0.5$) and it follows a type I behaviour, which is usually used to describe microporous materials ($< 2\text{ nm}$). Subsequently, in the relative pressure region from 0.1 to 1, the isotherm of COF-80 is slowly increasing and approaching a limit value. On the other hand, COF-77-A and COF-77-B showed adsorption isotherms of the type V with a gradual increase of N_2 uptake, which does not reach a limit value (Figure 95a,c). This kind of isotherm is usually observed for mesoporous (2-50 nm) adsorbents. The BET specific surface area values of COF-

⁸ The experiments have been performed in the groups of M. Fichtner in the Institute of Nanotechnology at the Karlsruhe Institute of Technology (KIT) by Dr. Z. Li, whom is greatly acknowledged.

80, COF-77-A and COF-77-B are $530 \text{ m}^2 \text{ g}^{-1}$, $230 \text{ m}^2 \text{ g}^{-1}$ and $60 \text{ m}^2 \text{ g}^{-1}$ respectively, indicating that the highest surface area was reached with COF-80, which was prepared *via* the solvothermal reaction performed at 400°C . The pore size distribution (PSD) is a key factor that characterizes porous materials. Pore size distributions for COF-80, COF-77-A and COF-77-B are depicted in Figure 96.

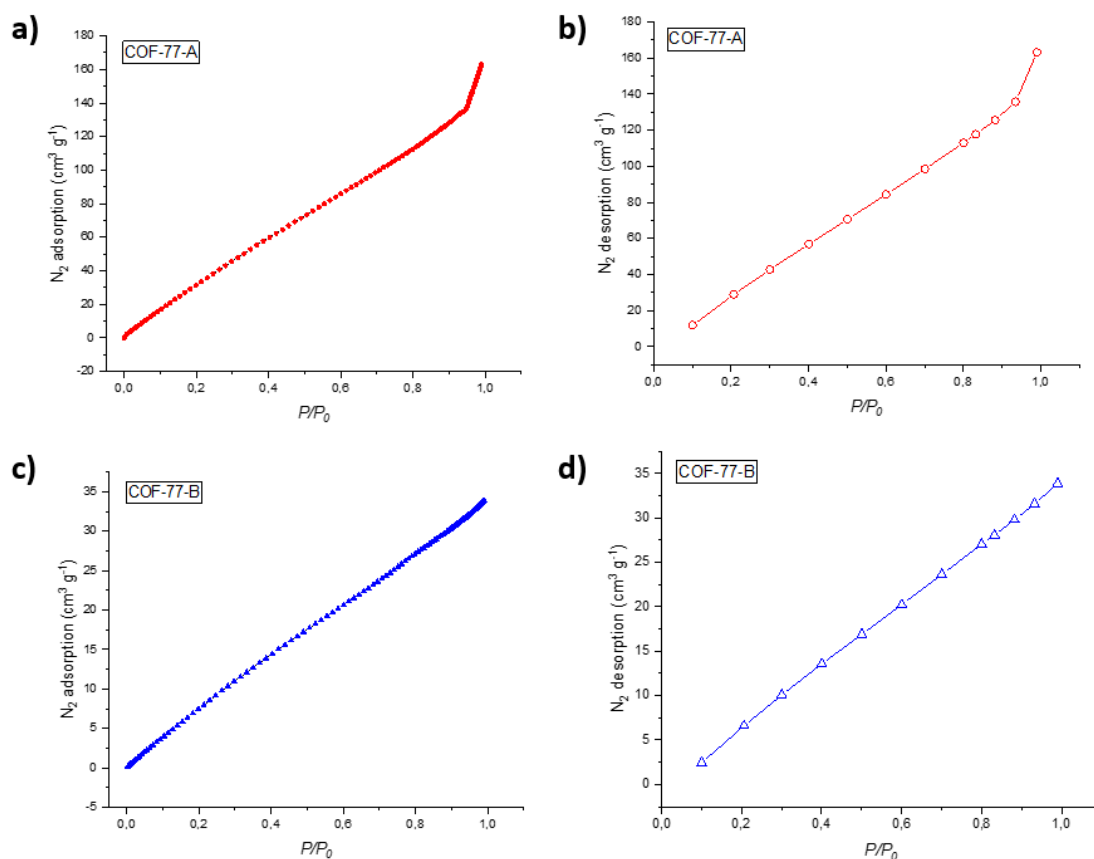


Figure 95. Nitrogen adsorption-desorption isotherms of COF-77-A and COF-77-B prepared in mild condition at low temperature using TFMSA as Brønsted acid catalyst for the cyclotrimerization reaction. a) N_2 adsorption isotherm of COF-77-A; b) N_2 desorption isotherm of COF-77-A; c) N_2 adsorption isotherm of COF-77-B; d) N_2 desorption isotherm of COF-77-B.

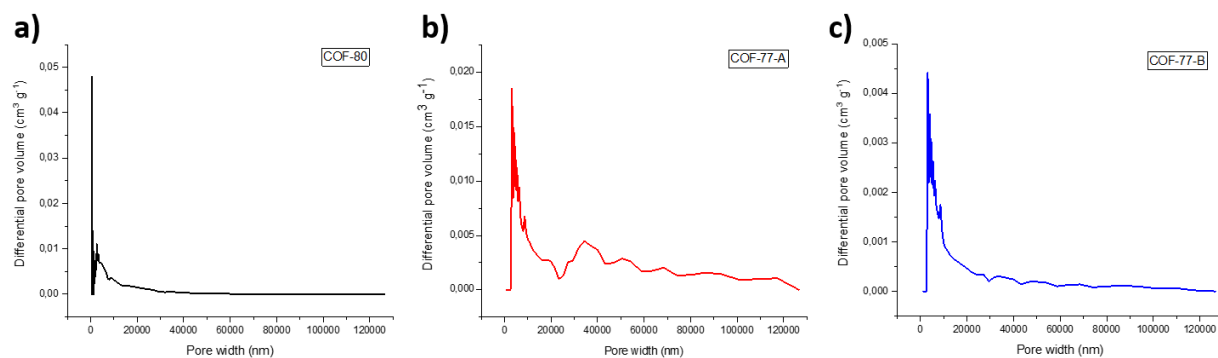


Figure 96. Pore size distribution (PSD) of COF-80 (a), COF-77-A (b) and COF-77-B. PSD were calculated using non-negative regularization, no smoothing density functional theory (DFT).

The PSD of COF-80 shows a homogeneous pore size distribution below 5 nm (microporous material), while for COF-77-A and COF-77-B the PSD is more heterogeneous and the pores are characterized by bigger size (mesoporous materials).

2.1.9 Conclusions

A novel family of star-shaped multi-photochromic molecules based on azobenzene photoswitches was designed and synthesized to study their photochromism as well as the supramolecular self-assembly at the solid (HOPG)/liquid interface. The photo-responsive compounds **3**, **27** and **23** bearing three, two and one azobenzene photochromic units respectively, are characterized by a peculiar structural geometry designed *ad hoc* to amplify the structural variation associated with the photoisomerization. The general structure consists on a benzene scaffold with three switchable and/or non-switchable molecular “arms” in the *meta* position reciprocally. The molecular design limits the π -conjugation and interactions between the azobenzene chromophores belonging to the same molecule, thus enabling their independent $E \leftrightarrow Z$ isomerization, but at the same time maintaining the rigidity of the structure. The analogous non-switchable derivative **10** and the linear azobenzenes **35** and **79** were employed as reference compounds for the studies. The investigation of photochromism of star-shaped tris(azobenzene) **3**, bis(azobenzene) **27** and mono(azobenzene) **23** molecules was performed using different techniques such as UV-Vis absorption spectroscopy, cyclic voltammetry (CV), differential pulse voltammetry (DPV), high performance liquid chromatography (HPLC), scanning tunnelling microscopy (STM) and advanced mass spectrometry methods as ion mobility (IMMS). UV-Vis absorption spectra, together with the presence of clear isosbestic points upon photoswitching and the photoisomerization quantum yields values of **3**, **27** and **23**, basically not different from the values obtained for the reference compounds **35** and **79**, provided evidence of almost complete absence of electron delocalization between the azobenzene units present in the same molecule. This was further observed by cyclic and differential pulse voltammetries showing that the reduction of the azobenzene moieties in our multi-photochromic star-shaped derivatives occurs at the same potential. IMMS experiments were performed to study for the first time such multi-chromophoric star-shaped molecules with this technique, revealing the occurrence of a large shape-variation upon photoisomerization. Finally, the self-assembly of **3** on graphite surface was investigated by means of STM both at the solid-liquid and at the solid-air interfaces. When no irradiated, the (*E,E,E*)-isomer form highly tight ordered 2D crystalline packing domains, which arise from the occurrence of strong π - π and van der Waals interactions between the planar all-(*E*)-isomer and the substrate. Subsequently, upon *in situ* irradiation with UV light, $E \rightarrow Z$ isomerization takes places causing a loss of the crystallinity associated with (*E,E,E*)-**3** and the visualization of ordered domains containing only (*E,Z,Z*)-**3** or (*E,E,Z*)-**3**. The experimental data were corroborated by MM/MD simulation of the self-assembly for each isomeric

species. Furthermore, no packing related to the all-(*Z*) form was observed, which can be explained because of the non-planarity of (*Z,Z,Z*)-**3** which results completely desorbed from the substrate. Star-shaped tris(azobenzene) **3** was proposed as a photoswitchable organic ligand for the construction of photoresponsive metal-organic frameworks. Although the deprotonated carboxylic groups introduced at the azobenzene unit termini might form a strong metal-oxygen bond characteristic of MOF architecture, no crystalline materials have been obtained by solvothermal method. Moreover, a novel star-shaped tris(CN-azobenzene) **30** was synthesized as a photoresponsive building block for the preparation of triazine-based covalent organic frameworks *via* cyclotrimerization of the benzonitrile termini. Interestingly, the attempts performed towards triazine-based COFs either *via* solvothermal reaction (COF-**80**) at high temperature in a ceramic oven using ZnCl₂ as Lewis acid-catalyst, or *via* a low temperature reaction (COF-**78** and COF-**79**) using TfOH as Brønsted acid-catalyst provided porous materials characterized by different specific surface areas. The obtained materials were analyzed by FTIR spectroscopy, nitrogen adsorption-desorption measurements and elemental analysis, which confirmed the formation of the triazine ring and the absence of the nitrile groups, as well as the porosity of the material. Whereas for COF-**80** the characteristic N₂-adsorption isotherm of a microporous material was observed, COF-**78** and COF-**79** were found to be mesoporous. Furthermore, COF-**80** exhibits the highest surface area value (530 m² g⁻¹) with respect to COF-**77-A** (230 m² g⁻¹) and COF-**77-B** (60 m² g⁻¹) prepared under milder conditions with TfOH.

2.2 Hexa-*peri*-hexabenzocoronene derivatives bearing azobenzene photoswitches⁹

Polycyclic aromatic hydrocarbons (PAHs) are a widely studied class of compounds featuring unique physical and chemical properties, which make these materials appealing candidates for applications in organic electronics.^[122] Among polycyclic aromatic hydrocarbons, disk-like PAHs such as hexa-*peri*-hexabenzocoronene (HBC)^[140] are particularly noteworthy. The symmetrical structure of HBC is characterized by an extended π -system, which allows supramolecular self-assembly into columns by means of strong π - π intermolecular interactions between the aromatic cores. The strong intermolecular forces occurring between HBC molecules make this material extremely stable and insoluble, and on the other hand, enable charge transport through the columnar axis, which is particularly important in semiconductive materials.

2.2.1 Motivation

In the present work the design, synthesis and characterization of a series of multi-photochromic systems based on HBC derivatives functionalized with azobenzene photoswitches are discussed (Figure 97). These molecules were proposed for the investigations of the influence of the azobenzene units on the HBC self-assembly into columnar structures (discotics) upon UV/Vis light irradiation and, on the other hand, for the study of the electronic conductivity through the assemblies. The azo-HBC derivatives proposed contain from three (**3-azo-HBC**) to six (**6-azo-HBC-01** and **6-azo-HBC-02**) azobenzene units. As aforementioned, due to the strong π - π staking interactions HBC compounds feature typical insolubility, which represents one of the main limitations of these materials. Therefore, long alkoxy chains were introduced into the structure to solve this issue. Whereas derivatives **6-azo-HBC-01** (**74**) and **6-azo-HBC-02** (**75**) contain six photoswitchable azobenzene units bearing long branched alkoxy chains at their termini, **3-azo-HBC** (**76**) consists of three cyano-azobenzene units, and the solubilizing alkoxy chains are introduced directly onto the HBC core. Furthermore, the geometry of **3-azo-HBC** reminds the molecular structure of star-shaped tris(CN-azobenzene) **30** in which the central benzene scaffold is replaced with the so-called “super-benzene” HBC core. Therefore, derivative **76** might also be conceived as a potential photoresponsive building block for the construction of optically triggered covalent organic frameworks.

⁹ The compounds discussed in this section were proposed for my 2nd secondment in the groups of Prof. K. Müllen and Dr. A. Narita at the Max-Planck Institute for Polymer Research (Mainz, Germany), whom are greatly acknowledged.

2.2.2 Synthesis of 6-azo-HBC-01 (74)

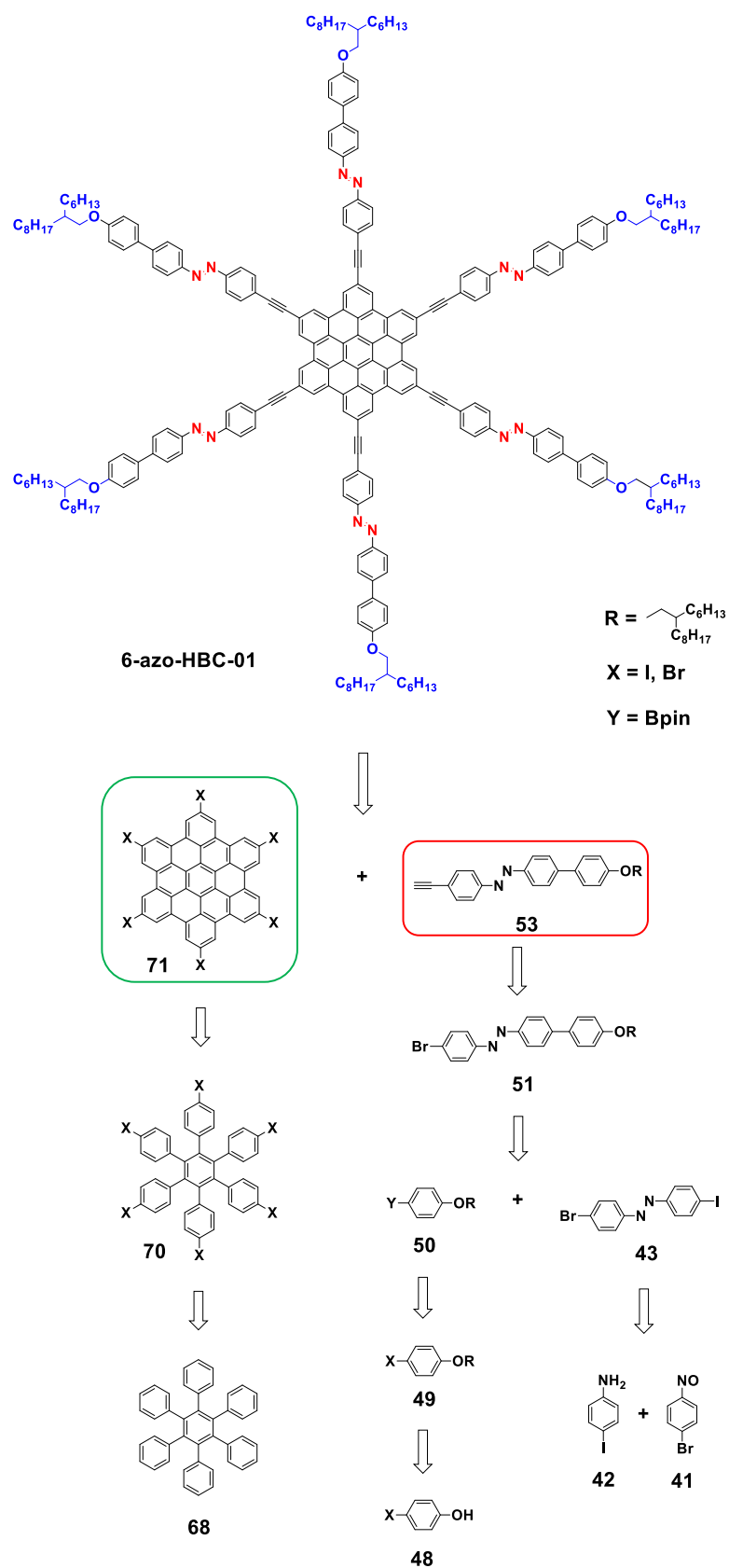


Figure 98. Retrosynthetic analysis towards **6-azo-HBC-01** (74) based on the assembly of two main building blocks: the photoswitchable azobenzene **53** and the rigid HBC core **71** via Sonogashira cross-coupling reaction.

The retrosynthetic approach towards **6-azo-HBC-01 (74)** is displayed in Figure 98. The two building blocks, namely the alkoxy-azobenzene **53** and 2,5,8,11,14,17-hexa-iodohexa-*peri*-hexabenzocoronene (**71**), were assembled *via* Sonogashira cross-coupling reaction. The HBC core was prepared through a two-steps synthesis, by Scholl oxidative coupling of hexakis(4-iodophenyl)benzene (**70**), which was obtained by iodination of hexaphenylbenzene (**68**). On the other hand, the photoswitchable alkoxy azobenzene **53** was prepared *via* Sonogashira cross-coupling reaction between trimethylsilylacetylene and azobenzene **51**. The latter was assembled *via* Suzuki-Miyaura reaction of 4-iodo-4'-bromoazobenzene (**43**) with the alkoxy-phenylpinacolboronic ester **50**. Azobenzene **43**, synthesized by Mills reaction between 4-iodoaniline (**41**) and 4-nitrosobromobenzene (**42**), was designed as modular building block for the preparation of different azobenzenes (**46**, **53** and **54**) used as photochromic “molecular-arms” for the functionalization of HBC derivatives **74-76**. Finally, derivative **50** was obtained *via* etherification of 4-bromophenol (**48**) with 7-(bromomethyl)pentadecane.

The synthesis towards ethynyl-alkoxyazobenzene **53** (Figure 99) was developed in a way that the synthetic intermediates can be employed as modular building blocks for the preparation of other structurally similar azobenzenes such as alkoxy-azobenzenepinacolboronic ester (**54**) and cyano-azobenzenepinacolboronic ester (**46**). The structure of target molecule **53** consists of two building blocks: an azobenzene and an alkoxyphenyl unit. The synthesis of 2-{4-[(2-hexyldecyl)oxy]phenyl}-4,4,5,5-tetramethyl-1,3,2-dioxaborolane (**50**), namely the alkoxyphenyl building block, starts with the introduction of a branched alkoxy chain into 4-bromophenol (**48**) in typical Williamson etherification conditions using K₂CO₃ as a base in acetone to afford the desired product **49** in 77% yield. Subsequently, 1-bromo-4-[(2-hexyldecyl)oxy]benzene (**49**) was converted into the corresponding pinacolboronic ester **50** *via* palladium-catalyzed Miyaura borylation using a slight excess of bis(pinacolato)diboron in dioxane in 83% yield. On the other hand, the synthesis of the azobenzene building block **43** begins with a Mills reaction between 4-iodoaniline (**42**) and 4-nitrosobromobenzene (**41**); the latter was freshly prepared by oxidation of 4-bromoaniline (**40**) with Oxone® in a biphasic system of H₂O and CH₂Cl₂ in 91% yield. The crude nitroso derivative **41** was directly used for the next reaction step, and it afforded the desired azobenzene **43** in 76% yield. Alkoxy-azobenzene **51** was prepared *via* Suzuki-Miyaura cross-coupling reaction between azobenzene **43** and derivative **50**. In order to selectively substitute the iodine atom with the alkoxyphenyl unit, only one equivalent of compound **50** at a lower reaction temperature was used affording the desired product **51** as an orange wax in 61% yield.

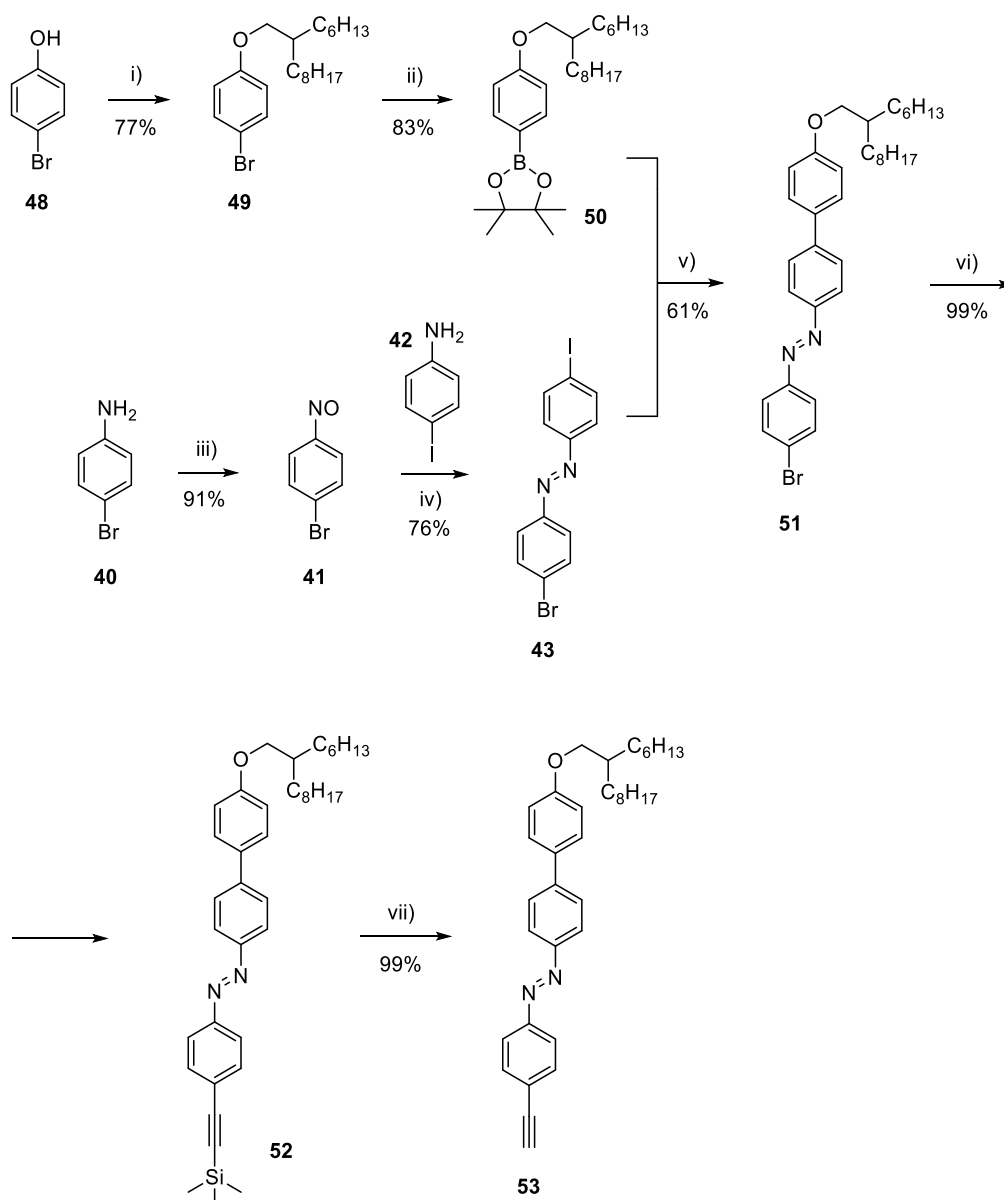


Figure 99. Synthetic strategy towards ethynyl-alkoxyazobenzene (**53**). Reagents and conditions: i) 7-(bromomethyl)pentadecane, K_2CO_3 , acetone, reflux; ii) bis(pinacolato)diboron, $\text{Pd}(\text{dppf})\text{Cl}_2$, AcOK, dioxane, 90 °C; iii) Oxone®, H_2O , CH_2Cl_2 , RT; iv) AcOH, RT; v) $\text{Pd}(\text{dppf})\text{Cl}_2$, K_2CO_3 , H_2O , dioxane, 85 °C; vi) ethynyltrimethylsilane, $\text{Pd}(\text{PPh}_3)_2\text{Cl}_2$, CuI, Et_3N , 65 °C; vii) K_2CO_3 , MeOH, THF, RT.

Sonogashira cross-coupling reaction between azobenzene **51** and a large excess of ethynyltrimethylsilane afforded derivative **52** in quantitative yield. The final hydrolysis of the latter under basic conditions yielded the desired ethynyl-alkoxyazobenzene **53** as an orange wax quantitatively.

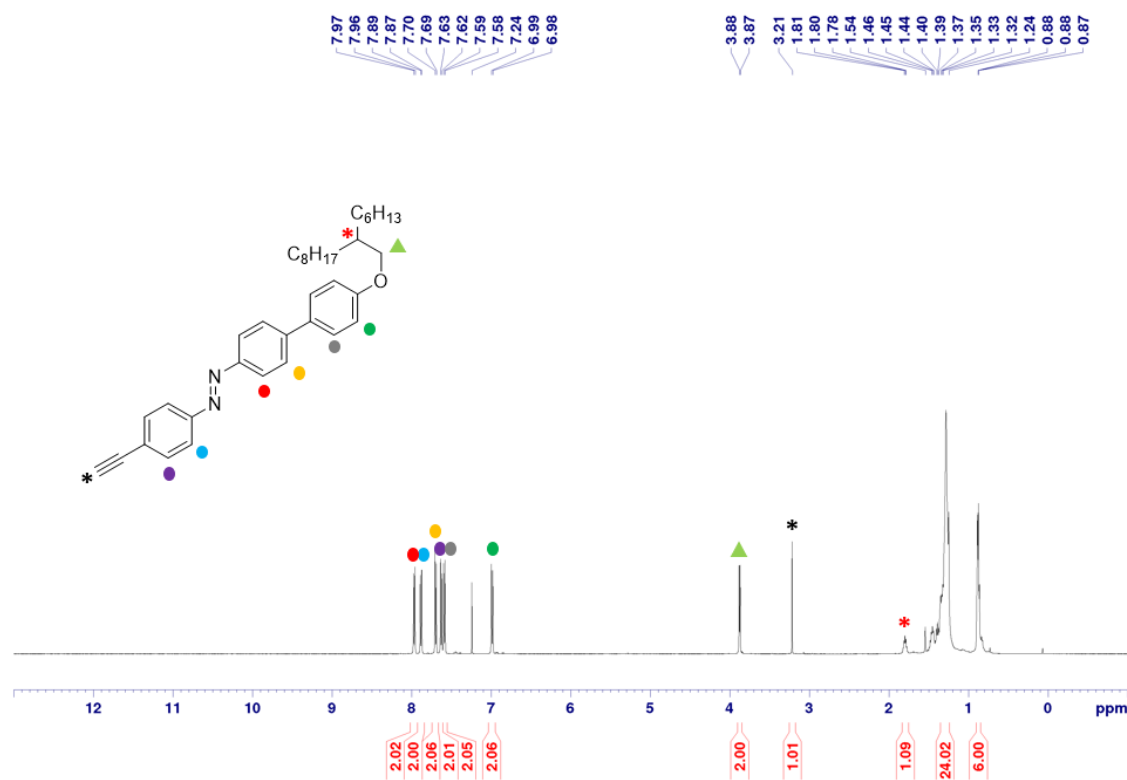


Figure 100. ^1H NMR spectrum of ethynyl-alkoxyazobenzene **53** measured in deuterated chloroform (CDCl₃) at RT.

The synthetic pathway towards the HBC building block **71** is outlined in Figure 101. The synthesis starts with the iodination of hexaphenylbenzene (**68**) using phenyliodine bis(trifluoroacetate) (PIFA) and iodine (I₂) to afford derivative **70** in quantitative yield. PIFA is an hypervalent iodine reagent known for its oxidative character. When treated with iodine in a chlorinated solvent, PIFA gives mild iodination reaction mixtures particularly useful in organic synthesis.^[275] Finally, the hexa-*peri*-hexabenzocoronene core was synthesized *via* Scholl oxidative coupling reaction following a modified literature procedure.^[276] The Scholl reaction is a crucial step for the preparation of HBC derivative. Although the reaction procedure appears easy and simple to perform, some critical aspects need to be considered. Firstly, the use of iron(III) chloride (anhydrous) as Lewis acid mild oxidative agent might cost side chlorination reactions because of the hydrochloric acid (HCl) generated during the reaction. Therefore, the reaction mixture needs to be constantly purged with an inert gas flow during the entire reaction time to prevent chlorination by removing the gaseous HCl. Secondly, non-stabilized dichloromethane needs to be used as a solvent to eliminate side reactions caused by stabilizing agents.

6-azo-HBC-01 (74) was finally assembled *via* Sonogashira cross-coupling reaction between HBC **71** and azobenzene **53** (Figure 103).

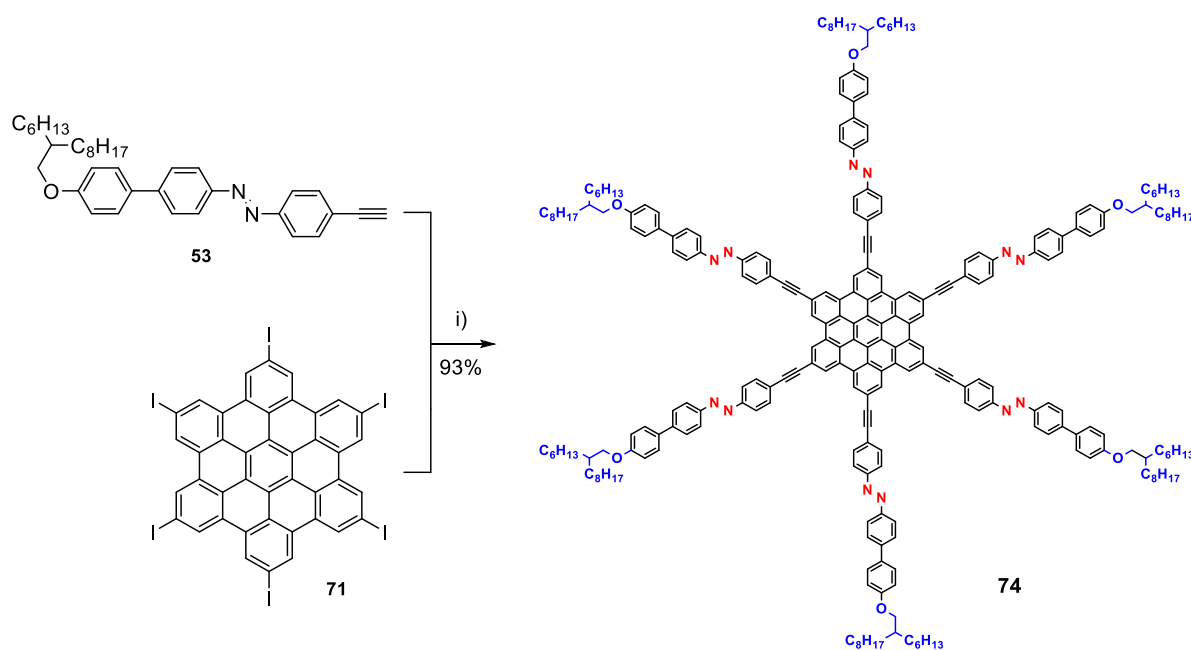


Figure 103. Synthesis of **6-azo-HBC-01 (74)** *via* Sonogashira cross-coupling reaction between HBC **71** and azobenzene derivative **53**. Reagents and conditions: i) Pd(PPh₃)₄, CuI, THF, piperidine, 60 °C.

The Sonogashira cross-coupling was performed according to a modified literature procedure reported by Dössel *et al.*^[277] At first, several attempts towards the synthesis of 2,5,8,11,14,17-hexakis[4-(*tert*-butyl)ethynyl]hexa-*peri*-hexabenzocoronene (**73**) *via* Sonogashira coupling between HBC **71** and 4-(*tert*-butyl)phenylacetylene (**72**) have been performed to optimize the reaction conditions (synthesis of derivative **73**, Experimental Part). Subsequently, it was possible to prepare the target molecule **74** in 93% yield. Due to the insolubility of HBC **71**, the cross-coupling reaction takes place at the interface between the solution containing azobenzene **53** and the insoluble HBC **71**. The latter became gradually more soluble after its coupling with the azobenzene units bearing solubilizing branched alkoxy chains. **6-azo-HBC-01 (74)** resulted thus well soluble in common organic solvents, and its characterization by solid-state techniques (MALDI-TOF MS, FTIR, EA) was also corroborated by NMR spectroscopy in solution. In the MALDI-TOF MS spectrum of **74** (Figure 104) a very weak peak corresponding to the product is observed. The low intensity of the molecular ion peak is due to the very low ionizability of such compounds. Moreover, due to the high tendency to form columnar aggregates, ¹H NMR spectrum measured at room temperature did not show any significant peak in the aromatic region. Thus, high temperature (at 383 K) ¹H NMR was measured using deuterated 1,1,2,2-tetrachloroethane (C₂D₂Cl₄) as a solvent (Figure 105). In the ¹H NMR spectrum measured at 383 K broad peaks are observed, and peaks corresponding to the alkoxy chains (δ ppm 1.44 – 1.01) are characterized by higher intensity.

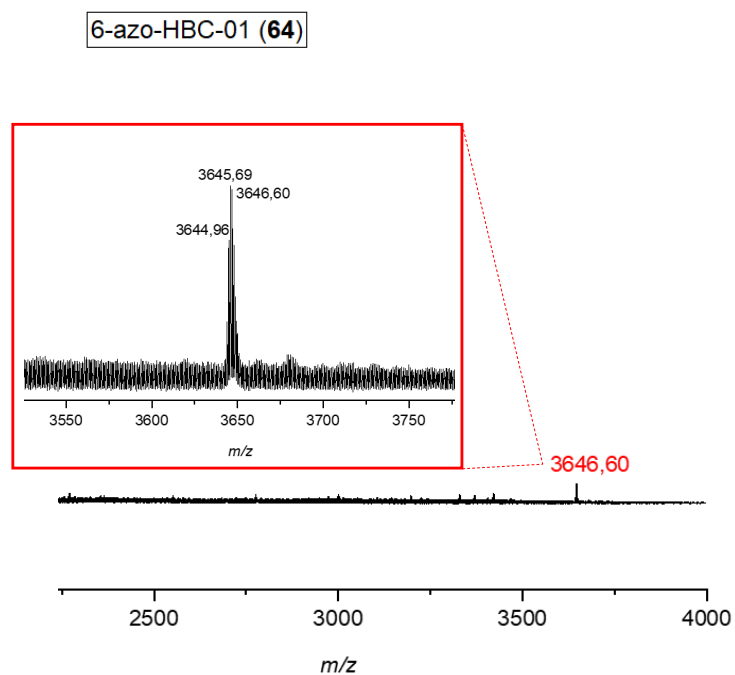


Figure 104. MALDI-TOF MS (+) spectrum of **6-azo-HBC-01 (74)** measured using TCNQ matrix. The weak intensity of the molecular ion peak is due to the low ionizability of such compound.

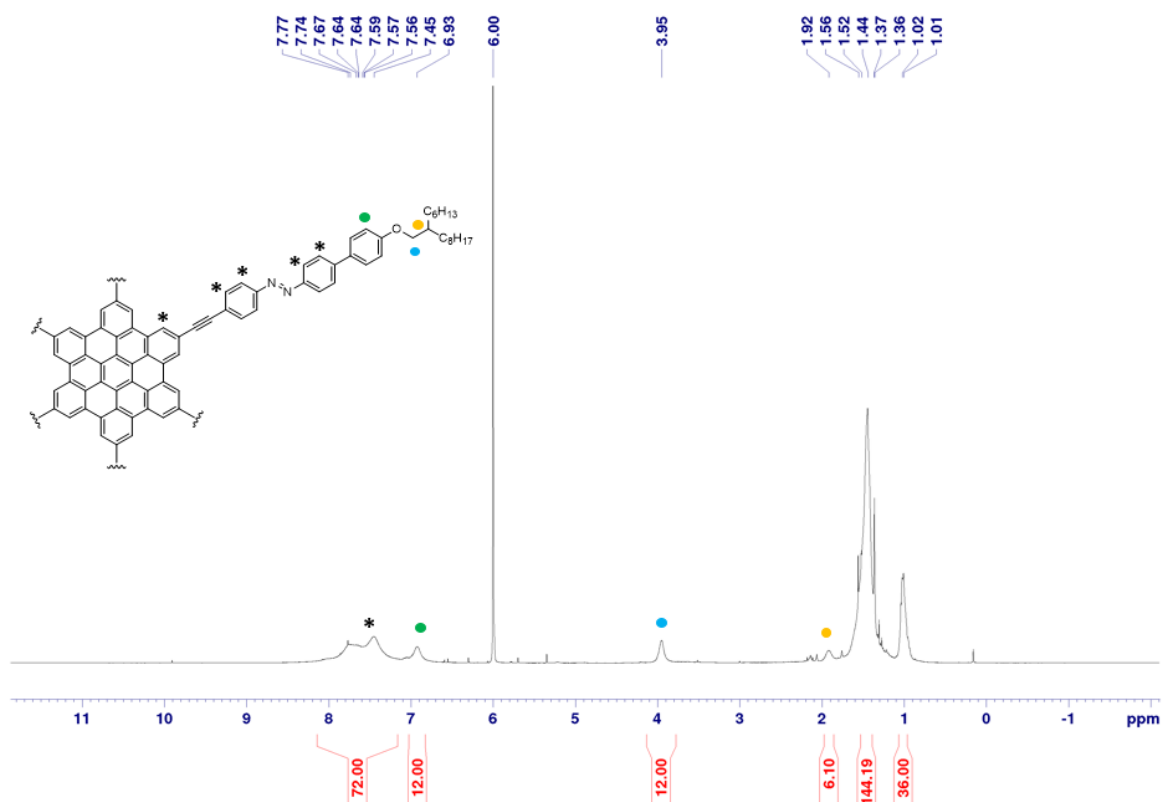


Figure 105. ^1H NMR spectrum of **6-azo-HBC-01 (74)**, measured in deuterated 1,1,2,2-tetrachloroethan ($\text{C}_2\text{D}_2\text{Cl}_4$) at 383 K.

Preliminary experiments on **6-azo-HBC-01** photochemical behavior have been performed by means of UV-Vis spectroscopy, and the absorption spectra obtained before and after UV irradiation are displayed in Figure 106.

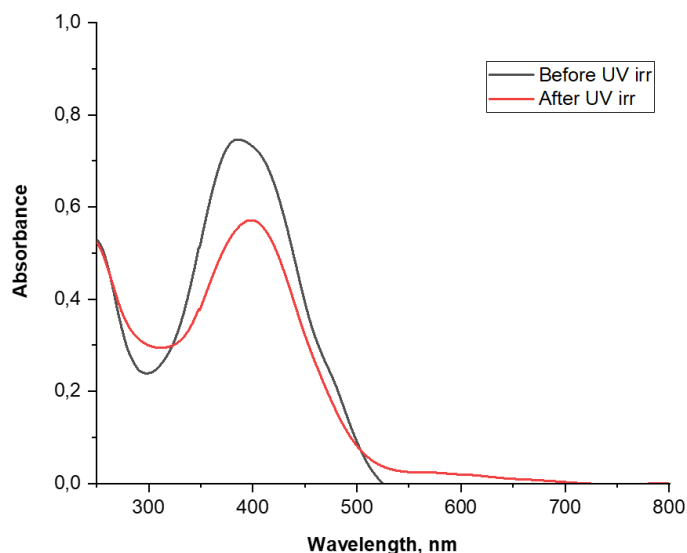


Figure 106. UV-Vis of **6-azo-HBC-01** (**74**) upon UV light irradiation ($\lambda_{\text{irr}} = 350$ nm) in DCM ($c = 10^{-6}$ M). *Black line*, no irradiation; *red line*, after 3 hours of irradiation with UV light.

The photoisomerization of **6-azo-HBC-01** (**74**) was investigated upon irradiation with UV light ($\lambda_{\text{irr}} = 350$) of a dichloromethane solution of compound **74** ($c = 10^{-6}$ M). Before UV irradiation, the UV/Vis spectrum shows an absorption band at *ca.* 385 nm, which according to our interpretation corresponds to the π - π^* transition band of azobenzene slightly red-shifted due to the extended conjugation within the structure. As the HBC core absorption falls in the same wavelength range of azobenzene π - π^* transition, the two absorption bands result overlapped. Interestingly, after irradiating the solution with UV light for 3 hours a decrease of absorption together with a bathochromic shift (*ca.* 14 nm) of the latter was observed. Furthermore, a weak absorption band at *ca.* 570 nm appeared.

2.2.3 Synthesis of 6-azo-HBC-02 (75)

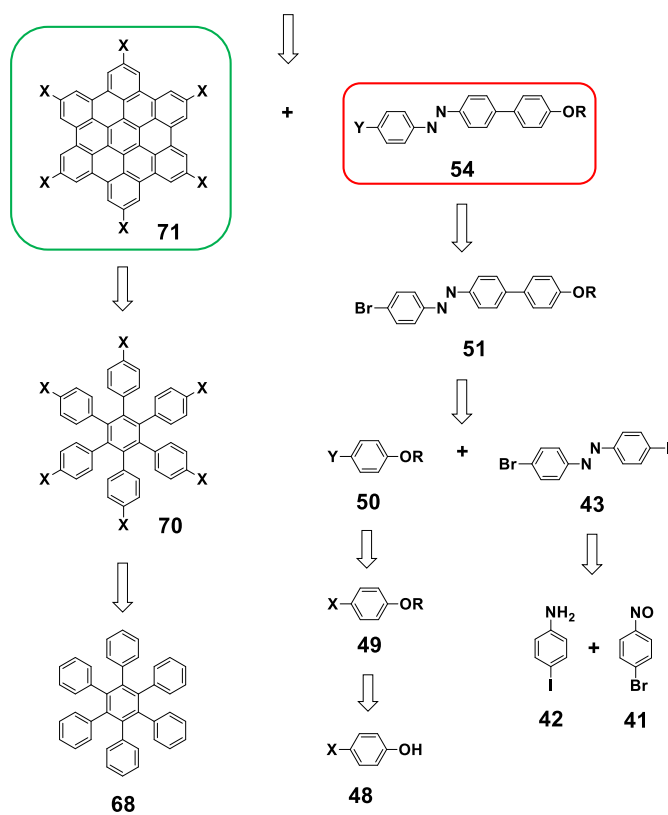
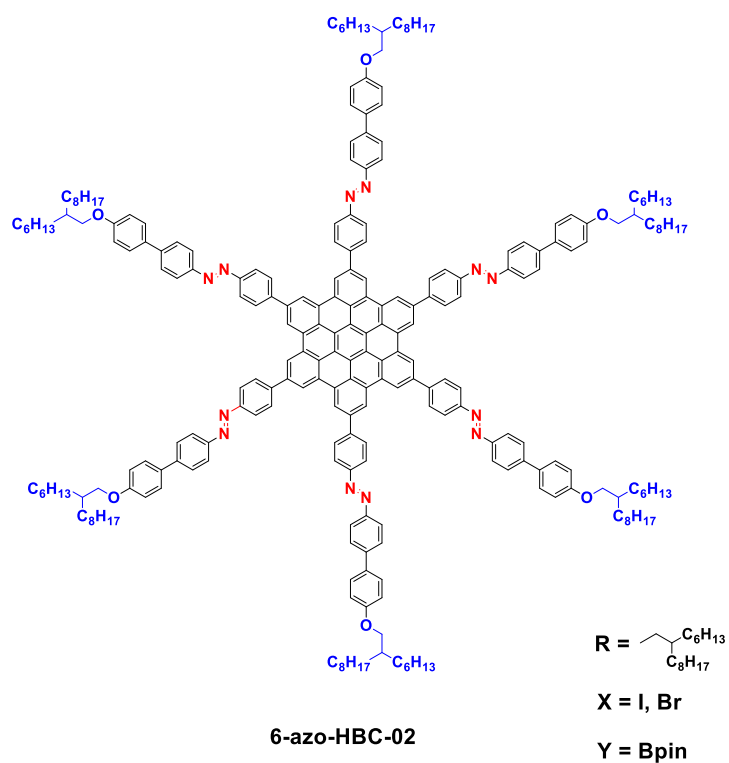


Figure 107. Retrosynthetic analysis towards **6-azo-HBC-02 (74)** based on the assembly of two main building blocks: the photoswitchable azobenzene **54** and the rigid HBC core **71** via Suzuki-Miyaura cross-coupling reaction.

The retrosynthetic approach towards **6-azo-HBC-02 (75)** is basically analogous to the one employed for the preparation of compound **74**. It consists on the assembly of the rigid HBC and the photoswitchable azobenzene units (Figure 107). Whereas in molecule **74** the two building blocks (HBC **71** and azobenzene **53**) were coupled *via* Sonogashira reaction, Suzuki-Miyaura cross-coupling reaction was employed for the final assembly of building blocks **71** and **54**. In such structure, the absence of acetylene bridges between the rigid HBC core and the photoswitchable azobenzene unit is responsible of a decreased planarity. Therefore, intermolecular aggregation between **6-azo-HBC-02** monomers is expected to be moderate with respect to **6-azo-HBC-01**. The synthetic pathway towards HBC **71** has been already discussed above (Figure 101). On the other hand, azobenzene **54** is obtained by Miyaura borylation of the alkoxyazobenzene **51**, whose synthesis has been already displayed in Figure 99.

The synthesis of azobenzene **54** follows the same synthetic steps performed for the preparation of azobenzene **53** with a difference in the two final steps (Figure 108). Azobenzene intermediate **51**, indeed, is directly converted to the desired pinacolboronic ester **54** *via* Miyaura borylation reaction in dioxane in 83% yield.

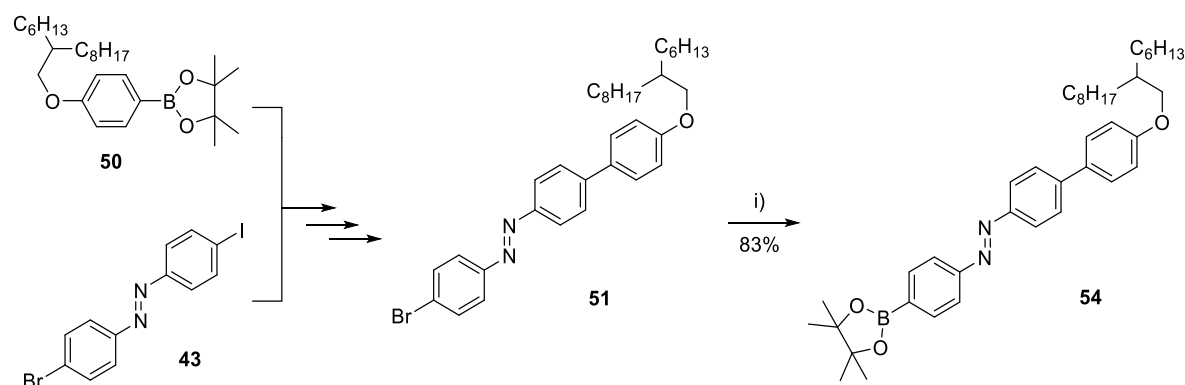


Figure 108. Synthetic pathway towards alkoxyazobenzene pinacolboronic ester **54**. Reagents and conditions: i) Bis(pinacolato)diboron, Pd(dppf)Cl₂, AcOK, dioxane, 90 °C.

With the two building blocks (azobenzene **54** and HBC **71**) in hands, it was finally possible to assemble target molecule **6-azo-HBC-02 (75)** *via* Suzuki-Miyaura cross-coupling reaction. As the first attempts performed under standard Suzuki conditions failed, the use of a ligand, whose palladium-complex exhibit high activity for the coupling, was required. To this purpose, 2-dicyclohexylphosphino-2',6'-dimethoxyphenyl (S-Phos) was employed as a ligand.^[278,279] The ligand-palladium complex facilitates the oxidative addition step and may prevent the catalyst decomposition.

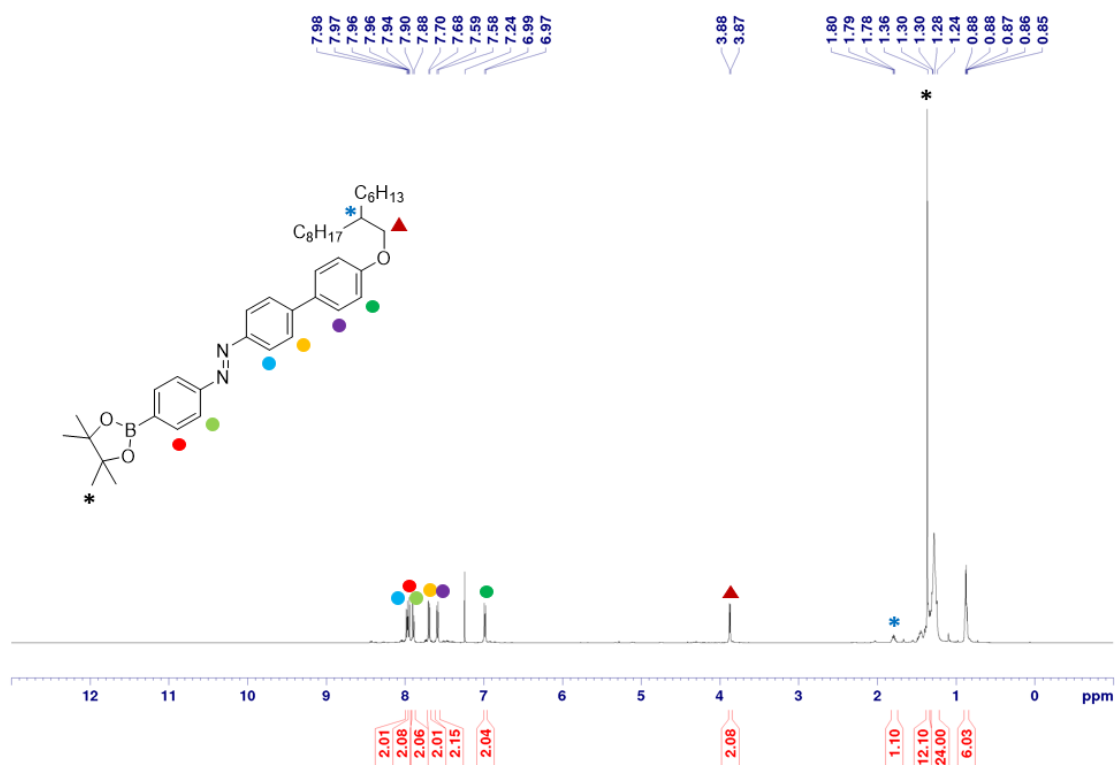


Figure 109. ^1H NMR spectrum (500 MHz) of alkoxyazobenzene pinacolboronic ester **54**, measured in deuterated chloroform (CDCl_3) at RT.

HBC **71** was reacted with a large excess of azobenzene **54** and S-Phos in Suzuki-Miyaura conditions to afford the target molecule **75** in 91% yield.

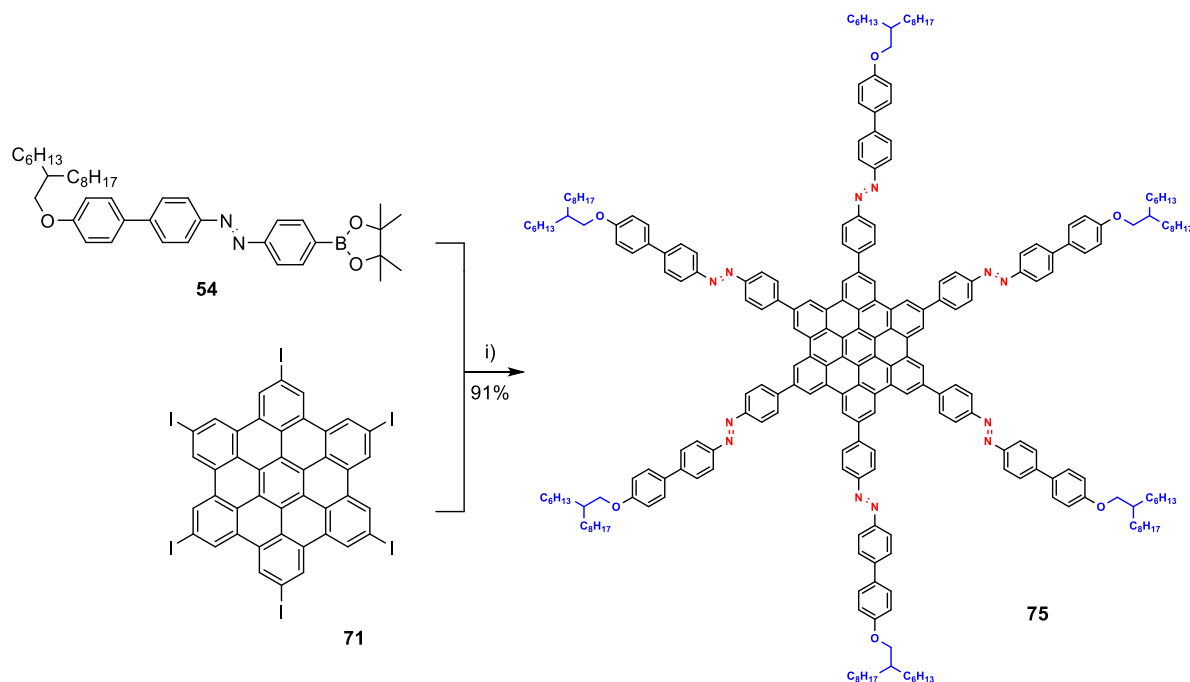


Figure 110. Synthesis of 6-azo-HBC-02 (**75**) via Suzuki-Miyaura cross-coupling reaction between HBC **71** and azobenzene derivative **54**. Reagents and conditions: i) $\text{Pd}(\text{PPh}_3)_4$, K_2CO_3 , S-Phos, H_2O , EtOH, toluene, 60°C .

6-azo-HBC-02 (75) was found to be nicely soluble in common organic solvents. MALDI-TOF MS results (Figure 111) were further corroborated by NMR spectroscopy (Figure 112), as well as FTIR spectroscopy, UV/VIS spectroscopy.

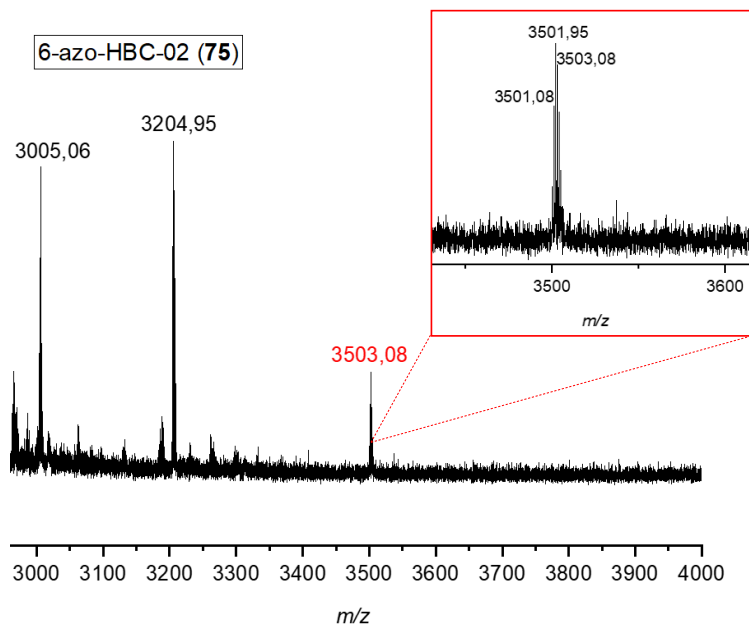


Figure 111. MALDI-TOF MS (+) spectrum of **6-azo-HBC-02 (75)** measured using TCNQ matrix. The weak intensity of the molecular ion peak is due to the low ionizability of such compound.

As already discussed for **6-azo-HBC-01 (74)**, **6-azo-HBC-02 (75)** is difficult to be ionized and therefore its MALDI spectrum displays a weak molecular ion peak. Moreover, the baseline noise observed in the spectrum was typical for HBC derivatives whose MALDI spectra were measured using TCNQ as a matrix. As for molecule **74**, the ^1H NMR spectrum of **75** was recorded at high temperature (383 K). The spectrum shows broad peaks, whose integration fits with the target molecule **75**. The signals with higher intensity at δ ppm 1.46 – 0.91 correspond to the alkoxy chains at the azobenzene termini. Preliminary experiments on photoisomerization of **6-azo-HBC-02 (75)** upon UV irradiation were performed on a solution of **75** in dichloromethane, and the absorption spectra obtained are depicted below (Figure 113). The photoisomerization of **75** ($c = 10^{-6}$ M in DCM) was studied upon irradiation with UV light ($\lambda_{\text{irr}} = 350$ nm). Before irradiation, an absorption band at *ca.* 384 nm was observed. Irradiation with UV light afforded a small decrease of absorbance together with a slight red shift of the absorption band of *ca.* 5 nm. As already mentioned for **6-azo-HBC-01 (74)**, the comprehensive explanation of the photochemical behavior of such compounds is still under investigation.

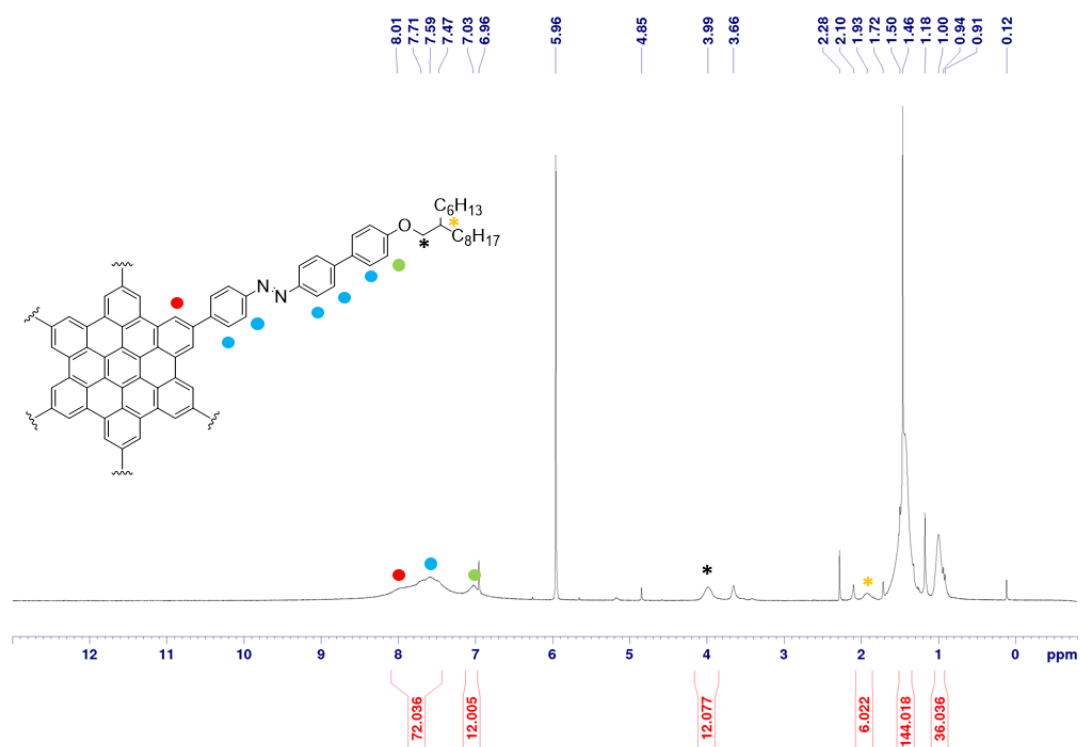


Figure 112. ^1H NMR spectrum of **6-azo-HBC-02 (75)**, measured in deuterated 1,1,2,2-tetrachloroethan (CD_2Cl_4) at 283 K.

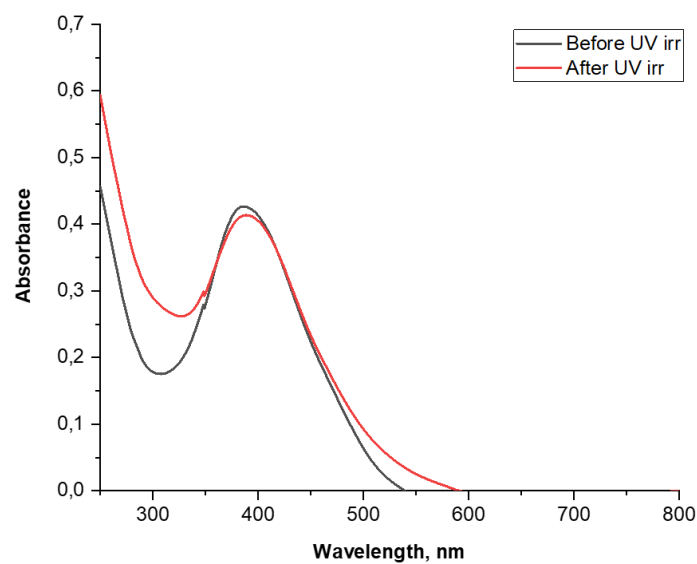


Figure 113. UV-Vis of **6-azo-HBC-02 (75)** upon UV light irradiation ($\lambda_{\text{irr}} = 350 \text{ nm}$) in DCM ($c = 10^{-6} \text{ M}$). *Black line*, no irradiation; *red line*, after 3 hours of irradiation with UV light.

2.2.4 Synthesis of 3-azo-HBC (76)

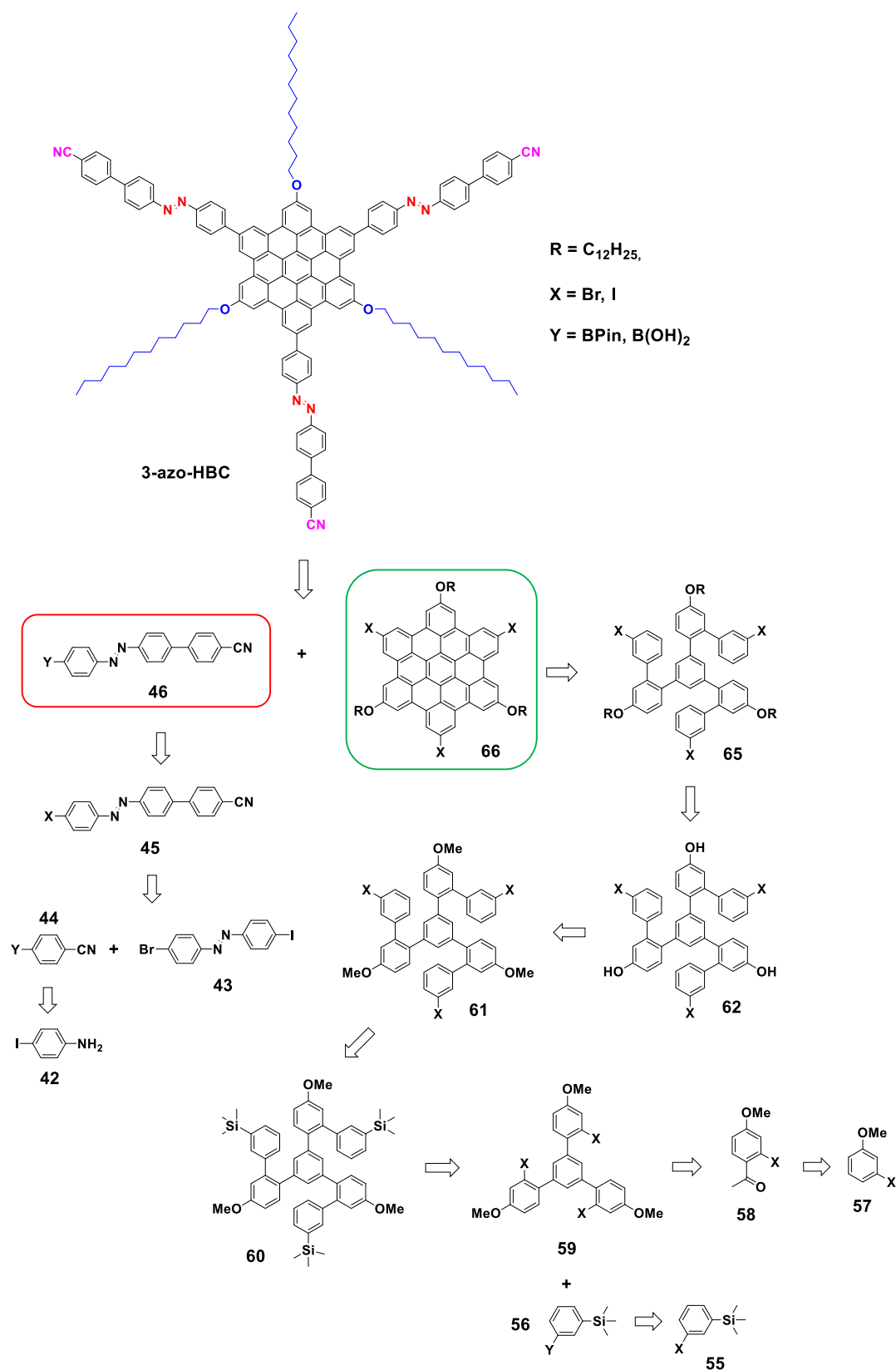


Figure 114. Retrosynthetic analysis towards **3-azo-HBC (76)** based on the assembly of two main building blocks: the photoswitchable azobenzene **46** and the rigid alkoxy-HBC core **66** via Suzuki-Miyaura cross-coupling reaction.

Target molecule **3-azo-HBC (76)** has been designed as analogous of star-shaped azobenzene derivatives already described in Chapter 2.1. In particular, its molecular structure reminds star-shaped tris(CN-azobenzene) **30** where the benzene core is replaced with the bigger aromatic HBC conferring a higher rigidity. Furthermore, long alkoxy chains have been introduced in the HBC core for solubilization of the material and thus, for its processability and for the investigations on self-assembly features. The retrosynthetic approach (Figure 114) towards **3-azo-HBC (76)** is based on the preparation of two building blocks: a photoswitchable azobenzene unit and an alkoxy-HBC core. The two building blocks were separately prepared and linked together *via* Suzuki-Miyaura cross-coupling reaction. In this molecule cyano groups were introduced as the azobenzene termini to employ **3-azo-HBC** as a photoresponsive unit in optically triggered COFs.

Azobenzene **46** was prepared following the same synthetic pathway used for the preparation of derivative **43**, which was then reacted with the 4-cyanophenylboronic acid (**44**) *via* Suzuki cross-coupling reaction. On the other hand, alkoxy-HBC **66** was obtained by Scholl oxidative coupling of derivative **65**, which was prepared by alkylation of trihydroxy derivative **62** under Mitsunobu conditions. The demethylation of trimethoxy derivative **61** using boron tribromide (BBr₃) afforded the trihydroxy compound **62**. Derivative **61** was obtained by iodination of the corresponding trimethylsilyl derivative **60**, which was previously assembled *via* Suzuki-Miyaura cross-coupling reaction between 1,3,5-triphenylbenzene **59** and pinacolboronic ester **56**. The latter was synthesized *via* Miyaura borylation of 3-trimethylsilyl-bromobenzene (**55**) with bis(pinacolato)diboron. Finally, 1,3,5-triphenylbenzene **59** was prepared *via* cyclotrimerization of 4-methoxy-2-bromoacetophenone **58**, which was obtained by Friedel-Crafts acylation of 3-bromoanisole (**57**) with acetyl chloride.

The synthetic strategy used for the preparation of cyano-azobenzene **46** is depicted in Figure 115. The synthesis of cyano-azobenzene building block (**46**) begins with the intermediate **43**, whose synthesis has been already discussed. Subsequently, the introduction of cyanophenyl group was achieved through a Suzuki-Miyaura reaction between azobenzene **43** and 4-cyanophenylboronic acid (**44**) in dioxane. In order to selectively obtain the mono-substituted product **45** only one equivalent of compound **44** was used, and the desired product **45** was isolated in 72% yield. Finally, Miyaura borylation of derivative **45** with bis(pinacolato)diboron afforded azobenzene **46** in 91% yield.

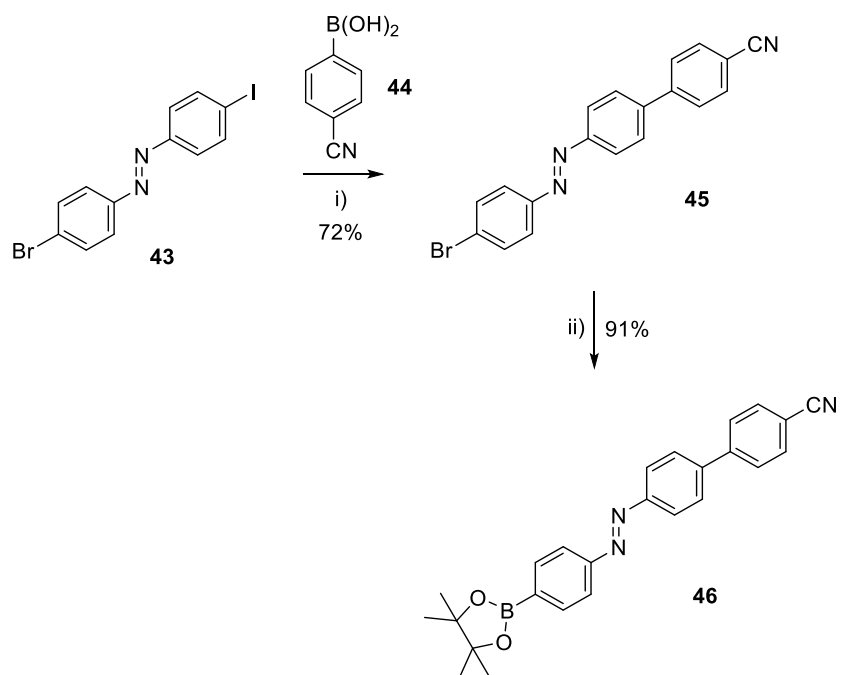


Figure 115. Synthetic strategy towards cyano azobenzene (**46**). Reagents and conditions: i) Pd(dppf)Cl₂, K₂CO₃, H₂O, dioxane, 90 °C; ii) bis(pinacolato)diboron, Pd(dppf)Cl₂, AcOK, dioxane, 90 °C.

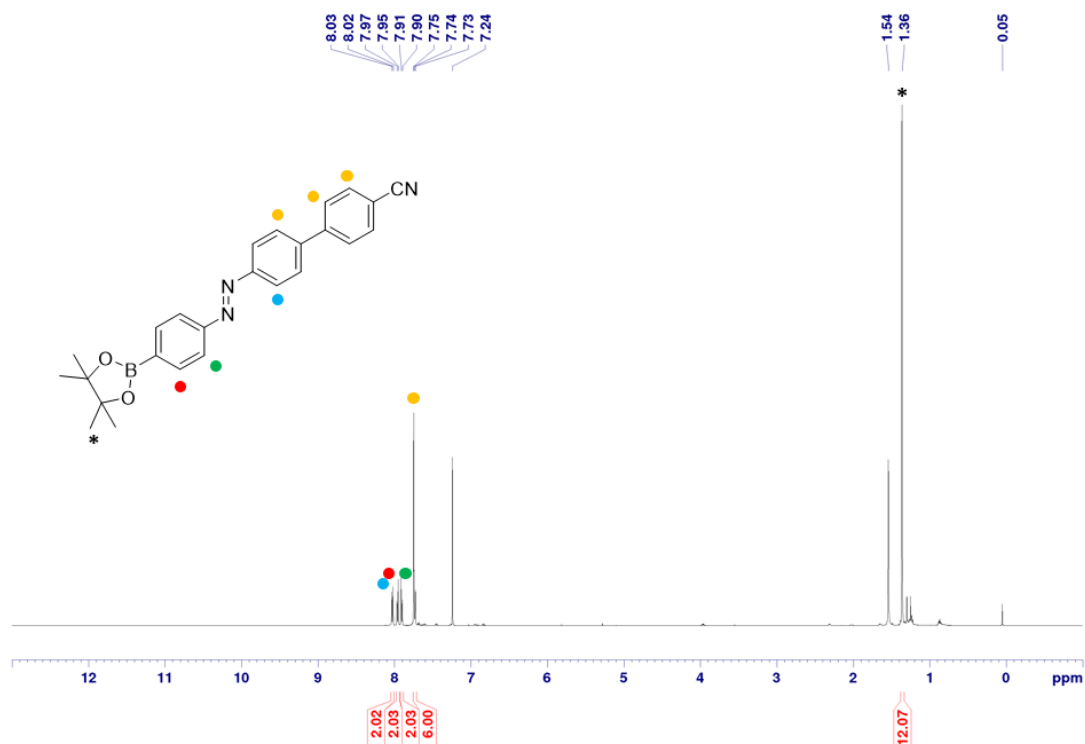


Figure 116. ¹H NMR spectrum of cyano-azobenzene **46** measured in deuterated chloroform (CDCl₃) at room temperature.

The synthetic pathway towards alkoxy-HBC **66** is outlined in Figure 117. It starts with the preparation of 4-methoxy-3-bromoacetophenone (**58**) from 3-bromoanisole (**57**) following the literature procedure reported by Cheng *et al.*^[280] The Friedel-Crafts acylation of 3-bromoanisole takes places at the *para* position to the methoxy and the *ortho* position to the bromo electron donating groups. The desired 3-bromoacetophenone (**58**) was isolated as a colorless oil in 74% yield. 1,3,5-Triarylbenzene **59** was synthesized through a cyclocondensation reaction of 3-bromoacetophenone **58** catalysed by silicon tetrachloride (SiCl₄) as a Lewis acid in ethanol (EtOH). The reaction was performed following a literature procedure to afford the desired product **59** in 62% yield.^[281] The 1,3,5-tris(biphenyl)benzene derivative **60** was assembled *via* Suzuki-Miyaura cross-coupling reaction between compound **59** and the pinacolboronic ester **56**, which was previously prepared under Miyaura borylation conditions in 93% yield. For the Suzuki coupling towards compound **60** an excess of pinacolboronic ester **56** was used to afford the target molecule **60** as a white foamy solid in 76% yield. Intermediate **61** was synthesized by iodination of compound **60** with iodine monochloride (ICl). Due to the higher electronegativity of chlorine, ICl is used as a source of electrophilic iodine. Initially, the attempts towards iodination of **60** afforded a mixture of polyiodinated side-products highly difficult to purify, because the strong electron-donating behaviour of methoxy groups causes the iodination of the methoxy functionalized phenyl rings. In order to prevent such a side-reaction and to selectively substitute TMS groups, the reaction was performed in an ice bath using a solution of iodine monochloride (1.0 M in CH₂Cl₂) in 1:1 stoichiometric ratio with TMS groups. ICl was added in three portions over 30 min and the progress of the reaction was continuously monitored by TLC yielding the desired product **61** quantitatively. Subsequently, the corresponding tri-hydroxy derivative **62** was prepared *via* demethylation of molecule **61** using boron tribromide^[282] and isolated in quantitative yield. Once prepared the trihydroxy intermediate **62** it was possible to proceed with the introduction of solubilizing long alkyl chains. Our original plan was to functionalize molecule **62** with branched alkyl chains (**63**, Figure 118), using 7-(bromomethyl)pentadecane already employed for the synthesis of alkoxy-azobenzene derivatives **53** and **54**.

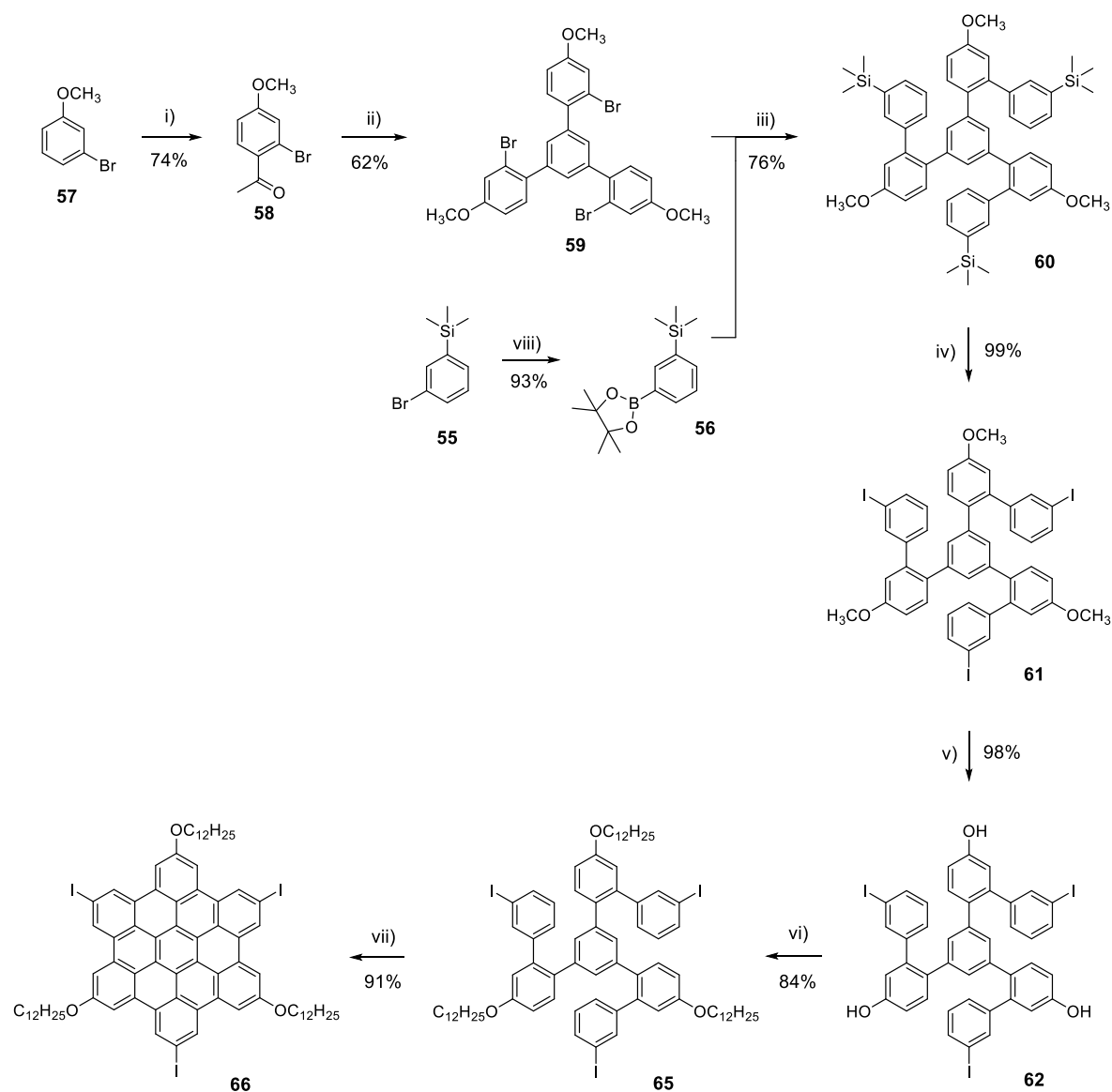


Figure 117. Synthetic pathway towards alkoxy-HBC building block (**66**). Reagents and conditions: i) CH_3COCl , AlCl_3 , CH_2Cl_2 , RT; ii) SiCl_4 , EtOH, RT; iii) $\text{Pd}(\text{PPh}_3)_4$, K_2CO_3 , H_2O , dioxane, 85°C ; iv) ICl , CH_2Cl_2 , 0°C ; v) BBr_3 , CH_2Cl_2 , RT; vi) $\text{C}_{12}\text{H}_{25}\text{OH}$, PPh_3 , DIAD , THF, RT; vii) FeCl_3 , CH_3NO_2 , CH_2Cl_2 , RT; viii) bis(pinacolato)diboron, $\text{Pd}(\text{dppf})\text{Cl}_2$, AcOK, dioxane, 90°C .

At first, the Williamson etherification reaction between derivative **62** and the alkylating agent 7-(bromomethyl)pentadecane was performed using a large excess of K_2CO_3 as base (**Method A**) for the deprotonation of hydroxy groups in DMF as a solvent, and the reaction mixture was refluxed for 48 hours providing the desired target molecule **63** in very low yield (11%). The reason of such a moderate yield was addressed to the base weakness, thus a second attempt towards **63** was performed using a stronger base (**Method B**) such as sodium hydride (NaH). However, the reaction yield in this case was found to be even lower than before (7% yield) and, after work up and purification, a second fraction containing the elimination product **64** was isolated in 11% yield. The moderated reaction yields are probably related to the low solubility of the tri-phenolate anion, which does not efficiently react with

7-(bromomethyl)pentadecane. Moreover, similar yield values have been reported in literature for analogous tri-hydroxy compounds.^[283,284]

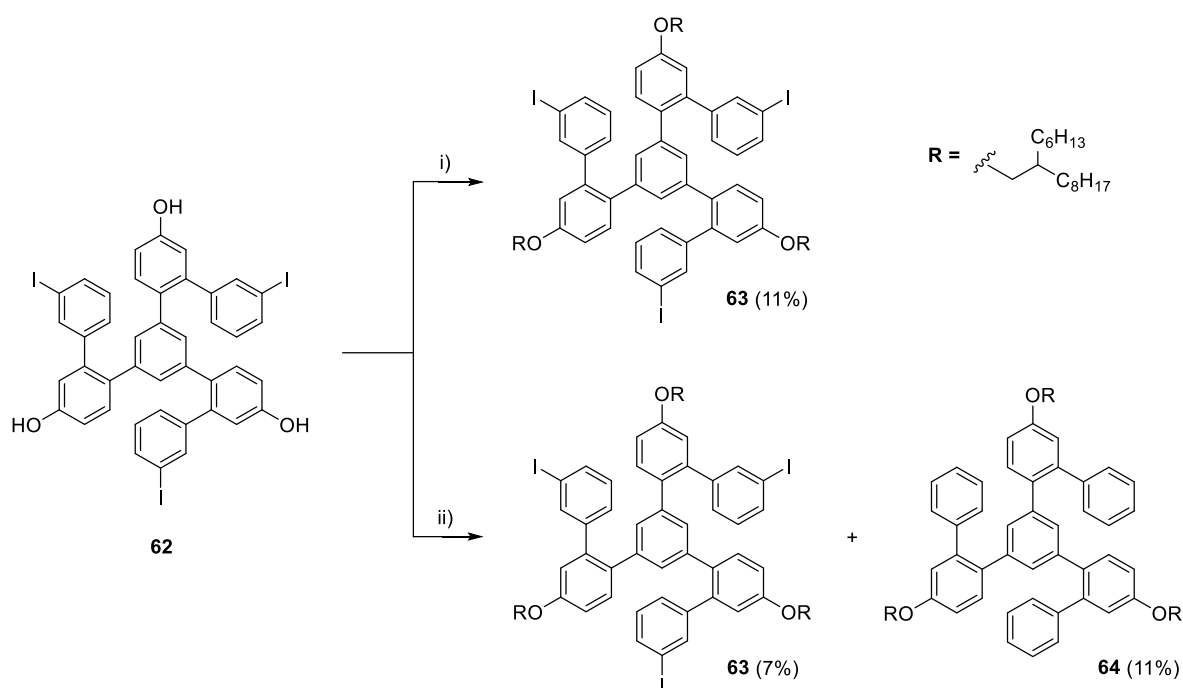


Figure 118. Synthetic approach towards **63**. Reagents and conditions: i) 7-(bromomethyl)pentadecane, K_2CO_3 , DMF, reflux (*Method A*); ii) 7-(bromomethyl)pentadecane, NaH, THF, 40 °C (*Method B*).

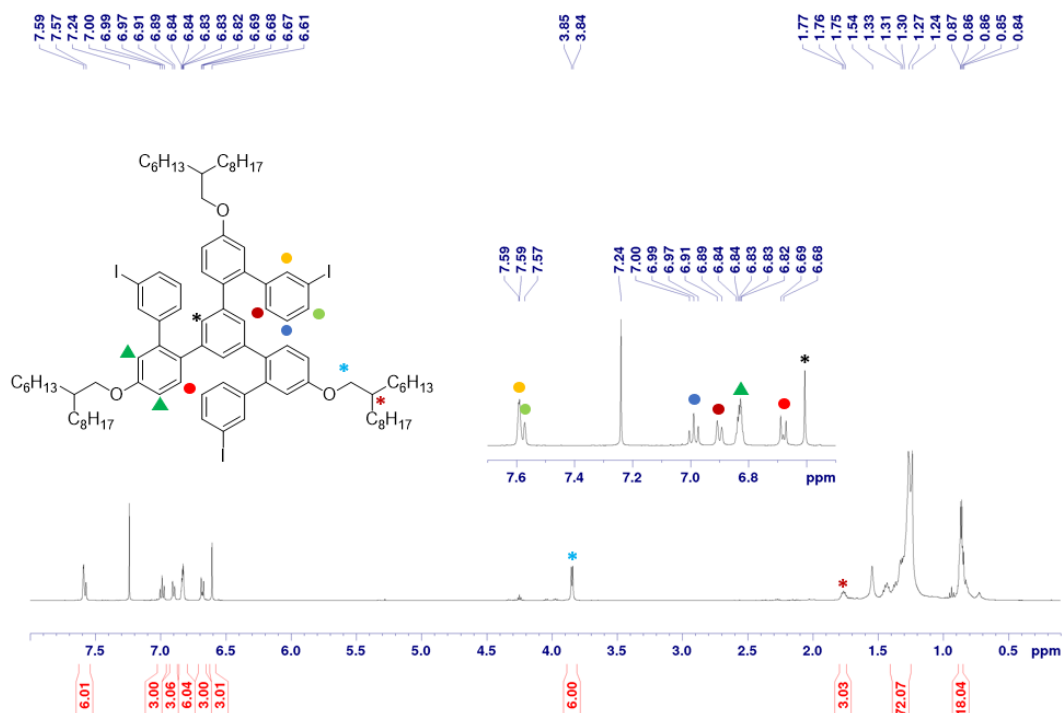


Figure 119. ^1H NMR spectrum (500 MHz) of derivative **63** measured in deuterated chloroform (CDCl_3) at room temperature.

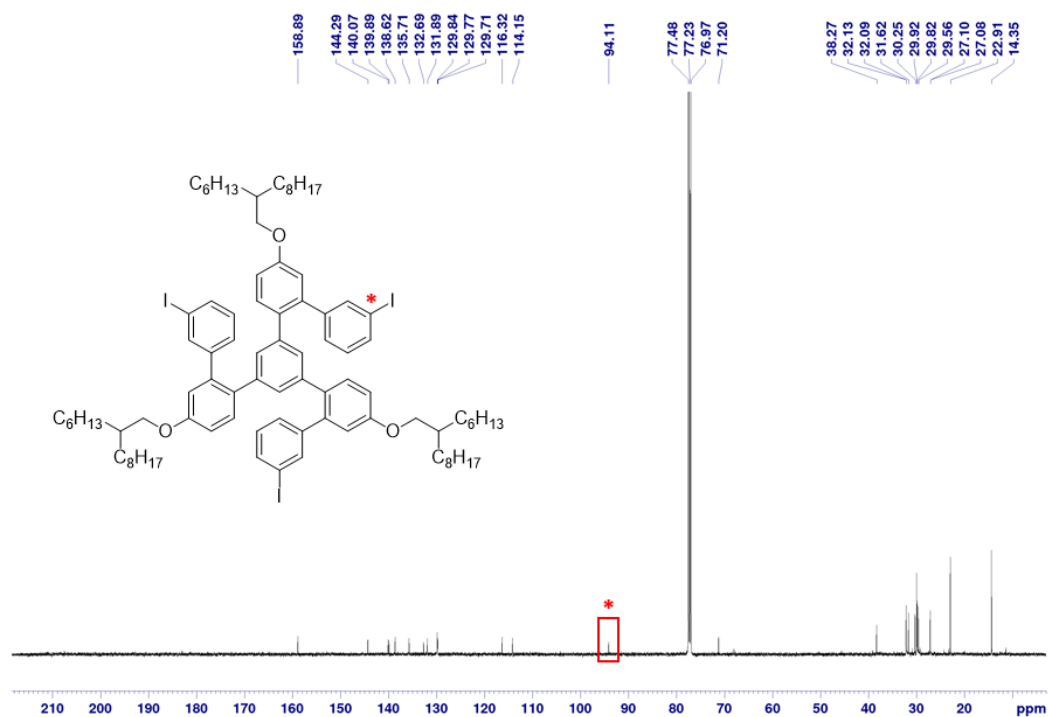


Figure 120. ^{13}C NMR spectrum (125.8 MHz) of compound **63** measured in deuterated chloroform (CDCl_3) at room temperature. The characteristic peak of the carbon bounded to the iodine around 90 ppm is highlighted in the picture.

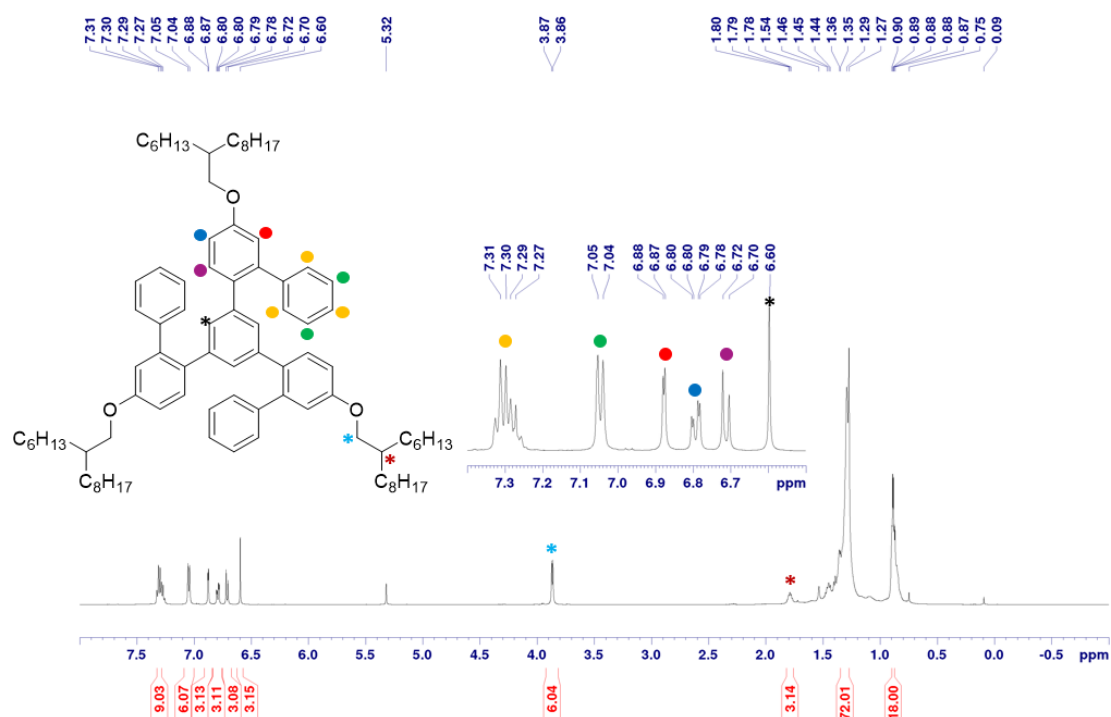


Figure 121. ^1H NMR spectrum (500 MHz) of the elimination product **64** measured in deuterated dichloromethane (CD_2Cl_2) at room temperature.

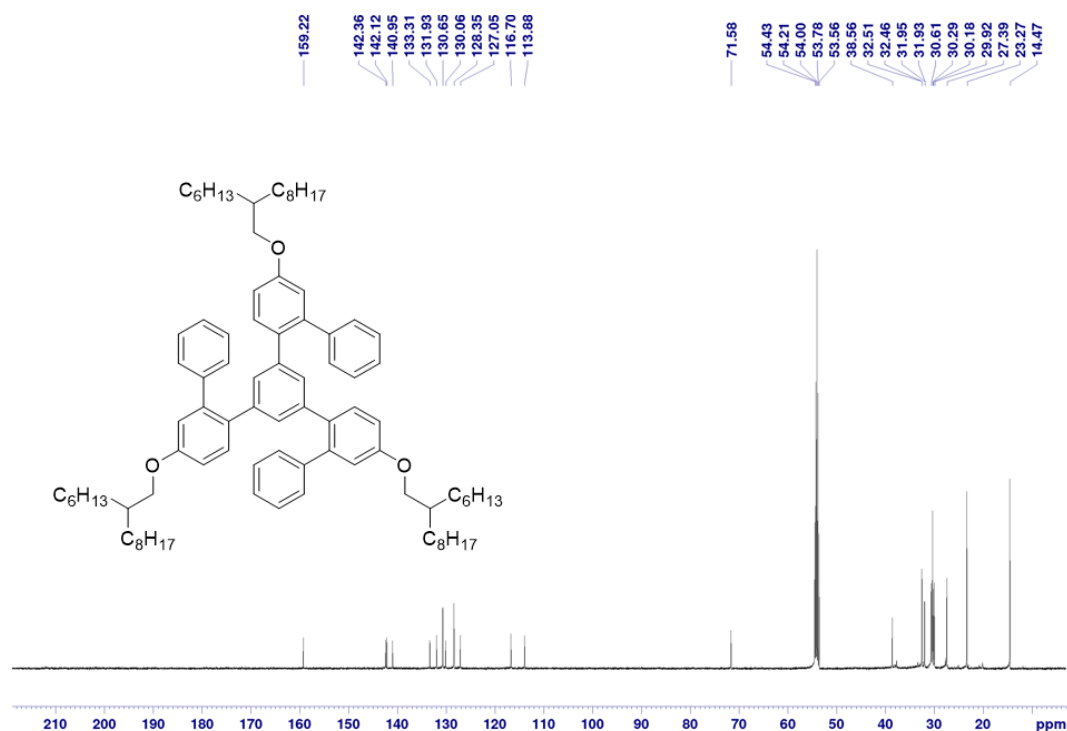


Figure 122. ^{13}C NMR spectrum (125.8 MHz) of the elimination product **64** measured in deuterated dichloromethane (CD_2Cl_2) at room temperature. The typical peak corresponding to the C bounded to the iodine atom around 90 ppm is not present.

On the other hand, the Mitsunobu reaction^[285] was found to be a smart solution to overcome the aforementioned issues. Mitsunobu reaction enables the conversion of primary and secondary alcohols into esters, phenyl ethers, thioethers and various other compounds (Figure 123). Therefore, the alkylation of compound **62** was performed under standard Mitsunobu conditions using triphenylphosphine (PPh_3) and diisopropyl azodicarboxylate (DIAD) in anhydrous tetrahydrofuran. PPh_3 is a nucleophile species that attacks the electrophilic DIAD generating a basic intermediate, which deprotonates the phenol group. Furthermore, the intermediated deprotonates the alcohol affording the corresponding alkoxide, which is finally converted into the electrophilic oxyphosphonium ion. The latter is thus attacked by the phenolate anion providing the desired ether and the triphenylphosphine oxide as a by-product. For the preparation of molecule **65**, a slight excess of 1-dodecanol was used for the alkylation to provide the desired product **65** as a yellow solid in 84% yield.

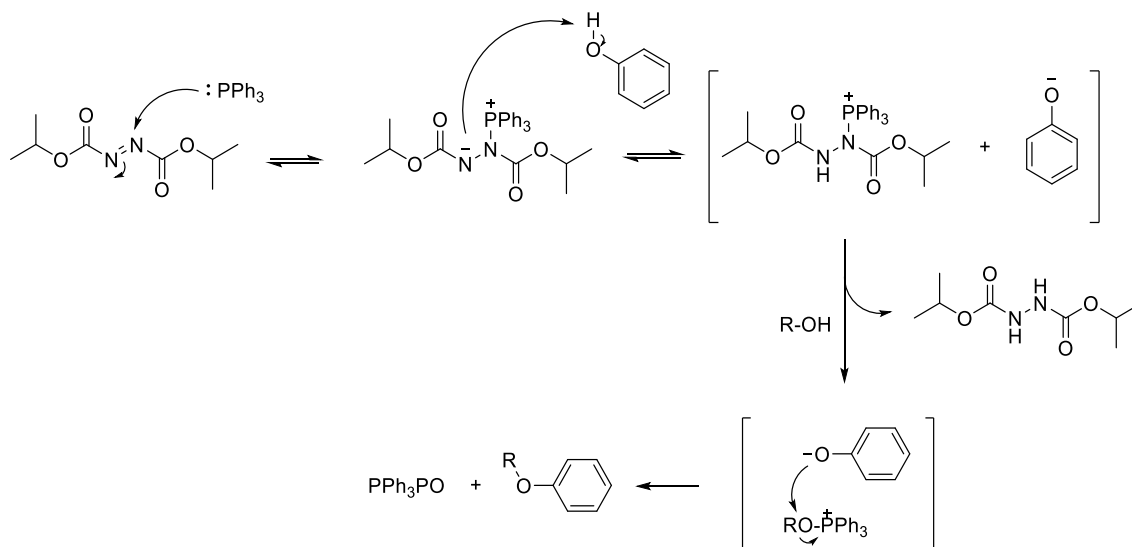


Figure 123. Mitsunobu reaction mechanism proposed for the formation of aromatic ethers. The nucleophilic attack of PPh_3 to DIAD (electrophile) generates a basic intermediate, which deprotonates the phenol and the alcohol derivatives. The formation of the alkoxide is crucial for the formation of the oxyphosphonium cation, which is attacked by the generated phenolate anion affording the desired aryl ether.

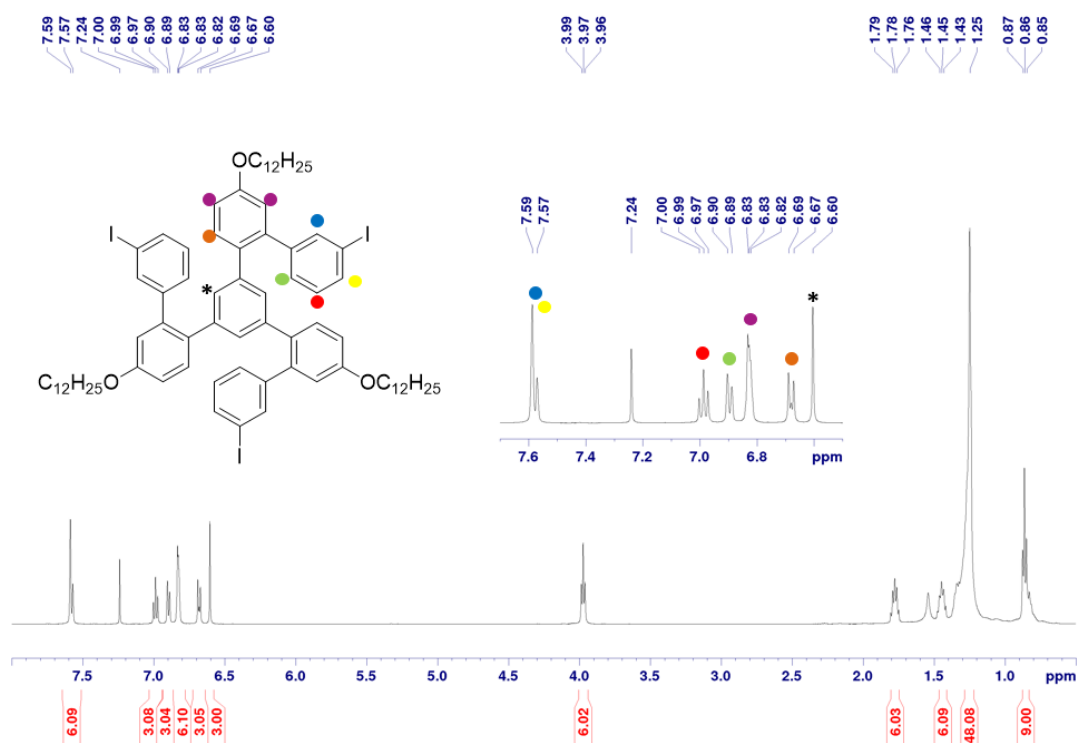


Figure 124. ^1H NMR spectrum (500 MHz) of derivative **65** obtained by Mitsunobu reaction, measured in deuterated chloroform (CDCl_3) at room temperature.

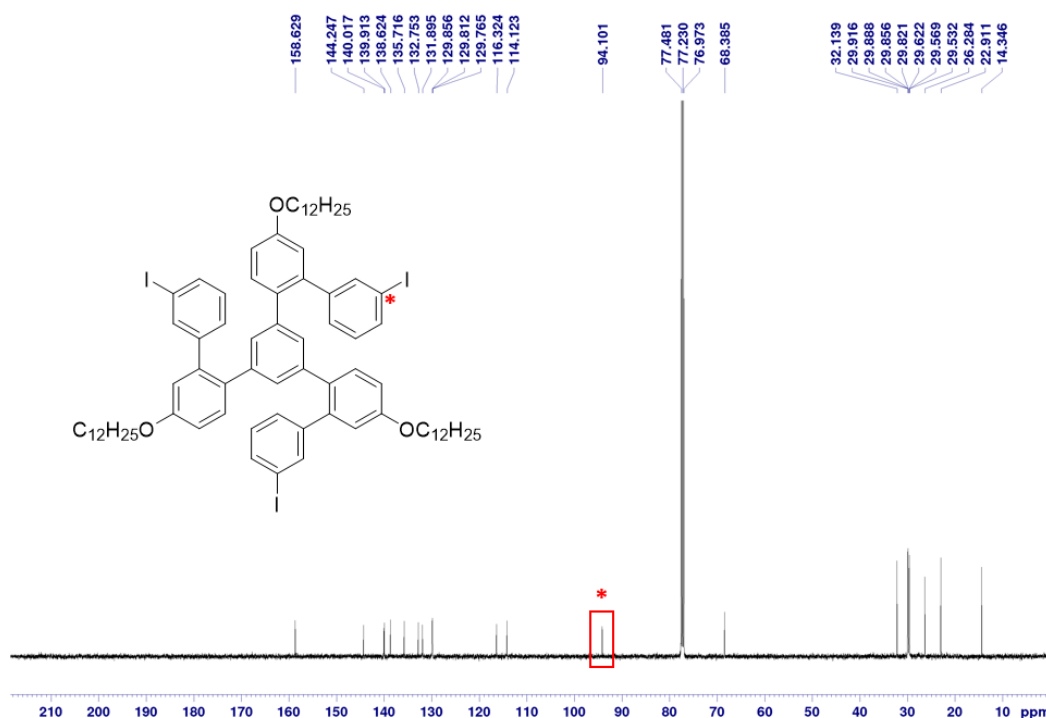


Figure 125. ^{13}C NMR spectrum (125.8 MHz) of derivative **65** measured in deuterated chloroform (CDCl_3) at room temperature. The characteristic peak corresponding to the C bounded to the iodine atom is highlighted in the red rectangle.

Finally, the alkylated derivative **65** was converted into the alkoxy-HBC **66** via Scholl oxidative coupling reaction. Although the reaction conditions used for the preparation of HBC **71** afforded the desired 2,5,8,11,14,17-hexa-iodohexa-*peri*-hexabenzocoronene in quantitative yield, they needed to be adjusted for the synthesis of alkoxy-HBC **66**, and the best results were obtained using 50 equivalents of FeCl_3 . The oxidative coupling afforded the target molecule **66** in 84% yield.

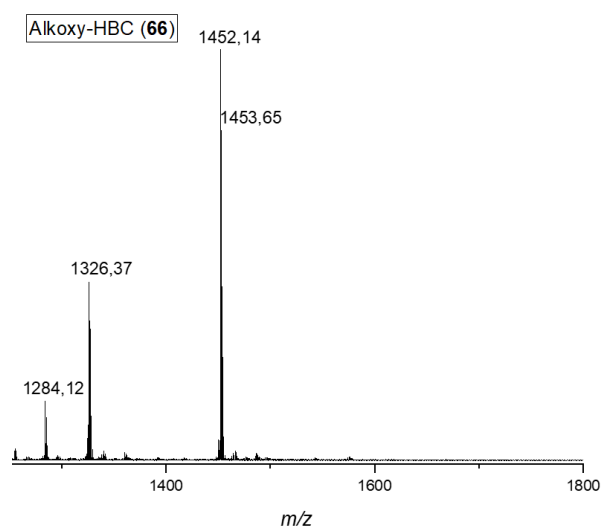


Figure 126. MALDI-TOF MS (+) spectrum of alkoxy-HBC **66** measured using DCTB matrix. The spectrum shows the peak corresponding to the molecular ion ($m/z = 1452.14$) with the highest intensity and fragmentations corresponding to the loss of iodine ($m/z = 1326.37$) and alkyl chain ($m/z = 1284.12$).

The reaction mixture was continuously purged with an argon flow for the entire reaction time and the process of the reaction constantly monitored by MALDI-TOF MS. In this case, better results were obtained using DCTB as matrix (Figure 126). Finally, target molecule **3-azo-HBC (76)** was assembled by Suzuki-Miyaura cross-coupling reaction between azobenzene **46** and alkoxy-HBC **66** (Figure 127) and isolated as a brown reddish solid in 90% yield.

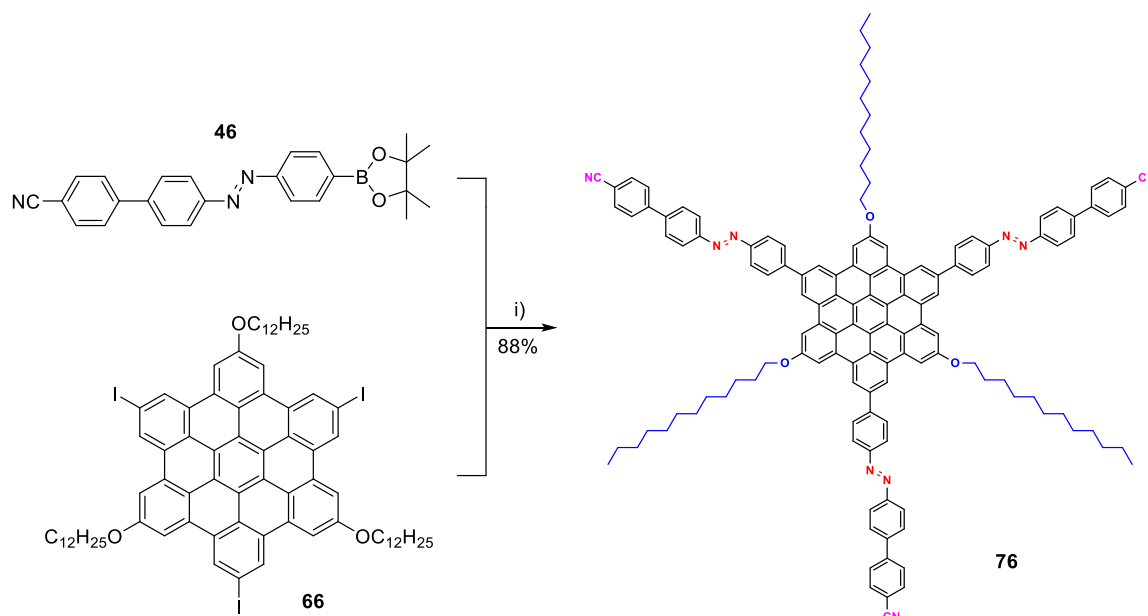


Figure 127. Synthesis of **3-azo-HBC (76)** via Suzuki-Miyaura cross-coupling reaction between alkoxy-HBC **66** and azobenzene derivative **46**. Reagents and conditions: i) Pd(PPh₃)₄, K₂CO₃, S-Phos, H₂O, EtOH, toluene, 65 °C.

As for derivatives **74** and **75**, ¹H NMR spectrum of **3-azo-HBC** was recorded using deuterated 1,1,2,2-tetrachloroethane (C₂D₂Cl₄) as a solvent for the measurement at high temperature (383 K). The ¹H NMR spectrum is depicted below (Figure 128) and it shows broadened peaks in the aromatic region (δ ppm 8.34 – 7.60) whose integration fits with the aromatic protons contained within the structure. The signals corresponding to the aliphatic protons close to the oxygen (red and blue dots, Figure 128) are weaker and broad, while the signals of the rest of the aliphatic protons, which are more far from the HBC core, are more intense. All the signals related with the protons contained in the aliphatic chain appear in the same region observed for derivative **65**, thus further confirming the influence of the self-assembly of the HBC units on the NMR results. MALDI-TOF MS measurements have also been performed either using TCNQ or DCTB as a matrix, and the latter afforded the best spectrum observed (Figure 129). However, in both cases it was possible to visualize a very weak peak corresponding to the molecular ion ($m/z = 1918.82$), while an intense fragmentation peak corresponding to the loss of the three cyano groups ($m/z = 1837.96$) was observed.

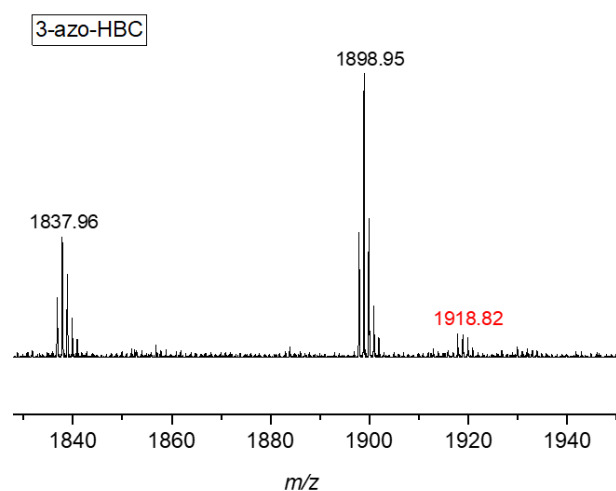


Figure 129. MALDI-TOF MS (+) of derivative **76** (**3-azo-HBC**) measured using DCTB as a matrix. The spectrum shows a weak peak corresponding to the molecular ion ($m/z = 1918.82$) and more intense fragmentation peaks ($m/z = 1898.95$, 1837.96).

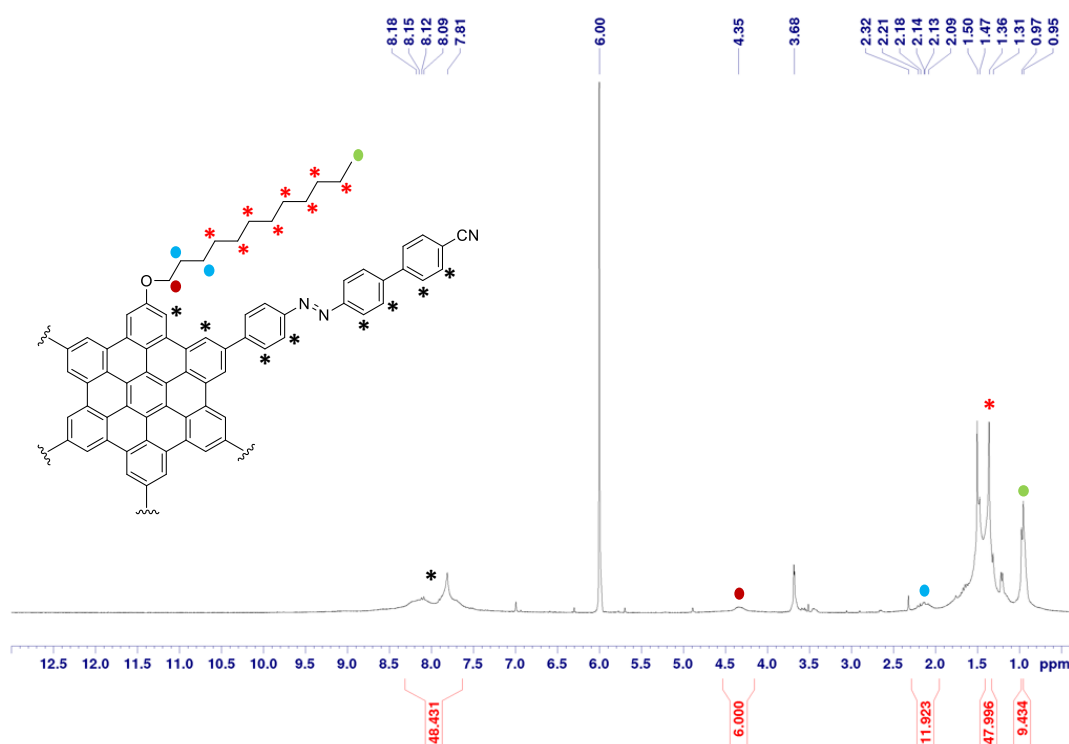


Figure 128. ^1H NMR spectrum (500 MHz) of **3-azo-HBC** measured in deuterated 1,1,2,2-tetrachloroethane ($\text{C}_2\text{D}_2\text{Cl}_4$) at 383 K.

Experiments on photoisomerization of **3-azo-HBC** (**76**) upon UV irradiation were performed on a solution of **76** in dichloromethane ($c = 10^{-5}$ M) by means of UV-Vis spectroscopy (Figure 130). The photoisomerization of **76** was studied upon irradiation with UV light ($\lambda_{\text{irr}} = 366$ nm). Before irradiation, an absorption band at *ca.* 371 nm was observed. After 3 hours of irradiation with a UV light a small decrease of absorbance together with a very small red shift of the absorption band of *ca.* 3 nm was

observed. The solution was stored in the dark for 20 hours, after which time it was possible to recover the initial state. This evidence was assigned to the thermal $Z \rightarrow E$ isomerization of the azobenzene units protruding from the HBC core. The evidence observed are still considered as preliminary results. The photochemical behavior of such compounds is still under investigation for a comprehensive explanation of their photochemistry.

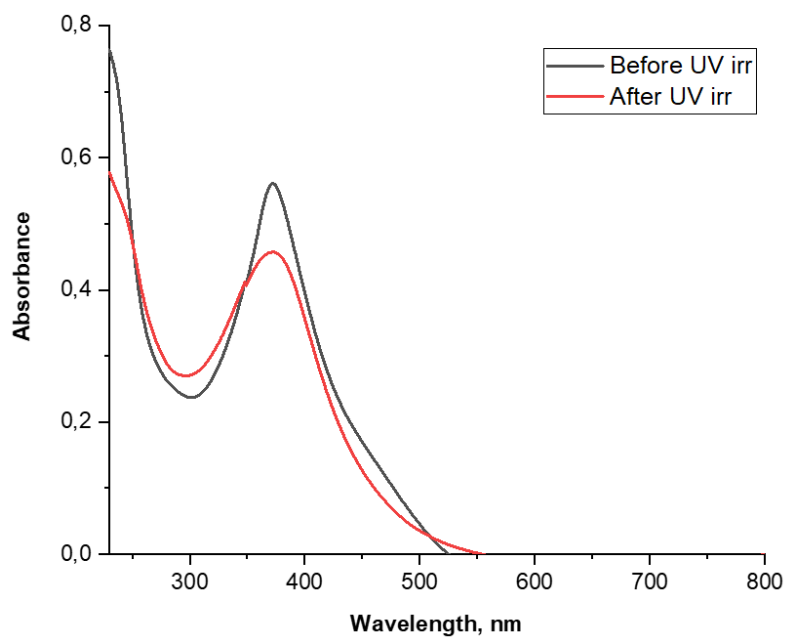


Figure 130. UV-Vis of **3-azo-HBC (76)** upon UV light irradiation ($\lambda_{\text{irr}} = 366$ nm) in DCM ($c = 10^{-5}$ M). *Black line*, no irradiation; *red line*, after 3 hours of irradiation with UV light.

2.2.4 Conclusions and outlooks

A series of novel multi-photochromic systems based on HBC derivatives (**3-azo-HBC**, **6-azo-HBC-01** and **6-azo-HBC-02**) bearing azobenzene photoswitchable units has been synthesized in order to study the influence of azobenzene photochromes onto HBC self-assembled discotic architectures upon irradiation with UV-Vis light. Furthermore, our interest was focused on the investigation of charge transport properties of such materials, as well as on their self-assembly on HOPG substrate upon UV/Vis light irradiation.

The molecules synthesized contain from three (**76**) to six (**74-75**) photoswitchable molecular branches able to undergo $E \leftrightarrow Z$ photoisomerization by means of UV/Vis light irradiation. Moreover, long alkoxy chains (branched in derivatives **74-75** and linear in derivative **76**) were introduced either onto the HBC rigid aromatic core (**76**) or at the azobenzene termini (**74-75**) to solubilize the compounds in common organic solvents and thus allowing their characterization in a solution.

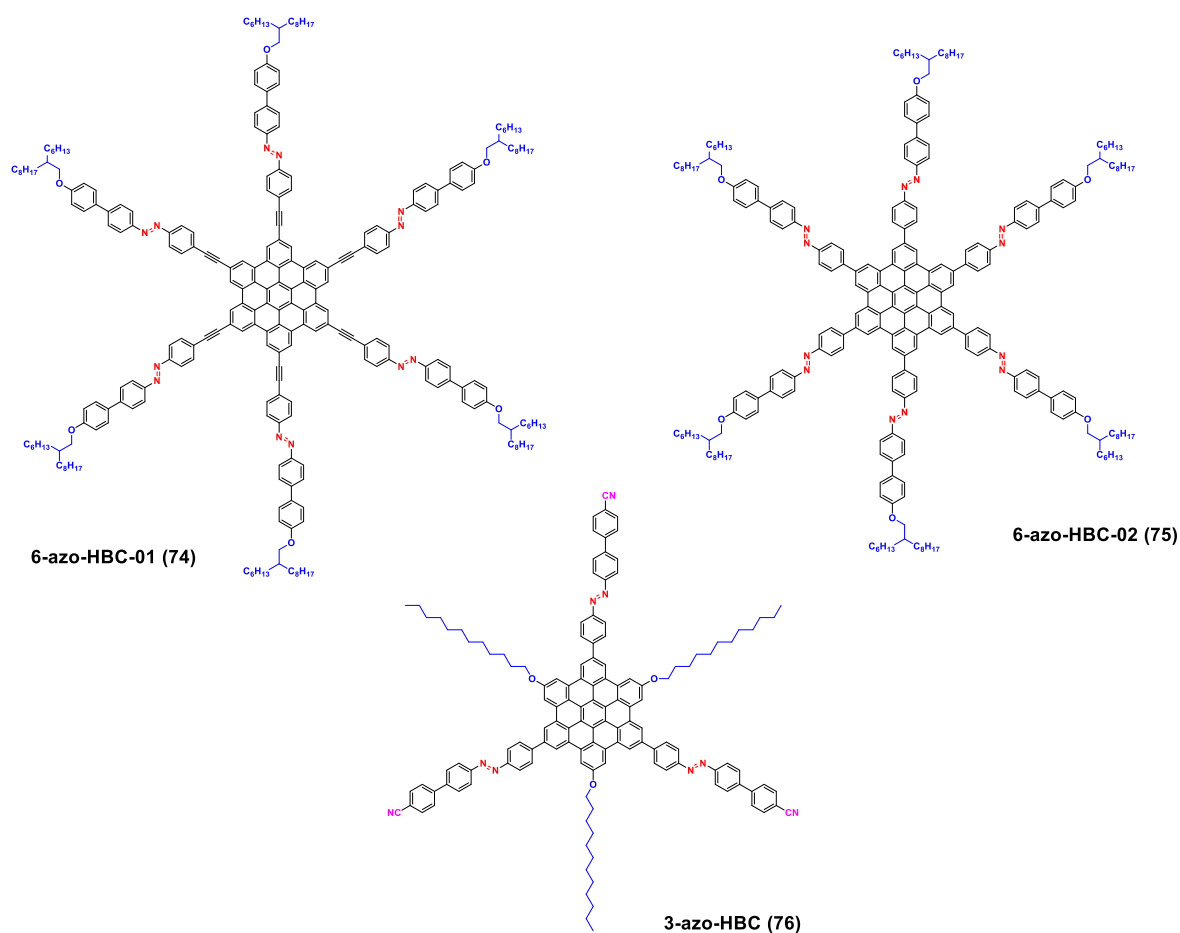


Figure 97. Molecular structures of our series of multi-chromophoric systems **6-azo-HBC-01 (74)**, **6-azo-HBC-02 (75)** and **3-azo-HBC (76)** based on HBC derivatives functionalized with azobenzene photoswitches.

For all the derivatives **74-76** the synthetic approach is based on the preparation of the two building blocks, namely the azobenzene and the HBC units, subsequently assembled *via* Sonogashira (**6-azo-**

HBC-01) or *via* Suzuki-Miyaura (**6-azo-HBC-02** and **3-azo-HBC**) cross-coupling reactions. The solid-state characterization by means of MALDI-TOF MS, FTIR and EA was further corroborated by NMR spectroscopy. However, the ^1H NMR spectra obtained displayed broadened beaks due to the strongly packed aggregation between the HBC core, even when measured at high temperature (383 K). Although preliminary studies on the photoisomerization of derivatives **74** and **75** by means of UV/Vis absorption spectroscopy showed a bathochromic shift of the adsorption band after irradiation with UVA light, the photochemistry of derivatives **74-75** is still under investigation. Once clarified the properties of such materials in solution, their behavior on graphite surface as well as their conductivity will be studied. On the other hand, the star-shaped molecular geometry of **3-azo-HBC (76)** was proposed for the preparation of triazine-based photoresponsive COFs. The synthesis of this molecule was achieved very recently. Therefore, all the studies are still on going. Preliminary STM experiments at the solid-liquid interface of derivative **74** have been performed, nevertheless it was not possible to visualize patterns suggesting the formation of 2D crystalline assemblies. Once clarified the photochemical behavior of such materials, as well as their self-assembly at the solid (HOPG)/liquid interface, their electrical properties will be investigated.

3 General conclusions

The research activity performed within this thesis has been focused on the design, synthesis and characterization of multi-photochromic systems based on azobenzene as the photoswitchable unit. Among the chromophores able to undergo isomerization by means of light irradiation azobenzene draws the attention of many scientists, due to its well-known, relatively fast and reversible $E \leftrightarrow Z$ photoisomerization and due to the structural and physical features of its isomers. The compounds presented in this thesis comprise azobenzene photochromic units, which have been attached onto a rigid aromatic scaffold aiming to the synthesis of novel photoresponsive molecular-scale actuators for applications in electronics.

In Chapter 2.1 the novel family of star-shaped azobenzene derivatives (**3**, **23**, **27**, Figure 131) has been presented. These molecules are characterized by a peculiar geometry bestowed by introducing either photoswitchable (azo) or non-photoswitchable (tolane) molecular “arms” in the position 1,3,5 of a benzene ring. The introduction of the photochromic units in the *meta* position reciprocally was chosen to reduce the π -conjugation between the azobenzene units belonging to the same molecule. In this way, the photoisomerization of each azo-unit results independent from the state of the others within the same molecular system.

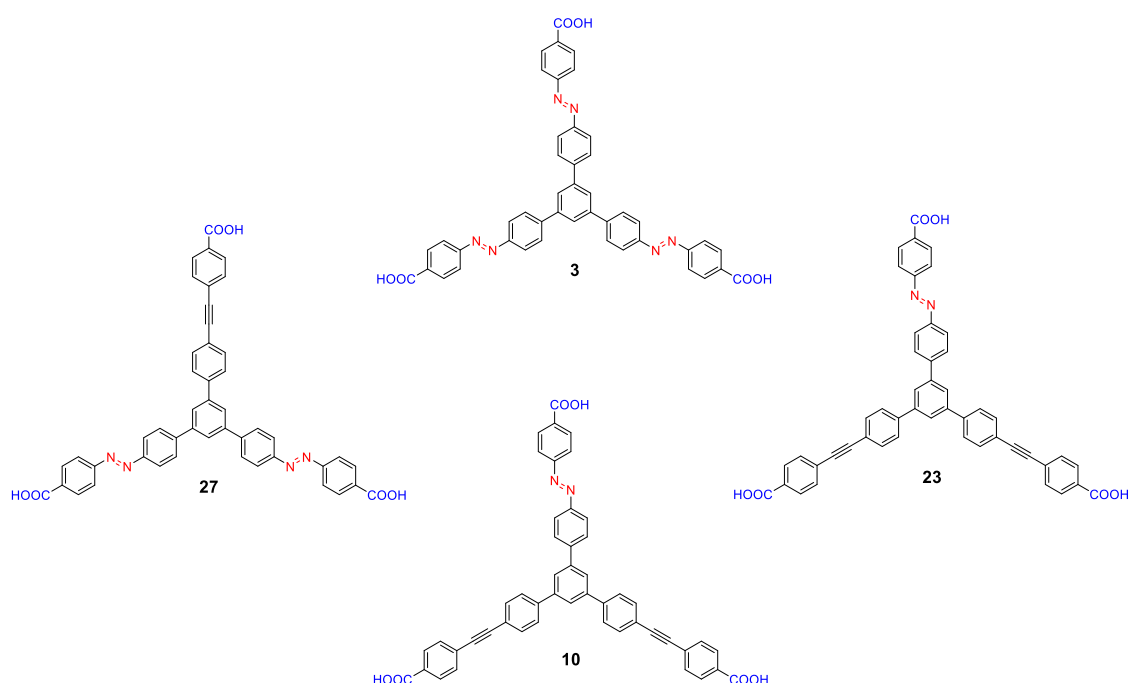


Figure 131. Molecular structures of star-shaped derivatives **3**, **10**, **23** and **27**.

The aim of the project was the investigation of the multi-photochromism of tris(azobenzene) **3**. Furthermore, its self-assembly on graphite (HOPG) surface was studied to realize 2D surface-confined

architectures whose topology may be triggered by means of light irradiation. All the studies were performed in comparison with bis(azobenzene) **27** and mono(azobenzene) **23**, which were designed by progressive substitution of the azobenzene units with a non-photoresponsive ethyn-1,2-diyl unit. The investigation of photochromism in solution was performed employing different techniques such as UV-Vis absorption spectroscopy, cyclic voltammetry (CV), differential pulse voltammetry (DPV), high performance liquid chromatography (HPLC) and advanced mass spectrometry methods as ion mobility (IMMS). Before irradiation, the UV-Vis adsorption spectra of derivatives **3**, **23** and **27** show the typical adsorption bands of azobenzene chromophores: the first related to the π - π^* transition (*ca.* 370 nm) and the second one related to the n - π^* transition (*ca.* 455 nm). The presence of clear isosbestic points upon irradiation together with the quantum yield values obtained for star-shaped derivatives **3**, **23** and **27** similar to the reference compounds (azobenzene **35** and 4-(phenylazo)benzoic acid) provided evidences of almost absent electron coupling between the azobenzene units. The absence of electronic coupling was also confirmed by cyclic voltammetry and differential pulse voltammetry studies. The reduction peaks observed for our star-shaped derivatives tris(azobenzene) **3**, bis(azobenzene) **27** and mono(azobenzene) **23** resulted substantially analogous to the one displayed by azobenzene and by the linear reference compounds **35** and **79**. Furthermore, the same study was performed on the non-photoswitchable compound **10**, which showed only the peak corresponding to the reduction of the carboxylic group, while the characteristic reduction peak of azobenzene was absent. Ion mobility mass spectrometry experiments have been performed and they unveiled a large shape-variation of such star-shaped compound upon irradiation, which is due to the photoisomerization of the azobenzene units from the large and extended all-(*E*) to the contracted and non-planar all-(*Z*) isomer. The introduction of carboxylic groups as the azobenzene termini was conceived to allow the 2D self-assembly on HOPG surface through intermolecular hydrogen-bonding interactions of the molecules. Moreover, the rigid molecular scaffold with the peculiar substitution pattern was specifically designed to enhance the conformational variation upon azobenzene photoisomerization. The self-assembly of tris(azobenzene) **3** was investigated by means of scanning tunneling microscope (STM) at the solid-liquid and solid-air interface, and the non-photoswitchable derivative **10** was employed as a reference compound for the study. Before UV irradiation, the (*E,E,E*)-**3** isomer forms highly ordered 2D crystalline domains where the molecules result tightly packed due to the strong π - π and van der Waals interactions with the substrate. Although the molecule **3** may be considered as an elongated analogous of trimesic acid, it does not form the expected “honeycomb” networking, suggesting that the self-assembly results from the balance between hydrogen-bonding and van der Waals intermolecular interactions. Therefore, the highly tight packing observed is thermodynamically favored with respect to the honeycomb organization where hydrogen-bonding interactions are predominant. Upon *in situ* irradiation with UV light a loss of crystallinity is observed, and it was possible to visualize the presence of ordered domains consisting of only (*Z,E,E*)-**3** or (*Z,Z,E*)-**3**. On the other hand, it was not possible to visualize any packing related to (*Z,Z,Z*)-**3** because of its non-planarity, which caused its desorption from the

substrate. The STM results were further corroborated by MM/MD simulation of the self-assembly for each isomer. Our star-shaped molecule bearing three photochromic units (**3**) was also proposed as a photoswitchable ligand for the preparation of optically triggered 3D architectures such as MOFs, which enable the variation of the pore size upon irradiation. However, all our attempts towards photoresponsive MOFs consisting of tris(azobenzene) **3** did not afford any crystalline material *via* solvothermal reaction. Therefore, a novel star-shaped tris(CN-azobenzene) **30** was synthesized as a photoswitchable organic ligand for the preparation of 3D COFs. In particular, the molecule **30** bears cyano groups as the azobenzene termini to enable the formation of triazine-based COFs *via* cyclotrimerization of the benzonitrile termini.

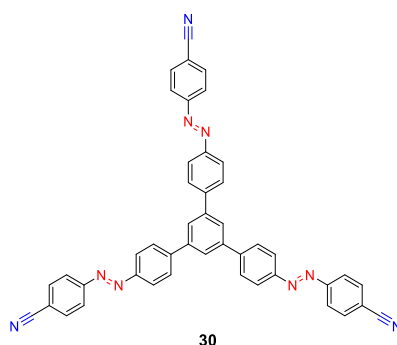


Figure 86. Molecular structure of tris(CN-azobenzene) **30** designed as photoswitchable organic ligand for the preparation triazine-based COFs *via* cyclotrimerization of the benzonitrile termini.

Our attempts towards triazine-based COFs have been performed either *via* solvothermal reaction at high temperature (400 °C) using zinc chloride as Lewis acid-catalyst (COF-**80**), or *via* a reaction at lower temperature (40 °C) using triflic acid as Brønsted acid-catalyst (COF-**77-A** and COF-**77-B**). The materials obtained have been characterized by different techniques such as FTIR, nitrogen adsorption-desorption and EA, and confirmed the formation of the triazine ring together with the absence of the nitrile groups. Furthermore, all the materials resulted porous and according to their absorption isotherms COF-**80** exhibits typical behaviour of microporous materials, while COF-**77-A** and COF-**77-B** resulted mesoporous. COF-**80** also exhibits the highest surface area value (530 m² g⁻¹).

In Chapter 2.2 the class of hexa-*peri*-hexabenzocoronenes (HBCs) bearing either three (**3-azo-HBC**) or six (**6-azo-HBC-01** and **6-azo-HBC-02**) azobenzene photoswitchable “arms” has been presented. In these molecules the flexible azobenzene branches protrude from a central rigid aromatic scaffold, namely the HBC unit. HBC derivatives are known to be extremely stable and insoluble materials due to the strong π - π intermolecular interactions, which enable the self-organization into columnar aggregates (discoics) where charge transport through the columnar axis is observed. The aim of this project was the synthesis of such intriguing and complex structures, as well as investigation of the effects of the azobenzene substitution on the HBC self-assembly and conductivity.

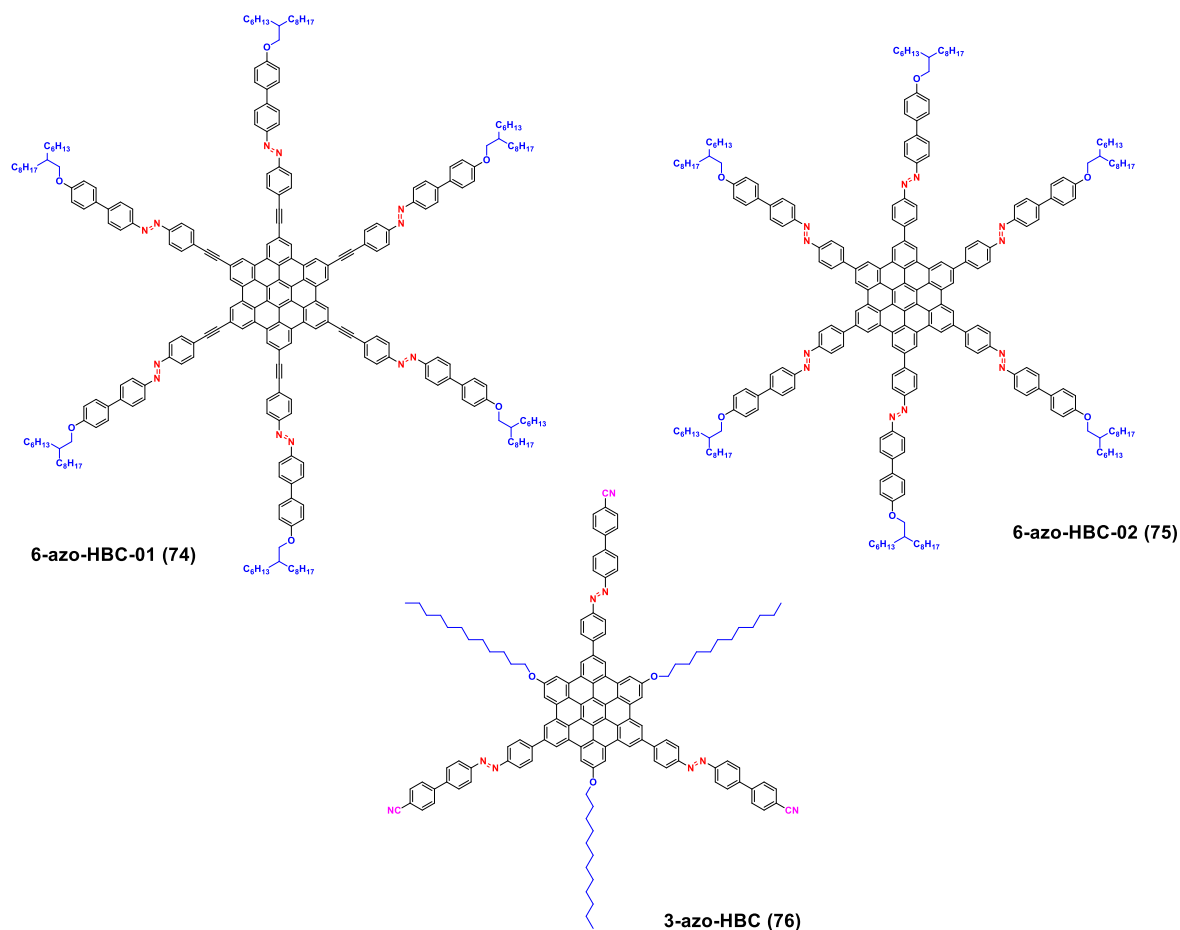


Figure 97. Molecular structures of our series of HBC derivatives **6-azo-HBC-01 (74)**, **6-azo-HBC-02 (75)** and **3-azo-HBC (76)** bearing azobenzene as the photoswitchable unit.

All the molecule synthesized contain long alkoxy chains (branched or linear), which have been introduced for a solubility reason. Derivatives **74** and **75** consist of six azobenzene photochromic units decorated with branched alkoxy chains as the termini, which have been attached to the HBC either *via* Sonogashira (**74**) or *via* Suzuki-Miyaura (**75**) cross-coupling reaction respectively. The structure of derivative **76** instead may be considered as an extended analogous of star-shaped tris(CN-azobenzene) **30**, where the central benzene ring has been replaced by the larger and rigid HBC core. The molecule also contains cyano groups as the azobenzene termini to enable the formation of triazine-based COFs, and the solubilizing linear alkoxy chains have been introduced directly to the HBC core. All the molecules have been characterized by MALDI-TOF MS using TCNQ or DCTB as a matrix, FTIR, UV-Vis spectroscopy and EA. The materials resulted rather difficult to ionize, thus MALDI spectra show molecular ion peaks with a low intensity. FTIR spectra were measured for a qualitative characterization and the vibrational bands corresponding to the alkyl chains and the aromatic core were clearly detected. Furthermore, for **3-azo-HBC** the typical peak for the nitrile group (2226 cm^{-1}) was observed, while the characteristic ethynyl stretching band (2202 cm^{-1}) was detected for **6-azo-HBC-01**. All molecules are nicely soluble in common organic solvents such as chloroform, dichloromethane, THF, and so on; thus, the solid-state characterization was further corroborated by ^1H NMR, which was

measured at high temperature (383 K) to disrupt the aggregation between the HBC cores. Although the spectra obtained show rather broadened peaks, their integration fits with the protons contained within the structure. Furthermore, very intense signals were observed for the terminal alkyl chains, which are not involved in the aggregation, even at room temperature suggesting that the π - π stacking between the HBC units highly affects the results. The experiments on the photochemistry of our derivatives have been performed by means of UV-Vis spectroscopy to study the photoisomerization of the azobenzene units upon UV irradiation. Upon UV irradiation, all the compound showed a decrease of the absorption band related to the π - π^* electronic transition together with a moderate bathochromic shift. The latter was more evident for molecule **74** (*ca.* 14 nm), while it was quite small for derivatives **75** (*ca.* 5 nm) and **76** (*ca.* 3 nm). However, these are preliminary results and the photochemical behaviour of these molecules is still under investigation. Once clarified the photoisomerization process in solution, STM experiments at the solid-liquid interface of graphite will be performed for studying the photoswitching on a surface. Subsequently, the influence of the azobenzene isomerization on the supramolecular aggregation of **74**, **75** and **76** in discotics will be investigated, as well as their conductivity for applications in electronics. Moreover, the star-shaped molecule like **3-azo-HBC** might be employed as photoresponsive organic building block for the preparation of photoactive triazine-based COFs.

4 Experimental Part

4.1 General remarks

Reagents and solvents

All starting materials and reagents were purchased from commercial suppliers (*Alfa Aesar* (Karlsruhe, Germany), *Sigma-Aldrich* (Schnelldorf, Germany), *TCI Chemicals Europe* (Zwijndrecht, Belgium), *Merck* (Darmstadt, Germany)) and used without further purification. Solvents utilized for crystallization, chromatography and extraction were used in technical grade. Thin Layer Chromatography (TLC) was performed on silica gel 60 F₂₅₄ aluminium plates (thickness of 0.25 mm) obtained from *Merck* and spots were detected either by fluorescence quenching under UV light at 254 or 366 nm or using a phosphomolybdic acid stain (PMA). Column chromatography was performed on silica gel 60 (particle size 0.040-0.063 mm). Size Exclusion Chromatography (SEC) was performed on *Bio-Beads S-X1* support (styrene divinylbenzene resin, 1% cross-linkage, 40-80 µm bead size, 600-14000 MW exclusion range) purchased from *BIO RAD*. All experimental manipulations with anhydrous solvents were carried out in cycles of freeze-vacuum-thaw in flame-dried glassware. Tetrahydrofuran was dried and distilled from sodium/benzophenone under argon atmosphere. Dichloromethane and trimethylamine were dried and distilled from CaH₂ under argon atmosphere.

¹H-Nuclear Magnetic Resonance (¹H NMR)

¹H NMR spectra were recorded on a *Bruker Avance III-NMR* (500 MHz) instrument. Chemical shifts (δ) are reported in parts per million (ppm) relative to residual solvent peaks (CDCl₃: 7.24 ppm, CD₂Cl₂: 5.32 ppm, Acetone-d₆: 2.05 ppm, DMSO-d₆: 2.50 ppm) or trimethylsilane (TMS: 0.00 ppm) and coupling constants (*J*) are cited in Hertz (Hz). The bond distance of the coupling constant is stated with a superscript number (^{*n*}*J*). If not mentioned otherwise, all spectra were measured at room temperature (RT). The spin multiplicities are specified as s = singlet, d = doublet, t = triplet, q = quartet, dd = doublet of doublet, m = multiplet, br = broad.

¹³C-Nuclear Magnetic Resonance (¹³C NMR)

¹³C NMR spectra with total decoupling of protons were recorded on a *Bruker Avance III-NMR* (125.8 MHz) instrument. Chemical shifts (δ) are cited in parts per million (ppm) relative to residual solvent peaks (CDCl₃: 77.23 ppm, CD₂Cl₂: 54.00, Acetone-d₆: 206.68 and 29.92 ppm, DMSO-d₆: 39.51 ppm) or trimethylsilane (TMS: 0.00 ppm) and coupling constants (*J*) are reported in Hertz (Hz). If not mentioned otherwise, all spectra were measured at room temperature (RT). For complete peak assignments of both ¹H and ¹³C NMR spectra, ¹H-¹H COSY, ¹³C-DEPT-135, HSQC and HMBC experiments were performed.

Mass Spectrometry (MS)

Electrospray Ionization (ESI) mass spectra were performed on a *Bruker Daltonics* (ESI micro TOF-QII) mass spectrometer. Matrix Assisted Laser Desorption Ionization Time of Flight (MALDI-TOF) mass spectra were recorded with a MALDI-TOF *Synapt G2-S High Definition* mass spectrometer using 7,7,8,8,-tetracyanoquinodimethane (TCNQ) or *trans*-2-[3-(4-*tert*-butylphenyl)-2-methyl-2-propenylidene]malononitrile (DCTB) as a matrix either by myself at the Institute of Nanotechnology (KIT – Karlsruhe, Germany) or by Mrs. Jutta Schnee at the Max-Planck Institute of Polymer Research (MPIP – Mainz, Germany). Electron impact (EI) mass spectra were obtained with a Thermo Scientific Trace 1300 GS/MS instrument with single quadrupole ISQ. Significant signals are given in mass units per charge (m/z).

Fourier Transfer Infrared Spectrometry (FT-IR)

IR spectra were measured with a *Perkin Elmer GX* spectrometer in KBr pellets. The bands intensity is indicated as w = weak, m = medium, s = strong or br =broad.

Ultraviolet – Visible Spectroscopy (UV-Vis)

UV-Vis spectra were measured with a *Varian Cary 500 Scan* spectrometer in optical quartz *114 – QS Hellma* cuvettes (1 cm light path) at room temperature using HPLC grade solvents. The excitation coefficient (ϵ) is given in units of $\text{L mol}^{-1} \text{cm}^{-1}$.

Elemental Analysis (EA)

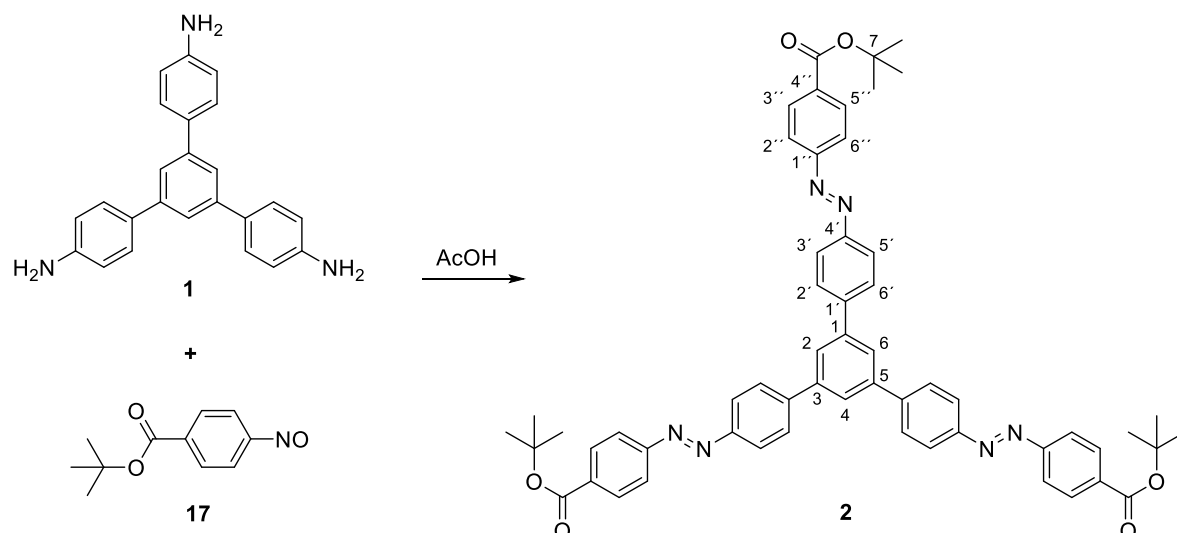
Elemental analyses were obtained with a *Vario MicroCube CHNS* analyzer and measured by Sven Stahl and Milena Staub. The values are expressed in mass percentage.

Melting Point

Melting points (m.p.) were measured with a *Büchi Melting point apparatus M – 565* and are not corrected.

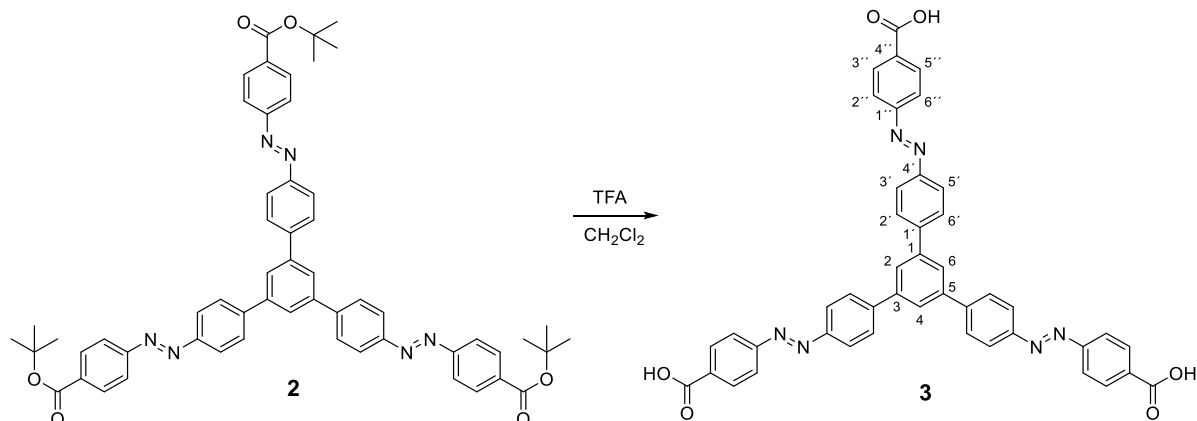
4.2 Synthetic Procedures

1,3,5-Tris(4'-[4''-(*tert*-butoxycarbonyl)phenyl]diazenyl)phenylbenzene (**2**)



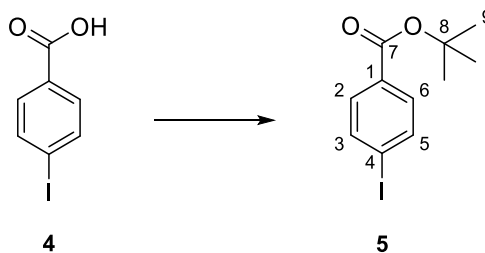
In a 100 mL Schlenk flask, freshly prepared nitroso derivative **17** (2.4 g, 11.6 mmol) was dissolved in glacial acetic acid (60 mL) under argon atmosphere. Subsequently 1,3,5-tris(4'-aminophenyl)benzene **1** (0.8 g, 2.28 mmol) was added. The reaction mixture was allowed to stir overnight at room temperature, during which time an orange precipitate formed. After 20 h, the reaction mixture was concentrated in vacuo and an orange precipitate was filtered off, washed with pentane (100 mL) and air dried. The crude product was purified on silica gel (600 g) in hexane/EtOAc (15:1) yielding the desired product **3** as an orange solid (1.71 g) in 81% yield. (R_f = 0.31, hexane/EtOAc 10:1); m.p. 141-142 °C; ^1H NMR (500 MHz, CDCl_3) δ ppm 8.14 (dd, 6H, $J_{\text{H,H}}$ = 8.5 Hz, $\text{C}^{3'',5''}\text{H}$), 8.08 (dd, 6H, $J_{\text{H,H}}$ = 8.5 Hz, $\text{C}^{3',5'}\text{H}$), 7.96 (dd, 6H, $J_{\text{H,H}}$ = 8.5 Hz, $\text{C}^{2'',6''}\text{H}$), 7.94 (s, 3H, $\text{C}^{2,4,6}\text{H}$), 7.89 (dd, 6H, $J_{\text{H,H}}$ = 8.5 Hz, $\text{C}^{2',6'}\text{H}$), 1.62 (s, 27H, CH_3); ^{13}C NMR (125.8 MHz, CDCl_3) δ ppm 165.4 (CO), 155.1 ($\text{C}^{1''}$), 152.2 ($\text{C}^{4'}$), 143.9 ($\text{C}^{1'}$), 141.9 ($\text{C}^{1,3,5}$), 134.0 ($\text{C}^{4''}$), 130.7 ($\text{C}^{3'',5''}\text{H}$), 128.3 ($\text{C}^{2',6'}\text{H}$), 126.1 ($\text{C}^{2,4,6}\text{H}$), 124.0 ($\text{C}^{3',5'}\text{H}$), 122.8 ($\text{C}^{2'',6''}\text{H}$), 81.7 (C^7), 28.4 (CH_3); IR (KBr) ν cm^{-1} : 3054 (w, $\nu(\text{CH})$), 2976(m, $\nu_{\text{as}}(\text{CH}_3)$), 2932 (w, $\nu_{\text{s}}(\text{CH}_3)$), 1716 (s, $\nu(\text{C=O})$), 1599 (s, $\nu(\text{C=C})$), 1500 (m), 1478 (w), 1457 (m, $\delta_{\text{as}}(\text{CH}_3)$), 1407 (m), 1393 (m, $\delta_{\text{s}}(\text{CH}_3)$), 1368 (s), 1291 (bs, $\nu(\text{CO})$), 1256 (m), 1171 (m), 1143 (m), 1115 (s, $\nu(\text{CO})$), 1012 (m), 865 (m), 847 (s, $\delta_{\text{as}}(\text{CH}_3)$), 796 (m), 775 (m), 694 (m, $\nu_{\text{as}}(\text{CC}_3)$); Elemental Anal. Calcd. (%) for $\text{C}_{57}\text{H}_{54}\text{N}_6\text{O}_6$ (919.10): C 74.49; H 5.92, N 9.14; Found: C 74.81, H 5.79, N 9.17.

1,3,5-Tris{4'-[(4''-carboxyphenyl)diazenyl]phenyl}benzene (**3**)



To a solution of *tert*-butyl ester **2** (0.3 g, 0.33 mmol) in dichloromethane (30 mL) was added TFA (15 mL) and dark red solution was stirred overnight. After 16 h, the reaction mixture was diluted with EtOH (80 mL), and an orange precipitate was filtered off. After washing with EtOH (2 × 50 mL), water (60 mL), diethyl ether (150 mL), and subsequent drying, the desired product **3** (219 mg) was obtained in 88% yield as an orange solid. m.p. 324-325 °C; ¹H NMR (500 MHz, d₆-DMSO) δ ppm 13.25 (bs, 3H, COOH), 8.14 (bd, 12H, C^{2',6'}H, C^{3'',5''}H), 8.11 (s, 3H, C^{2,4,6}H), 8.03 (dd, 6H, *J*_{H,H} = 8 Hz, C^{3',5'}H), 7.97 (dd, 6H, *J*_{H,H} = 8 Hz, C^{2'',6''}H); ¹³C NMR (125.8 MHz, d₆-DMSO) δ ppm 166.7 (CO), 154.3 (C^{1''}), 151.3 (C^{4'}), 143.1 (C^{1'}), 140.5 (C^{1,3,5}), 132.9 (C^{4''}), 130.7 (C^{3'',5''}H), 128.4 (C^{2',6'}H), 125.4 (C^{2,4,6}H), 123.5 (C^{3',5'}H), 122.6 (C^{2'',6''}H); IR (KBr) ν cm⁻¹: 3042 (bw, ν(OH)), 1689 (bs, ν(C=O)), 1598 (s, ν(C=C)), 1499 (m), 1411 (m, δ(OH)), 1281 (bm, ν(CO)), 1220 (m), 1143 (m), 1096 (w), 1010 (m, δ(OH)), 863 (w), 836 (m), 775 (m); ESI (-) MS Calcd for C₄₅H₂₉N₆O₆ ([M - H]⁻, 749.21), Found *m/z* 749.17; Elemental Anal. Calcd. (%) for C₄₅H₃₀N₆O₆ (750.77): C 71.99; H 4.03, N 11.19; Found: C 70.61, H 3.86, N 10.83.

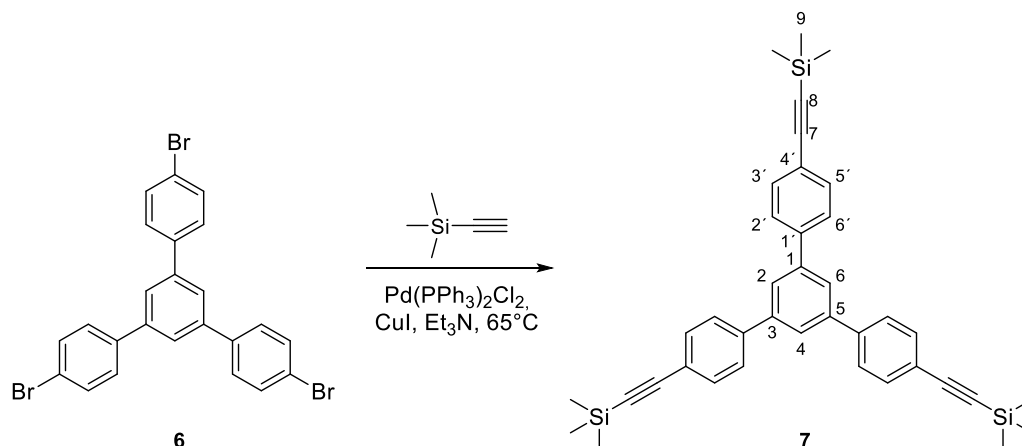
***tert*-butyl-4-iodobenzoate (5)**



Method A: This compound was prepared according to a modified procedure.^[249] In a 100 mL Schlenk flask, 4-iodobenzoic acid **4** (5.00 g, 0.020 mol) was dissolved in 15 mL of thionyl chloride (0.20 mol). A drop of DMF was added to the reaction mixture and the reaction was allowed to reflux (around 75°C) for 30 min under argon atmosphere. After cooling to RT, all unreacted SOCl₂ was removed by distillation in a fume hood. The light brown solid benzoyl chloride was dissolved in dry DCM (30 mL) and a solution of *tert*-BuOK (2.47 g, 0.022 mol) in dry THF (140 mL) was slowly added via a cannula and allowed to stir at RT under argon until all benzoyl chloride was consumed. Subsequently, the reaction mixture was poured over ice water (100 mL) and extracted with DCM (3 x 100 mL), dried over MgSO₄, filtered off and all volatile solvents were evaporated under vacuum. The pure product was isolated as a yellow oil (3.80 g) in 62% yield. (*R*_f = 0.36, *n*-hexane/EtOAc 20:1); ¹H NMR (500 MHz, CDCl₃) δ ppm 7.73 (dd, 2H, ³*J*_{H,H} = 8.3 Hz, C^{3,5}H), 7.66 (dd, 2H ³*J*_{H,H} = 8.3 Hz, C^{2,6}H), 1.55 (s, 9H, C⁹H₃); ¹³C NMR (125.8 MHz, CDCl₃) δ ppm 165.34 (C⁷), 137.64 (C^{3,5}H), 131.64 (C¹), 131.10 (C^{2,6}H), 100.22 (C⁴), 81.59 (C⁸), 28.32 (C⁹H₃).

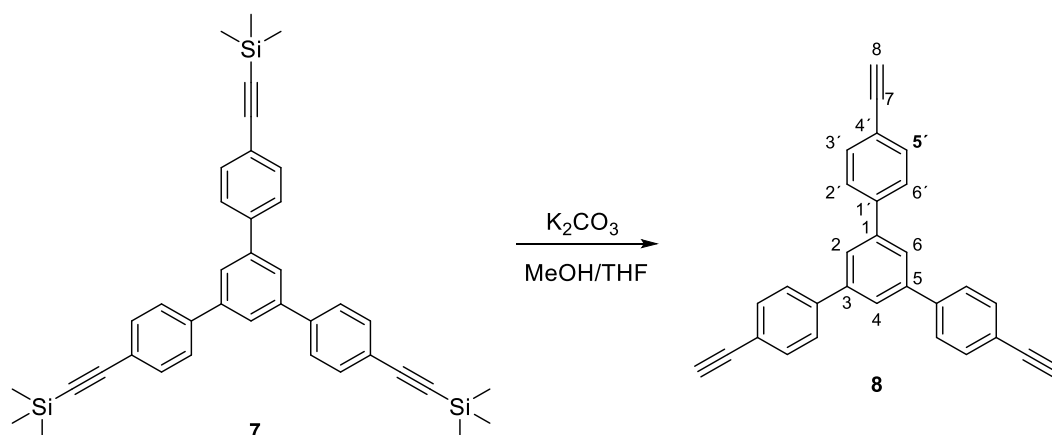
Method B: This compound was prepared according to a modified procedure.^[250] In a 250 mL Schlenk flask, 4-iodobenzoic acid **4** (1.00 g, 4.03 mmol), DMAP (985 mg, 8.06 mmol) and (BOC)₂O (1.32 g, 6.04 mmol) were dissolved in *tert*-BuOH (200 mL). The mixture was allowed to stir at 40°C for 18 h under argon atmosphere. After cooling at RT, the reaction was quenched with H₂O (150 mL) and extracted with DCM (3 x 200 mL), washed with brine (200 mL), dried over MgSO₄, filtered through a short pad of silica gel, and all volatile solvents were evaporated under vacuum. The pure product was isolated as a yellow oil (1.19 g) in 97% yield.

1,3,5-Tris{4'-[(trimethylsilyl)ethynyl]phenyl}benzene (7)



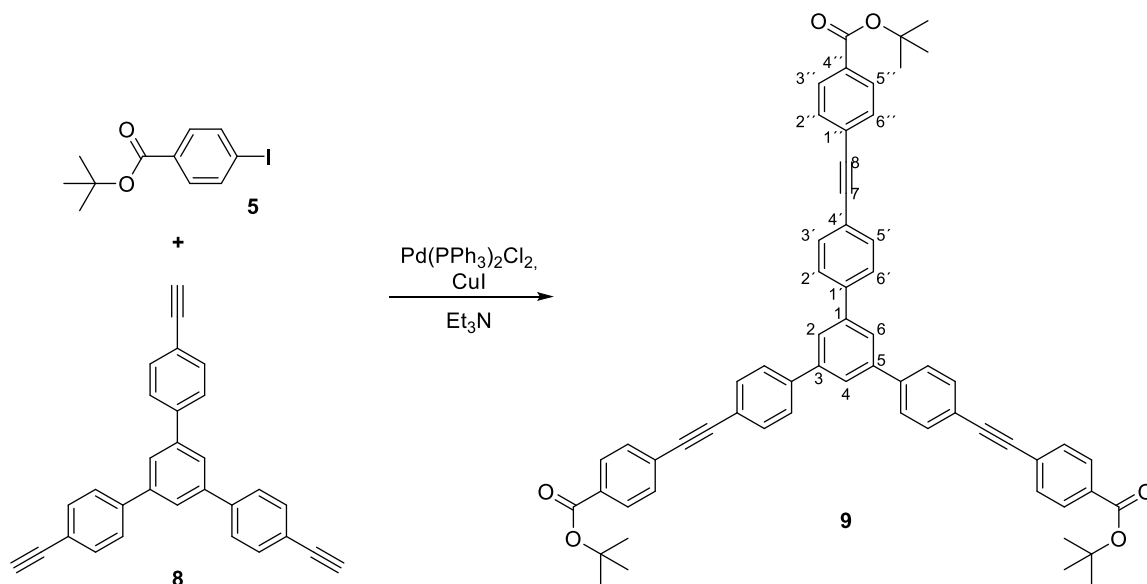
This compound was prepared according to a modified procedure.^[286] In a 50 mL Schlenk flask under argon atmosphere, 1,3,5-tris(4-bromophenyl)benzene **6** (1.00 g, 1.84 mmol), Pd(PPh₃)₂Cl₂ (64.7 mg, 0.092 mmol), and CuI (8.76 mg, 0.046 mmol) were dissolved in anhydrous Et₃N (20 mL). The solution was purged with argon for 15 min, and ethynyltrimethylsilane (1.26 g, 12.90 mmol) was added. The reaction mixture was allowed to stir at 65 °C for 18 h under argon atmosphere. After cooling to the RT, the mixture was diluted with diethyl ether (20 mL) and filtered through a short pad of silica gel. All volatile solvents were evaporated under vacuum. The residue was purified by column chromatography on silica gel (*n*-hexane/EtOAc, 20:1) and the desired product was isolated as a yellowish powder (990 mg) in 90% yield. (*R*_f = 0.31, *n*-hexane/EtOAc 20:1); ¹H NMR (500 MHz, CDCl₃) δ ppm 7.73 (s, 3H, C^{2,4,6}H), 7.61 (dd, 6H, ³*J*_{H,H} = 8 Hz, C^{3',5'}H), 7.55 (dd, 6H, ³*J*_{H,H} = 8 Hz, C^{2',6'}H) 0.26 (s, 27H, CH₃); ¹³C NMR (125.8 MHz, CDCl₃) δ ppm 141.9 (C^{1'}), 140.9 (C^{1,3,5}), 132.7 (C^{3',5''}H), 127.3 (C^{2',6'}H), 125.4 (C^{2,4,6}H), 122.7 (C^{4'}), 105.0 (C⁷), 95.4 (C⁸), 0.2 (C⁹H₃).

1,3,5-Tris[4'-(ethynyl)phenyl]benzene (8)



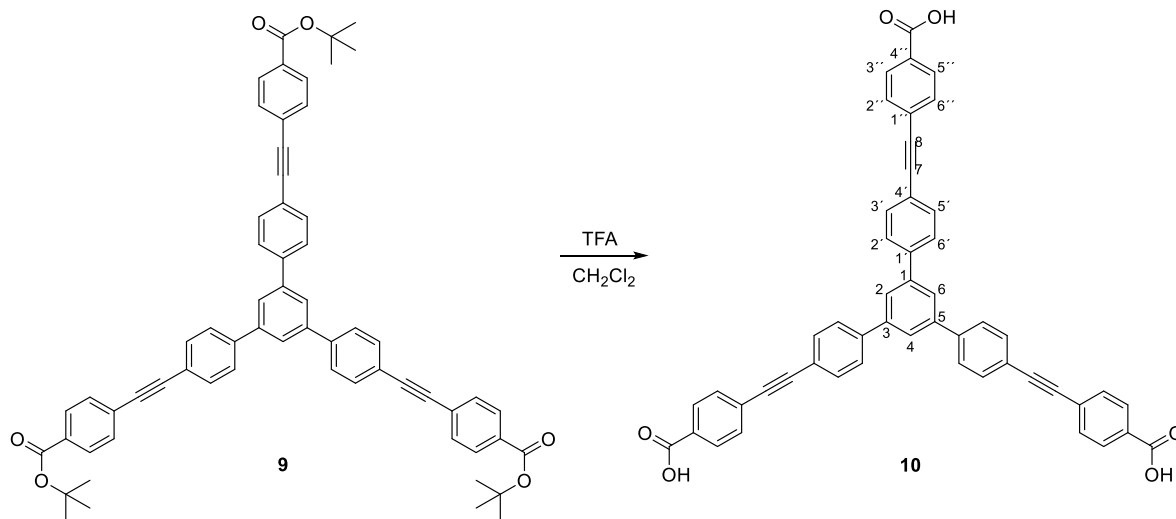
This compound was prepared according to a modified procedure.^[286] Compound **7** (900 mg, 1.51 mmol) was dissolved in the mixture of THF/MeOH (100 mL, 1/4 v/v). K_2CO_3 (1.25 g, 9.06 mmol) was added to a round bottom flask and the reaction mixture was allowed to stir at room temperature for 16 h. The mixture was diluted with diethyl ether (30 mL), filtered through a short pad of silica gel (30 g), washed with diethyl ether (50 mL), and all solvents were evaporated under the reduced pressure. The crude product was purified by column chromatography on silica gel (*n*-hexane/EtOAc, 30:1) and the pure product was isolated as a white solid (400 mg) in 70% yield. (R_f = 0.29, *n*-hexane/EtOAc 20:1); 1H NMR (500 MHz, $CDCl_3$) δ ppm 7.74 (s, 3H, $C^{2,4,6}H$), 7.63 (dd, 6H, $^3J_{H,H}$ = 8 Hz, $C^{3',5'}H$), 7.59 (dd, 6H, $^3J_{H,H}$ = 8 Hz, $C^{2',6'}H$), 3.14 (s, 3H, C^8H); ^{13}C NMR (125.8 MHz, $CDCl_3$) δ ppm 141.9 ($C^{1'}$), 141.3 ($C^{1,3,5}$), 132.9 ($C^{3',5'}H$), 127.4 ($C^{2',6'}H$), 125.5 ($C^{2,4,6}H$), 121.7 ($C^{4'}$), 83.6 (C^7), 78.3 (C^8H).

1,3,5-Tris{4-[4''-(*tert*-butoxycarbonyl)phenylethynyl]phenyl}benzene (9)



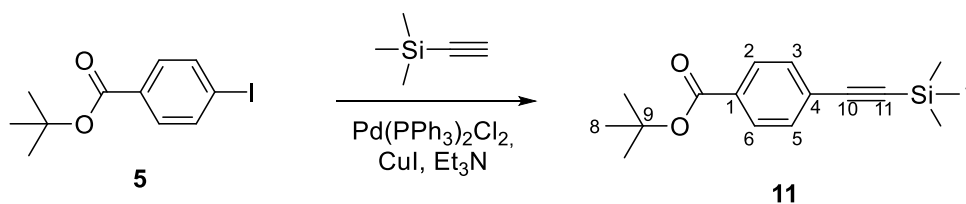
In a 50 ml Schlenk flask, *tert*-butyl-4-iodobenzoate **5** (702 mg, 2.31 mmol) and Pd(PPh₃)₂Cl₂ (23.2 mg, 0.033 mmol) were dissolved in anhydrous Et₃N (30 mL) and the solution was purged with argon for 15 min. Compound **8** (250 mg, 0.66 mmol) and CuI (3.1 mg, 0.017 mmol) were added, and the reaction mixture was allowed to stir at room temperature for 18 h under argon atmosphere. The mixture was diluted with diethyl ether (20 mL) and filtered through a short pad of silica gel (30 g, Et₂O). After evaporation of all volatiles, the residue was purified by column chromatography on silica gel (*n*-hexane/EtOAc, 10:1) and the pure product was isolated as a white solid (437 mg) in 73% yield. (*R*_f = 0.33, *n*-hexane/EtOAc, 10:1). m.p. 129-131 °C. ¹H NMR (500 MHz, CDCl₃) δ ppm 7.97 (dd, 6H, ³*J*_{H,H} = 8.5 Hz, C^{3'',5''}H), 7.81 (s, 3H, C^{2,4,6}), 7.70 (dd, 6H, ³*J*_{H,H} = 8 Hz, C^{3',5'}H), 7.65 (dd, 6H, ³*J*_{H,H} = 8 Hz, C^{2',6'}H), 7.58 (dd, 6H, ³*J*_{H,H} = 8.5 Hz, C^{2'',6''}H), 1.59 ppm (s, 27H, CH₃); ¹³C NMR (125.8 MHz, CDCl₃) δ ppm 165.4 (CO), 141.9 (C^{1'}), 141.2 (C^{1,3,5}), 132.5 (C^{3',5'}H), 131.7 (C^{2',6''}H), 131.6 (C^{3'',5''}H), 129.6 (C^{2',6'}H), 127.52 (C^{1''}), 125.5 (C^{2,4,6}H), 122.5 (C^{4'}), 92.0 (C⁷), 90.0 (C⁸), 81.6 (C-CH₃), 28.4 (CH₃); IR (KBr) ν cm⁻¹: 3080 (w) and 3038 (w, ν (=CH)), 2976 (m, ν_{as}(CH₃)), 2931 (m, ν_s(CH₃)), 2214 (m, ν (C≡C)), 1710 (s, ν (C=O)), 1601 (m, ν (C=C)), 1294 (s, ν (C-O)), 1164 (s, ν (COO-C)); UV/Vis (CH₂Cl₂) λ_{max} (ε) = 324 nm (50 400); MALDI-TOF MS (+) calcd. for C₆₃H₅₄O₆ (M⁺, 907.40), found: 907.35; Elemental Anal. Calcd. (%) for C₆₃H₅₄O₆ (907.12): C 83.42, H 6.00. Found: C 83.79, H 6.33.

1,3,5-Tris-{4'[-(carboxyphenyl)ethynyl]phenyl}benzene (10)



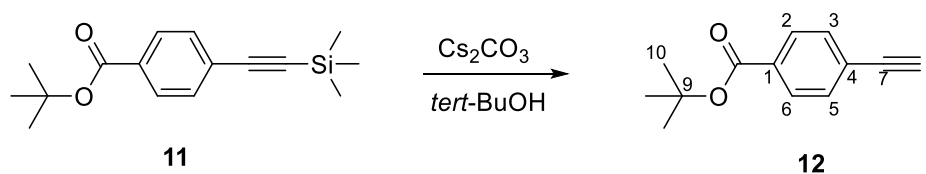
This compound was prepared according to a modified procedure.^[286] *tert*-Butyl ester **9** (170 mg, 0.187 mmol) was dissolved in CH₂Cl₂ (8 mL). To the yellowish solution was dropwise added TFA (4 mL), and the reaction mixture was stirred at room temperature for 18 h. The product was quantitatively precipitated by addition of 2 mL of EtOH. The precipitate was filtered off and continuously washed with EtOH (60 mL), water (30 mL) and CH₂Cl₂ (30 mL). After air and vacuum drying, the desired product was obtained as a white powder (134 mg) in 97% yield. m.p. > 400 °C (dec.); ¹H NMR (500 MHz, d₆-DMSO) δ ppm 13.16 (bs, 3H, COOH), 8.03 (s, 3H, C^{2,4,6}H), 8.01 (d, 6H, ³J_{H,H} = 8 Hz, C^{3',5''}H), 7.98 (d, 6H, ³J_{H,H} = 8 Hz, C^{2'',6''}H), 7.72 (d, 6H, ³J_{H,H} = 8.5 Hz, C^{3',5'}H), 7.70 (d, 6H, ³J_{H,H} = 8.5 Hz, C^{2',6'}H); ¹³C NMR (125.8 MHz, d₆-DMSO) δ ppm 166.7 (COOH), 140.7 (C^{1'}), 140.3 (C^{1,3,5}), 132.1 (C^{3',5'}H), 131.6 (C^{2'',6''}H), 130.6 (C^{3'',5''}H), 129.6 (C^{4''}), 127.6 (C^{2',6'}H), 126.6 (C^{1''}), 124.8 (C^{2,4,6}H), 121.2 (C^{4'}), 91.9 (C⁷), 89.5 (C⁸); IR (KBr) ν cm⁻¹: 3026 (bm), 2654 (bw) and 2526 (bw, ν(OH)), 2212 (w, ν (C≡C)), 1689 (s, ν (C=O)), 1601 (m, ν (C=C)), 1275 (m, ν (C-O)); UV/Vis (DMSO) λ_{max} (ε) = 321 nm (62 400); Elemental Anal. Calcd. (%) for C₅₁H₃₀O₆ (738.80): C 82.91, H 4.09. Found: C 81.48, H 4.20.

***tert*-butyl-4-[(trimethylsilyl)ethynyl]benzoate (**11**)**



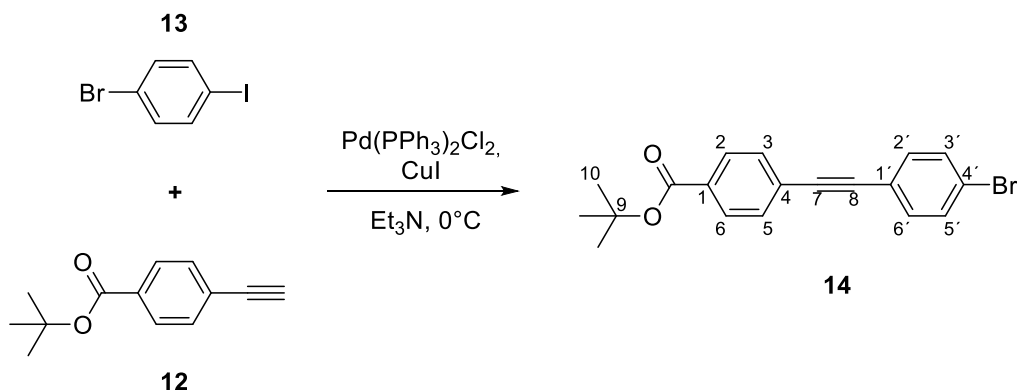
This compound was prepared according to a modified procedure.^[249] In a 250 mL Schlenk flask, *tert*-butyl 4-iodobenzoate **5** (3.00 g, 9.86 mmol), Pd(PPh₃)₂Cl₂ (346 mg, 0.49 mmol) and CuI (46.9 mg, 0.25 mmol) were dissolved in anhydrous Et₃N (80 mL). The solution was purged with argon for 15 min, and ethynyltrimethylsilane (1.94 g, 19.7 mmol) was added. The reaction mixture was allowed to stir at room temperature for 18 h under argon atmosphere. The mixture was diluted with diethyl ether (20 mL) and filtered through a short pad of silica gel. All volatile solvents were evaporated under vacuum. The residue was purified by column chromatography on silica gel (*n*-hexane/EtOAc, 30:1) and the desired product was isolated as a yellowish powder (2.67 g) in 99 % yield. (*R*_f = 0.45, *n*-hexane/EtOAc, 20:1); ¹H NMR (500 MHz, CDCl₃) δ ppm 7.88 (dd, 2H, *J*_{H,H} = 8.4 Hz, C^{2,6}H), 7.46 (dd, 2H, *J*_{H,H} = 8.4 Hz, C^{3,5}H), 1.57 (s, 9H, C⁸H₃), 0.24 (s, 9H, C⁷H₃); ¹³C NMR (125.8 MHz, CDCl₃) δ ppm 165.4 (CO), 131.9 (C^{3,5}H), 131.8 (C^{2,6}H), 129.4 (C¹), 127.4 (C⁴), 104.5 (C¹⁰), 97.4 (C¹¹), 81.5 (C⁹), 28.4 (C⁸H₃), 0.1 (C⁷H₃).

***tert*-butyl-4-ethynylbenzoate (**12**)**



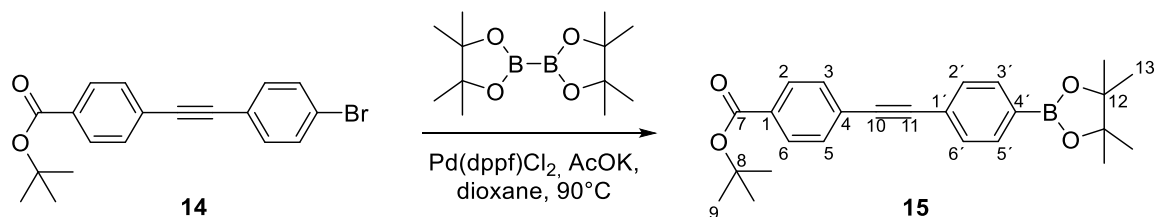
This compound was prepared according to a modified procedure.^[287] Compound **11** (2.50 g, 9.11 mmol) was dissolved in 50 mL of *tert*-BuOH. Cs₂CO₃ (14.8 g, 45.5 mmol) was added to the round bottom flask and the reaction mixture was allowed to stir at 45 °C for 8 h. After cooling to RT, the mixture was diluted with diethyl ether (30 mL) and filtered through a short pad of silica gel. The organic phase was washed with water (2 × 30 mL), brine (30 mL), dried over MgSO₄ and filtered. Evaporation of all volatile solvents under vacuum provides the desired product as a yellowish powder (1.82 g) in 99 % yield. (*R*_f = 0.43, *n*-hexane/EtOAc, 15:1); ¹H NMR (500 MHz, CDCl₃) δ ppm 7.91 (dd, 2H, *J*_{H,H} = 8 Hz, C^{2,6}H), 7.50 (dd, 2H, *J*_{H,H} = 8 Hz, C^{3,5}H), 3.19 (s, 1H, C⁸H), 1.57 (s, 9H, C¹⁰H₃); ¹³C NMR (125.8 MHz, CDCl₃) δ ppm 165.3 (CO), 132.3 (C^{3,5}H), 132.1 (C¹), 129.5 (C^{2,6}H), 126.4 (C⁴), 83.2 (C⁷), 81.6 (C⁹), 79.9 (C⁸H), 28.38 (C¹⁰H₃).

***tert*-Butyl-4[(4'-bromophenyl)ethynyl]benzoate (**14**)**



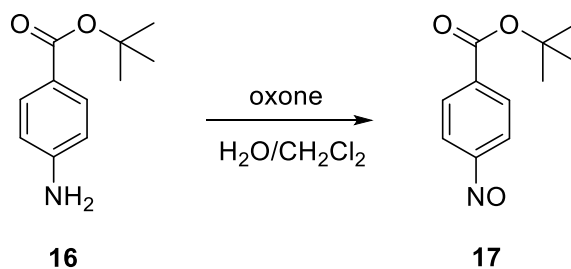
In a 100 mL Schlenk flask, 1-bromo-4-iodobenzene **13** (3.98 g, 14.1 mmol), Pd(PPh₃)₂Cl₂ (329 mg, 0.470 mmol) and CuI (61.7 mg, 0.234 mmol) were dissolved in anhydrous Et₃N (40 mL). The solution was purged with argon for 15 min, and compound **12** (1.90 g, 9.39 mmol) was added. The reaction mixture was cooled at 0 °C and allowed to stir for 16 h under argon atmosphere. The mixture was diluted with diethyl ether (20 mL) and filtered through a short pad of silica gel. All volatile solvents were evaporated under vacuum. The residue was purified by column chromatography on silica gel (*n*-hexane/EtOAc, 30:1) and the desired product isolated as a yellow solid (2.92 g) in 87 % yield. (*R*_f = 0.31, *n*-hexane/EtOAc, 20:1); m.p. 121 °C. ¹H NMR (500 MHz, CDCl₃) δ ppm 7.94 (dd, 2H, *J*_{H,H} = 8.60 Hz, C^{2,6}H), 7.53 (dd, 2H, *J*_{H,H} = 8.60 Hz, C^{3,5}H), 7.48 (dd, 2H, *J*_{H,H} = 8.60 Hz, C^{3',5'}H), 7.38 (dd, 2H, *J*_{H,H} = 8.60 Hz, C^{2',6'}H), 1.58 (s, 9H, C¹⁰H₃); ¹³C NMR (125.8 MHz, CDCl₃) δ ppm 165.4 (CO), 133.3 (C^{2',6'}H), 131.9 (C^{3,5}H), 131.9 (C^{3',5'}H), 131.6 (C¹), 129.6 (C^{2,6}H), 127.2 (C⁴), 123.2 (C^{4'}), 122.0 (C^{1'}), 91.1 (C⁸), 90.1 (C⁷), 81.6 (C⁹), 28.4 (C¹⁰H₃); IR (KBr) ν cm⁻¹ 3005 (m, ν (=CH)), 2978 (m, ν_{as} (CH₃)), 2930 (m, ν_s (CH₃)), 2365 (m, ν (C≡C)), 1715 (s, ν (C=O)), 1605 (m, ν (C=C)), 1294 (s, ν (C-O)), 1008 (m, ν (COO-O)); UV-Vis (CH₂Cl₂) λ_{max} (ε) = 302 nm (32 800), 321 nm (29 800); EI MS *m/z* (%) for C₁₉H₁₇BrO₂ (356.04): 358.0 (18), 356.0 (18, M⁺), 301.9 (98), 299.9 (100), 282.9 (27), 280.9 (27), 176.1 (47), 150.0 (14), 85.1 (21), 71.9 (23), 57.1 (32); Elemental Anal. Calcd. (%) for C₁₉H₁₇BrO₂ (357.25): C, 63.88; H, 4.80. Found: C, 63.96; H, 4.83.

***tert*-Butyl-4{[4'-(4,4,5,5-tetramethyl-1,3,2-dioxaborolan-2-yl)phenyl]ethynyl}benzoate
(15)**



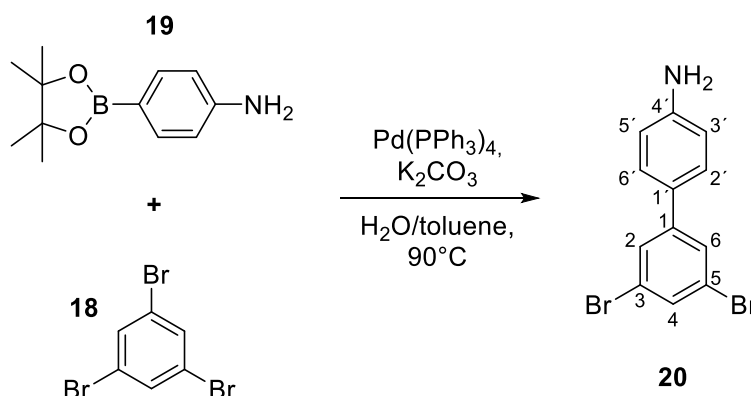
In a 250 mL Schlenk flask, compound **14** (1.00 g, 2.80 mmol), bis(pinacolato)diboron (1.07 g, 4.20 mmol), AcOK (1.37 g, 14.0 mmol) and Pd(dppf)Cl₂ (114 mg, 0.14 mmol) were dissolved in anhydrous dioxane (130 mL). The solution was purged with argon for 15 min and then allowed to stir at 90 °C for 18 h under argon atmosphere. After cooling to RT, the mixture was diluted with diethyl ether (30 mL) and filtered through a short pad of silica gel. All volatile solvents were evaporated under vacuum. The desired product was purified by column chromatography on silica gel (*n*-hexane/EtOAc, 20:1) and isolated as a white solid (1.07 g) in 95 % yield. (*R*_f = 0.27, *n*-hexane/EtOAc, 20:1); m.p. 164 °C. ¹H NMR (500 MHz, CDCl₃) δ ppm 7.94 (dd, 2H, *J*_{H,H} = 8.6 Hz, C^{2,6}H), 7.78 (dd, 2H, *J*_{H,H} = 8.6 Hz, C^{3',5'}H), 7.54 (dd, 2H, *J*_{H,H} = 8.6 Hz, C^{3,5}H) 7.52 (dd, 2H, *J*_{H,H} = 8.6 Hz, C^{2',6'}H), 1.58 (s, 9H, C⁹H₃), 1.33 (s, 12H, C¹³H₃); ¹³C NMR (125.8 MHz, CDCl₃) δ ppm 165.4 (C⁷), 134.9 (C^{3',5'}H), 131.7 (C^{2',6'}H), 131.6 (C^{3,5}H), 131.1 (C^{4'}), 129.6 (C^{2,6}H), 127.5 (C¹), 125.6 (C⁴), 92.3 (C¹¹), 90.3 (C¹⁰), 84.2 (C¹²), 81.5 (C⁸), 28.4 (C⁹H₃), 25.1 (C¹³H₃); IR (KBr) ν cm⁻¹ 3077 (w) and 3036 (w, ν (=CH)), 2957 (m) and 2927 (s, ν_{as}(CH₃)), 2855 (m, ν_s(CH₃)), 2345 (w, ν (C≡C)), 1707 (s, ν (C=O)), 1609 (s, ν (C=C)), 1361 (s) and 1296 (s, ν (C-O)), 1017 (m, ν (COO-C)); UV-Vis (CH₂Cl₂) λ_{max} (ε) = 304 nm (31 100), 324 nm (28 900); EI MS *m/z* (%) for C₂₅H₂₉BO₄ (404.22): 404.2 (12, M⁺), 348.2 (31), 303.1 (9), 262.0 (13), 248.0 (15), 97.1 (14), 83.1 (16), 57.1 (32), 56.1 (74), 41.0 (69); Elemental Anal. Calcd. (%) for C₂₅H₂₉BO₄ (404.22): C, 74.27; H, 7.23. Found: C, 76.16, H, 8.86.

***tert*-Butyl-4-nitrosobenzoate (17)**



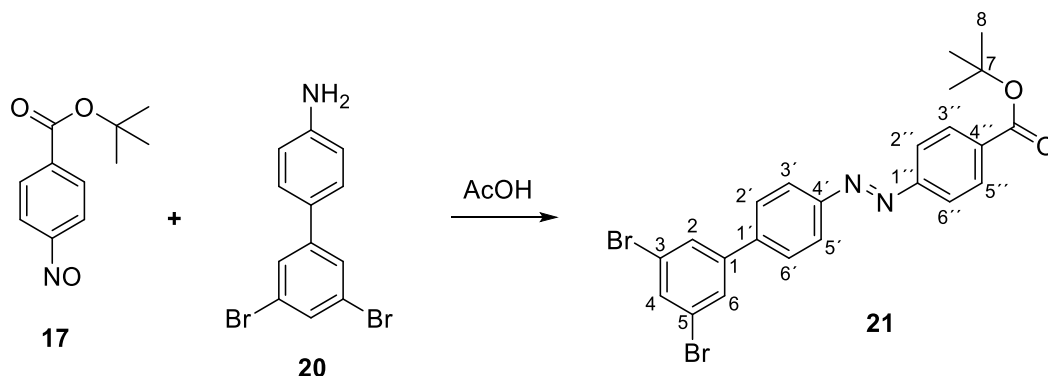
To a solution of *tert*-Butyl-4-aminobenzoate **16** (2.5 g, 12.9 mmol) in distilled dichloromethane (60 mL) was added an aqueous solution of Oxone® (15.9 g, 25.8 mmol) in water (100 mL). The reaction mixture was stirred for 16 h at room temperature and the reaction progress was checked by TLC in the mixture of dichloromethane/*n*-hexane (3:1). The two layers were separated, and the aqueous layer was washed with dichloromethane (2 x 50 mL). The combined organic layer was washed sequentially with HCl (100 mL, 1M), NaHCO_3 (100 mL, saturated), brine (100 mL), dried over MgSO_4 and filtered. Solvents were evaporated under reduced pressure and the resulting crude product was purified on a short pad of silica gel (300 g) in dichloromethane/*n*-hexane (2:1). The isolated product, a greenish solid (2.51 g, 94%), is unstable and hence was used without further purification in the subsequent Mills reaction ($R_f = 0.55$, dichloromethane/*n*-hexane, 3:1).

4-Amino-3',5'-dibromobiphenyl (**20**)



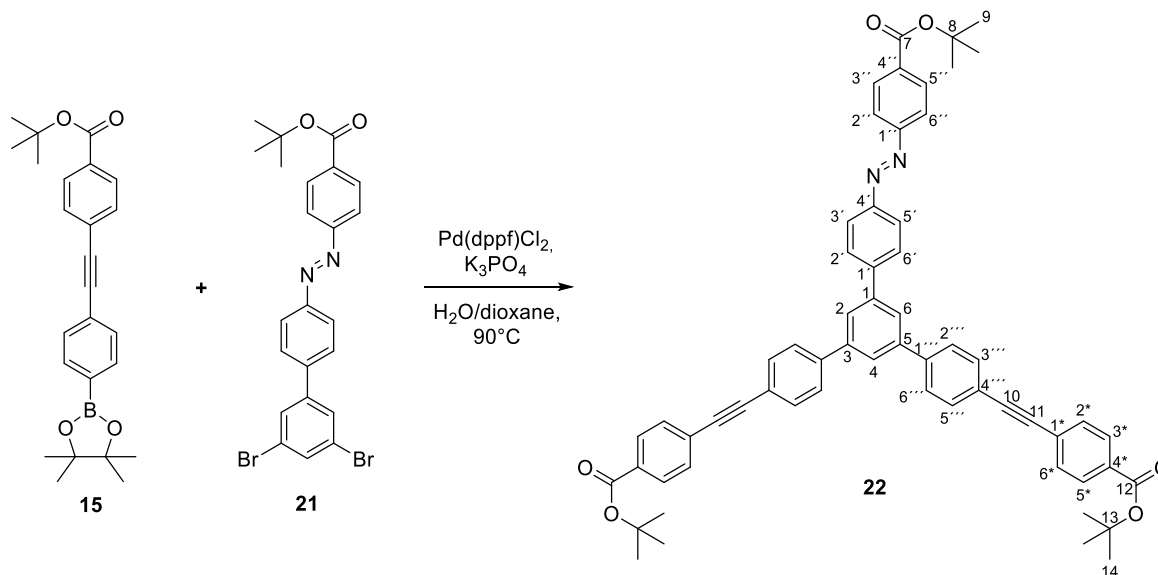
In a 100 mL Schlenk flask, 1,3,5-tribromobenzene **18** (800 mg, 2.54 mmol) and 4-aminophenylboronic acid pinacol ester **19** (834 mg, 3.81 mmol) were dissolved in anhydrous dioxane (30 mL). The solution was purged with argon for 15 min. To the degassed solution an aqueous solution of Cs₂CO₃ (2.48 g, 7.62 mmol) in 3 mL of water was added and the reaction mixture was purged with argon for 15 min. Subsequently Pd(PPh₃)₄ (293 mg, 0.254 mmol) was added and the mixture was allowed to stir at 90 °C for 16 h under argon atmosphere. After cooling down to RT, the reaction mixture was diluted with ethyl acetate (50 mL) and washed with water (3 × 50 mL). The organic phase was further washed with Na₂CO₃ (50 mL, saturated), brine (50 mL), dried over MgSO₄ and filtered. All volatile solvents were evaporated under vacuum. The desired product was purified by column chromatography on silica gel (*n*-hexane/EtOAc, 3:1) and isolated as a yellow solid (357 mg) in 43 % yield. (*R*_f = 0.42, *n*-hexane/EtOAc, 7:3); m.p. 116°C. ¹H NMR (500 MHz, DMSO-*d*₆) δ ppm 7.72 (d, 2H, *J*_{H,H} = 1.8 Hz, C^{2,6}H), 7.61 (t, 1H, *J*_{H,H} = 1.7 Hz, C⁴H), 7.41 (dd, 2H, *J*_{H,H} = 8.6 Hz C^{2',6'}H), 6.62 (dd, 2H, *J*_{H,H} = 8.6 Hz C^{3',5'}H), 5.44 (s, 2H, NH₂); ¹³C NMR (125.8 MHz, DMSO-*d*₆) δ ppm 149.6 (C⁴), 144.8 (C¹), 130.0 (C⁴), 127.6 (C^{2',6'}H), 126.8 (C^{2,6}H), 123.7 (C^{1'}), 123.0 (C^{3,5}H), 114.1 (C^{3',5'}H); IR (KBr) ν cm⁻¹ 3422 (m) and 3321 (m, ν (N-H)), 3067 (w, ν (=CH)), 1604 (m, ν (C=C)), 1282 (m, ν (C-N)); UV-Vis (CH₂Cl₂) λ_{max} (ε) = 298 nm (16 200); MALDI-TOF MS (+) calcd. for C₁₂H₁₀Br₂N (M⁺, 326.91), found: 326.87; Elemental Anal. Calcd. (%) for C₁₂H₉Br₂N (327.02): C, 44.07; H, 2.77; N, 4.28. Found: C, 44.71; H, 3.18; N, 4.29.

***tert*-Butyl-4-[(3',5'-dibromobiphenyl-4-yl)diazenyl]benzoate (**21**)**



In a 100 mL Schlenk flask, *tert*-butyl 4-nitrosobenzoate **17** (634 mg, 3.06 mmol) was dissolved in glacial acetic acid (40 mL) under argon atmosphere. Subsequently, amine **20** (500 mg, 1.53 mmol) was added to the green solution. The reaction mixture was allowed to stir at RT for 20 h under argon atmosphere, during which time an orange precipitate was formed. The precipitate was filtered off, washed with AcOH and air-dried. The desired product was isolated without further purification as an orange solid (553 mg) in 70 % yield. (R_f = 0.32, *n*-hexane/EtOAc, 20:1); m.p. 111 °C. ^1H NMR (500 MHz, CDCl_3) δ ppm 8.13 (dd, 2H, $J_{\text{H,H}}$ = 8.6 Hz, $\text{C}^{3'',5''}\text{H}$), 8.01 (dd, 2H, $J_{\text{H,H}}$ = 8.5 Hz, $\text{C}^{3',5'}\text{H}$), 7.93 (dd, 2H, $J_{\text{H,H}}$ = 8.5 Hz, $\text{C}^{2'',6''}\text{H}$), 7.71 (d, 2H, $J_{\text{H,H}}$ = 1.8 Hz, $\text{C}^{2,6}\text{H}$), 7.68 (m, 3H, C^4H and $\text{C}^{2',6'}\text{H}$), 1.61 (s, 9H, C^8H_3); ^{13}C NMR (125.8 MHz, CDCl_3) δ ppm 165.3 (CO), 155.0 ($\text{C}^{1''}$), 152.5 ($\text{C}^{4'}$), 143.8 (C^1), 141.4 ($\text{C}^{1'}$), 134.2 ($\text{C}^{4''}$), 133.5 (C^4H), 130.7 ($\text{C}^{3'',5''}\text{H}$), 129.2 ($\text{C}^{2,6}\text{H}$), 128.1 ($\text{C}^{2',6'}\text{H}$), 124.0 ($\text{C}^{3',5'}\text{H}$), 123.7 ($\text{C}^{3,5}$), 122.8 ($\text{C}^{2'',6''}\text{H}$), 81.8 (C^7), 28.4 (C^8H_3); IR (KBr) ν cm^{-1} 3060 (w, ν (=CH)), 2977 (m, ν_{as} (CH_3)), 2928 (m, ν_{s} (CH_3)), 1708 (s, ν (C=O)), 1548 (m, ν (C=C)), 1457 (m, ν (N=N)), 1290 (s, ν (C-N)); UV-Vis (THF) λ_{max} (ϵ) = 349 nm (41 900), 456 (1 400); ESI (-) MS calcd. for $\text{C}_{23}\text{H}_{20}\text{Br}_2\text{N}_2\text{O}_2$ (M^- , 515.99), found: 515.95; Elemental Anal. Calcd. (%) for $\text{C}_{23}\text{H}_{20}\text{Br}_2\text{N}_2\text{O}_2$ (516.23): C, 53.51; H, 3.91; N, 5.43. Found: C, 53.74; H, 4.29; N, 5.39.

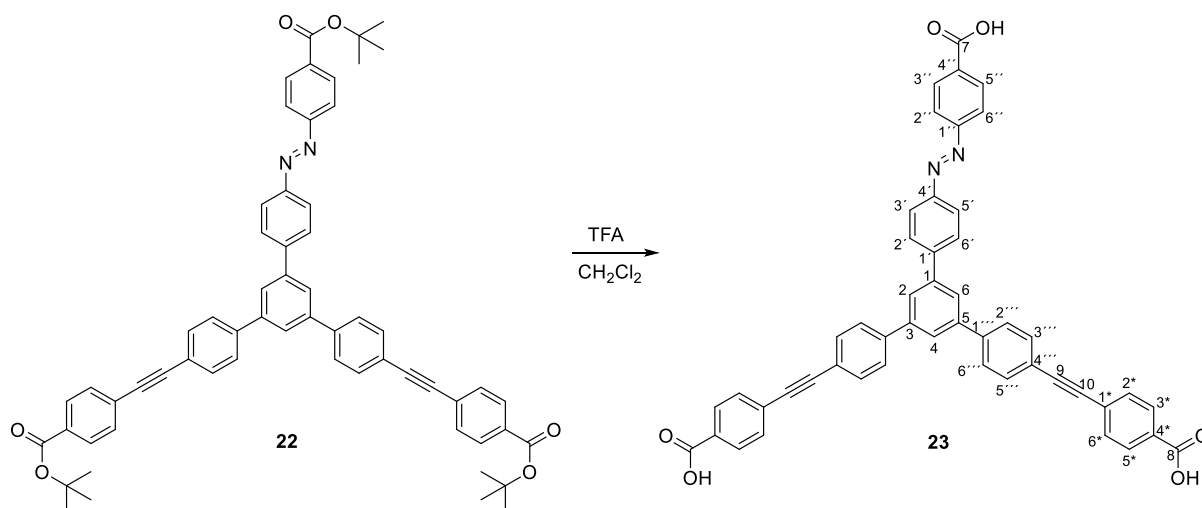
***tert*-Butyl 4-{{[3',5'-bis(4'-{{[4''-(*tert*-butoxycarbonyl)phenyl]ethynyl}phenyl)biphenyl-4-yl]diazenyl}benzoate (**22**)**



In a 100 mL Schlenk flask, compound **21** (200 mg, 0.387 mmol) and compound **15** (391 mg, 0.970 mmol) were dissolved in anhydrous dioxane (24 mL). After purging the solution with argon for 15 min, an aqueous solution of K_3PO_4 (410 mg, 1.93 mmol) in 4 mL of H_2O was added and the reaction mixture purged for an additional 15 min. Subsequently $Pd(dppf)Cl_2$ (31.6 mg, 0.039 mmol) was added and the degassed mixture was allowed to stir at 90 °C for 30 min under argon atmosphere. After cooling to RT, the mixture was diluted with water (30 mL) and extracted with CH_2Cl_2 (3 × 30 mL). The organic phases were combined, dried over $MgSO_4$ and the solvent evaporated under vacuum. The desired product was purified by column chromatography on silica gel (*n*-hexane/EtOAc, 20:1) and isolated as orange powder (290 mg) in 82 % yield. (R_f = 0.24, *n*-hexane/EtOAc, 15:1); m.p. 126 °C. 1H NMR (500 MHz, $CDCl_3$) δ ppm 8.14 (dd, 2H, $J_{H,H}$ = 8.3 Hz, $C^{3'',5''}$ H), 8.06 (dd, 2H, $J_{H,H}$ = 8.2 Hz, $C^{3',5'}$ H), 7.97 (m, 6H, $C^{3*,5*}$ H and $C^{2'',6''}$ H), 7.86 (m, 4H, $C^{2,6}$ H and $C^{2',6'}$ H), 7.83 (s, 1H, C^4 H), 7.71 (dd, 4H, $J_{H,H}$ = 8.3 Hz, $C^{2'',6''}$ H), 7.66 (dd, 4H, $J_{H,H}$ = 8.3 Hz, $C^{3'',5''}$ H), 7.58 (dd, 4H, $J_{H,H}$ = 8.3 Hz, $C^{2*,6*}$ H), 1.62 (s, 9H, C^9H_3), 1.60 (s, 18H, $C^{14}H_3$); ^{13}C NMR (125.8 MHz, $CDCl_3$) δ ppm 165.4 (C^7 and C^{12}), 155.1 ($C^{1'}$), 152.2 ($C^{4'}$), 144.1 ($C^{1'}$), 142.0 (C^{1*}), 141.8 (C^1), 141.1 ($C^{1''}$), 134.0 ($C^{4''}$), 132.5 ($C^{3'',5''}$ H), 131.7 (C^{4*} and $C^{3,5}$), 131.6 ($C^{2*,6*}$ H), 130.7 ($C^{3'',5''}$ H), 129.6 ($C^{3*,5*}$ H), 128.3 ($C^{2,6}$ H), 127.5 ($C^{2'',6''}$ H), 125.7 (C^4 H), 125.6 ($C^{2,6}$ H), 124.0 ($C^{3',5'}$ H), 122.8 ($C^{2'',6''}$ H), 122.5 ($C^{4''}$), 92.0 (C^{10}), 90.1 (C^{11}), 81.7 (C^8), 81.5 (C^{13}), 29.9 (C^9H_3), 28.4 ($C^{14}H_3$); IR (KBr) ν cm^{-1} 3043 (w, ν (=CH)), 2975 (m) and 2930 (m, ν_{as} (CH_3)), 2854 (w, ν_s (CH_3)), 2362 (w) and 2337 (w, ν ($C\equiv C$)), 1712 (s, ν ($C=O$)), 1601 (m, ν ($C=C$)), 1517 (m, ν ($N=N$)), 1368 (m, ν ($C-N$)), 1293 (s, ν ($C-O$)), 1016 (m, ν ($COO-C$)); UV-Vis (THF) λ_{max} (ϵ) = 327 nm (96 100), 442 (1 400); ESI (+) MS calcd. for $C_{61}H_{54}N_2O_6Na$ (933.39), found: 933.40;

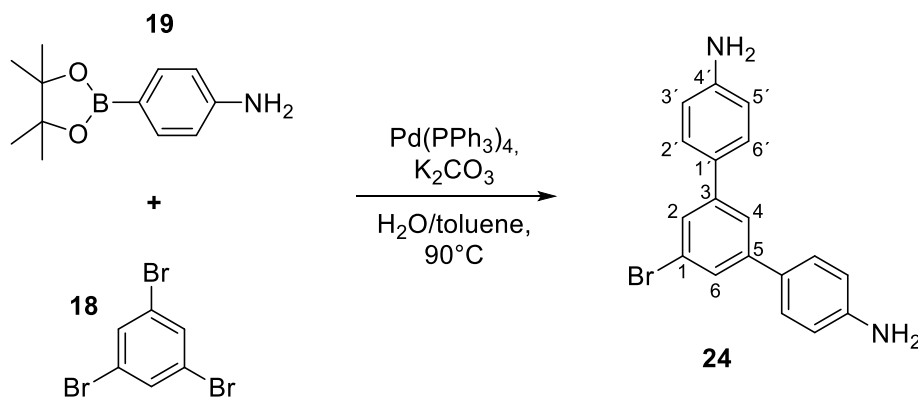
Elemental Anal. Calcd. (%) for $C_{61}H_{54}N_2O_6$ (911.11): C, 80.41; H, 5.97; N, 3.07. Found: C, 80.48; H, 6.39; N, 3.04.

4-[(3',5'-Bis{4'-[(4''-carboxyphenyl)ethynyl]phenyl}biphenyl-4-yl)diazenyl]benzoic acid (23**)**



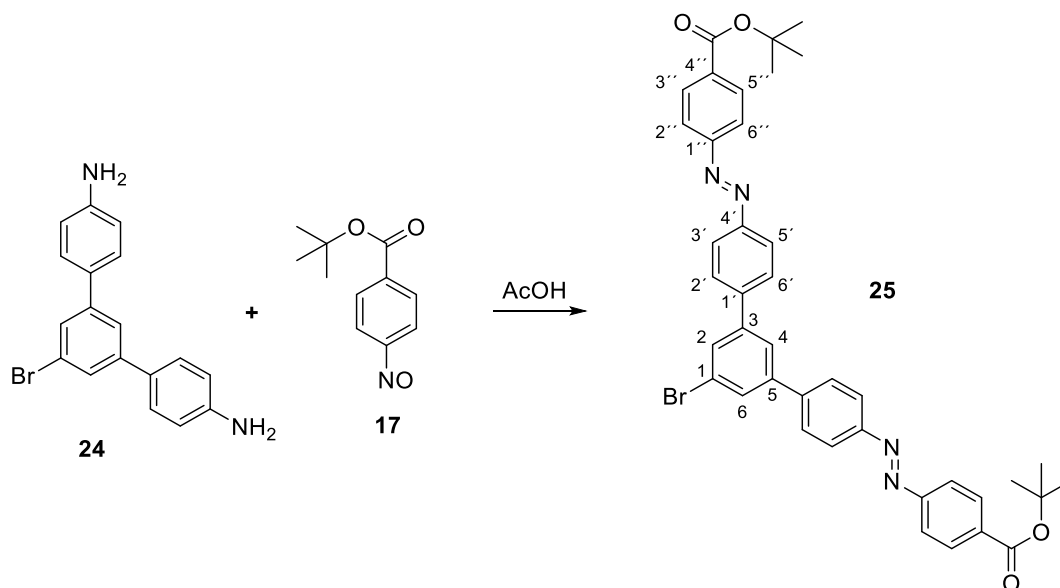
To a solution of *tert*-butyl ester **22** (200 mg, 0.220 mmol) in dichloromethane (10 mL) was added TFA (5 mL) and the dark red solution was allowed to stir at RT for 20 h. The product was quantitatively precipitated by addition of 2 mL of EtOH. The precipitate was filtered off and continuously washed with EtOH (60 mL), water (30 mL) and CH_2Cl_2 (30 mL). After air and vacuum drying, the desired product was isolated as light orange powder (158 mg) in 97 % yield. m.p. 310 °C. 1H NMR (500 MHz, $DMSO-d_6$) δ ppm 8.19 (dd, 2H, $J_{H,H} = 8.5$ Hz, $C^{2',6'}H$), 8.16 (dd, 2H, $J_{H,H} = 8.5$ Hz, $C^{3'',5''}H$), 8.10-7.98 (m, 13H, C^4H , $C^{3',5'}H$, $C^{2'',6''}H$, $C^{2''',6'''H}$, $C^{3*,5*}H$), 7.73 (dd, 4H, $J_{H,H} = 8.5$ Hz, $C^{3''',5'''}H$), 7.71 (dd, 4H, $J_{H,H} = 8.5$ Hz, $C^{2*,6*}H$); ^{13}C NMR (125.8 MHz, $DMSO-d_6$) δ ppm 166.7 (C^7 and C^8), 154.3 ($C^{1''}$), 151.3 ($C^{4'}$), 143.3 ($C^{1'}$), 140.7 (C^1), 140.5 ($C^{3,5}$), 140.3 ($C^{1'''}$), 133.0 ($C^{4''}$), 132.2 ($C^{3'',5''}H$), 131.6 ($C^{2*,6*}H$), 130.7 ($C^{3''',5'''}H$), 129.6 ($C^{3*,5*}H$), 128.4 ($C^{2',6'}H$), 127.6 ($C^{2''',6'''H}$), 126.6 (C^{1*}), 125.2 (C^4H), 125.0 ($C^{2,6}H$), 123.5 ($C^{2'',6''}H$), 122.6 ($C^{3',5'}H$), 121.2 ($C^{4'''}$), 91.9 (C^9), 89.6 (C^{10}); IR (KBr) ν cm^{-1} 2922 (m), 2852 (m), 2657 (m) and 2539 (m, ν (O-H)), 2213 (w, ν ($C\equiv C$)), 1690 (s, ν ($C=O$)), 1601 (s, ν ($C=C$)), 1418 (s, ν ($N=N$)), 1279 (m, ν ($C-O$)); UV-Vis (DMSO) λ_{max} (ϵ) = 331 (92 100), 453 (1 400); ESI (-) MS calcd. for $C_{49}H_{29}N_2O_6$ ($[M-H]^-$, 741.20), found: 741.65; Elemental Anal. Calcd. (%) for $C_{49}H_{30}N_2O_6$ (742.79): C, 79.23; H, 4.07; N, 3.77. Found: C, 78.37; H, 4.83; N, 3.12.

5'-Bromo-(1,1':3',1''-terphenyl)-4,4''-diamine (24)



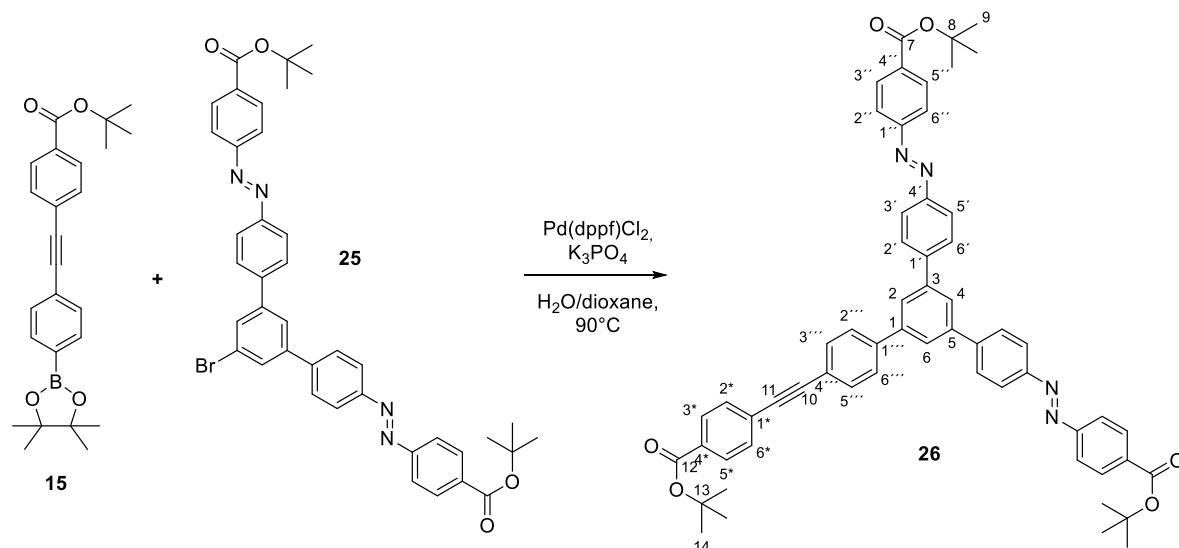
In a 100 mL Schlenk flask, 1,3,5-tribromobenzene **18** (800 mg, 2.54 mmol) and 4-aminophenylboronic acid pinacol ester **19** (1.39 g, 6.35 mmol) were dissolved in anhydrous dioxane (30 mL). The solution was purged with argon for 15 min. To the degassed solution was added an aqueous solution of K_2CO_3 (1.04 g, 7.62 mmol) in 3 mL of water and the reaction mixture was purged with argon for 15 min. Subsequently $\text{Pd(PPh}_3)_4$ (293 mg, 0.254 mmol) was added and the mixture was allowed to stir at 90°C for 16 h under argon atmosphere. After cooling to RT, the reaction mixture was diluted with ethyl acetate (50 mL) and washed with water (3 x 50 mL). The organic phase was further washed with Na_2CO_3 (50 mL, saturated), brine (50 mL), dried over MgSO_4 and filtered. All volatile solvents were evaporated under vacuum. The desired product was purified by column chromatography on silica gel (*n*-hexane/EtOAc, 1:1) and isolated as yellow solid (413 mg) in 48 % yield. (R_f = 0.34, *n*-hexane/EtOAc, 1:1); m.p. 137°C . ^1H NMR (500 MHz, $\text{DMSO-}d_6$) δ ppm 7.63 (t, 1H, $J_{\text{H,H}}$ = 1.6 Hz, C^4H), 7.51 (d, 2H, $J_{\text{H,H}}$ = 1.6 Hz, $\text{C}^{2,6}\text{H}$), 7.44 (dd, 4H, $J_{\text{H,H}}$ = 8.5 Hz, $\text{C}^{2',6'}\text{H}$), 6.64 (dd, 4H, $J_{\text{H,H}}$ = 8.5 Hz, $\text{C}^{3',5'}\text{H}$), 5.32 (s, 4H, NH_2); ^{13}C NMR (125.8 MHz, $\text{DMSO-}d_6$) δ ppm 149.0 ($\text{C}^{4'}$), 143.4 ($\text{C}^{3,5}$), 127.5 ($\text{C}^{2,6}\text{H}$), 125.8 ($\text{C}^{1'}$), 125.0 ($\text{C}^{2',6'}\text{H}$), 123.0 (C^1), 121.3 (C^4H), 114.1 ($\text{C}^{3',5'}\text{H}$); IR (KBr) ν cm^{-1} 3422 (m) and 3321 (m, ν (N-H)), 3067 (w, ν (=CH)), 1604 (m, ν (C=C)), 1282 (m, ν (C-N)); UV-Vis (CH_2Cl_2) λ_{max} (ϵ) = 290 nm (76 000); MALDI-TOF MS (+) calcd. for $\text{C}_{18}\text{H}_{16}\text{BrN}_2$ ($[\text{M}+\text{H}]^+$, 339.05), found: 339.08; Elemental Anal. Calcd. (%) for $\text{C}_{18}\text{H}_{15}\text{BrN}_2$ (339.23): C 63.73, H 4.46, N 8.86. Found: C 64.90, H 5.08, N 7.60.

1-Bromo-3,5-di(4'-{[4''-(*tert*-butoxycarbonyl)phenyl]diazenyl}phenyl)benzene (25)



In a 100 mL Schlenk flask, *tert*-butyl 4-nitrosobenzoate **17** (914 mg, 4.41 mmol) was dissolved in glacial acetic acid (40 mL) under argon atmosphere. Subsequently diamine **24** (500 mg, 1.47 mmol) was added to the green solution. The reaction mixture was allowed to stir at RT for 20 h under argon atmosphere, during which time an orange precipitate was formed. The precipitate was filtered off, washed with AcOH and air dried. The desired product was isolated without further purification as orange solid (770 mg) in 73 % yield. (R_f = 0.26, *n*-hexane/EtOAc, 15:1); m.p. 137 °C. ^1H NMR (500 MHz, CDCl_3) δ ppm 8.13 (dd, 4H, $J_{\text{H,H}}$ = 8.70 Hz, $\text{C}^{3'',5''}\text{H}$), 8.05 (dd, 4H, $J_{\text{H,H}}$ = 8.70 Hz, $\text{C}^{3',5'}\text{H}$), 7.95 (dd, 4H, $J_{\text{H,H}}$ = 8.70 Hz, $\text{C}^{2'',6''}\text{H}$), 7.83 (m, 1H, C^4H), 7.81 (m, 2H, $\text{C}^{2,6}\text{H}$), 7.79 (dd, 4H, $J_{\text{H,H}}$ = 8.70 Hz, $\text{C}^{2',6'}\text{H}$), 1.62 (s, 18H, CH_3); ^{13}C NMR (125.8 MHz, CDCl_3) δ ppm 165.4 (CO), 155.1 ($\text{C}^{1''}$), 152.4 ($\text{C}^{4'}$), 143.0 ($\text{C}^{1'}$), 142.7 ($\text{C}^{3,5}$), 134.1 (C^1), 130.7 ($\text{C}^{3'',5''}\text{H}$), 129.9 ($\text{C}^{2,6}\text{H}$), 128.2 ($\text{C}^{2',6'}\text{H}$), 125.1 (C^4H), 124.0 ($\text{C}^{3',5'}\text{H}$), 122.8 ($\text{C}^{2'',6''}\text{H}$), 81.7 (C- CH_3), 28.4 (CH_3); IR (KBr) ν cm^{-1} 3055 (w, ν (=CH)), 2975 (m) and 2925 (m, $\nu_{\text{as}}(\text{CH}_3)$), 2854 (w, $\nu_{\text{s}}(\text{CH}_3)$), 1715 (s, ν (C=O)), 1559 (m, ν (C=C)), 1368 (m, ν (C-N)), 1292 (s, ν (C-O)); UV-Vis (THF) λ_{max} (ϵ) = 358 nm (58 400), 447 nm (2 700); MALDI-TOF MS (-) calcd. for $\text{C}_{40}\text{H}_{37}\text{BrN}_4\text{O}_4$ (M^- , 716.20), found: 716.46; Elemental Anal. Calcd. (%) for $\text{C}_{40}\text{H}_{37}\text{BrN}_4\text{O}_4$ (717.66): C, 66.94; H, 5.20; N, 7.81. Found: C, 67.37; H, 5.71; N, 7.35.

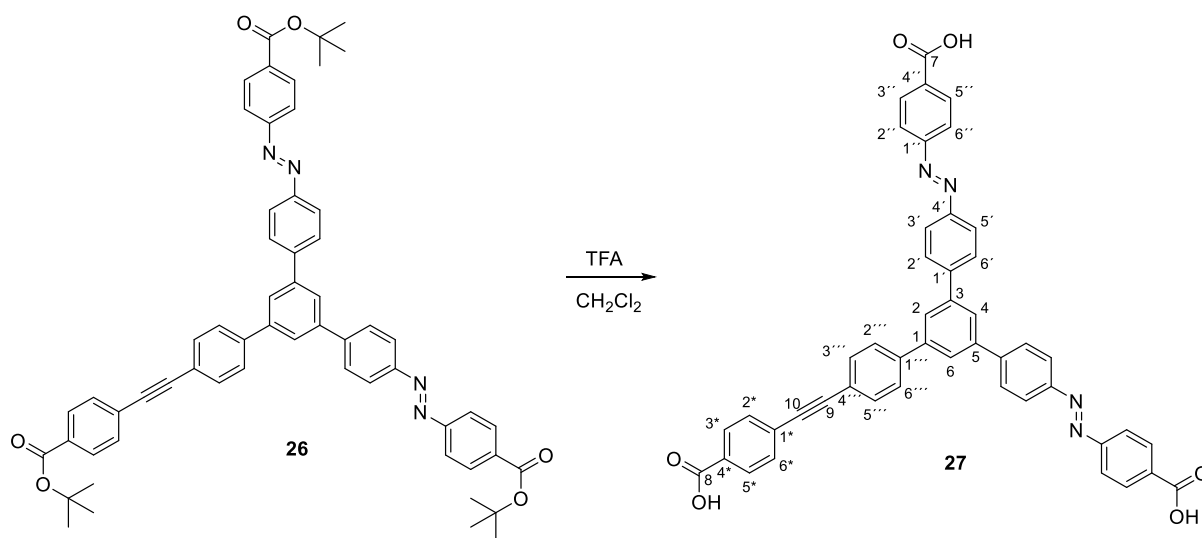
***tert*-Butyl 4-[[[3',5'-bis(4'-{[4''-(*tert*-butoxycarbonyl)phenyl]diazenyl}phenyl)biphenyl-4-yl]ethynyl]benzoate (**26**)**



In a 100 mL Schlenk flask, compound **25** (200 mg, 0.280 mmol) and compound **15** (170 mg, 0.420 mmol) were dissolved in anhydrous dioxane (24 mL). The resulting solution was stirred for 15 min while purging with argon, then an aqueous solution of K_3PO_4 (297 mg, 1.40 mmol) in 4 mL of H_2O was added, and the reaction mixture purged for an additional 15 min. Subsequently $Pd(dppf)Cl_2$ (22.8 mg, 0.028 mmol) was added and the degassed mixture was allowed to stir at 90 °C for 30 min under argon atmosphere. After cooling to RT, the mixture was diluted with water (30 mL) and extracted with CH_2Cl_2 (3 × 30 mL). The organic phases were combined, dried over $MgSO_4$ and all solvents were evaporated under vacuum. The desired product was purified by column chromatography on silica gel (*n*-hexane/EtOAc, 15:1) and isolated as an orange powder (213 mg) in 83 % yield. (R_f = 0.21, *n*-hexane/EtOAc, 15:1); m.p. 111-113 °C. 1H NMR (500 MHz, $CDCl_3$) δ ppm 8.14 (dd, 4H, $J_{H,H}$ = 8.70 Hz, $C^{3'',5''}H$), 8.08 (dd, 4H, $J_{H,H}$ = 8.70 Hz, $C^{3',5'}H$), 7.96 (m, 6H, $C^{3*,5*}H$ and $C^{2',6'}H$), 7.92 (m, 1H, C^4H), 7.88 (m, 6H, $C^{2,6}H$ and $C^{2'',6''}H$), 7.73 (dd, 2H, $J_{H,H}$ = 8.20 Hz, $C^{3''',5'''}H$), 7.67 (dd, 2H, $J_{H,H}$ = 8.20, $C^{2*,6*}H$), 7.58 (dd, 2H, $J_{H,H}$ = 8.20, $C^{2''',6'''}H$), 1.62 (s, 18H, C^9H_3), 1.59 (s, 9H, $C^{14}H_3$); ^{13}C NMR (125.8 MHz, $CDCl_3$) δ ppm 165.4 (C^7 and C^{12}), 155.1 ($C^{1'}$), 152.2 ($C^{4'}$), 144.0 ($C^{1'}$), 142.1 ($C^{1''}$), 141.8 (C^1 and $C^{3,5}$), 141.1 ($C^{4''}$), 134.1 (C^{4*}), 132.6 ($C^{2*,6*}H$), 131.7 (C^{1*}), 131.6 ($C^{2'',6''}H$), 130.7 ($C^{3'',5''}H$), 129.6 ($C^{3*,5*}H$), 128.3 ($C^{2'',6''}H$), 127.6 ($C^{3''',5'''}H$), 125.9 ($C^{2,6}H$), 125.8 (C^4H), 124.0 ($C^{3',5'}H$), 122.8 ($C^{2',6'}H$), 122.6 ($C^{4''}$), 92.0 (C^{10}), 90.1 (C^{11}), 81.7 (C^8), 81.6 (C^{13}), 28.4 (C^9H_3), 27.1 ($C^{14}H_3$); IR (KBr) ν cm^{-1} 3043 (w, ν (=CH)), 2975 (m, ν_{as} (CH_3)), 2929 (m, ν_s (CH_3)), 2363 (w, ν ($C\equiv C$)), 1715 (s, ν ($C=O$)), 1599 (m, ν ($C=C$)), 1368 (m, ν ($C-N$)), 1293 (s, ν ($C-O$)); UV-Vis (THF) λ_{max} (ϵ) = 343 (63 800), 445 (2 500); MALDI-TOF MS (+) calcd. for $C_{59}H_{55}N_4O_6$ ($[M+H]^+$, 915.41),

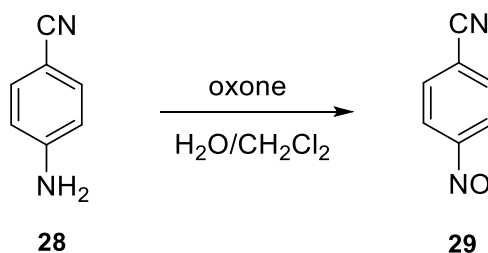
found: 915.36; Elemental Anal. Calcd. (%) for $C_{59}H_{54}N_4O_6$ (915.10): C, 77.44; H, 5.95; N, 6.12. Found: C, 72.37; H, 6.20; N, 5.62.

4-[(3',5'-Bis{4'-[(4''-carboxyphenyl)diazenyl]phenyl}biphenyl-4-yl)ethynyl]benzoic acid (27)



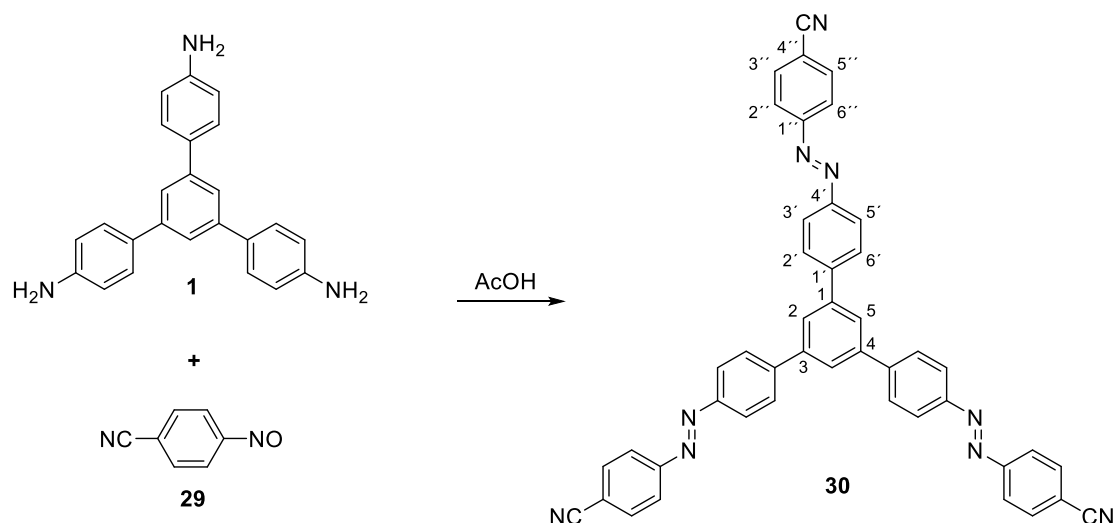
To a solution of *tert*-butyl ester **26** (200 mg, 0.219 mmol) in dichloromethane (10 mL) was added TFA (5 mL) and the dark red solution was allowed to stir at RT for 20 h. The product was quantitatively precipitated by addition of 2 mL of EtOH. The precipitate was filtered off and continuously washed with EtOH (60 mL), water (30 mL) and CH_2Cl_2 (30 mL). After air and vacuum drying, the desired product was isolated as a light orange powder (159 mg) in 97 % yield. m.p. 326 °C. 1H NMR (500 MHz, $DMSO-d_6$) δ ppm 8.20 (dd, 4H, $J_{H,H} = 8.30$ Hz, $C^{3'',5''}H$), 8.16 (dd+s, 5H, $J_{H,H} = 8.30$ Hz, $C^{3',5'}$ and C^4), 8.13 (s, 2H, $C^{2,6}H$), 8.07 (dd, 4H, $J_{H,H} = 8.30$ Hz, $C^{2',6'}H$), 8.04 (dd, 2H, $J_{H,H} = 8.60$ Hz, $C^{3*,5*}H$), 8.00 (m, 6H, $C^{2'',6''}H$ and $C^{3''',5'''}H$), 7.74 (dd, 2H, $J_{H,H} = 8.60$ Hz, $C^{2*,6*}H$), 7.70 (dd, 2H, $J_{H,H} = 8.60$ Hz, $C^{2'',6''}H$); ^{13}C NMR (125.8 MHz, $DMSO-d_6$) δ ppm 166.7 (C^7 and C^8), 154.3 ($C^{1''}$), 151.4 ($C^{4'}$), 143.2 ($C^{1'}$), 140.8 ($C^{1'''}$), 140.6 (C^1 and $C^{3,5}$), 140.3 ($C^{4''}$), 133.1 (C^{4*}), 132.2 ($C^{3''',5'''}H$), 131.6 (C^{4H} and $C^{3',5'}H$), 130.7 ($C^{3'',5''}H$), 129.6 ($C^{3*,5*}H$), 128.4 ($C^{2*,6*}H$ and $C^{2''',6'''}H$), 127.7 ($C^{2,6}H$), 123.5 ($C^{2',6'}H$), 122.6 ($C^{2'',6''}H$), 121.3 (C^{1*}), 91.9 (C^9), 89.6 (C^{10}); IR (KBr) ν cm^{-1} 2967 (m), 2643 (m) and 2530 (m, ν (O-H)), 2349 (w, ν ($C\equiv C$)), 1689 (s, ν ($C=O$)), 1598 (s, ν ($C=C$)), 1410 (m, ν ($N=N$)), 1277 (m, ν ($C-N$)), 1240 (m, ν ($C-O$)); UV-Vis ($DMSO$) λ_{max} (ϵ) = 344 nm (54 400), 458 (2 800); ESI (-) MS calcd. for $C_{47}H_{29}N_4O_6$ ($[M-H]^-$, 745.21), found: 745.65; Elemental Anal. Calcd. (%) for $C_{47}H_{30}N_4O_6$ (746.78): C, 75.59; H, 4.05; N, 7.50. Found: C, 74.61; H, 4.19; N, 7.27.

4-Nitrosobenzonitrile (**29**)



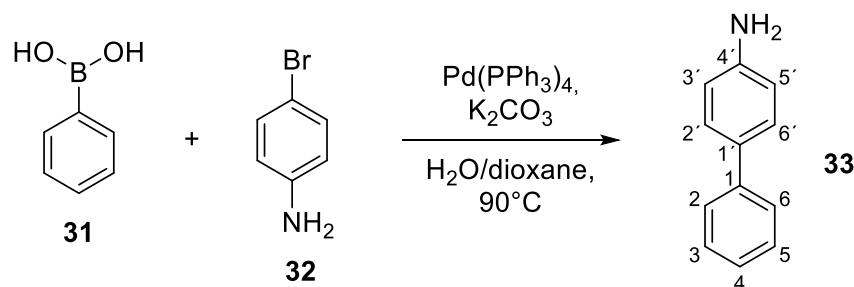
To a solution of 4-aminobenzonitrile **28** (2.0 g, 0.017 mol) in distilled dichloromethane (60 mL) was added an aqueous solution of Oxone® (10.4 g, 0.034 mol) in water (100 mL). The reaction mixture was stirred for 16 h at room temperature and the reaction progress was checked by TLC in the mixture of dichloromethane/*n*-hexane (3:1). The two layers were separated, and the aqueous layer was washed with dichloromethane (2 x 50 mL). The combined organic layer was washed sequentially with HCl (100 mL, 1M), NaHCO₃ (100 mL, saturated), brine (100 mL), dried over MgSO₄ and filtered. Solvents were evaporated under reduced pressure and the resulting crude product was purified on a short pad of silica gel (300 g) in dichloromethane/*n*-hexane (2:1). The isolated product, a greenish solid (2.13 g, 95%), is unstable and hence was used without further purification in the subsequent Mills reaction (R_f = 0.49, dichloromethane/*n*-hexane, 3:1).

1,3,5-Tris{4'-[(4''-cyanophenyl)diazenyl]phenyl}benzene (30)



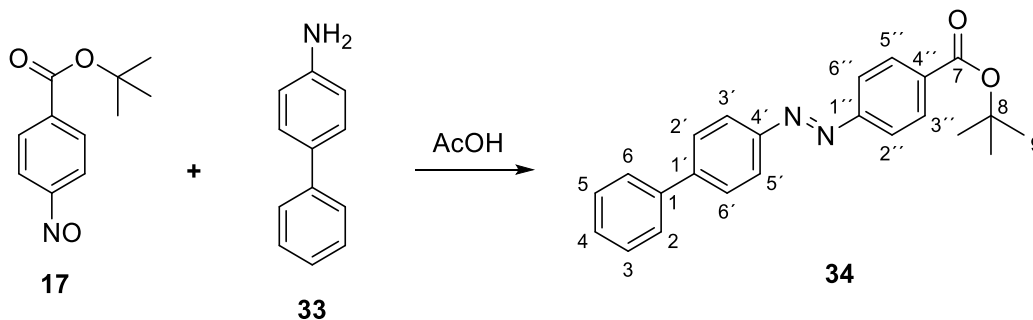
In a 250 mL Schlenk flask, 4-nitrosobenzonitrile **29** (1.5 g, 11.34 mmol) was dissolved in glacial acetic acid (130 mL) under argon atmosphere. Subsequently 1,3,5-Tris(4-aminophenyl)benzene **1** (570 mg, 1.62 mmol) was added to the green solution. The reaction mixture was allowed to stir at RT for 20 h under argon atmosphere, during which time an orange precipitate was formed. The precipitate was filtered off, washed with AcOH and air-dried. The desired product was isolated without further purification as an orange solid (1.11 g) in 99 % yield. (R_f = 0.25, $\text{CH}_2\text{Cl}_2/n\text{-hexane}$, 2:1); m.p. 238.9 °C. ^1H NMR (500 MHz, CDCl_3) δ ppm 8.09 (dd, 6H, $^3J_{\text{H,H}}$ = 8.41 Hz, $\text{C}^{5',3'}$ H), 8.02 (dd, 6H, $^3J_{\text{H,H}}$ = 8.41 Hz, $\text{C}^{2'',6''}$ H), 7.96 (s, 3H, $\text{C}^{2,4,6}$ H), 7.90 (dd, 6H, $^3J_{\text{H,H}}$ = 8.41 Hz, $\text{C}^{2',6'}$ H), 7.83 (dd, 6H, $^3J_{\text{H,H}}$ = 8.41 Hz, $\text{C}^{3'',5''}$ H); ^{13}C NMR (125.8 MHz, CDCl_3) δ ppm 154.76 ($\text{C}^{1''}$), 152.06 ($\text{C}^{4'}$), 144.48 ($\text{C}^{1'}$), 141.83 ($\text{C}^{1,3,5}$), 133.49 ($\text{C}^{3'',5''}$ H), 128.43 ($\text{C}^{2',6'}$ H), 126.21 ($\text{C}^{2,4,6}$ H), 124.28 ($\text{C}^{3',5'}$ H), 123.65 ($\text{C}^{2'',6''}$ H), 118.67 ($\text{C}\equiv\text{N}$), 114.31 ($\text{C}^{4''}$); IR (KBr) ν cm^{-1} 3015 (w, ν ($=\text{CH}$)), 2226 (m, ν ($\text{C}\equiv\text{N}$)), 1598 (s, ν ($\text{C}=\text{C}$)), 1456 (m, ν ($\text{N}=\text{N}$)), 1142 (m, ν ($\text{C}-\text{N}$)); UV-Vis (CH_2Cl_2) λ_{max} (ϵ) = 365 nm (81 560), 454 (4 300); ESI (+) MS calcd. for $\text{C}_{45}\text{H}_{27}\text{N}_9\text{Cl}$ (727.43), found: 728.02; Elemental Anal. Calcd. (%) for $\text{C}_{45}\text{H}_{27}\text{N}_9$ (693.77): C, 77.91; H, 3.92; N, 18.17. Found: C, 76.36; H, 4.03; N, 16.69.

4-Aminobiphenyl (**33**)



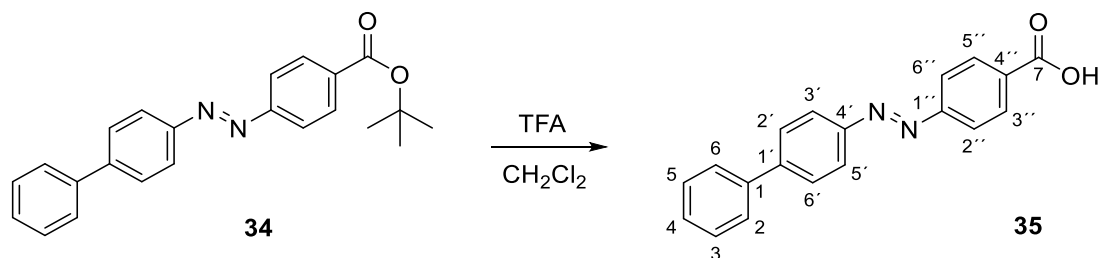
This compound was prepared using a modified procedure.^[288] In a 250 mL Schlenk flask, 4-bromoaniline **32** (1.00 g, 5.91 mmol) and phenylboronic acid **31** (1.08 g, 8.86 mmol) were dissolved in anhydrous dioxane (80 mL). The resulting solution was stirred for 15 min while purging with argon, then an aqueous solution of K_2CO_3 (4.08 g, 29.6 mmol) in 20 mL of water was added. After subsequent addition of $\text{Pd(PPh}_3)_4$ (683 mg, 0.591 mmol), the degassed mixture was allowed to stir at 90°C for 20 h under argon atmosphere. After cooling to RT, the reaction mixture was diluted with dichloromethane and filtered through a short pad of silica gel. All volatiles were evaporated under vacuum, the desired product was purified by column chromatography on silica gel (pure CH_2Cl_2) and obtained as a yellow solid (608 mg) in 61 % yield. ($R_f = 0.30$, CH_2Cl_2); ^1H NMR (500 MHz, CDCl_3) δ ppm 7.52 (dd, 2H, $J_{\text{H,H}} = 8.50$ Hz, $\text{C}^{2',6'}\text{H}$), 7.40 (m, 4H, $\text{C}^{2,6}\text{H}$ and $\text{C}^{3,5}\text{H}$), 7.26 (d, 1H, C^4H), 6.74 (dd, 2H, $J_{\text{H,H}} = 8.50$ Hz, $\text{C}^{3',5'}\text{H}$), 3.70 (bs, 2H, NH_2); ^{13}C NMR (125.8 MHz, CDCl_3) δ ppm 146.0 ($\text{C}^{4'}$), 141.4 (C^1), 131.8 ($\text{C}^{1'}$), 128.9 ($\text{C}^{3,5}\text{H}$), 128.2 ($\text{C}^{2',6'}\text{H}$), 126.6 ($\text{C}^{2,6}\text{H}$), 126.5 (C^4H), 115.6 ($\text{C}^{3',5'}\text{H}$).

***tert*-Butyl-4-[(biphenyl-4-yl)diazenyl]benzoate (**34**)**



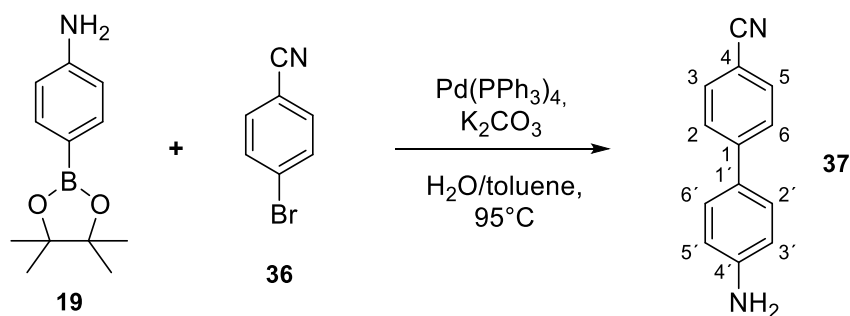
In a 100 mL Schlenk flask, *tert*-Butyl 4-nitrosobenzoate **17** (490 mg, 2.36 mmol) was dissolved in glacial acetic acid (20 mL) under argon atmosphere. Subsequently 4-aminobiphenyl **33** (200 mg, 1.18 mmol) was added to the green solution. The reaction mixture was allowed to stir at RT for 20 h under argon atmosphere, during which time an orange precipitate was formed. The precipitate was filtered off, washed with AcOH and air-dried. The desired product was isolated without further purification as an orange solid (310 mg) in 73 % yield. (R_f = 0.31, *n*-hexane/EtOAc, 20:1); m.p. 140 °C. ¹H NMR (500 MHz, CDCl₃) δ ppm 8.13 (dd, 2H, $J_{\text{H,H}}$ = 8.20 Hz, C^{3'',5''}H), 8.01 (dd, 2H, $J_{\text{H,H}}$ = 8.20 Hz, C^{3',5'}H), 7.93 (dd, 2H, $J_{\text{H,H}}$ = 8.20 Hz, C^{2'',6''}H), 7.75 (dd, 2H, $J_{\text{H,H}}$ = 8.20 Hz, C^{2',6'}H), 7.66 (d, 2H, $J_{\text{H,H}}$ = 7.80 Hz, C^{2,6}H), 7.47 (dd, 2H, $J_{\text{H,H}}$ = 7.40 Hz, C^{3,5}H), 7.39 (dd, 1H, $J_{\text{H,H}}$ = 7.10 Hz, C⁴H), 1.62 (s, 9H, C⁹H₃); ¹³C NMR (125.8 MHz, CDCl₃) δ ppm 165.4 (C⁷), 155.2 (C^{1''}), 151.9 (C^{4'}), 144.6 (C^{1'}), 140.3 (C¹), 133.9 (C^{4''}), 130.7 (C^{3'',5''}H), 129.2 (C^{3,5}H), 128.3 (C⁴H), 128.1 (C^{2',6'}H), 127.4 (C^{2,6}H), 123.9 (C^{3',5'}H), 122.7 (C^{2'',6''}H), 81.7 (C⁸), 28.4 (C⁹H₃); IR (KBr) ν cm⁻¹ 3058 (w, ν (=CH)), 2977 (m) and 2930 (m, ν_{as} (CH₃)), 1680 (s, ν (C=O)), 1601 (m, ν (C=C)), 1482 (m, ν (N=N)), 1367 (m, ν (C-N)), 1291 (s, ν (C-O)), 1113 (m, ν (COO-C)); UV-Vis (THF) λ_{max} (ϵ) = 355 (39 000), 462 (1 700); EI-MS m/z (%) for C₂₃H₂₂N₂O₂ (358.17): 358.2 (6, M⁺), 302.1 (11), 181.12 (7), 153.1 (81), 121.0 (13), 56.1 (51), 40.1 (50), 32.0 (56); Elemental Anal. Calcd. (%) for C₂₃H₂₂N₂O₂ (358.44): C, 77.07; H, 6.19; N, 7.82. Found: C, 76.81; H, 6.34; N, 7.83.

4-[(Biphenyl-4-yl)diazenyl]benzoic acid (**35**)



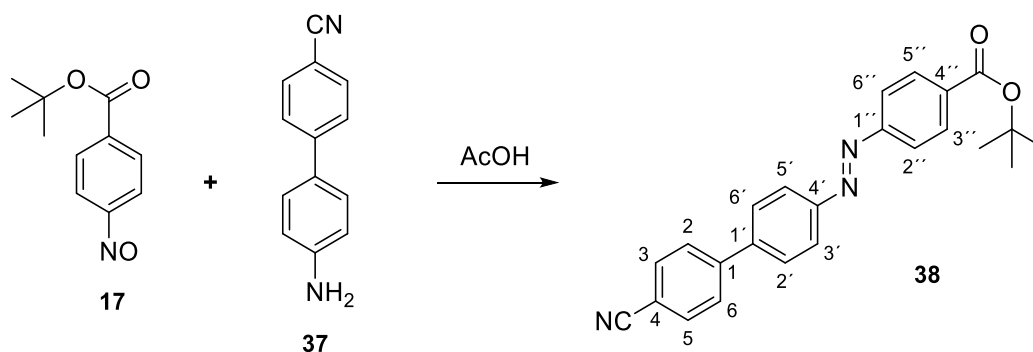
To a solution of *tert*-Butyl ester **34** (250 mg, 0.697 mmol) in dichloromethane (12 mL) was added TFA (6 mL) and the dark red solution was allowed to stir at RT for 20 h. The product was quantitatively precipitated by addition of 2 mL of EtOH. The precipitate was filtered off and continuously washed with EtOH (80 mL), water (40 mL) and CH₂Cl₂ (40 mL). After air and vacuum drying, the desired product was isolated as a light orange powder (209 mg) in 99 % yield. m.p. 296 °C. ¹H NMR (500 MHz, DMSO-*d*₆) δ ppm 13.25 (bs, 1H, C-OH), 7.99 (m, 10H, C^{2,6}H, C^{2',6'}H, C^{3',5'}H, C^{2'',6''}H, C^{3'',5''}H), 7.51 (s, 3H, C^{3,5}H and C⁴H); ¹³C NMR (125.8 MHz, DMSO-*d*₆) δ ppm 166.7 (C⁷), 154.3 (C^{1''}), 151.0 (C⁴), 143.6 (C^{1'}), 138.8 (C¹), 132.8 (C^{4''}), 130.7 (C^{3'',5''}H), 129.1 (C^{3,5}H), 128.4 (C⁴H), 127.8 (C^{2',6'}H), 126.9 (C^{2,6}H), 123.5 (C^{3',5'}H), 122.6 (C^{2'',6''}H); IR (KBr) ν cm⁻¹ 2982 (m), 2888 (m), 2674 (m) and 2548 (m, ν (O-H)), 1684 (s, ν (C=O)), 1600 (m) and 1581 (m, ν (C=C)), 1484 (m, ν (N=N)), 1429 (s, ν (C-N)), 1291 (s, ν (C-O)); UV-Vis (DMSO) λ_{max} (ε) = 360 (37 900), 457 (2 000); MALDI-TOF MS (+) calcd. for C₁₉H₁₄N₂O₂ (M⁺, 302.11), found: 302.06; Elemental Anal. Calcd. (%) for C₁₉H₁₄N₂O₂ (302.33): C, 75.48; H, 4.67; N, 9.27. Found: C, 73.35; H, 4.73; N, 9.11.

4'-Aminobiphenyl-4-carbonitrile (**37**)



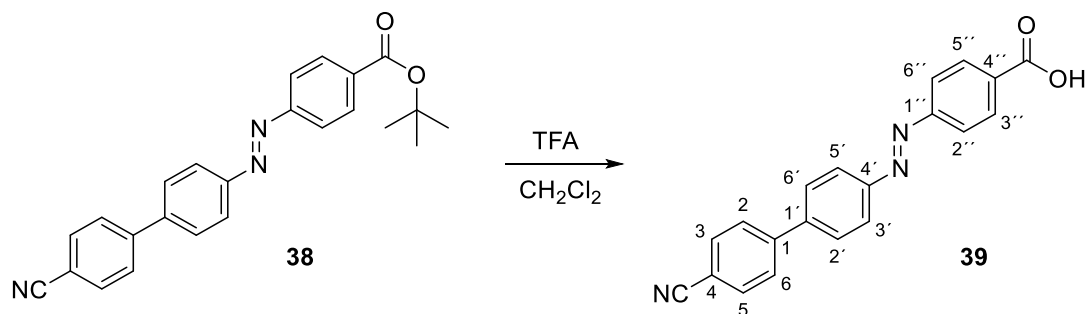
This compound was prepared using a modified procedure.^[289] In a 50 mL Schlenk flask, 4-bromobenzonitrile **36** (250 mg, 1.37 mmol) and 4-aminophenylboronic acid pinacol ester **19** (451 mg, 2.06 mmol) were dissolved in toluene (20 mL). The resulting solution was stirred for 15 min while purging with argon, then an aqueous solution of K_2CO_3 (947 mg, 6.85 mmol) in 5 mL of water was added. After subsequent addition of $\text{Pd(PPh}_3)_4$ (158 mg, 0.137 mmol), the degassed mixture was allowed to stir at 95°C for 18 h under argon atmosphere. After cooling to RT, the reaction mixture was diluted with ethyl acetate and filtered through a short pad of silica gel. The yellow solution was washed with H_2O (50 mL), Na_2CO_3 (50 mL, saturated), brine (50 mL) and dried over MgSO_4 . All volatiles were evaporated under vacuum, the desired product was purified by column chromatography on silica gel (*n*-hexane/EtOAc, 1:1) and isolated as a light brown solid (239 mg) in 90 % yield. (R_f = 0.49, *n*-hexane/EtOAc, 1:1); m.p. 183.6°C . ^1H NMR (500 MHz, CDCl_3) δ ppm 7.64 (dd, 2H, $^3J_{\text{H,H}}$ = 8.34 Hz, $\text{C}^{3,5}\text{H}$), 7.59 (dd, 2H, $^3J_{\text{H,H}}$ = 8.34 Hz, $\text{C}^{2,6}\text{H}$), 7.40 (dd, 2H, $^3J_{\text{H,H}}$ = 8.34 Hz, $\text{C}^{2',6'}\text{H}$), 6.75 (dd, 2H, $^3J_{\text{H,H}}$ = 8.34 Hz, $\text{C}^{3',5'}\text{H}$), 3.83 (s, 2H, NH_2); ^{13}C NMR (125.8 MHz, CDCl_3) δ ppm 147.38 (C^1), 145.75 ($\text{C}^{4'}$), 132.74 ($\text{C}^{3,5}\text{H}$), 129.24 ($\text{C}^{1'}$), 128.44 ($\text{C}^{2',6'}\text{H}$), 126.82 ($\text{C}^{2,6}\text{H}$), 119.50 ($\text{C}\equiv\text{N}$), 115.58 ($\text{C}^{3',5'}\text{H}$), 109.69 (C^4); IR (KBr) ν cm^{-1} 3444 (m) and 3364 (m, ν (N-H)), 3036 (w, ν ($=\text{CH}$)), 2226 (m, ν ($\text{C}\equiv\text{N}$)), 1635 (m, δ (N-H)), 1594 (s, ν ($\text{C}=\text{C}$)), 1494 (s, ν ($\text{C}-\text{N}$)).

***tert*-Butyl-4-[(4'-cyanobiphenyl-4-yl)diazenyl]benzoate (**38**)**



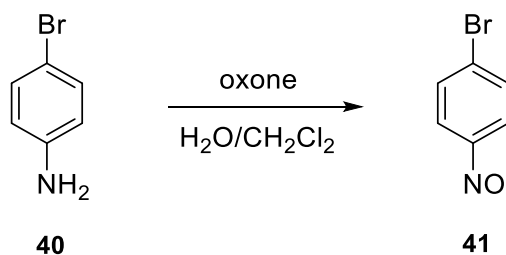
In a 50 mL Schlenk flask, *tert*-Butyl 4-nitrosobenzoate **17** (448 mg, 2.16 mmol) was dissolved in glacial acetic acid (20 mL) under argon atmosphere. Subsequently 4'-aminobiphenyl-4-carbonitrile **37** (210 mg, 1.08 mmol) was added to the green solution. The reaction mixture was allowed to stir at RT for 20 h under argon atmosphere, during which time an orange precipitate was formed. The precipitate was filtered off, washed with AcOH and air-dried. The desired product was isolated without further purification as an orange solid (323 mg) in 78 % yield. (R_f = 0.22, *n*-hexane/EtOAc, 20:1); m.p. 300.8 °C. ^1H NMR (500 MHz, CDCl_3) δ ppm 8.13 (dd, 2H, $^3J_{\text{H,H}}$ = 8.60 Hz, $\text{C}^{3'',5''}\text{H}$), 8.04 (dd, 2H, $^3J_{\text{H,H}}$ = 8.60 Hz, $\text{C}^{2'',6''}\text{H}$), 7.94 (dd, 2H, $^3J_{\text{H,H}}$ = 8.41 Hz, $\text{C}^{3',5'}\text{H}$), 7.75 (s+dd, 6H, $\text{C}^{2',6'}\text{H}$, $\text{C}^{2,6}\text{H}$ and $\text{C}^{3,5}\text{H}$), 1.61 (s, 9H, CH_3); ^{13}C NMR (125.8 MHz, CDCl_3) δ ppm 165.33 (C=O), 155.00 ($\text{C}^{1''}$), 152.64 ($\text{C}^{4'}$), 144.72 (C^1), 142.21 ($\text{C}^{4''}$), 134.26 ($\text{C}^{1'}$), 132.95 ($\text{C}^{2',6'}\text{H}$), 130.68 ($\text{C}^{3',5'}\text{H}$), 128.29 ($\text{C}^{3,5}\text{H}$), 128.05 ($\text{C}^{2,6}\text{H}$), 124.09 ($\text{C}^{2'',6''}\text{H}$), 122.84 ($\text{C}^{3',5'}\text{H}$), 118.97 ($\text{C}\equiv\text{N}$), 111.85 (C^4), 81.78 (C- CH_3), 28.42 (CH_3); IR (KBr) ν cm^{-1} 3021 (w, ν (=C-H)), 2984 (w, ν (C-H)), 2224 (m, ν ($\text{C}\equiv\text{N}$), 1702 (s, ν (C=O)), 1603 (m, ν (C=C)), 1490 (w, ν (N=N)), 1369 (m, ν (C-N)), 1299 (s) and 1258 (m, δ (C-H)); UV-Vis (CH_2Cl_2) λ_{max} (ϵ) = 348 nm (48 900), 440 (2 300); ESI (+) MS calcd. for $\text{C}_{24}\text{H}_{21}\text{N}_3\text{O}_2\text{Na}$ (406.15), found: 406.14; Elemental Anal. Calcd. (%) for $\text{C}_{24}\text{H}_{21}\text{N}_3\text{O}_2$ (406.15): C, 75.18; H, 5.52; N, 10.96. Found: C, 79.21; H, 8.06; N, 11.12.

4-[(4'-Cyanobiphenyl-4-yl)diazenyl]benzoic acid (**39**)



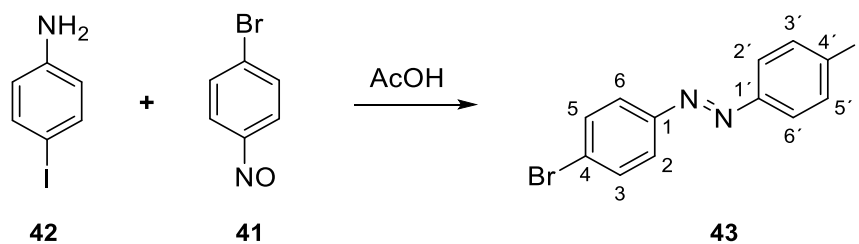
To a solution of *tert*-Butyl ester **38** (250 mg, 0.652 mmol) in dichloromethane (12 mL) was added TFA (6 mL) and the dark red solution was allowed to stir at RT for 20 h. The product was quantitatively precipitated by addition of 2 mL of EtOH. The precipitate was filtered off and continuously washed with EtOH (80 mL), water (40 mL) and CH₂Cl₂ (40 mL). After air and vacuum drying, the desired product was isolated as a light orange powder (205 mg) in 96 % yield. m.p. 300.1 °C. ¹H NMR (500 MHz, DMSO-*d*₆) δ ppm 8.16 (dd, 2H, ³*J*_{H,H} = 8.58 Hz, C^{3'',5''}H), 8.07 (dd, 2H, ³*J*_{H,H} = 8.58 Hz, C^{2'',6''}H), 8.03 (dd, 2H, ³*J*_{H,H} = 8.58 Hz, C^{3,5}H), 8.02 – 7.98 (m, 6H, C^{2,6}H, C^{2',6'}H and C^{3',5'}H); ¹³C NMR (125.8 MHz, DMSO-*d*₆) δ ppm 166.74 (CO), 154.21 (C^{1''}), 151.74 (C^{4'}), 143.30 (C¹), 141.51 (C^{4''}), 133.02 (C^{1'} and C^{3'',5''}H), 130.67 (C^{2',6'}H), 128.40 (C^{3,5}H), 127.88 (C^{2,6}H), 123.60 (C^{2'',6''}H), 122.67 (C^{3',5'}H), 118.78 (C≡N), 110.81 (C⁴); IR (KBr) ν cm⁻¹ above 3200 (bm, ν (O-H)), 2980 (w, ν (=CH)), 2225 (m, ν (C≡N)), 1687 (s, ν (C=O)), 1604 (m, ν (C=C)), 1425 (m, ν (N=N)), 1304 (m, ν (C-N)), 1146 (m, ν (C-O)); ESI (-) MS calcd. for C₂₀H₁₃N₃O₂ ([M-H]⁻, 326.04), found: 326.04; Elemental Anal. Calcd. (%) for C₂₀H₁₃N₃O₂ (327.44): C, 73.38; H, 4.00; N, 12.48. Found: C, 73.09; H, 4.04; N, 13.13.

4-Bromo-nitrosobenzene (**41**)



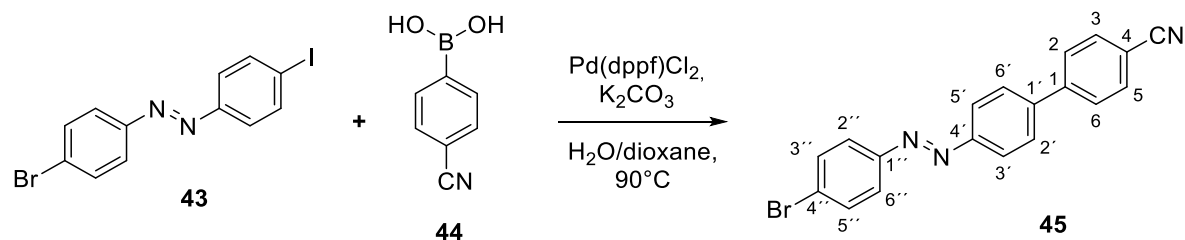
To a solution of 4-bromoaniline **40** (6.0 g, 0.035 mol) in distilled dichloromethane (80 mL) was added an aqueous solution of Oxone® (21.5 g, 0.07 mol) in water (160 mL). The reaction mixture was stirred for 16 h at room temperature and the reaction progress was checked by TLC in the mixture of dichloromethane/*n*-hexane (1:1). The two layers were separated, and the aqueous layer was washed with dichloromethane (2 x 50 mL). The combined organic layer was washed sequentially with HCl (150 mL, 1M), NaHCO₃ (150 mL, saturated), brine (150 mL), dried over MgSO₄ and filtered. Solvents were evaporated under reduced pressure and the resulting crude product was purified on a short pad of silica gel (300 g) in dichloromethane/*n*-hexane (2:1). The isolated product, a greenish solid (5.92 g, 91%), is unstable and hence was used without further purification in the subsequent Mills reaction (*R_f* = 0.54, dichloromethane/*n*-hexane, 1:1).

1-(4-Bromophenyl)-2-(4-iodophenyl)diazene (**43**)



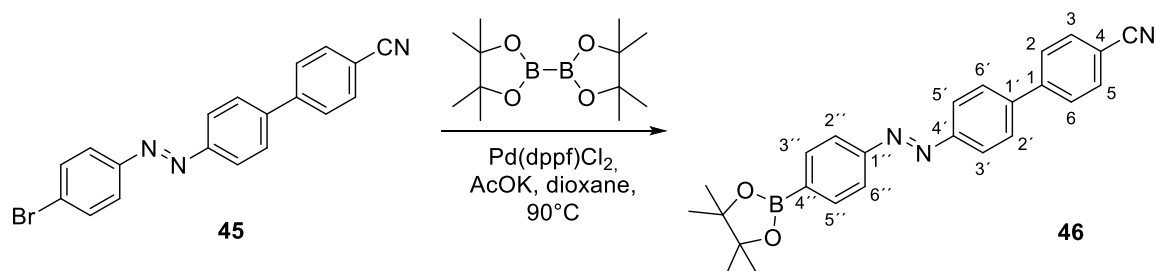
This compound was prepared using a modified procedure.^[95] In a 50 mL Schlenk flask, 4-bromonitrosobenzene **41** (4.46 g, 0.024 mol) was dissolved in glacial acetic acid (300 mL) under argon atmosphere. Subsequently 4-iodoaniline **42** (3.5 g, 0.016 mol) was added to the green solution. The reaction mixture was allowed to stir at RT for 20 h under argon atmosphere, during which time an orange precipitate was formed. The precipitate was filtered off, washed with AcOH and air dried. The desired product was purified by column chromatography on silica gel (*n*-hexane/CHCl₃, 7:1) as an orange solid (4.72 g) in 76 % yield. (*R_f* = 0.38, *n*-hexane/CHCl₃, 7:1); m.p. 208.7 °C. ¹H NMR (500 MHz, CDCl₃) δ ppm 7.87 (dd, 2H, ³*J*_{H,H} = 8.58 Hz, C^{3',5'}H), 7.79 (dd, 2H, ³*J*_{H,H} = 8.58 Hz, C^{2',6'}H), 7.65 (dd, 2H, ³*J*_{H,H} = 8.58 Hz, C^{3,5}H), 7.64 (dd, 2H, ³*J*_{H,H} = 8.58 Hz, C^{2,6}H), ¹³C NMR (125.8 MHz, CDCl₃) δ ppm 151.76 (C^{1'}), 151.16 (C¹), 138.45 (C^{3',5'}H), 132.43 (C^{3,5}H), 125.82 (C⁴), 124.53 (C^{2,6}H), 124.46 (C^{2',6'}H); IR (KBr) ν cm⁻¹ 1564 (m, ν (C=C)), 1470 (m, ν (N=N)), 1394 (m, ν (C-N)); UV-Vis (CH₂Cl₂) λ_{max} (ε) = 343 nm (48 700), 428 (2 900); Elemental Anal. Calcd. (%) for C₁₂H₈BrIN₂ (387.02): C, 37.24; H, 2.08; N, 7.24. Found: C, 39.55; H, 2.51; N, 7.09.

4'-[(4-Bromophenyl)diazenyl]biphenyl-4-carbonitrile (**45**)



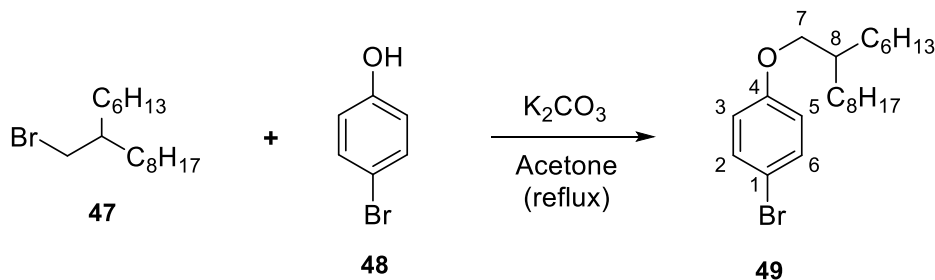
In a 100 mL Schlenk flask, 1-(4-bromophenyl)-2-(4-iodophenyl)diazene **43** (600 mg, 1.55 mmol) and 4-cyanophenylboronic acid **44** (197 mg, 1.55 mmol) were dissolved in anhydrous dioxane (50 mL). The resulting solution was stirred for 15 min while purging with argon, then an aqueous solution of K_2CO_3 (1.07 g, 7.75 mmol) in 3.5 mL of water was added. After subsequent addition of $Pd(dppf)Cl_2$ (63.7 mg, 0.078 mmol), the degassed mixture was allowed to stir at 90 °C for 16 h under argon atmosphere. After cooling to RT, the reaction mixture was diluted with dichloromethane and filtered through a short pad of silica gel. All volatiles were evaporated under vacuum, the desired product was purified by column chromatography on silica gel (n-hexane/ CH_2Cl_2 , 2:1) and obtained as an orange solid (402 mg) in 72 % yield. (R_f = 0.31, n-hexane/ CH_2Cl_2 , 1:1); m.p. 253.2 °C. 1H NMR (500 MHz, $CDCl_3$) δ ppm 8.01 (dd, 2H, $^3J_{H,H}$ = 8.25 Hz, $C^{3',5'}$ H), 7.81 (dd, 2H, $^3J_{H,H}$ = 8.25 Hz, $C^{2'',6''}$ H), 7.74 (m, 6H, $C^{2,3,5,6,2',6'}$ H), 7.65 (dd, 2H, $^3J_{H,H}$ = 8.25 Hz, $C^{3'',5''}$ H); ^{13}C NMR (125.8 MHz, $CDCl_3$) δ ppm 152.55 ($C^{4'}$), 151.55 ($C^{1''}$), 144.76 (C^1), 141.95 ($C^{1'}$), 132.94 ($C^{3,5}$ H), 132.64 ($C^{3'',5''}$ H), 128.28 ($C^{2',6'}$ H), 128.02 ($C^{2,6}$ H), 126.01 ($C^{4''}$), 124.69 ($C^{2'',6''}$ H), 123.92 ($C^{3',5'}$ H), 118.97 ($C\equiv N$), 111.80 (C^4); IR (KBr) ν cm^{-1} 3086, 3055 and 3037 (w, ν (=CH)), 2223 (m, ν ($C\equiv N$)), 1600 and 1569 (m, ν ($C=C$)), 1476 (m, ν ($N=N$)), 1396 (m, ν ($C-N$)); UV-Vis (CH_2Cl_2) λ_{max} (ϵ) = 349 nm (86 800), 449 (3 700); ESI (+) MS calcd. for $C_{19}H_{12}BrN_3Na$ (384.01), found: 384.01; Elemental Anal. Calcd. (%) for $C_{19}H_{12}BrN_3$ (362.22): C, 63.00; H, 3.34; N, 11.60. Found: C, 62.98; H, 3.16; N, 12.28.

4'-[4-(4,4,5,5-Tetramethyl-1,3,2-dioxaborolan-2-yl)phenyl]diazenyl}biphenyl-4-carbonitrile (46)



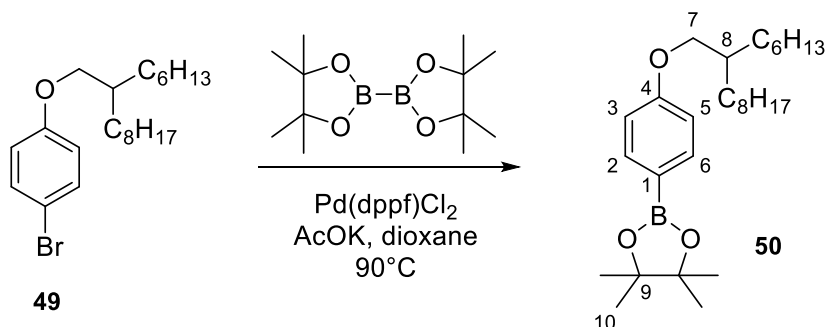
In a 100 mL Schlenk flask, compound **45** (500 mg, 1.38 mmol), bis(pinacolato)diboron (526 mg, 2.07 mmol), AcOK (622 mg, 6.90 mmol) and Pd(dppf)Cl₂ (56.3 mg, 0.069 mmol) were dissolved in anhydrous dioxane (60 mL). The solution was purged with argon for 15 min and allowed to stir at 90 °C for 18 h under argon atmosphere. After cooling to RT, the mixture was diluted with dichloromethane (30 mL) and filtered through a short pad of silica gel. All volatile solvents were evaporated under vacuum. The desired product was purified by column chromatography on silica gel (*n*-hexane/CH₂Cl₂, 1:1) and isolated as an orange solid (514 mg) in 91 % yield. (*R*_f = 0.38, *n*-hexane/CH₂Cl₂, 1:1); m.p. 194.6 °C. ¹H NMR (500 MHz, CDCl₃) δ ppm 8.02 (dd, 2H, ³J_{H,H} = 8.60 Hz, C^{3',5'}H), 7.96 (dd, 2H, ³J_{H,H} = 8.60 Hz, C^{3'',5''}H), 7.90 (dd, 2H, ³J_{H,H} = 8.60 Hz, C^{2',6'}H), 7.74 (m, 6H, C^{2,3,5,6,2',6'}H), 1.36 (s, 12H, CH₃); ¹³C NMR (125.8 MHz, CDCl₃) δ ppm 154.54 (C^{1''}), 152.79 (C^{4'}), 144.85 (C¹), 141.79 (C^{1'}), 135.91 (C^{3'',5''}H), 132.93 (C^{3,5}H), 128.23 (C^{2,6}H), 128.03 (C^{2',6'}H), 127.82 (C^{4''}), 123.93 (C^{3',5'}H), 122.30 (C^{2'',6''}H), 84.35 (C-CH₃), 25.13 (CH₃); IR (KBr) ν cm⁻¹ 3047 (w, ν (=CH)), 2980 (m, ν (C-H)), 2225 (m, ν (C≡N)), 1603 (m, ν (C=C)), 1502 (m, ν (N=N)), 1392 (m) and 1353 (s, δ_{sym} (C-H)); UV-Vis (CH₂Cl₂) λ_{max} (ε) = 346 nm (55 400), 448 (2 300); ESI (+) MS calcd. for C₂₅H₂₄BN₃O₂Na (432.19), found: 432.18; Elemental Anal. Calcd. (%) for C₂₅H₂₄BN₃O₂ (409.30): C, 73.36; H, 5.91; N, 10.27. Found: C, 72.40; H, 6.33; N, 9.94.

1-Bromo-4-[(2-hexyldecyl)oxy]benzene (**49**)



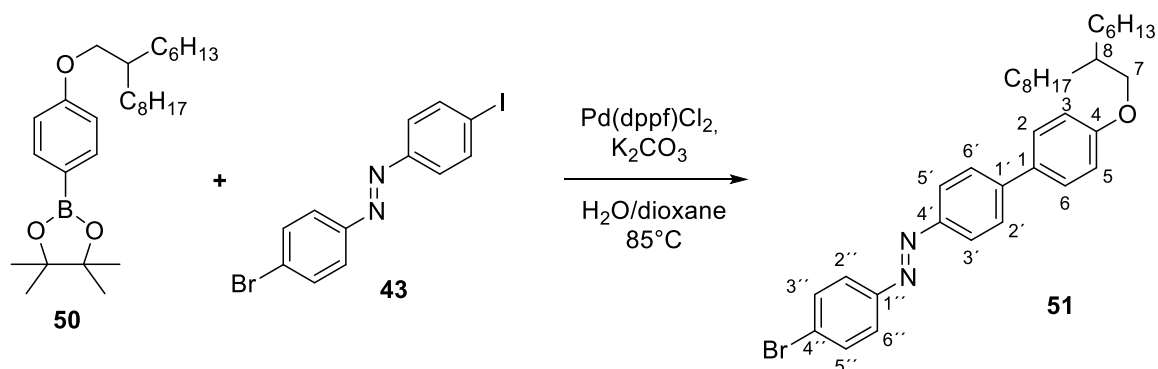
This compound was prepared using a modified procedure.^[290] To a solution of 4-bromophenol **48** (1.20 g, 6.94 mmol) in acetone (60 mL) was added an excess of K₂CO₃ (4.79 g, 34.7 mmol) and the mixture was stirred at room temperature for 30 min. Subsequently, 7-(bromomethyl)pentadecane **47** (2.97 g, 9.72 mmol) was added and the reaction mixture was allowed to reflux for 30 h. After cooling down to RT, the white precipitate was filtered off, washed with acetone (50 mL) and dichloromethane (50 mL) and air-dried. The desired product was purified by column chromatography on silica gel (*n*-hexane/EtOAc, 20:1) and isolated as a yellowish oil (2.12 g) in 77 % yield. (*R*_f = 0.55, *n*-hexane/EtOAc, 20:1). ¹H NMR (500 MHz, CDCl₃) δ ppm 7.33 (dd, 2H, ³*J*_{H,H} = 9.14 Hz, C^{2,6}H), 6.75 (dd, 2H, ³*J*_{H,H} = 9.14 Hz, C^{3,5}H), 3.72 (d, 2H, ³*J*_{H,H} = 4.44 Hz, C⁷H₂), 1.74 (t, 1H, ³*J*_{H,H} = 6.03 Hz, C⁸H), 1.26 (bs, 24H, CH₂), 0.91 (t, 6H, *J*_{H,H} = 7.05 Hz, CH₃); ¹³C NMR (125.8 MHz, CDCl₃) δ ppm 158.72 (C⁴), 132.34 (C^{2,6}H), 116.54 (C^{3,5}H), 112.65 (C¹), 71.39 (C⁷H₂), 38.10 (C⁸H), 32.12, 32.06, 31.54, 31.52, 30.21, 29.88, 29.79, 27.03, 27.01, 22.89 (CH₂), 14.32 (CH₃); IR (KBr) ν cm⁻¹ 2923 (s) and 2855 (s, ν (C-H)), 1591 (w, ν (C=C)), 1490 (m) and 1468 (s, δ_{sim} (C-H)), 1244 (m, ν (C-O)).

2-[4-[(2-Hexyldecyl)oxy]phenyl]-4,4,5,5-tetramethyl-1,3,2-dioxaborolane (50)



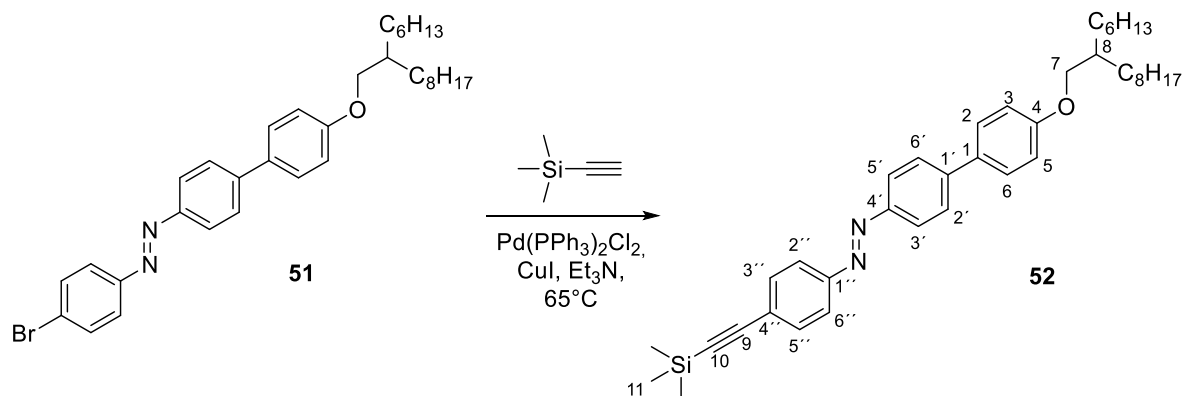
This compound was prepared using a modified procedure.^[291] In a 250 mL Schlenk flask, compound **49** (1.50 g, 3.77 mmol), bis(pinacolato)diboron (1.24 g, 4.90 mmol), AcOK (1.85 g, 18.85 mmol) and Pd(dppf)Cl₂ (154 mg, 0.188 mmol) were dissolved in anhydrous dioxane (100 mL). The solution was purged with argon for 15 min and allowed to stir at 90 °C for 18 h under argon atmosphere. After cooling to RT, the mixture was diluted with diethyl ether (30 mL) and filtered through a short pad of silica gel. All volatile solvents were evaporated under vacuum. The desired product was purified by column chromatography on silica gel (*n*-hexane/EtOAc, 20:1) and isolated as a colorless oil (1.39 g) in 83 % yield. (*R*_f = 0.45, *n*-hexane/EtOAc, 20:1). ¹H NMR (500 MHz, CDCl₃) δ ppm 7.72 (dd, 2H, ³*J*_{H,H} = 8.60 Hz, C^{3,5}H), 6.87 (dd, 2H, ³*J*_{H,H} = 8.60 Hz, C^{2,6}H), 3.82 (d, 2H, ³*J*_{H,H} = 6.00 Hz, C⁷H₂), 1.75 (t, 1H, ³*J*_{H,H} = 6.00 Hz, C⁸H), 1.31 (s, 12H, C¹⁰H₃), 1.25 (bs, 24H, CH₂), 0.86 (t, 6H, *J*_{H,H} = 6.05 Hz, CH₃); ¹³C NMR (125.8 MHz, CDCl₃) δ ppm 162.18 (C¹), 136.59 (C^{3,5}H), 127.85 (C⁴), 114.06 (C^{2,6}H), 83.64 (C⁹), 70.84 (C⁷H₂), 38.04 (C⁸H), 32.05, 32.00, 31.51, 31.50, 30.16, 29.83, 29.73, 29.47, 27.06, 26.97, 26.94, 25.00 (C¹⁰H₃), 22.92 (CH₂), 14.26 (CH₃); IR (KBr) ν cm⁻¹ 2927 (s) and 2857 (s, ν (C-H)), 1606 (m, ν (C=C)), 1398 (m) and 1360 (s, δ_{sym} (C-H)), 1246 (m, ν (C-O)).

1-(4-Bromophenyl)-2-{4'-[(2-hexyldecyl)oxy]biphenyl}-4-yl}diazene (**51**)



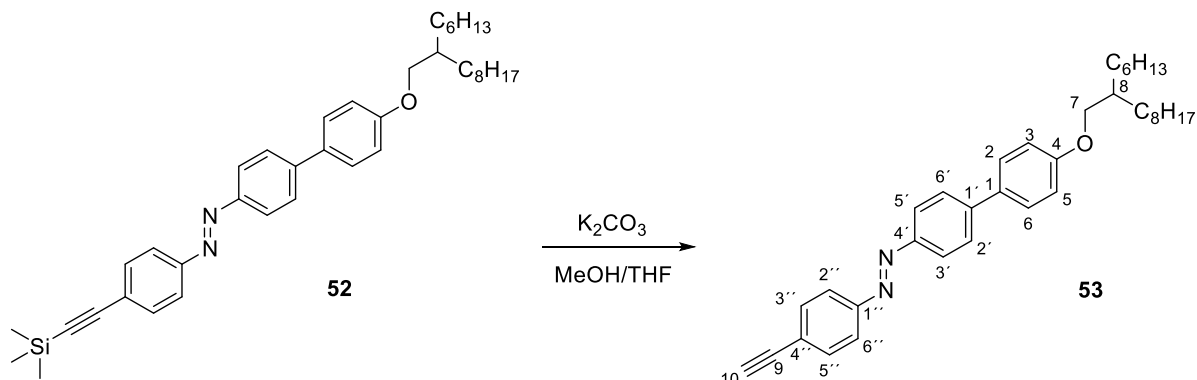
In a 100 mL Schlenk flask, 1-(4-bromophenyl)-2-(4-iodophenyl)diazene **43** (500 mg, 1.29 mmol) and alkoxy pinacolboronic ester **50** (573 mg, 1.29 mmol) were dissolved in anhydrous dioxane (60 mL). The resulting mixture was stirred for 15 min while purging with argon, then an aqueous solution of K_2CO_3 (891 mg, 6.45 mmol) in 5 mL of water was added. After subsequent addition of $Pd(dppf)Cl_2$ (52.7 mg, 0.065 mmol), the degassed mixture was allowed to stir at 85 °C for 16 h under argon atmosphere. After cooling to RT, the reaction mixture was diluted with dichloromethane and filtered through a short pad of silica gel. All volatiles were evaporated under vacuum, the desired product was purified by column chromatography on silica gel (*n*-hexane/EtOAc, 30:1) and obtained as an orange wax (454 mg) in 61 % yield. (R_f = 0.45, *n*-hexane/EtOAc, 30:1). 1H NMR (500 MHz, $CDCl_3$) δ ppm 7.95 (dd, 2H, $^3J_{H,H}$ = 8.50 Hz, $C^{2'',6''}H$), 7.79 (dd, 2H, $^3J_{H,H}$ = 8.50 Hz, $C^{3',5'}H$), 7.69 (dd, 2H, $^3J_{H,H}$ = 8.50 Hz, $C^{2',6'}H$), 7.63 (dd, 2H, $^3J_{H,H}$ = 8.50 Hz, $C^{3'',5''}H$), 7.58 (dd, 2H, $^3J_{H,H}$ = 8.50 Hz, $C^{2,6}H$), 6.98 (dd, 2H, $^3J_{H,H}$ = 8.50 Hz, $C^{3,5}H$), 3.87 (d, 2H, $^3J_{H,H}$ = 5.64 Hz, C^7H_2), 1.79 (t, 1H, $^3J_{H,H}$ = 5.73 Hz, C^8H), 1.27 (bs, 24H, CH_2), 0.87 (t, 6H, $^3J_{H,H}$ = 4.03 Hz, CH_3); ^{13}C NMR (125.8 MHz, $CDCl_3$) δ ppm 159.85 (C^4), 151.72 ($C^{1''}$), 151.34 ($C^{4'}$), 144.07 ($C^{1'}$), 132.53 ($C^{3'',5''}H$), 132.31 ($C^{1'}$), 128.41 ($C^{2,6}H$), 127.41 ($C^{2',6'}H$), 125.37 ($C^{4''}$), 124.53 ($C^{3',5'}$), 123.73 ($C^{2'',6''}$), 115.20 ($C^{3,5}H$), 71.28 (C^7H_2), 38.19 (C^8H), 32.12, 32.08, 31.61, 31.59, 30.25, 29.92, 29.81, 29.55, 27.07, 27.05, 22.9 (CH_2), 14.34 (CH_3); IR (KBr) ν cm^{-1} 2954 (m), 2923 (s) and 2855 (s, ν (C-H)), 1598 (m, ν (C=C)), 1491 (m, ν (N=N)), 1398 (m, δ_{sym} (C-H)), 1252 (s, ν (C-O)); UV-Vis (CH_2Cl_2) λ_{max} (ϵ) = 370 nm (41 000); ESI (+) MS calcd. for $C_{34}H_{45}BrN_2O$ ($[M+H]$, 579.27), found: 579.28; Elemental Anal. Calcd. (%) for $C_{34}H_{45}BrN_2O$ (577.65): C, 70.70; H, 7.85; N, 4.85. Found: C, 70.93; H, 8.01; N, 4.82.

**1-{4'-[(2-Hexyldecyl)oxy]biphenyl]-4-yl}-2-{4-[(trimethylsilyl)ethynyl]phenyl}diazene
(52)**



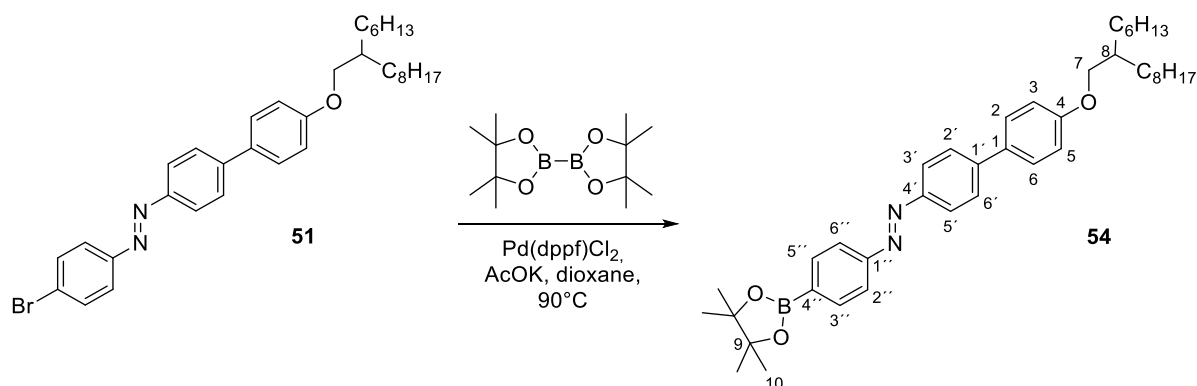
In a 50 mL Schlenk flask under argon atmosphere, azobenzene **51** (450 mg, 0.780 mmol), Pd(PPh₃)₂Cl₂ (27.4 mg, 0.039 mmol), and CuI (3.80 mg, 0.02 mmol) were dissolved in a dry mixture of THF/Et₃N (40 mL, 1/3 v/v). The solution was purged with argon for 15 min, and ethynyltrimethylsilane (536 mg, 5.46 mmol) was added. The reaction mixture was allowed to stir at 65 °C for 18 h under argon atmosphere. After cooling to RT, the mixture was diluted with diethyl ether (20 mL) and filtered through a short pad of silica gel. All volatile solvents were evaporated under vacuum. The residue was purified by column chromatography on silica gel (*n*-hexane/EtOAc, 30:1) and the desired product was isolated as an orange wax (458 mg) in 99% yield. (*R*_f = 0.40, *n*-hexane/EtOAc 30:1). ¹H NMR (500 MHz, CDCl₃) δ ppm 7.95 (dd, 2H, ³*J*_{H,H} = 8.50 Hz, C^{3',5'}H), 7.85 (dd, 2H, ³*J*_{H,H} = 8.50 Hz, C^{2'',6''}H), 7.68 (dd, 2H, ³*J*_{H,H} = 8.50 Hz, C^{2',6'}H), 7.59 (dd, 2H, ³*J*_{H,H} = 8.50 Hz, C^{3'',5''}H), 7.57 (dd, 2H, ³*J*_{H,H} = 8.50 Hz, C^{2,6}H), 6.98 (dd, 2H, ³*J*_{H,H} = 8.50 Hz, C^{3,5}H), 3.86 (d, 2H, ³*J*_{H,H} = 5.78 Hz, C⁷H₂), 1.79 (t, 1H, ³*J*_{H,H} = 6.58 Hz, C⁸H), 1.27 (bs, 24H, CH₂), 0.86 (t, 6H, ³*J*_{H,H} = 4.94 Hz, CH₃), 0.26 (s, 9H, C¹¹H₃); ¹³C NMR (125.8 MHz, CDCl₃) δ ppm 159.84 (C⁴), 152.30 (C^{4'} and C^{1''}), 144.16 (C^{1'}), 133.03 (C^{3'',5''}H), 132.36 (C¹), 128.42 (C^{2,6}H), 127.40 (C^{2',6'}H), 125.81 (C^{4''}), 123.74 (C^{3',5'}H), 122.96 (C^{2'',6''}H), 115.20 (C^{3,5}H), 83.77 (C⁹), 76.84 (C¹⁰), 71.28 (C⁷H₂), 38.19 (C⁸H), 32.13, 32.08, 31.59, 30.25, 29.92, 29.82, 29.56, 27.07, 27.05, 22.90 (CH₂), 14.34 (CH₃), 0.14 (C¹¹H₃); IR (KBr) ν cm⁻¹ 3041 (w, ν (=CH)); 2957 (m), 2927 (s) and 2854 (m, ν (C-H)), 1598 (m, ν (C=C)), 1491 (m) and 1469 (m, ν (N=N)), 1377 (m, δ_{sym} (C-H)), 1249 (s, ν (C-O)); UV-Vis (CH₂Cl₂) λ_{max} (ε) = 378 nm (26 000); Elemental Anal. Calcd. (%) for C₃₉H₅₄N₂OSi (594.96): C, 78.73; H, 9.15; N, 4.71. Found: C, 78.15; H, 8.95; N, 4.90.

1-(4-Ethynylphenyl)-2-{4'-[(2-hexyldecyl)oxy]biphenyl-4-yl}diazene (**53**)



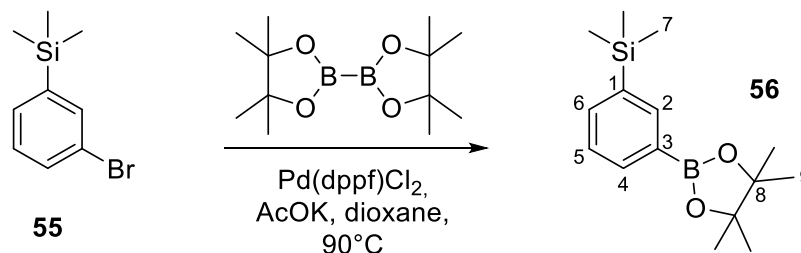
Compound **52** (400 mg, 0.672 mmol) was dissolved in the mixture of THF/MeOH (50 mL, 1/4 v/v). K_2CO_3 (464 mg, 3.36 mmol) was added to a round bottom flask and the reaction mixture was allowed to stir at room temperature for 16 h. The mixture was diluted with diethyl ether (30 mL), filtered through a short pad of silica gel and solvents were evaporated under the reduced pressure. The crude product was purified by column chromatography on silica gel (*n*-hexane/EtOAc, 60:1) and isolated as an orange wax (349 mg) in 99% yield. (R_f = 0.38, *n*-hexane/EtOAc 30:1). 1H NMR (500 MHz, $CDCl_3$) δ ppm 7.97 (dd, 2H, $^3J_{H,H}$ = 8.15 Hz, $C^{3',5'}H$), 7.88 (dd, 2H, $^3J_{H,H}$ = 8.15 Hz, $C^{2'',6''}H$), 7.70 (dd, 2H, $^3J_{H,H}$ = 8.15 Hz, $C^{2',6'}H$), 7.63 (dd, 2H, $^3J_{H,H}$ = 8.15 Hz, $C^{3'',5''}H$), 7.59 (dd, 2H, $^3J_{H,H}$ = 8.15 Hz, $C^{2,6}H$), 6.99 (dd, 2H, $^3J_{H,H}$ = 8.15 Hz, $C^{3,5}H$), 3.87 (d, 2H, $^3J_{H,H}$ = 5.60 Hz, C^7H_2), 3.21 (s, 1H, $C^{10}H$), 1.80 (t, 1H, $^3J_{H,H}$ = 5.60 Hz, C^8H), 1.28 (bs, 24H, CH_2), 0.88 (t, 6H, $J_{H,H}$ = 5.06 Hz, CH_3); ^{13}C NMR (125.8 MHz, $CDCl_3$) δ ppm 159.98 (C^4), 152.70 ($C^{4'}$), 151.58 ($C^{1''}$), 144.23 ($C^{1'}$), 133.32 ($C^{3'',5''}H$), 132.52 ($C^{1'}$), 128.54 ($C^{2,6}H$), 127.51 ($C^{2',6'}H$), 124.81 ($C^{4''}$), 123.93 ($C^{3',5'}H$), 123.14 ($C^{2'',6''}H$), 115.32 ($C^{3,5}H$), 83.71 ($C^{10}H$), 79.70 (C^9), 71.34 (C^7H_2), 38.33 (C^8H_3), 32.30, 32.28, 32.23, 31.73, 30.40, 30.08, 30.04, 29.97, 29.74, 29.71, 27.46, 27.27, 27.22, 27.20 and 23.05 (CH_2), 14.48 (CH_3); IR (KBr) ν cm^{-1} 3317 (m, ν ($\equiv C-H$)), 3041 (w, ν ($=C-H$)), 2956 (m), 2923 (s) and 2856 (s, ν ($C-H$)), 2106 (w, ν ($C\equiv C$)), 1597 (m, ν ($C=C$)), 1491 (m) and 1468 (m, ν ($N=N$)), 1250 (m, ν ($C-O$)); UV-Vis (CH_2Cl_2) λ_{max} (ϵ) = 377 nm (42 600); ESI (+) MS calcd. for $C_{36}H_{46}N_2O$ ($[M+H]$, 523.36), found: 523.37; Elemental Anal. Calcd. (%) for $C_{36}H_{46}N_2O$ (522.78): C, 82.71; H, 8.87; N, 5.36. Found: C, 82.82; H, 9.09; N, 5.95.

1-{4'-[(2-Hexyldecyl)oxy]biphenyl-4-yl}-2-[4-(4,4,5,5-tetramethyl-1,3,2-dioxaborolan-2-yl)phenyl]diazene (54**)**



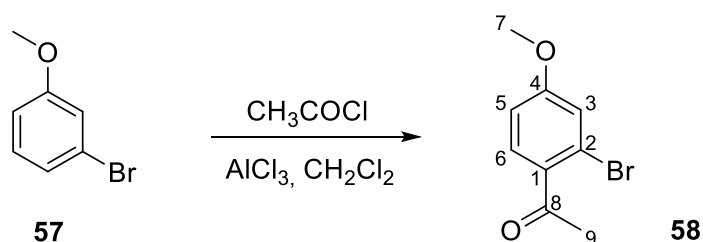
In a 250 mL Schlenk flask, compound **51** (1.50 g, 3.77 mmol), bis(pinacolato)diboron (1.24 g, 4.90 mmol), AcOK (1.85 g, 18.85 mmol) and Pd(dppf)Cl₂ (154 mg, 0.188 mmol) were dissolved in anhydrous dioxane (100 mL). The solution was purged with argon for 15 min and allowed to stir at 90 °C for 18 h under argon atmosphere. After cooling to RT, the mixture was diluted with diethyl ether (30 mL) and filtered through a short pad of silica gel. All volatile solvents were evaporated under vacuum. The desired product was purified by column chromatography on silica gel (*n*-hexane/EtOAc, 20:1) and isolated as a dark orange wax (1.39 g) in 83 % yield. (*R*_f = 0.45, *n*-hexane/EtOAc, 20:1). ¹H NMR (500 MHz, CDCl₃) δ ppm 7.97 (dd, 2H, ³*J*_{H,H} = 9.13 Hz, C^{3',5'}H), 7.95 (dd, 2H, ³*J*_{H,H} = 7.60 Hz, C^{3'',5''}H), 7.89 (dd, 2H, ³*J*_{H,H} = 7.60 Hz, C^{2'',6''}H), 7.69 (dd, 2H, ³*J*_{H,H} = 9.13 Hz, C^{2',6'}H), 7.58 (dd, 2H, ³*J*_{H,H} = 9.13 Hz, C^{2,6}H), 6.98 (dd, 2H, ³*J*_{H,H} = 9.13 Hz, C^{3,5}H), 3.87 (d, 2H, ³*J*_{H,H} = 5.70 Hz, C⁷H₂), 1.79 (t, 1H, ³*J*_{H,H} = 5.01 Hz, C⁸H), 1.36 (s, 12H, C¹⁰H₃), 1.28 (bs, 24H, CH₂), 0.87 (t, 6H, *J*_{H,H} = 4.00 Hz, CH₃); ¹³C NMR (125.8 MHz, CDCl₃) δ ppm 159.79 (C⁴), 154.72 (C^{1''}), 151.57 (C^{4'}), 143.90 (C^{1'}), 135.86 (C^{3'',5''}H), 135.62 (C^{4''}), 132.47 (C¹), 128.41 (C^{2,6}H), 127.36 (C^{2',6'}H), 123.74 (C^{3',5'}H), 122.16 (C^{2'',6''}H), 115.17 (C^{3,5}H), 84.26 (C⁹), 71.25 (C⁷H₂), 38.18 (C⁸H), 32.13, 32.08, 31.60, 31.58, 30.25, 29.92, 29.81, 29.55, 27.06 and 27.05 (CH₂), 25.13 (C¹⁰H₃), 22.90 (CH₂), 14.34 (CH₃); IR (KBr) ν cm⁻¹ 2926 (s) and 2855 (s, ν (C-H)), 1600 (m, ν (C=C)), 1492 (m) and 1468 (m, ν (N=N)), 1355 (s, δ_{sym} (C-H)), 1249 (m, ν (C-O)); UV-Vis (CH₂Cl₂) λ_{max} (ε) = 366 nm (33 100); MALDI-TOF MS (+) calcd. for C₄₀H₅₇BN₂O₃ (M⁺, 624.45), found: 624.54; Elemental Anal. Calcd. (%) for C₄₀H₅₇BN₂O₃ (624.87): C, 76.91; H, 9.20; N, 4.48. Found: C, 77.09; H, 9.12; N, 4.49.

Trimethyl[3-(4,4,5,5-tetramethyl-1,3,2-dioxaborolan-2-yl)phenyl]silane (56**)**



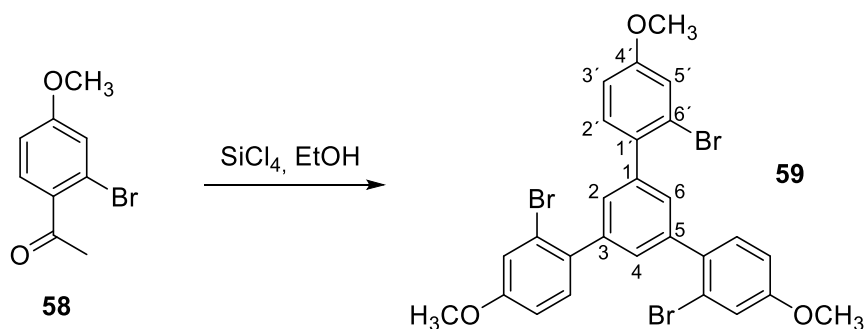
This compound was prepared using a modified literature procedure.^[292] In a 250 mL Schlenk flask, 3-trimethylsilyl-bromobenzene **55** (4.60 g, 0.020 mol), bis(pinacolato)diboron (6.12 g, 0.024 mol), AcOK (9.01 g, 0.1 mol) and Pd(dppf)Cl₂ (1.14 g, 1.40 mmol) were dissolved in anhydrous dioxane (150 mL). The solution was purged with argon for 15 min and then allowed to stir at 90 °C for 18 h under argon atmosphere. After cooling to RT, the mixture was diluted with ethyl acetate (50 mL) and filtered through a short pad of silica gel. All volatile solvents were evaporated under vacuum. The desired product was purified by column chromatography on silica gel (*n*-hexane/EtOAc, 20:1) and isolated as a yellow oil (5.14 g) in 93 % yield. (*R*_f = 0.30, *n*-hexane/EtOAc, 20:1). ¹H NMR (500 MHz, CDCl₃) δ ppm 7.95 (s, 1H, C²H), 7.79 (d, 1H, ³*J*_{H,H} = 7.50 Hz, C⁶H), 7.61 (d, 1H, ³*J*_{H,H} = 7.50 Hz, C⁴H), 7.34 (t, 1H, ³*J*_{H,H} = 7.50 Hz, C⁵H), 1.33 (s, 12H, C⁹H₃), 0.27 (s, 9H, C⁷H₃); ¹³C NMR (125.8 MHz, CDCl₃) δ ppm 139.83 (C²H), 139.74 (C¹ and C³), 136.48 (C⁴H), 135.53 (C⁶H), 127.24 (C⁵H), 83.93 (C⁸), 25.07 (C⁹H₃), -0.840 (C⁷H₃); IR (KBr) ν cm⁻¹ 2980 (m) and 2958 (m, ν (C-H)), 1592 (m, ν (C=C)), 1392 (m) and 1353 (s, δ_{sym} (C-H)), 1251 (m, ν (C-O)).

2-Bromo-4-methoxyacetophenone (**58**)



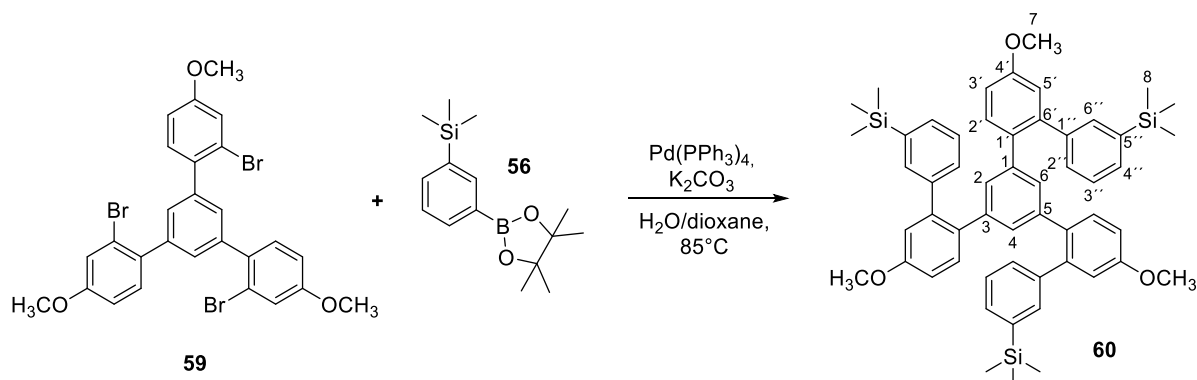
This compound was prepared using a modified literature procedure.^[280] In a 100 mL Schlenk flask, 3-bromoanisole **57** (8.00 g, 43.0 mmol) and AlCl₃ (6.93 g, 52.0 mmol) were dissolved in dichloromethane (40 mL). The mixture was cooled down to 5°C in an ice bath, and acetyl chloride (3.37 g, 43.0 mmol) was added dropwise. The yellow mixture was allowed to reach room temperature and stirred for 1.5 h under argon atmosphere, then poured into ice – water (60 mL) containing concentrated HCl (9 mL) and stirred until RT was reached. The aqueous phase was extracted with CH₂Cl₂ (2 x 150 mL), then the organic phases were combined, concentrated and washed with H₂O (100 mL), NaOH (100 mL, 10% aqueous solution), brine (100 mL) and dried over MgSO₄. All volatile solvents were evaporated under vacuum. The desired product was isolated by column chromatography on silica gel (pentane/diethyl ether, 5:1) and obtained as a colorless oil (7.20 g) in 74% yield. (*R_f* = 0.40, pentane/diethyl ether, 5:1). ¹H NMR (500 MHz, CD₂Cl₂) δ ppm 7.59 (d, 1H, ³*J*_{H,H} = 8.60 Hz, C⁶H), 7.16 (d, ³*J*_{H,H} = 2.54 Hz, C³H), 6.89 (dd, 1H, ³*J*_{H,H} = 2.54 Hz, C⁵H), 3.83 (s, 3H, C⁷H₃), 2.57 (s, 3H, C⁹H₃); ¹³C NMR (125.8 MHz, CD₂Cl₂) δ ppm 198.98 (C⁸=O), 162.44 (C⁴O), 133.00 (C¹), 132.14 (C⁶H), 121.51 (C²), 120.14 (C³H), 113.49 (C⁵H), 56.30 (C⁷H₃), 30.23 (C⁹H₃); IR (KBr) ν cm⁻¹ 3080 (w, ν (=CH)), 2970 (m), and 2941 (m, ν (C-H)), 1689 (s, ν (C=O)), 1592 (m, ν (C=H)), 1356 (s, δ_{sym} (C-H)), 1253 (m, ν (C-O)).

1,3,5-Tris-(2-bromo-4-methoxyphenyl)benzene (59)



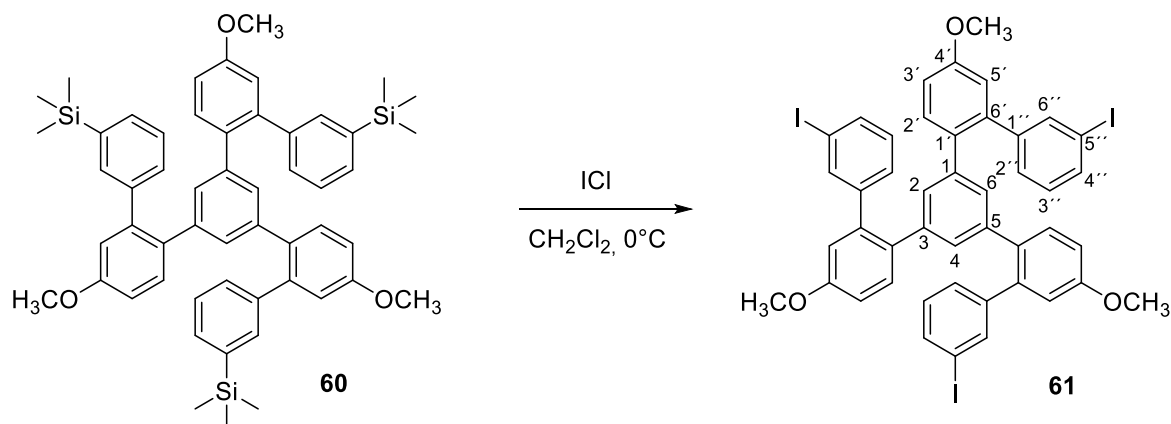
This compound was prepared using a modified literature procedure.^[281] In a 50 mL Schlenk flask, 2-bromo-4-methoxyacetophenone **58** (1.50 g, 6.55 mmol) was dissolved in absolute EtOH (24 mL). SiCl₄ (2.23 g, 13.1 mmol) was added dropwise and the resulting yellow solution allowed to stir at room temperature under argon atmosphere for 16 h. The reaction mixture was diluted with CH₂Cl₂ (30 mL) and washed with H₂O (2 x 50 mL), the organic phases were combined, concentrated, washed with brine and dried over MgSO₄. All volatile solvents were evaporated under vacuum and the desired product purified by column chromatography on silica gel (*n*-hexane/CH₂Cl₂, 5:3) and isolated as a white powder (855 mg) in 62% yield. (*R_f* = 0.30, *n*-hexane/CH₂Cl₂, 5:3); m.p. 86.6 °C. ¹H NMR (500 MHz, CD₂Cl₂) δ ppm 7.40 (s, 3H, C^{2,4,6}H), 7.24 (d, 3H, ³*J*_{H,H} = 8.40 Hz, C²H), 7.21 (d, 3H, ³*J*_{H,H} = 2.72 Hz, C³H), 6.90 (dd, 3H, ³*J*_{H,H} = 2.72 Hz, C⁵H), 3.82 (s, 9H, CH₃); ¹³C NMR (125.8 MHz, CD₂Cl₂) δ ppm 159.54 (C^{4'}), 140.16 (C^{1,3,5}), 134.80 (C^{1'}), 132.19 (C²H), 129.91 (C^{2,4,6}H), 123.05 (C^{6'}), 118.48 (C³H), 113.49 (C⁵H), 55.83 (CH₃); IR (KBr) ν cm⁻¹ 2927 (m, ν (C-H)), 1602 (s, ν (C=C)), 1391 (w, δ_{sym} (C-H)), 1288 (m, ν (C-O)); UV-Vis (CH₂Cl₂) λ_{max} (ε) = 259 nm (83 200).

4'''',5'-Dimethoxy-5''-[5-methoxy-3'-(trimethylsilyl)biphenyl-2-yl]-3,3''''-bis(trimethylsilyl)-[1,1':2',1'':3'',1''':2''',1''''-quinquephenyl (60)



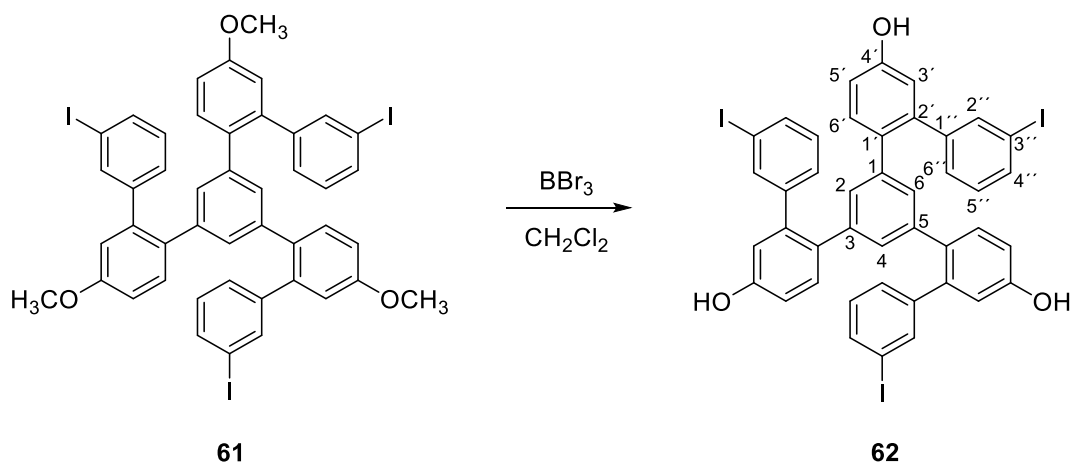
In a 250 mL Schlenk flask, compound **59** (2.00 g, 3.16 mmol) and pinacolboronic ester **56** (3.50 g, 12.6 mmol) were dissolved in dioxane (160 mL). The solution was purged with argon for 15 min. To the degassed solution an aqueous solution of K_2CO_3 (2.18 g, 15.8 mmol) in 3.5 mL of water was added and the reaction mixture was purged with argon for 15 min. Subsequently $Pd(PPh_3)_4$ (365 mg, 0.316 mmol) was added and the mixture was allowed to stir at 80 °C for 20 h under argon atmosphere. After cooling down to RT, the reaction mixture was diluted with diethyl ether (50 mL) and filtered through a short pad of silica gel. All volatile solvents were evaporated under vacuum. The desired product was purified by column chromatography on silica gel (*n*-hexane/EtOAc, 30:1) and isolated as a white foamy solid (2.02 g) in 76 % yield. (R_f = 0.26, *n*-hexane/EtOAc, 20:1); m.p. 164.4 °C. 1H NMR (500 MHz, $CDCl_3$) δ ppm 7.40 (d, 3H, $^3J_{H,H}$ = 7.35 Hz, $C^{4'}H$), 7.33 (s, 3H, $C^{2,4,6}H$), 7.21 (t, 3H, $^3J_{H,H}$ = 7.35 Hz, $C^{2''}H$), 6.88 (m, 6H, $C^{5'}H$ and $C^{3''}H$), 6.72 (dd, 3H, $^3J_{H,H}$ = 3.27 Hz, $C^{3'}H$), 6.54 (s, 3H, $C^{6''}H$), 6.49 (d, 3H, $^3J_{H,H}$ = 8.17 Hz, $C^{2'}H$), 3.81 (s, 9H, C^7H_3), 0.15 (s, 27H, C^8H_3); ^{13}C NMR (125.8 MHz, $CDCl_3$) δ ppm 158.77 ($C^{4'}$), 142.09 ($C^{1,3,5}$), 141.18 ($C^{6'}$), 140.39 ($C^{1'}$), 139.91 ($C^{5''}$), 135.06 ($C^{2,4,6}H$), 133.48 ($C^{1''}$), 131.61 ($C^{2'}H$), 131.58 ($C^{4''}H$), 130.78 ($C^{6''}H$), 129.79 ($C^{3''}H$), 127.38 ($C^{2''}$), 115.61 ($C^{5'}H$), 112.85 ($C^{3'}H$), 55.59 (C^7H_3), -0.93 (C^8H_3); IR (KBr) ν cm^{-1} 3046, (w, ν (=CH)), 2954 (m), 2901 (w) and 2836 (w, ν (C-H)), 1606 (s, ν (C=C)), 1387 (m) and 1316 (m, δ_{sym} (C-H)), 1297 (m, ν (C-O)), 1248 (s) and 838 (s, ν (Si-CH₃)); UV-Vis (dioxane) λ_{max} (ϵ) = 266 nm (56 400); ESI (+) MS calcd. for $C_{54}H_{60}O_3Si_3Na$ (863.37), found: 863.37; Elemental Anal. Calcd. (%) for $C_{54}H_{60}O_3Si_3$ (841.33): C, 77.09; H, 7.19. Found: C, 76.62; H, 7.22.

3,3'''-Diiodo-5''-(3'-iodo-5-methoxy)biphenyl-2-yl)-4'',5'-dimethoxy-1,1':2',1'':3'',1''':2''',1''''-quinquephenyl (61)



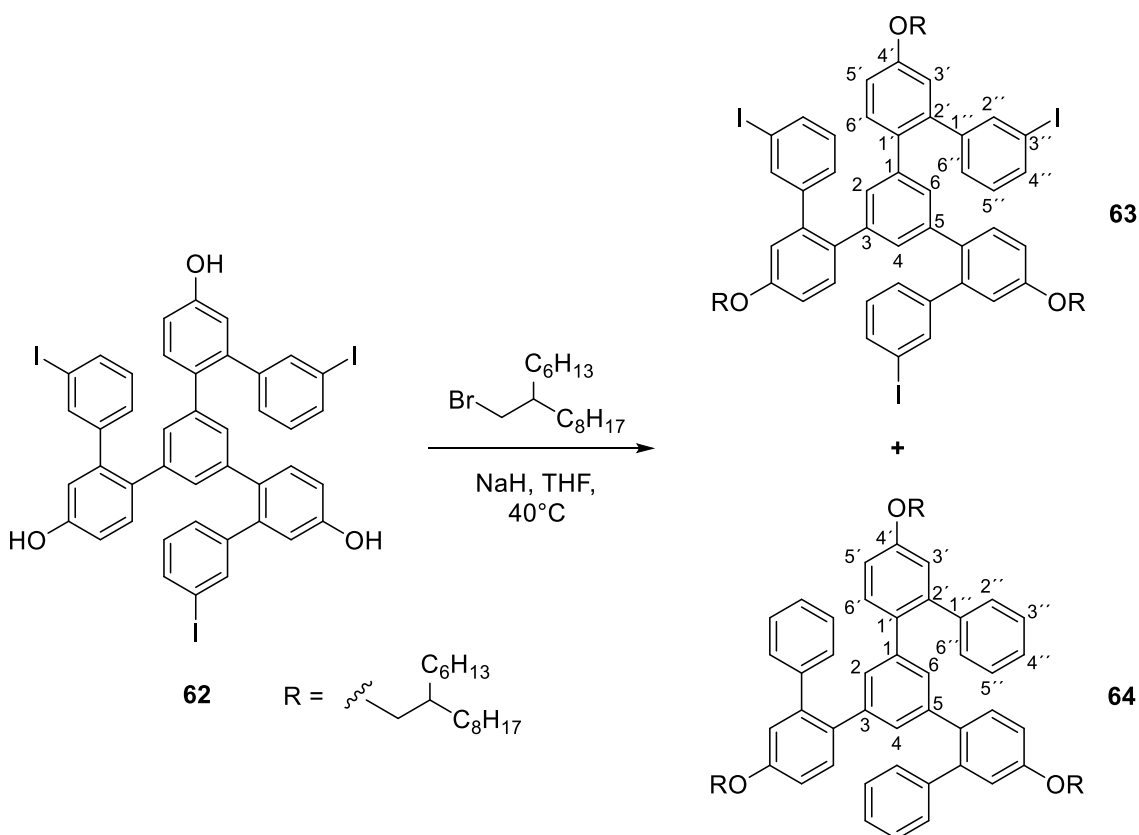
In a 50 mL Schlenk flask, compound **60** (200 mg, 0.238 mmol) was dissolved in anhydrous dichloromethane (15 mL) and the solution was cooled down to 0 °C in an ice bath. Subsequently, was added ICl solution (1.0 M in CH₂Cl₂, 116 mg, 0.714 mmol) was added in three portions over 30 min and the progress of the reaction was continuously monitored by TLC. The mixture was allowed to stir in an ice bath for 30 min under argon atmosphere, then diluted with CH₂Cl₂ (40 mL) and filtered through a short pad of silica gel. The organic phase was further washed with Na₂S₂O₃ (saturated aqueous solution, 50 mL), H₂O (50 mL), brine (50 mL) and dried over MgSO₄. All volatile solvents were evaporated under vacuum providing the desired pure product as a yellow solid (236 mg) in 99% yield. (*R_f* = 0.28, *n*-hexane/EtOAc, 10:1); m.p. 202.9 °C. ¹H NMR (500 MHz, CDCl₃) δ ppm 7.59 (d, 3H, ³*J*_{H,H} = 5.43 Hz, C^{4''}H), 7.59 (s, 3H, C^{6''}), 7.00 (t, 3H, ³*J*_{H,H} = 8 Hz, C^{3''}H), 6.91 (d, 3H, ³*J*_{H,H} = 7.71 Hz, C^{2''}H), 6.86 (d, 3H, ³*J*_{H,H} = 3 Hz, C^{5'}H), 6.84 (s, 3H, C^{5'}H), 6.70 ³*J*_{H,H} = 8 Hz, C^{2'}H), 6.62 (s, 3H, C^{2,4,6}H), 3.84 (s, 9H, CH₃); ¹³C NMR (125.8 MHz, CDCl₃) δ ppm 159.04 (C^{4'}), 144.16 (C^{1'}), 139.97 (C^{1,3,5,6'}), 138.62 (C^{6''}H), 135.78 (C^{4''}H), 132.94 (C^{1'}), 131.91 (C^{2'}H), 129.89 (C^{2,4,6}H), 129.81 (C^{3''}H), 129.77 (C^{2''}H), 115.70 (C^{5'}H), 113.67 (C^{3'}H), 94.12 (C^{5''}), 55.66 (CH₃); IR (KBr) ν cm⁻¹ 3028 (w, ν (=CH)), 2954 (w), 2927 (w) and 2897 (w, ν (C-H)), 1604 (s, ν (C=C)), 1393 (m, δ_{sym} (C-H)), 1219 (m, ν (C-O)); UV-Vis (dioxane) λ_{max} (ε) = 265 nm (39 200); ESI (+) MS calcd. for C₄₅H₃₃I₃O₃Na (1024.96), found: 1024.95; Elemental Anal. Calcd. (%) for C₄₅H₃₃I₃O₃ (1002.47): C, 53.92; H, 3.32. Found: C, 53.86; H, 3.58.

4''',5'-Dihydroxy-5''-(5-hydroxy-3'-iodo-biphenyl-2-yl)-3,3''''-diiodo-1,1':2',1'':3'',1''':2''',1''''-quinquephenyl (62)



In a 25 mL Schlenk flask, compound **61** (350 mg, 0.350 mmol) was dissolved in anhydrous dichloromethane (9 mL) and the solution cooled below -70 °C in a dry ice/acetone bath. To the cold solution an excess of BBr₃ solution (1.0 M in CH₂Cl₂, 526 mg, 2.10 mmol) was added dropwise. The mixture was allowed to reach RT and stirred under argon atmosphere for 16 h. The reaction was quenched with HCl (1.0 M aqueous solution, 20 mL). The aqueous phase was extracted with ethyl acetate (3 x 50 mL), the organic phases were combined, washed with H₂O (2 x 50 mL), brine (50 mL) and dried over MgSO₄. All volatile solvents were evaporated under vacuum providing the desired product as a white solid (329 mg) in 98% yield. (*R*_f = 0.25, *n*-hexane/EtOAc, 1:1); m.p. 163.9 °C. ¹H NMR (500 MHz, acetone-*d*₆) δ ppm 8.58 (s, 3H, OH), 7.68 (d, 3H, ³*J*_{H,H} = 8 Hz, C^{4'}H), 7.63 (s, 3H, C^{2''}H), 7.17 (t, 3H, ³*J*_{H,H} = 7.63 Hz, C^{5''}H), 7.01 (d, ³*J*_{H,H} = 7.63 Hz, C^{6''}H), 7.83 (m, 6H, C^{3',5'}H), 6.69 (d, 3H, ³*J*_{H,H} = 8.60 Hz, C^{6'}H), 6.63 (s, 3H, C^{2,4,6}H); ¹³C NMR (125.8 MHz, acetone-*d*₆) δ ppm 157.76 (C^{4'}), 145.25 (C^{1''}), 141.01 (C^{1,3,5}), 140.78 (C^{2'}), 139.23 (C^{2''}H), 136.50 (C^{4''}H), 132.67 (C^{6'}H), 132.46 (C^{1'}), 130.92 (C^{5''}H), 130.47 (C^{6''}H), 130.33 (C^{2,4,6}H), 117.79 (C^{3'}H), 115.95 (C^{5'}H), 94.48 (C^{3''}); IR (KBr) ν cm⁻¹ 3350-3200, (bm, ν (O-H)), 3050 (w), and 3028 (w, ν (=CH)), 1606 (s, ν (C=C)), 1198 (bs, ν (C-O)); UV-Vis (dioxane) λ_{max} (ε) = 264 nm (39 600); ESI (-) MS calcd. for C₄₂H₂₇I₃O₃ ([M-H]⁻, 958.90), found: 958.91; Elemental Anal. Calcd. (%) for C₄₂H₂₇I₃O₃ (960.39): C, 52.53; H, 2.83. Found: C, 52.32; H, 3.17.

4'''',5'-Bis[(2-hexyldecyl)oxy]-5''-[5-[(2-hexyldecyl)oxy]-3'-iodo-biphenyl-2-yl]-3,3''''-diiodo-1,1':2',1'':3'',1''':2''',1''''-quinquephenyl (63)



Method A: In a 50 mL round bottom flask, compound **62** (100 mg, 0.104 mmol) was dissolved in anhydrous THF (10 mL) and the solution was cooled to 0 °C in an ice bath. To the cold solution was added an excess of NaH (60% dispersion in mineral oil, 20 mg, 0.832 mmol) and the mixture stirred for 30 min at that temperature, then the suspension was allowed to reach RT and stirred for 1 h. Subsequently, 7-(bromomethyl)pentadecane (320 mg, 1.04 mmol) was added dropwise and the reaction allowed to stir at 40 °C under argon atmosphere for 18 h. The reaction was quenched with H₂O (15 mL), the insoluble particles filtered off and washed with CH₂Cl₂ (40 mL). The organic phase was washed with brine (50 mL) and dried over MgSO₄. All volatile solvents were evaporated under vacuum and the product (**63**) was isolated by flash column chromatography on silica gel (*n*-hexane/CH₂Cl₂, 30:1) as a dark yellow oil (12 mg) in 7% yield. (*R_f* = 0.58, *n*-hexane/EtOAc, 30:1). A second fraction containing the elimination product (**64**) was isolated as a brown oil (19 mg) in 11% yield.

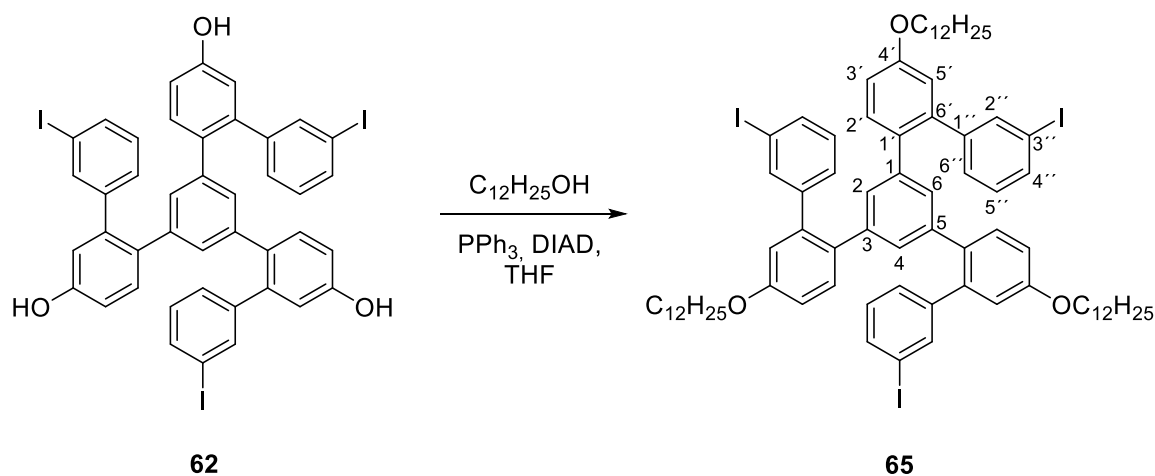
For **63**: ¹H NMR (500 MHz, CD₂Cl₂) δ ppm 7.59 (s, 3H, C^{2''}H), 7.58 (d, 3H, ³*J*_{H,H} = 8 Hz, C^{4''}H), 6.99 (t, 3H, ³*J*_{H,H} = 8 Hz, C^{5''}H), 6.89 (d, 3H, ³*J*_{H,H} = 8 Hz, C^{6''}H), 6.82 (m, 6H, C^{3';5'}H), 6.68 (d, 3H, ³*J*_{H,H} = 9 Hz, C^{6'}H), 6.61 (s, 3H, C^{2,4,6}H), 3.84 (d, 6H, ³*J*_{H,H} = 6 Hz, OCH₂), 1.76 (t, 3H, ³*J*_{H,H} = 5.20 Hz, CH),

1.27 (bs, 72H, CH₂), 0.86 (m, 18H, CH₃); ¹³C NMR (125.8 MHz, CDCl₃) δ ppm 158.89 (C^{4'}), 144.29 (C^{1''}), 140.07 (C^{1,3,5}), 139.89 (C^{2'}), 138.62 (C^{2''}H), 135.71 (C^{4''}H), 132.69 (C^{1'}), 131.89 (C^{6'}H), 129.84 (C^{2,4,6}H), 129.77 (C^{6''}H), 129.71 (C^{5''}H), 116.32 (C^{3'}H), 114.15 (C^{5'}H), 94.11 (C^{3''}), 71.20 (OCH₂), 38.27 (CH), 32.13, 32.09, 30.25, 29.92, 29.82, 29.56, 27.10, 27.08 and 22.91 (CH₂), 14.35 (CH₃); IR (KBr) ν cm⁻¹ 2955 (m), 2923 (s) and 2855 (m, ν (CH)), 1605 (m, ν (C=C)), 1467 (m, δ (O-CH₂)), 1380 (w, δ_{sym} (CH)), 1204 (m, ν (C-O)); UV-Vis (dioxane) λ_{max} (ε) = 268 nm (42 000); Elemental Anal. Calcd. (%) for C₉₀H₁₂₃O₃I₃ (1633.68): C, 66.17; H, 7.59. Found: C, 68.38; H, 8.64.

For **64**: ¹H NMR (500 MHz, CD₂Cl₂) δ ppm 7.33 – 7.27 (m, 9H, C^{2'',4'',6''}H), 7.04 (d, 6H, ³J_{H,H} = 7.74 Hz, C^{3'',5''}H), 6.87 (d, 3H, ³J_{H,H} = 2.54 Hz, C^{3'}H), 6.79 (dd, 3H, ³J_{H,H} = 2.70 Hz, C^{5'}H), 6.71 (d, 3H, ³J_{H,H} = 8.45 Hz, C^{6'}H), 6.60 (s, 3H, C^{2,4,6}H), 3.87 (d, 6H, ³J_{H,H} = 5.72 Hz, OCH₂), 1.79 (t, 3H, ³J_{H,H} = 6 Hz, CH), 1.29 (bs, 72H, CH₂), 0.88 (m, 18H, CH₃); ¹³C NMR (125.8 MHz, CDCl₃) δ ppm 159.22 (C^{4'}), 142.36 (C^{2'}), 142.12 (C^{1''}), 140.95 (C^{1,3,5}), 133.31 (C^{1'}), 131.93 (C^{6'}H), 130.65 (C^{3'',5''}H), 130.06 (C^{2,4,6}H), 128.35 (C^{2'',6''}H), 127.05 (C^{4''}H), 116.70 (C^{3'}H), 113.88 (C^{5'}H), 71.58 (OCH₂), 38.56 (CH), 32.51, 32.46, 31.95, 31.93, 30.61, 30.29, 30.18, 29.92, 27.39 and 23.27 (CH₂), 14.47 (CH₃); IR (KBr) ν cm⁻¹ 3032 (w, ν (=CH)), 2923 (s) and 2854 (s, ν (CH)), 1603 (m, ν (C=C)), 1468 (m, δ (O-CH₂)), 1315 (m, δ_{sym} (CH)), 1203 (m, ν (C-O)); UV-Vis (dioxane) λ_{max} (ε) = 268 nm (42 000); ESI (-) MS calcd. for C₉₀H₁₂₆O₃Na (1255.98), found: 1256.01; Elemental Anal. Calcd. (%) for C₉₀H₁₂₆O₃ (1256.00): C, 86.07; H, 10.11. Found: C, 84.54; H, 11.19.

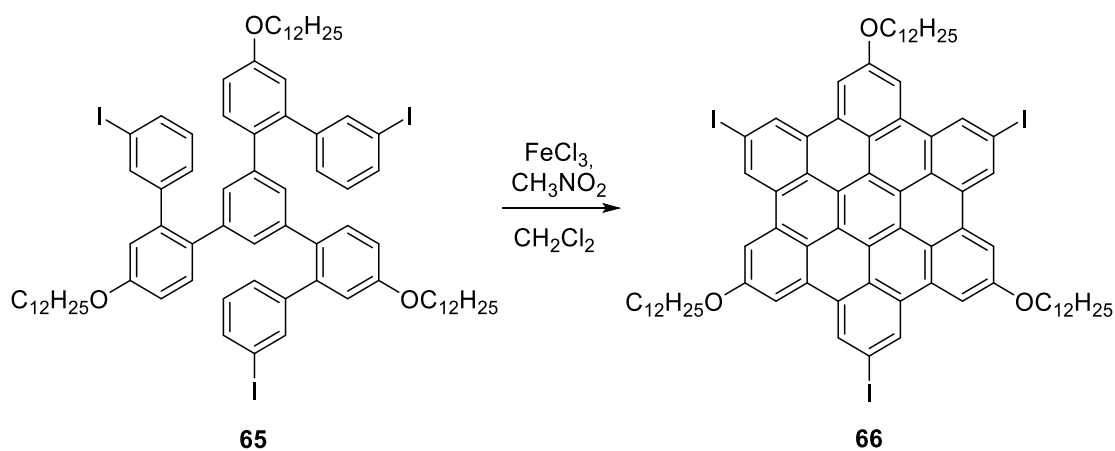
Method B: In a 25 mL round bottom flask, compound **62** (100 mg, 0.104 mmol) was dissolved in anhydrous DMF (8 mL). An excess of K₂CO₃ (216 mg, 1.56 mmol) was added and the suspension was stirred at RT for 30 min. Subsequently, 7-(bromomethyl)pentadecane (190 mg, 0.624 mmol) was added dropwise, and the mixture was refluxed for 48 h. After cooling to RT, the inorganic salts were removed via filtration; the resulting solution was diluted with H₂O and extracted with diethyl ether (3 x 50 mL). The organic phases were combined, washed with HCl (1.0 M aqueous solution, 50 mL), H₂O (50 mL), brine (50 mL) and dried over MgSO₄. All volatile solvents were evaporated under vacuum, the residue was purified by column chromatography on silica gel (*n*-hexane/EtOAc, 20:1) and isolated as a dark yellow oil (19 mg) in 11% yield.

4'''',5'-Bis(dodecyloxy)-5''-[5-(dodecyloxy)-3'-iodo-biphenyl-2-yl]-3,3''''-diiodo-1,1':2',1'':3'',1''':2''',1''''-quinquephenyl (65)



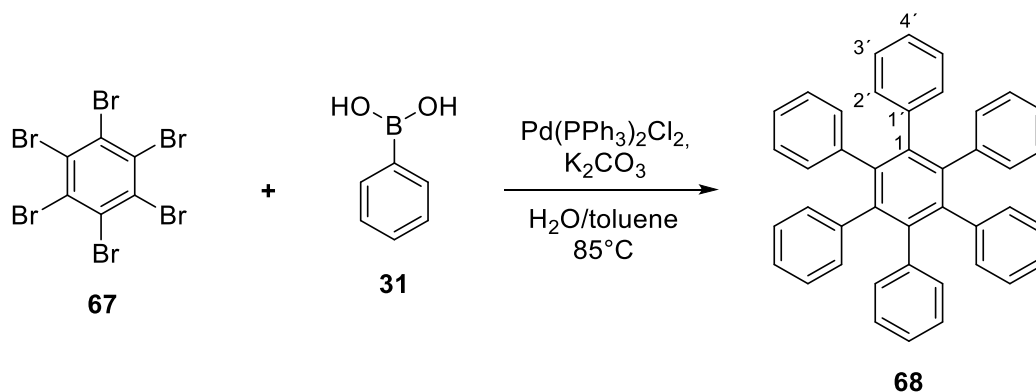
In a 50 mL Schlenk flask, compound **62** (400 mg, 0.416 mmol), PPh_3 (982 mg, 3.74 mmol) and 1-dodecanol (697 mg, 3.74 mmol) were dissolved in anhydrous THF (30 mL). The mixture was sonicated for 15 min until a yellow neat solution was obtained, afterwards DIAD (756 mg, 7.34 mmol) was slowly added dropwise over 20 min. The light orange solution was allowed to stir at RT under argon atmosphere for 16 h. The mixture was diluted with ethyl acetate and filtered through a short pad of silica gel, all volatile solvents were evaporated under vacuum and the desired product was isolated after column chromatography on silica gel (*n*-hexane/EtOAc, 20:1) as a yellow wax (512 mg) in 84% yield. (R_f = 0.38, *n*-hexane/EtOAc, 20:1). ^1H NMR (500 MHz, CDCl_3) δ ppm 7.59 (s, 3H, $\text{C}^{2''}\text{H}$), 7.58 (d, 3H, $^3J_{\text{H,H}}$ = 8.54 Hz, $\text{C}^{4''}\text{H}$), 6.99 (t, 3H, $^3J_{\text{H,H}}$ = 7.83 Hz, $\text{C}^{5''}\text{H}$), 6.89 (d, 3H, $^3J_{\text{H,H}}$ = 7.83 Hz, $\text{C}^{6''}\text{H}$), 6.83 (m, 6H, $\text{C}^{3',5'}\text{H}$), 6.68 (d, 3H, $^3J_{\text{H,H}}$ = 9.25 Hz, $\text{C}^{2'}\text{H}$), 6.60 (s, 3H, $\text{C}^{2,4,6}\text{H}$), 3.97 (t, 6H, $^3J_{\text{H,H}}$ = 6.30 Hz, OCH_2), 1.77 (t, 6H, $^3J_{\text{H,H}}$ = 6.93 Hz, OCH_2CH_2), 1.45 (t, 6H, $^3J_{\text{H,H}}$ = 6.93 Hz, CH_2), 1.25 (bs, 48H, CH_2), 0.86 (t, 9H, $^3J_{\text{H,H}}$ = 6.93 Hz, CH_3); ^{13}C NMR (125.8 MHz, CDCl_3) δ ppm 158.63 ($\text{C}^{4'}$), 144.25 ($\text{C}^{1''}$), 140.02 ($\text{C}^{6'}$), 139.91 ($\text{C}^{1,3,5}$), 138.62 ($\text{C}^{2''}\text{H}$), 135.72 ($\text{C}^{4''}$), 132.75 ($\text{C}^{1'}$), 131.89 ($\text{C}^{2'}\text{H}$), 129.86 ($\text{C}^{5''}\text{H}$), 129.81 ($\text{C}^{6''}\text{H}$), 129.77 ($\text{C}^{2,4,6}\text{H}$), 116.32 ($\text{C}^{5'}\text{H}$), 114.12 ($\text{C}^{3'}\text{H}$), 94.10 ($\text{C}^{3''}$), 68.39 (OCH_2), 32.14 (OCH_2CH_2), 29.92, 29.89, 29.86, 29.82, 29.62, 29.57, 29.53, 26.28 and 22.92 (CH_2), 14.35 (CH_3); IR (KBr) ν cm^{-1} 3049 (w, ν ($=\text{CH}$)), 2923 (s) and 2853 (s, ν (CH)), 1604 (m, ν ($\text{C}=\text{C}$)), 1468 (m, δ ($\text{O}-\text{CH}_2$)), 1388 (m, δ_{sym} (CH)), 1202 (m, ν ($\text{C}-\text{O}$)); UV-Vis (CH_2Cl_2) λ_{max} (ϵ) = 269 nm (44 300); Elemental Anal. Calcd. (%) for $\text{C}_{78}\text{H}_{99}\text{O}_3\text{I}_3$ (1465.36): C, 63.93; H, 6.81. Found: C, 65.88; H, 7.71.

2,8,14-Tris(dodecyloxy)-5,11,17-triiodohexa-*peri*-hexabenzocoronene (66)



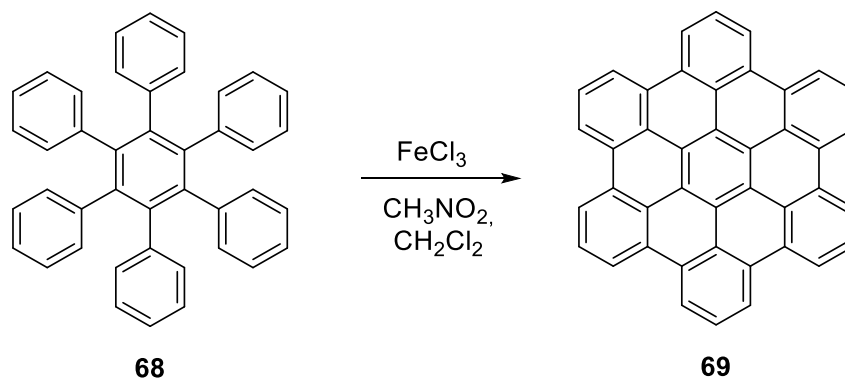
In a 50 mL round bottom flask, compound **65** (50 mg, 0.068 mmol) was dissolved in unstabilized dichlorometane (16 mL), and the solution was purged with argon for 30 min. To the degassed solution FeCl_3 (547 mg, 3.4 mmol) solution in 5 mL of anhydrous nitromethane was added and the reaction mixture allowed to stir at RT for 16 h. A constant flow of argon was purged through the mixture for the whole reaction time. The reaction was quenched with MeOH (60 mL) and the brown precipitated was filtered off, washed with MeOH, H_2O and dried under vacuum. The desired product was isolated as a dark brown solid (42 mg) in 84% yield. IR (KBr) $\nu \text{ cm}^{-1}$ 2922 (s) and 2851 (s, ν (CH)), 1608 (m, ν (C=C)), 1462 (m, δ (O-CH₂)), 1361 (m, δ_{sym} (CH)), 1195 (m, ν (C-O)); UV-Vis (CH_2Cl_2) λ_{max} (ϵ) = 367 nm (34 100); MALDI-TOF MS (+) calcd. for $\text{C}_{78}\text{H}_{87}\text{I}_3\text{O}_3$ (M^+ , 1452.38), found: 1452.14.

Hexaphenylbenzene (**68**)



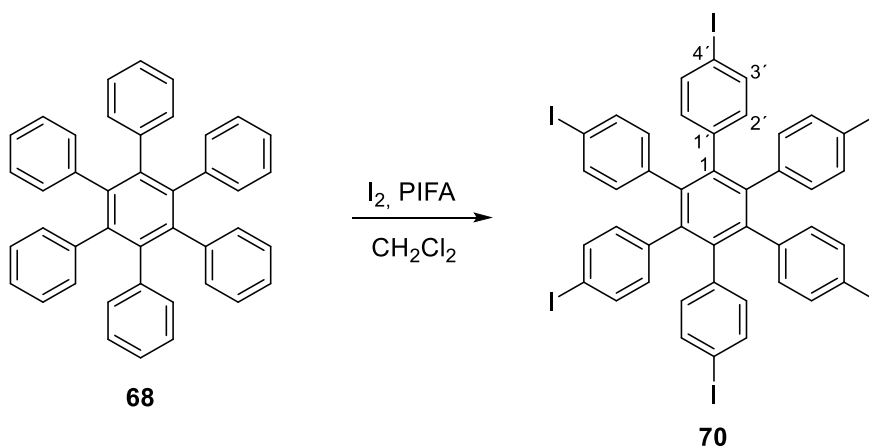
This compound was prepared using a modified literature procedure.^[293] In a 500 mL Schlenk flask, hexabromobenzene **67** (2.00 g, 3.63 mmol) and phenylboronic acid **31** (3.50 g, 29.04 mmol) were dissolved in toluene (200 mL). The solution was purged with argon for 15 min. To the degassed solution an aqueous solution of K₂CO₃ (2.50 g, 18.2 mmol) in 10 mL of water was added and the reaction mixture was purged with argon for 15 min. Subsequently, Pd(PPh₃)Cl₂ (178 mg, 0.254 mmol) was added and the mixture was allowed to stir at 85 °C for 24 h under argon atmosphere. After cooling down to RT, the reaction mixture was diluted with ethyl acetate (200 mL) and filtered through a short pad of silica gel. All volatile solvents were evaporated under vacuum. The desired product was purified by column chromatography on silica gel (*n*-hexane/EtOAc, 20:1) and isolated as a white solid (1.18 g) in 61 % yield. (*R*_f = 0.44, *n*-hexane/EtOAc, 20:1). ¹H NMR (500 MHz, CDCl₃) δ ppm 6.85-6.80 (m, 30H); ¹³C NMR (125.8 MHz, CDCl₃) δ ppm 140.60 (C¹), 140.31 (C^{1'}), 131.43 (C^{3'}H), 126.58 (C²H), 125.19 (C^{4'}H).

Hexa-*peri*-hexabenzocoronene (69)



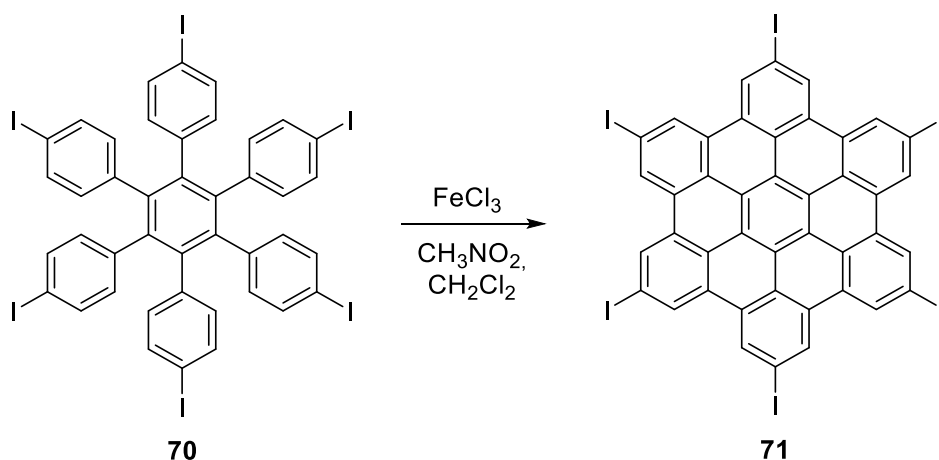
This compound was prepared using a modified literature procedure.^[294] In a 250 mL round bottom flask, hexaphenylbenzene **68** (250 mg, 0.468 mmol) was dissolved in unstabilized dichloromethane (80 mL) and the solution was purged with argon for 30 min. To the degassed solution FeCl_3 (3.42 g, 21.06 mmol) solution in 20 mL of anhydrous nitromethane was added and the reaction mixture was allowed to stir at RT for 18 h. A constant flow of argon was purged through the mixture for the whole reaction time. The reaction was quenched with MeOH (100 mL) and the dark brown precipitate was filtered off, washed with MeOH, H_2O , CH_2Cl_2 , and dried under vacuum. The desired product was isolated as an insoluble dark brown solid (242 mg) in 99% yield. IR (KBr) ν cm^{-1} 3077 (w, ν ($=\text{CH}$)), 1582 (m, ν ($\text{C}=\text{C}$)), 759 (s) and 738 (s, γ ($=\text{CH}$)); MALDI-TOF MS (+) calcd. for $\text{C}_{42}\text{H}_{18}$ (M^+ , 522.14), found: 522.06.

Hexakis(4-iodophenyl)benzene (70)



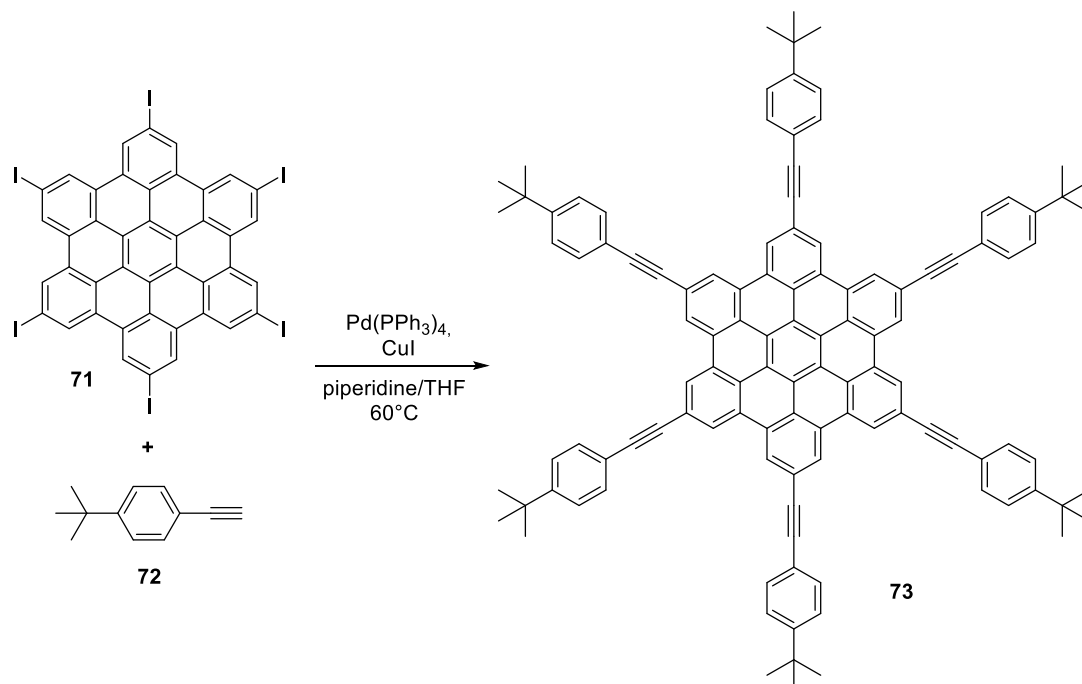
This compound was prepared using a modified literature procedure.^[295] In a 250 mL Schlenk flask, hexaphenylbenzene **68** (1.00 g, 1.87 mmol), PIFA (2.73 g, 6.36 mmol) and I_2 (1.57 g, 6.17 mmol) were dissolved in anhydrous dichloromethane (100 mL) and the mixture was allowed to stir at RT under argon atmosphere for 48 h. The reaction mixture was diluted with *n*-hexane (150 mL) turning into light purple solution with a white precipitate. The precipitate was filtered off, washed with *n*-hexane (50 mL) and dissolved in chloroform (100 mL). The organic phase was washed with $Na_2S_2O_3$ (saturated aqueous solution, 100 mL), H_2O (100 mL), brine (100 mL) and dried over $MgSO_4$. All volatile solvents were evaporated under vacuum, the desired product purified by column chromatography on silica gel (*n*-hexane/EtOAc, 10:1) and isolated as a white solid (2.39 g) in 99% yield. (R_f = 0.27, *n*-hexane/EtOAc, 20:1); m.p. > 400 °C. 1H NMR (500 MHz, $CDCl_3$) δ ppm 7.22 (d, 12H, $^3J_{H,H}$ = 8 Hz, C^3H), 6.44 (d, 12H, $^3J_{H,H}$ = 8 Hz, C^2H); ^{13}C NMR (125.8 MHz, $CDCl_3$) δ ppm 139.70 (C^1), 139.19 ($C^{1'}$), 136.55 (C^3H), 133.01 (C^2H), 92.16 (C^4).

2,5,8,11,14,17-Hexa-iodohexa-*peri*-hexabenzocoronene (71)



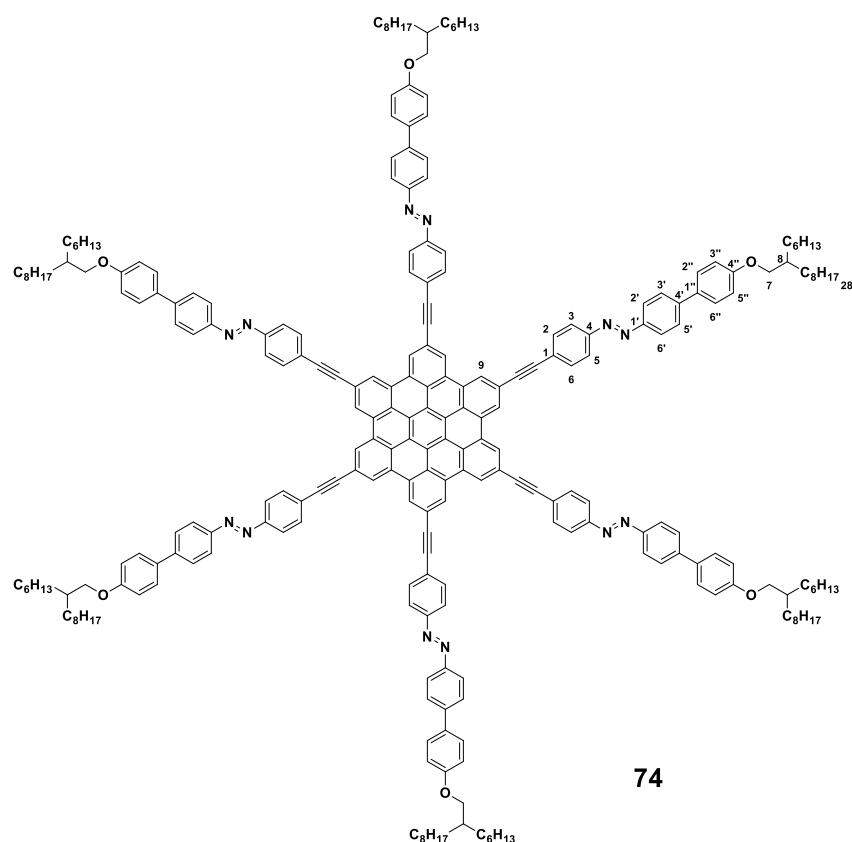
This compound was prepared using a modified literature procedure.^[276] In a 250 mL round bottom flask, hexakis(4-iodophenyl)benzene **70** (200 mg, 0.155 mmol) was dissolved in unstabilized dichloromethane (80 mL) and the solution was purged with argon for 30 min. To the degassed solution FeCl_3 (6.95 g, 26.7 mmol) solution in 20 mL of anhydrous nitromethane was added and the reaction mixture was allowed to stir at RT for 2 h. A constant flow of argon was purged through the mixture for the whole reaction time. The reaction was quenched with MeOH (150 mL) and the brown precipitate was filtered off and washed with MeOH, H_2O , CH_2Cl_2 and dried under vacuum. The desired product was isolated as an insoluble brown solid (196 mg) in 98% yield. MALDI-TOF MS (+) calcd. for $\text{C}_{42}\text{H}_{12}\text{I}_6$ (M^+ , 1277.52), found: 1277.61; Elemental Anal. Calcd. (%) for $\text{C}_{42}\text{H}_{12}\text{I}_6$ (1277.98): C, 39.47; H, 0.95. Found: C, 39.08; H, 1.15.

2,5,8,11,14,17-Hexakis((4-(tert-butyl)phenyl)ethynyl)hexa-*peri*-hexabenzocoronene (73)



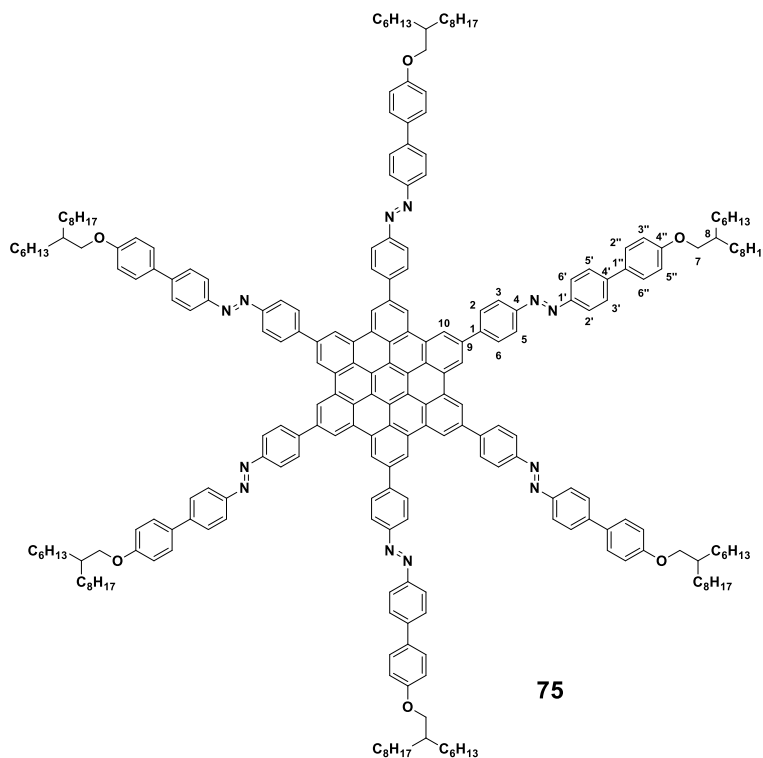
In a 50 mL Schlenk flask, 2,5,8,11,14,17-hexa-4-iodohexa-*peri*-hexabenzocoronene **71** (150 mg, 0.117 mmol), Pd(PPh₃)₄ (39.5 mg, 0.034 mmol), and CuI (13.3 mg, 0.07 mmol) were dissolved in an anhydrous mixture of THF/piperidine (20 mL, 1/3 v/v). The reaction mixture was degassed by three freeze – vacuum – thaw cycles, and 4-*tert*-butylphenylacetylene **72** (222 mg, 1.40 mmol) was added. The reaction was allowed to stir at 60 °C for 20 h under argon atmosphere. After cooling to RT, the crude product was precipitated with MeOH (60 mL), filtered off, washed with MeOH (50 mL), H₂O (50 mL) and dried under vacuum. The desired product was purified by size exclusion chromatography on a *BioBeads S-X1* resin purchased from BIO RAD (eluted in toluene). All volatile solvents were evaporated under vacuum and the pure product was isolated as a dark brown solid (166.3 mg) in 97% yield. IR (KBr) ν cm⁻¹ 3033 (w, ν (=CH)), 2955 (s), 2902 (m) and 2864 (m, (w, ν (CH))), 2207 (w, ν (C \equiv C)), 1600 (m, ν (C=C)), 1363 (m, δ_{sim} (CH)); MALDI-TOF MS (+) calcd. for C₁₁₄H₉₀ (M⁺, 1459.71), found: 1460.16; Elemental Anal. Calcd. (%) for C₁₁₄H₉₀ (1459.97): C, 93.79; H, 6.21. Found: C, 90.11; H, 5.97.

2,5,8,11,14,17-Hexakis[4-{4-(2-hexyldecyloxy)biphenyl-4'-yl}diazenyl]phenyl)ethynyl]hexa-*peri*-hexabenzocoronene (74)



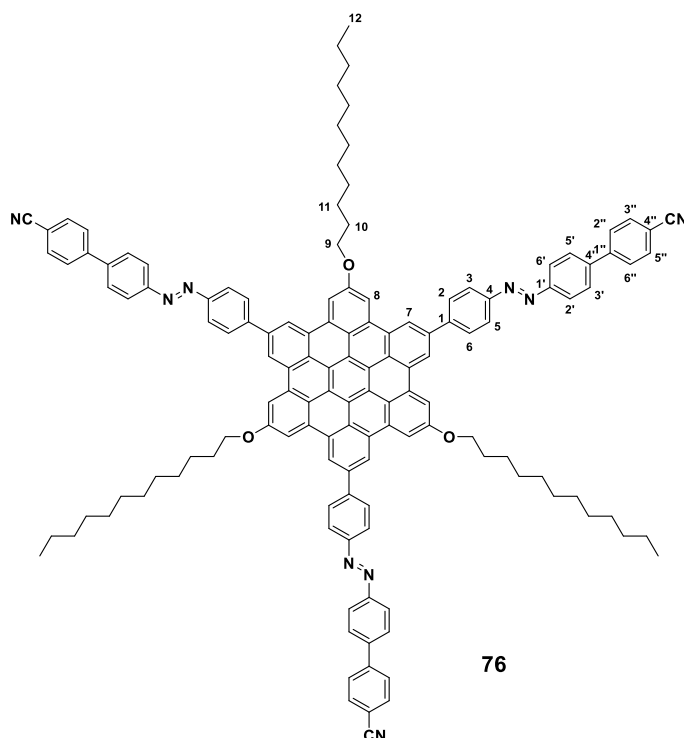
In a 10 mL Schlenk tube, 2,5,8,11,14,17-hexa-4-iodohexa-*peri*-hexabenzocoronene **71** (35 mg, 0.027 mmol), Pd(PPh₃)₄ (9.40 mg, 0.008 mmol), and CuI (3.08 mg, 0.016 mmol) were dissolved in an anhydrous mixture of THF/piperidine (5 mL, 2/3 v/v). The reaction mixture was degassed by three freeze – vacuum – thaw cycles, and azobenzene derivative **53** (167 mg, 0.324 mmol) was added. The reaction was allowed to stir at 60 °C for 48 h under argon atmosphere. After cooling to RT, the crude product was precipitated with MeOH (60 mL), filtered off, washed with MeOH (50 mL), H₂O (50 mL) and dried under vacuum. The desired product was purified by size exclusion chromatography on a *BioBeads S-X1* resin purchased from BIO RAD (eluted in THF). All volatile solvents were evaporated under vacuum providing the product as a red solid (92 mg) in 93% yield. ¹H NMR (500 MHz, C₂D₂Cl₄, 383 K) δ ppm 8.14 – 7.15 (br, 72H, C⁹H, C^{2,3,5,6}H, C^{2',3',5',6'}H, C^{2'',6''}H), 6.93 (br, 12H, C^{3'',5''}H), 3.95 (br, 12H, C⁷H₂), 1.92 (br, 6H, C⁸H), 1.56 – 1.36 (br, 144H, CH₂), 1.02 (br, 36H, CH₃); IR (KBr) ν cm⁻¹ 2953 (s), and 2853 (m, ν (CH)), 2202 (w, ν (C≡C)), 1598 (s, ν (C=C)), 1490 (m) and 1461 (m, ν (N=N)), 1248 (s, ν (C-O)); UV-Vis (CH₂Cl₂) λ_{max} (ε) = 385 nm (74 900); MALDI-TOF MS (+) calcd. for C₂₅₈H₂₈₂N₁₂O₆ (M⁺, 3647.22), found: 3647.87; Elemental Anal. Calcd. (%) for C₂₅₈H₂₈₂N₁₂O₆ (3647.08): C, 84.97; H, 7.79; N, 4.61. Found: C, 82.19; H, 7.79; N, 5.61.

2,5,8,11,14,17-Hexakis-(4-{[4-(2-hexyldecyloxy)biphenyl-4'-yl]diazenyl}phenyl)hexa-*peri*-hexabenzocoronene (75)



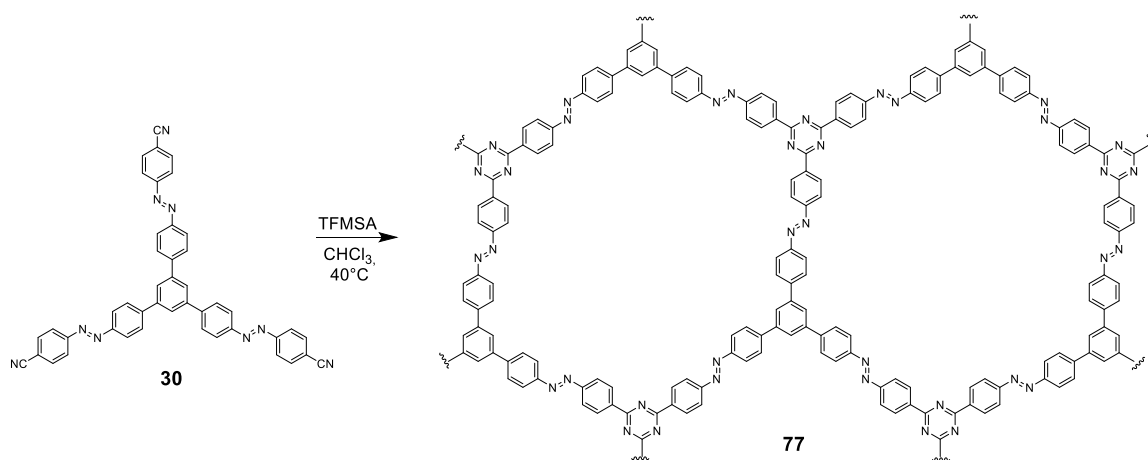
In a 25 mL Schlenk flask, compound **71** (50 mg, 0.039 mmol), azobenzene pinacolboronic ester **54** (292 mg, 0.468 mmol) and SPhos (2.39 mg, 0.006 mmol) were dissolved in toluene (5 mL). Subsequently, a large excess of K_2CO_3 (750 mg, 5.43 mmol) dissolved in a mixture of $H_2O/EtOH$ (2 mL, 1/1 v/v) was added and the reaction mixture was degassed by one freeze – vacuum – thaw cycle. Finally, $Pd(PPh_3)_4$ (3.60 mg, 0.004 mmol) was added, the mixture was degassed by two freeze – vacuum – thaw cycles and the reaction was allowed to stir at 60 °C for 96 h under argon atmosphere. After cooling to RT, the crude product was precipitated with MeOH (20 mL), filtered off, washed with MeOH (50 mL), H_2O (50 mL) and dried under vacuum. The desired product was purified by size exclusion chromatography on a *BioBeads S-XI* resin purchased from BIO RAD (with THF). All volatile solvents were evaporated under vacuum providing the desired product as a brown reddish solid (124 mg) in 91% yield. 1H NMR (500 MHz, $C_2D_2Cl_4$, 383 K) δ ppm 8.26 – 7.25 (bm, 72 H, $C^{2,3,5,6}H$, $C^{2',3',5',6'}H$, $C^{2'',6''}H$, $C^{10}H$), 7.13 – 6.98 (br, 12H, $C^{3'',5''}H$), 4.07 – 3.92 (br, 12H, C^7H_2), 2.00 – 1.84 (br, 6H, C^8H), 1.61 – 1.32 (br, 144H, CH_2), 0.99 – 0.91 (br, 36H, CH_3); IR (KBr) ν cm^{-1} 2921 (s), and 2852 (m, ν (CH)), 1599 (s, ν (C=C)), 1488 (m) and 1465 (m, ν (N=N)), 1246 (s, ν (C-O)); UV-Vis (CH_2Cl_2) λ_{max} (ϵ) = 384 nm (42 900); MALDI-TOF MS (+) calcd. for $C_{246}H_{282}N_{12}O_6$ (M^+ , 3502.22), found: 3501.95; Elemental Anal. Calcd. (%) for $C_{246}H_{282}N_{12}O_6$ (3503.04): C, 84.35; H, 8.11; N, 4.80. Found: C, 75.39; H, 6.63; N, 3.39.

2,8,14-Tris{4-[(4'-cyanobiphenyl-4-yl)diazenyl]phenyl}-5,11,17-tris(dodecyloxy)hexa-*peri*-hexabenzocoronene (76)



In a 25 mL Schlenk flask, compound **66** (50 mg, 0.034 mmol), azobenzene pinacolboronic ester **46** (83.5 mg, 0.204 mmol) and SPhos (2.10 mg, 0.005 mmol) were dissolved in toluene (6 mL). Then, a large excess of K_2CO_3 (750 mg, 5.43 mmol) dissolved in a mixture of $H_2O/EtOH$ (2 mL, 1/1 v/v) was added and the reaction mixture was degassed by one freeze – vacuum – thaw cycle. Subsequently, $Pd(PPh_3)_4$ (3.47 mg, 0.003 mmol) was added, the solution was degassed by two freeze – vacuum – thaw cycles and the reaction mixture was allowed to stir at 65 °C for 48 h under argon atmosphere. After cooling to RT, the crude product was precipitated with MeOH (20 mL), filtered off, washed with MeOH (50 mL), H_2O (50 mL) and dried under vacuum. The desired product was purified by size exclusion chromatography on a *BioBeads S-XI* resin purchased from BIO RAD (eluted with THF) and the desired product isolated as a dark brown solid (75 mg) in 88% yield. 1H NMR (500 MHz, $C_2D_2Cl_4$, 383 K) δ ppm 8.34 – 7.60 (br, 48H, $C^{2,3,5,6}H$, $C^{2',3',5',6'}H$, $C^{2'',3'',5'',6''}H$, C^7H and C^8H), 4.35 (br, 6H, C^9H_2), 2.27 – 1.90 (br, 12H, $C^{10}H_2$ and $C^{11}H_2$), 1.36 (br, 48H, CH_2), 0.97 (br, 9H, $C^{12}H_3$); IR (KBr) ν cm^{-1} 2962 (m), 2920 (s) and 2851 (m, ν (CH)), 2226 (m, ν ($C\equiv N$)), 1603 (s, ν ($C=C$)), 1433 (m, ν ($N=N$)), 1364 (m, δ_{sym} (CH)), 1261 (s, ν (C-O)); UV-Vis (CH_2Cl_2) λ_{max} (ϵ) = 373 nm (56 600); MALDI-TOF MS (+) calcd. for $C_{135}H_{123}N_9O_3$ (M^+ , 1918.98), found: 1918.82; Elemental Anal. Calcd. (%) for $C_{135}H_{123}N_9O_3$ (1919.53): C, 84.47; H, 6.46; N, 6.57. Found: C, 75.64; H, 7.26; 3.08.

Triazine based COF-77



Method A: In a 50 mL Schlenk flask, trifluoromethanesulfonic acid (51 μ L, 0.58 mmol) was dissolved in 1 mL of anhydrous CHCl₃, and the solution was cooled down to 0 °C in an ice bath. To the cold solution azobenzene derivative **30** (90 mg, 0.144 mmol) dissolved in anhydrous CHCl₃ (20 mL), was added dropwise over 30 min under stirring. The reddish mixture was stirred at 0 °C for 2 h. Subsequently, the reaction mixture was stirred at 40 °C for 60 h under argon atmosphere. The reaction color turned from colorless to purple and a solid precipitate was formed. After cooling down to RT, 220 mL of H₂O containing 11 mL of ammonia solution (25%) was added, and the suspension was stirred for 2 h. The obtained precipitate was isolated by vacuum filtration and copiously washed with H₂O (70 mL), EtOH (100 mL), acetone (100 mL) and CHCl₃ (150 mL). The desired product was dried under vacuum at 120 °C for 12 h to afford COF-77-A as a dark orange powder (36 mg) in 40% yield. IR (KBr) ν cm⁻¹ 2224 (w, ν (C \equiv N)), 1511 (s, ν (C=N)), 1371 (s, ν (C=N)), 837 (m, ν (C-H)); Elemental Anal. Calcd. (%) for C₄₅H₂₇N₉ (693.77): C, 77.91; H, 3.92; N, 18.17. Found: C, 71.05; H, 4.74; N, 13.85.

Method B: In a 50 mL Schlenk flask, trifluoromethanesulfonic acid (440 μ L, 4.97 mmol) was dissolved in 5 mL of anhydrous CH₂Cl₄, and the solution cooled at 0 °C in an ice bath. To the cold solution was added azobenzene derivative **30** (230 mg, 0.332 mmol) dissolved in anhydrous CHCl₃ (30 mL), slowly dropwise, with a dropping funnel, over 45 min under stirring. The purple mixture was stirred at 0 °C for 2 h. Subsequently, the reaction was allowed to reach 40 °C and stirred for 80 h under argon atmosphere. The reaction mixture turned from colorless to purple and a solid precipitate was formed. After cooling down at RT, 220 mL of H₂O containing 11 mL of ammonia solution (25%) was added, and the mixture stirred for 2 h. The precipitate was isolated by vacuum filtration and washed with H₂O

(150 mL), EtOH (50 mL), acetone (50 mL) and CHCl_3 (50 mL). The product was dried under vacuum at 120 °C for 12 h. COF-77-B was obtained as dark purple balls (232 mg) in quantitative yield. IR (KBr) $\nu \text{ cm}^{-1}$ 1507 (m, ν (C=N)), 1356 (m, ν (C=N)), 819 (m, ν (C-H)); Elemental Anal. Calcd. (%) for $\text{C}_{45}\text{H}_{27}\text{N}_9$ (693.77): C, 77.91; H, 3.92; N, 18.17. Found: C, 73.18; H, 6.98; N, 15.90.

Triazine based COF-80

A quartz tube (1.5×10 cm) was charged with tris(CN-azobenzene) **30** (100 mg, 0.144 mmol) and a large excess of anhydrous ZnCl_2 (197 mg, 1.44 mmol) under argon atmosphere, and then sealed under vacuum. The reaction mixture was heated at 400 °C for 30 h in a ceramic oven. After cooling down to room temperature, spontaneously, the black solid was poured into H_2O (50 mL), stirred in water for 18 h, filtered off and copiously washed with H_2O . Subsequently, the filtered solid was poured into an aqueous solution of HCl (1.0 M), stirred for 2 h, filtered off, washed with HCl (1.0 M), H_2O and dried at 120 °C under vacuum for 48 h. IR (KBr) $\nu \text{ cm}^{-1}$ 1609 (m, ν (C=C)), 1206 (m, ν (C-N)), 859 (m, ν (C-H)); Elemental Anal. Calcd. (%) for $\text{C}_{45}\text{H}_{27}\text{N}_9$ (693.77): C, 77.91; H, 3.92; N, 18.17. Found: C, 72.97; H, 3.52; N, 8.71.

5 List of Abbreviations

2D	Two-dimensional
3D	Three-dimensional
Å	Angstrom
AB	Azobenzene
AcCl	Acetyl chloride
AcOH	Acetic acid
AcOK	Potassium acetate
AFM	Atomic Force Microscopy
aq.	Aqueous
ATD	Arrival time distribution
<i>BE</i>	Binding energy
BET	Braunauer – Emmer – Teller
Boc	<i>tert</i> -Butyloxycarbonyl
(BOC) ₂ °	Di- <i>tert</i> -butyl-dicarbonate
(Bpin) ₂	Bis(pinacolato)diboron
br	Broad
Brine	Saturated aqueous NaCl solution
C	Celsius
Calcd.	Calculated
CCS	Collisional cross-section
CE	Collisional energy
COF	Covalent organic framework
COSY	Homonuclear correlation spectroscopy
CV	Cyclovoltammetry
d	Doublet
DCM	Dichloromethane
dd	Doublet of doublet
DCvC	Dynamic covalent chemistry
DCTB	trans-2-[3-(4- <i>tert</i> -Butylphenyl)-2-methyl-2-propenylidene]malononitrile
DDQ	2,3-Dichloro-5,6-dicyano-1,4-benzoquinone
DEF	<i>N,N</i> -Diethylformamide
DIAD	Diisopropyl azodicarboxylate
DMAP	4-Dimethylaminopyridine
DME	Dimethoxyethane

DMF	<i>N,N</i> -Dimethylformamide
DMSO	Dimethyl sulfoxide
dppf	1,1'-Bis(diphenylphosphino)ferrocene
DPV	Differential Pulse Voltammetry
DSC	Differential scanning calorimetry
DTE	Dithienylethene
EA	Elemental Analysis
E_{ads}	Adsorption energy
EDG	Electron – donating group
EI	Electron Impact
eq.	Equivalents
ESI	Electron Spray Ionization
Et	Ethyl
Et ₃ N	Triethylamine
Et ₂ O	Diethyl ether
EtOAc	Ethyl acetate
EtOH	Ethanol
EWG	Electron – withdrawing group
Fc	Ferrocene
FTIR	Fourier transform infrared spectroscopy
g	Grams
GC-MS	Gas chromatography – mass spectrometry
h	hours
HBC	Hexa- <i>peri</i> -hexabenzocoronene
HHTP	2,3,6,7,10,11-hexahydroxytriphenylene
HOPG	Highly oriented pyrolytic graphite
HPB	Hexaphenylbenzene
HMBC	Heteronuclear multiple bond correlation spectroscopy
HPLC	High-performance liquid chromatography
HR-TEM	High-resolution transmission electron microscopy
HSQC	Heteronuclear single quantum correlation spectroscopy
Hz	Hertz
IMMS	Ion mobility mass spectrometry
IMS	Ion mobility spectrometry
<i>i</i> -Pr	Isopropyl
IUPAC	International Union of Pure and Applied Chemistry
K	Kelvin

KOPh	Potassium phenoxide
LB	Langmuir-Blodgett
m	Multiplet
M	Molar
MALDI	Matrix-Assisted Laser Desorption/Ionization
m/z	mass per charge
MD	Molecular dynamics
Me	Methyl
ME	Molecular electronics
MeOH	Methanol
MHz	Megahertz
MIMs	Mechanically interlocked molecules
MOF	Metal-organic framework
m.p.	Melting point
MS	Mass spectrometry
NL-DFT	Non-linear density functional theory
NMP	<i>N</i> -methyl-2-pyrrolidone
NMR	Nuclear magnetic resonance
NP	Nanoparticle
OFET	Organic field-effect transistor
OPV	Organic photovoltaic
OTf	Trifluoromethanesulfonate (triflate)
PAH	Polycyclic aromatic hydrocarbon
Pd	Palladium
PE	4-(phenylethynyl)-1,1'-biphenyl
Ph	Phenyl
PIFA	Phenyliodine bis(trifluoroacetate)
PMA	Phosphomolybdic acid stain
POM	Polarized optical microscopy
PPh ₃	Triphenylphosphine
ppm	Parts per million
PSD	Pore size distribution
PSM	Post-synthetic modification
PSS	Photostationary state
PXRD	Powder X-ray diffraction
q	Quartet
RT	Room temperature

s	Singlet
SAM	Self – assembled monolayer
S _E	Electrophilic substitution
SEC	Size exclusion chromatography
S _N	Nucleophilic substitution
SOCl ₂	Thionyl chloride
S-Phos	2-Dicyclohexylphosphino-2',6'-dimethoxybiphenyl
STM	Scanning Tunneling Microscopy
t	Triplet
T	Temperature
TBPM	Tetra(4-dihydroxyboronylphenyl)methane
TBPS	Tetra(4-dihydroxyboronylphenyl)silane
TCNQ	7,7,8,8-tetracyanoquinodimethane
TD-DFT	Time-dependent density functional theory
TEM	Transmission electron microscopy
<i>tert</i> -Bu	<i>tert</i> -Butyl
<i>tert</i> -BuOCl	<i>tert</i> -Butyl hypochlorite
<i>tert</i> -BuOH	<i>tert</i> -Butanol
TFA	Trifluoroacetic acid
TfOH	Trifluoromethanesulfonic acid (triflic acid)
THF	Tetrahydrofuran
TLC	Thin layer chromatography
TM-AFM	Tapping-mode atomic force microscopy
TMA	Benzene 1,3,5-tricarboxylic acid (trimesic acid)
TMS	Trimethylsilyl
TOF	Time of flight
UV/Vis	Ultraviolet/visible absorption spectroscopy
V	Volt
vdW	van der Waals
WAXD	Wide-angle X-ray diffraction

6 References

- [1] J. J. P. Eckert, J. W. Mauchly, *Electronic Numerical Integrator and Computer*, **1964**, US3120606A.
- [2] R. P. Feynman, *Engineering and Science* **1960**, *23*, 22–36.
- [3] S. A. DiBenedetto, A. Facchetti, M. A. Ratner, T. J. Marks, *Advanced Materials* **2009**, *21*, 1407–1433.
- [4] “Molecular Logic Circuits - Balzani - 2003 - ChemPhysChem - Wiley Online Library,” can be found under <https://onlinelibrary.wiley.com/doi/full/10.1002/cphc.200390007>, **n.d.**
- [5] M. F. Budyka, *Russ. Chem. Rev.* **2017**, *86*, 181.
- [6] A. Koçer, M. Walko, W. Meijberg, B. L. Feringa, *Science* **2005**, *309*, 755–758.
- [7] J. M. Mativetsky, G. Pace, M. Elbing, M. A. Rampi, M. Mayor, P. Samorì, *J. Am. Chem. Soc.* **2008**, *130*, 9192–9193.
- [8] K. Hüll, J. Morstein, D. Trauner, *Chem. Rev.* **2018**, DOI 10.1021/acs.chemrev.8b00037.
- [9] N. Katsonis, M. Lubomska, M. M. Pollard, B. L. Feringa, P. Rudolf, *Progress in Surface Science* **2007**, *82*, 407–434.
- [10] M. Alemani, M. V. Peters, S. Hecht, K.-H. Rieder, F. Moresco, L. Grill, *J. Am. Chem. Soc.* **2006**, *128*, 14446–14447.
- [11] I. Aprahamian, *Chem. Commun.* **2017**, *53*, 6674–6684.
- [12] “Mechanisms of Opsin Activation,” can be found under <http://www.jbc.org/content/271/34/20621.abstract>, **n.d.**
- [13] W. R. Browne, B. L. Feringa, *Annual Review of Physical Chemistry* **2009**, *60*, 407–428.
- [14] M. Halik, A. Hirsch, *Advanced Materials* **2011**, *23*, 2689–2695.
- [15] R. Klajn, *Pure and Applied Chemistry* **2010**, *82*, 2247–2279.
- [16] K. Morgenstern, *Progress in Surface Science* **2011**, *86*, 115–161.
- [17] N. Fuentes, A. Martín-Lasanta, L. Á. de Cienfuegos, M. Ribagorda, A. Parra, J. M. Cuerva, *Nanoscale* **2011**, *3*, 4003–4014.
- [18] A. Operamolla, G. M. Farinola, *European Journal of Organic Chemistry* **2011**, *2011*, 423–450.
- [19] W. Wu, Y. Liu, D. Zhu, *Chem. Soc. Rev.* **2010**, *39*, 1489–1502.
- [20] F. Moresco, G. Meyer, K.-H. Rieder, H. Tang, A. Gourdon, C. Joachim, *Phys. Rev. Lett.* **2001**, *86*, 672–675.
- [21] B. J. Coe, S. Houbrechts, I. Asselberghs, A. Persoons, *Angewandte Chemie International Edition* **1999**, *38*, 366–369.
- [22] M. Albrecht, G. van Koten, *Angewandte Chemie International Edition* **2001**, *40*, 3750–3781.
- [23] D. J. Cram, J. M. Cram, *Science* **1974**, *183*, 803–809.
- [24] J.-P. Desvergne, H. Bouas-Laurent, *J. Chem. Soc., Chem. Commun.* **1978**, *0*, 403–404.
- [25] S. Shinkai, T. Nakaji, Y. Nishida, T. Ogawa, O. Manabe, *J. Am. Chem. Soc.* **1980**, *102*, 5860–5865.
- [26] Z. Liu, S. K. M. Nalluri, J. F. Stoddart, *Chem. Soc. Rev.* **2017**, *46*, 2459–2478.
- [27] T. Brotin, J.-P. Dutasta, *Chem. Rev.* **2009**, *109*, 88–130.
- [28] G. Crini, *Chem. Rev.* **2014**, *114*, 10940–10975.
- [29] Q.-D. Hu, G.-P. Tang, P. K. Chu, *Acc. Chem. Res.* **2014**, *47*, 2017–2025.
- [30] Y. Wang, N. Ma, Z. Wang, X. Zhang, *Angewandte Chemie International Edition* **2007**, *46*, 2823–2826.
- [31] H. Yan, C. Teh, S. Sreejith, L. Zhu, A. Kwok, W. Fang, X. Ma, K. T. Nguyen, V. Korzh, Y. Zhao, *Angewandte Chemie International Edition* **2012**, *51*, 8373–8377.
- [32] C. Gropp, B. L. Quigley, F. Diederich, *J. Am. Chem. Soc.* **2018**, *140*, 2705–2717.
- [33] A. R. Pease, J. O. Jeppesen, J. F. Stoddart, Y. Luo, C. P. Collier, J. R. Heath, *Acc. Chem. Res.* **2001**, *34*, 433–444.
- [34] R. A. Bissell, E. Córdova, A. E. Kaifer, J. F. Stoddart, *Nature* **1994**, *369*, 133–137.

- [35] L. Zhang, D. P. August, J. Zhong, G. F. S. Whitehead, I. J. Vitorica-Yrezabal, D. A. Leigh, *J. Am. Chem. Soc.* **2018**, *140*, 4982–4985.
- [36] L. Zhang, A. J. Stephens, A. L. Nussbaumer, J.-F. Lemonnier, P. Jurček, I. J. Vitorica-Yrezabal, D. A. Leigh, *Nature Chemistry* **2018**, *10*, 1083.
- [37] L. Jiang, J. Okano, A. Orita, J. Otera, *Angewandte Chemie International Edition* **2004**, *43*, 2121–2124.
- [38] H. Murakami, A. Kawabuchi, R. Matsumoto, T. Ido, N. Nakashima, *J. Am. Chem. Soc.* **2005**, *127*, 15891–15899.
- [39] Y. Aeschi, S. Drayss-Orth, M. Valášek, F. Raps, D. Häussinger, M. Mayor, *European Journal of Organic Chemistry* **2017**, *2017*, 4091–4103.
- [40] C. Dugave, L. Demange, *Chem. Rev.* **2003**, *103*, 2475–2532.
- [41] Hirshberg, *Compt. Rend. Acad. Sci.* **1950**, *231*, 903.
- [42] B. L. Feringa, “The Art of Building Small: From Molecular Switches to Molecular Motors,” DOI 10.1021/jo070394d can be found under <https://pubs.acs.org/doi/full/10.1021/jo070394d>, **2007**.
- [43] C. Petermayer, H. Dube, *Accounts of Chemical Research* **2018**, DOI 10.1021/acs.accounts.7b00638.
- [44] M. Irie, *Pure and Applied Chemistry* **2015**, *87*, 617–626.
- [45] Y. Yokoyama*, “Fulgides for Memories and Switches,” DOI 10.1021/cr980070c can be found under <https://pubs.acs.org/doi/abs/10.1021/cr980070c>, **2000**.
- [46] A. Perrier, F. Maurel, D. Jacquemin, “Single Molecule Multiphotochromism with Diarylethenes,” DOI 10.1021/ar200214k can be found under <https://pubs.acs.org/doi/abs/10.1021/ar200214k>, **2012**.
- [47] M. Natali, S. Giordani, *Chem. Soc. Rev.* **2012**, *41*, 4010–4029.
- [48] D. H. Waldeck, *Chem. Rev.* **1991**, *91*, 415–436.
- [49] B. S. Lukyanov, M. B. Lukyanova, *Chem Heterocycl Compd* **2005**, *41*, 281–311.
- [50] Fischer, E., *J. Chem. Soc.* **1952**, 4522–4524.
- [51] R. Rosario, D. Gust, M. Hayes, F. Jahnke, J. Springer, A. A. Garcia, *Langmuir* **2002**, *18*, 8062–8069.
- [52] K. Matsuda, M. Irie, *Journal of Photochemistry and Photobiology C: Photochemistry Reviews* **2004**, *5*, 169–182.
- [53] R. Klajn, *Chem. Soc. Rev.* **2013**, *43*, 148–184.
- [54] M. Irie, *Chem. Rev.* **2000**, *100*, 1685–1716.
- [55] S. Nakamura, M. Irie, *J. Org. Chem.* **1988**, *53*, 6136–6138.
- [56] M. Irie, M. Mohri, *J. Org. Chem.* **1988**, *53*, 803–808.
- [57] Mitscherlich, *Annalen der Pharmacie* **1834**, *12*, 311–314.
- [58] A. A. Beharry, G. A. Woolley, *Chem. Soc. Rev.* **2011**, *40*, 4422–4437.
- [59] M. Banghart, K. Borges, E. Isacoff, D. Trauner, R. H. Kramer, *Nature Neuroscience* **2004**, *7*, 1381–1386.
- [60] A. Mourot, M. A. Kienzler, M. R. Banghart, T. Fehrentz, F. M. E. Huber, M. Stein, R. H. Kramer, D. Trauner, *ACS Chem. Neurosci.* **2011**, *2*, 536–543.
- [61] M. V. Westphal, M. A. Schafroth, R. C. Sarott, M. A. Imhof, C. P. Bold, P. Leippe, A. Dhopeswarkar, J. M. Grandner, V. Katritch, K. Mackie, et al., *J. Am. Chem. Soc.* **2017**, *139*, 18206–18212.
- [62] O. Kulikovska, L. M. Goldenberg, J. Stumpe, *Chem. Mater.* **2007**, *19*, 3343–3348.
- [63] A. Archut, F. Vögtle, L. D. Cola, G. C. Azzellini, V. Balzani, P. S. Ramanujam, R. H. Berg, *Chemistry – A European Journal* **1998**, *4*, 699–706.
- [64] A. Natansohn, P. Rochon, J. Gosselin, S. Xie, *Macromolecules* **1992**, *25*, 2268–2273.
- [65] D. Wang, X. Wang, *Progress in Polymer Science* **2013**, *38*, 271–301.
- [66] E. Léonard, F. Mangin, C. Villette, M. Billamboz, C. Len, *Catal. Sci. Technol.* **2016**, *6*, 379–398.
- [67] K. Ichimura, *Chem. Rev.* **2000**, *100*, 1847–1874.

- [68] M. Müri, K. C. Schuermann, L. D. Cola, M. Mayor, *European Journal of Organic Chemistry* **2009**, 2009, 2562–2575.
- [69] G. S. Hartley, *Nature* **1937**, 140, 281.
- [70] E. Wagner-Wysiecka, N. Łukasik, J. F. Biernat, E. Luboch, *J Incl Phenom Macrocycl Chem* **2018**, 90, 189–257.
- [71] R. Turanský, M. Konôpka, N. L. Doltsinis, I. Štich, D. Marx, *Phys. Chem. Chem. Phys.* **2010**, 12, 13922–13932.
- [72] J. Henzl, M. Mehlhorn, H. Gawronski, K.-H. Rieder, K. Morgenstern, *Angewandte Chemie International Edition* **2006**, 45, 603–606.
- [73] T. Cusati, G. Granucci, M. Persico, G. Spighi, *J. Chem. Phys.* **2008**, 128, 194312.
- [74] H. M. Dhammika Bandara, S. C. Burdette, *Chemical Society Reviews* **2012**, 41, 1809–1825.
- [75] E. Wei-Guang Diao, *J. Phys. Chem. A* **2004**, 108, 950–956.
- [76] T. Schultz, J. Quenneville, B. Levine, A. Toniolo, T. J. Martínez, S. Lochbrunner, M. Schmitt, J. P. Shaffer, M. Z. Zgierski, A. Stolow, *J. Am. Chem. Soc.* **2003**, 125, 8098–8099.
- [77] C. R. Crecca, A. E. Roitberg, *J. Phys. Chem. A* **2006**, 110, 8188–8203.
- [78] C. Ciminelli, G. Granucci, M. Persico, *Chemistry – A European Journal* **2004**, 10, 2327–2341.
- [79] J. García-Amorós, D. Velasco, *Beilstein Journal of Organic Chemistry* **2012**, 8, 1003–1017.
- [80] E. Merino, *Chem. Soc. Rev.* **2011**, 40, 3835–3853.
- [81] F. Hamon, F. Djedaini-Pilard, F. Barbot, C. Len, *Tetrahedron* **2009**, 65, 10105–10123.
- [82] H. Langhals, *Angewandte Chemie International Edition* **2004**, 43, 5291–5292.
- [83] C. A. Hunter, L. D. Sarson, *Tetrahedron Letters* **1996**, 37, 699–702.
- [84] D. R. Reddy, B. G. Maiya, *J. Phys. Chem. A* **2003**, 107, 6326–6333.
- [85] A. Tsuge, T. Moriguchi, S. Mataka, M. Tashiro, *J. Chem. Soc., Perkin Trans. 1* **1993**, 0, 2211–2215.
- [86] J. Y. Kim, G. Kim, C. R. Kim, S. H. Lee, J. H. Lee, J. S. Kim, *J. Org. Chem.* **2003**, 68, 1933–1937.
- [87] C. Mills, *J. Chem. Soc., Trans.* **1895**, 67, 925–933.
- [88] M. H. Davey, V. Y. Lee, R. D. Miller, T. J. Marks, *J. Org. Chem.* **1999**, 64, 4976–4979.
- [89] A. Baeyer, *Berichte der deutschen chemischen Gesellschaft* **1874**, 7, 1638–1640.
- [90] B. G. Gowenlock, G. B. Richter-Addo, *J. Chem. Educ.* **2008**, 85, 1243.
- [91] Piloty, O., *Ber.* **1898**, 31, 452–458.
- [92] B. G. Gowenlock, G. B. Richter-Addo, *Chem. Rev.* **2004**, 104, 3315–3340.
- [93] H. Z. Caro, *Angew. Chem.* **1898**, 11, 845–846.
- [94] B. Priewisch, K. Rück-Braun, *J. Org. Chem.* **2005**, 70, 2350–2352.
- [95] B.-C. Yu, Y. Shirai, J. M. Tour, *Tetrahedron* **2006**, 62, 10303–10310.
- [96] C. Tie, J. C. Gallucci, J. R. Parquette, *J. Am. Chem. Soc.* **2006**, 128, 1162–1171.
- [97] E. Buncel, *Acc. Chem. Res.* **1975**, 8, 132–139.
- [98] E. S. Bacon, D. H. Richardson, *J. Chem. Soc.* **1932**, 0, 884–888.
- [99] H. S. Fry, P. E. Bowman, *J. Am. Chem. Soc.* **1930**, 52, 1531–1536.
- [100] R. F. Nystrom, W. G. Brown, *J. Am. Chem. Soc.* **1948**, 70, 3738–3740.
- [101] R. O. Hutchins, D. W. Lamson, L. Rua, C. Milewski, B. Maryanoff, *J. Org. Chem.* **1971**, 36, 803–806.
- [102] G. A. Olah, K. Dunne, D. P. Kelly, Y. K. Mo, *J. Am. Chem. Soc.* **1972**, 94, 7438–7447.
- [103] D. Combata, P. Concepción, A. Corma, *Journal of Catalysis* **2014**, 311, 339–349.
- [104] G. Richner, J. A. van Bokhoven, Y.-M. Neuhold, M. Makosch, K. Hungerbühler, *Phys. Chem. Chem. Phys.* **2011**, 13, 12463–12471.
- [105] Y.-K. Lim, K.-S. Lee, C.-G. Cho, *Org. Lett.* **2003**, 5, 979–982.
- [106] H.-M. Kang, Y.-K. Lim, I.-J. Shin, H.-Y. Kim, C.-G. Cho, *Org. Lett.* **2006**, 8, 2047–2050.
- [107] L. Wang, Q. Li, *Chem. Soc. Rev.* **2018**, 47, 1044–1097.
- [108] V. Ferri, M. Elbing, G. Pace, M. D. Dickey, M. Zharnikov, P. Samorì, M. Mayor, M. A. Rampi, *Angewandte Chemie International Edition* **2008**, 47, 3407–3409.
- [109] R. E. Dawson, S. F. Lincoln, C. J. Easton, *Chem. Commun.* **2008**, 0, 3980–3982.

- [110] G. Ragazzon, M. Baroncini, S. Silvi, M. Venturi, A. Credi, *Nature Nanotechnology* **2015**, *10*, 70–75.
- [111] W. Szymański, J. M. Beierle, H. A. V. Kistemaker, W. A. Velema, B. L. Feringa, *Chem. Rev.* **2013**, *113*, 6114–6178.
- [112] L. Peng, M. You, C. Wu, D. Han, I. Öçsoy, T. Chen, Z. Chen, W. Tan, *ACS Nano* **2014**, *8*, 2555–2561.
- [113] L. Zhu, H. Yan, C. Y. Ang, K. T. Nguyen, M. Li, Y. Zhao, *Chemistry – A European Journal* **2012**, *18*, 13979–13983.
- [114] H. Zhao, S. Sen, T. Udayabhaskararao, M. Sawczyk, K. Kučanda, D. Manna, P. K. Kundu, J.-W. Lee, P. Král, R. Klajn, *Nature Nanotechnology* **2016**, *11*, 82–88.
- [115] N. Crivillers, E. Orgiu, F. Reinders, M. Mayor, P. Samorì, *Advanced Materials* **2011**, *23*, 1447–1452.
- [116] O. Shekhah, J. Liu, R. A. Fischer, C. Wöll, *Chem. Soc. Rev.* **2011**, *40*, 1081–1106.
- [117] T. Murase, S. Sato, M. Fujita, *Angewandte Chemie International Edition* **2007**, *46*, 5133–5136.
- [118] J. Park, D. Yuan, K. T. Pham, J.-R. Li, A. Yakovenko, H.-C. Zhou, *J. Am. Chem. Soc.* **2012**, *134*, 99–102.
- [119] R. Lyndon, K. Konstas, B. P. Ladewig, P. D. Southon, P. C. J. Kepert, M. R. Hill, *Angewandte Chemie International Edition* **2013**, *52*, 3695–3698.
- [120] D. J. Gundlach, J. E. Royer, S. K. Park, S. Subramanian, O. D. Jurchescu, B. H. Hamadani, A. J. Moad, R. J. Kline, L. C. Teague, O. Kirillov, et al., *Nature Materials* **2008**, *7*, 216–221.
- [121] J. E. Anthony, *Angewandte Chemie International Edition* **2008**, *47*, 452–483.
- [122] J. Wu, W. Pisula, K. Müllen, *Chem. Rev.* **2007**, *107*, 718–747.
- [123] S. Rondeau-Gagné, J.-F. Morin, *Chem. Soc. Rev.* **2013**, *43*, 85–98.
- [124] S. H. Goh, R. G. Harvey, *J. Am. Chem. Soc.* **1973**, *95*, 242–243.
- [125] R. G. Harvey, J.-T. Zhang, E. Luna, J. Pataki, *J. Org. Chem.* **1998**, *63*, 6405–6408.
- [126] M. D. Watson, A. Fechtenkötter, K. Müllen, *Chem. Rev.* **2001**, *101*, 1267–1300.
- [127] J. E. Anthony, *Chem. Rev.* **2006**, *106*, 5028–5048.
- [128] G. R. Desiraju, A. Gavezzotti, *J. Chem. Soc., Chem. Commun.* **1989**, *0*, 621–623.
- [129] M. Kastler, W. Pisula, D. Wasserfallen, T. Pakula, K. Müllen, *J. Am. Chem. Soc.* **2005**, *127*, 4286–4296.
- [130] W. Pisula, Ž. Tomović, C. Simpson, M. Kastler, T. Pakula, K. Müllen, *Chem. Mater.* **2005**, *17*, 4296–4303.
- [131] I. Fischbach, T. Pakula, P. Minkin, A. Fechtenkötter, K. Müllen, H. W. Spiess, K. Saalwächter, *J. Phys. Chem. B* **2002**, *106*, 6408–6418.
- [132] D. Wasserfallen, I. Fischbach, N. Chebotareva, M. Kastler, W. Pisula, F. Jäckel, M. D. Watson, I. Schnell, J. P. Rabe, H. W. Spiess, et al., *Advanced Functional Materials* **2005**, *15*, 1585–1594.
- [133] L. Brunsveld, B. J. B. Folmer, E. W. Meijer, R. P. Sijbesma, *Chem. Rev.* **2001**, *101*, 4071–4098.
- [134] W. Pisula, Ž. Tomović, B. El Hamaoui, M. D. Watson, T. Pakula, K. Müllen, *Advanced Functional Materials* **2005**, *15*, 893–904.
- [135] M. Lee, J.-W. Kim, S. Peleshanko, K. Larson, Y.-S. Yoo, D. Vaknin, S. Markutsya, V. V. Tsukruk, *J. Am. Chem. Soc.* **2002**, *124*, 9121–9128.
- [136] W. Pisula, A. Menon, M. Stepputat, I. Lieberwirth, U. Kolb, A. Tracz, H. Sirringhaus, T. Pakula, K. Müllen, *Advanced Materials* **2005**, *17*, 684–689.
- [137] A. Tracz, J. K. Jeszka, M. D. Watson, W. Pisula, K. Müllen, T. Pakula, *J. Am. Chem. Soc.* **2003**, *125*, 1682–1683.
- [138] D. W. Breiby, O. Bunk, W. Pisula, T. I. Sølling, A. Tracz, T. Pakula, K. Müllen, M. M. Nielsen, *J. Am. Chem. Soc.* **2005**, *127*, 11288–11293.
- [139] E. Clar, C. T. Ironside, *Proc. Chem. Soc.* **1958**, 150.
- [140] H. Seyler, B. Purushothaman, D. J. Jones, A. B. Holmes, W. W. H. Wong, *Pure and Applied Chemistry* **2012**, *84*, 1047–1067.
- [141] A. Stabel, P. Herwig, K. Müllen, J. P. Rabe, *Angewandte Chemie International Edition in English* **1995**, *34*, 1609–1611.

- [142] C. Kübel, K. Eckhardt, V. Enkelmann, G. Wegner, K. Müllen, *J. Mater. Chem.* **2000**, *10*, 879–886.
- [143] K. P. C. Vollhardt, *Angewandte Chemie* **1984**, *96*, 525–541.
- [144] F. Xue, Y. K. Loh, X. Song, W. J. Teo, J. Y. D. Chua, J. Zhao, T. S. A. Hor, *Chemistry – An Asian Journal* **2017**, *12*, 168–173.
- [145] X. Feng, W. Pisula, L. Zhi, M. Takase, K. Müllen, *Angewandte Chemie International Edition* **2008**, *47*, 1703–1706.
- [146] S. Ito, M. Wehmeier, J. D. Brand, C. Kübel, R. Epsch, J. P. Rabe, K. Müllen, *Chemistry – A European Journal* **2000**, *6*, 4327–4342.
- [147] A. Fechtenkötter, N. Tchegbotareva, M. Watson, K. Müllen, *Tetrahedron* **2001**, *57*, 3769–3783.
- [148] A. Suzuki, *Journal of Organometallic Chemistry* **1999**, *576*, 147–168.
- [149] N. Miyaoura, K. Yamada, A. Suzuki, *Tetrahedron Letters* **1979**, *20*, 3437–3440.
- [150] N. Miyaoura, A. Suzuki, *J. Chem. Soc., Chem. Commun.* **1979**, *0*, 866–867.
- [151] J. Wu, M. Baumgarten, M. G. Debije, J. M. Warman, K. Müllen, *Angewandte Chemie International Edition* **2004**, *43*, 5331–5335.
- [152] R. Scholl, J. Mansfeld, *Berichte der deutschen chemischen Gesellschaft* **1910**, *43*, 1734–1746.
- [153] M. Grzybowski, K. Skonieczny, H. Butenschön, D. T. Gryko, *Angewandte Chemie International Edition* **2013**, *52*, 9900–9930.
- [154] C. Li, Y. Yang, Q. Miao, *Chemistry – An Asian Journal* **2018**, *13*, 884–894.
- [155] C. D. Simpson, J. D. Brand, A. J. Berresheim, L. Przybilla, H. J. Räder, K. Müllen, *Chemistry – A European Journal* **2002**, *8*, 1424–1429.
- [156] C. Nacci, A. Viertel, S. Hecht, L. Grill, *Angewandte Chemie International Edition* **2016**, *55*, 13724–13728.
- [157] T. Fujikawa, Y. Segawa, K. Itami, *J. Am. Chem. Soc.* **2016**, *138*, 3587–3595.
- [158] P. Rempala, J. Kroulík, B. T. King, *J. Org. Chem.* **2006**, *71*, 5067–5081.
- [159] L. Zhai, R. Shukla, R. Rathore, *Org. Lett.* **2009**, *11*, 3474–3477.
- [160] G. M. Paternò, Q. Chen, X.-Y. Wang, J. Liu, S. G. Motti, A. Petrozza, X. Feng, G. Lanzani, K. Müllen, A. Narita, et al., *Angewandte Chemie International Edition* **2017**, *56*, 6753–6757.
- [161] L. Zhai, R. Shukla, S. H. Wadumethrige, R. Rathore, *J. Org. Chem.* **2010**, *75*, 4748–4760.
- [162] Z. Zeng, Z. Guan, Q.-H. Xu, J. Wu, *Chemistry – A European Journal* **2011**, *17*, 3837–3841.
- [163] G. A. Clowes, *J. Chem. Soc. C* **1968**, *0*, 2519–2526.
- [164] M. Di Stefano, F. Negri, P. Carbone, K. Müllen, *Chemical Physics* **2005**, *314*, 85–99.
- [165] P. Rempala, J. Kroulík, B. T. King, *J. Am. Chem. Soc.* **2004**, *126*, 15002–15003.
- [166] M. Keil, P. Samorí, D. A. dos Santos, J. Birgerson, R. Friedlein, A. Dkhissi, M. Watson, K. Müllen, J. L. Brédas, J. P. Rabe, et al., *J. Chem. Phys.* **2002**, *116*, 10854–10860.
- [167] K. Mukai, M. Harada, Y. Kikuzawa, T. Mori, J. Sugiyama, *Electrochem. Solid-State Lett.* **2011**, *14*, A52–A55.
- [168] A. M. van de Craats, J. M. Warman, *Advanced Materials* **2001**, *13*, 130–133.
- [169] I. O. Shklyarevskiy, P. Jonkheijm, N. Stutzmann, D. Wasserberg, H. J. Wondergem, P. C. M. Christianen, A. P. H. J. Schenning, D. M. de Leeuw, Ž. Tomović, J. Wu, et al., *J. Am. Chem. Soc.* **2005**, *127*, 16233–16237.
- [170] L. Schmidt-Mende, A. Fechtenkötter, K. Müllen, E. Moons, R. H. Friend, J. D. MacKenzie, *Science* **2001**, *293*, 1119–1122.
- [171] L. Schmidt-Mende, M. Watson, K. Müllen, R. H. Friend, *Molecular Crystals and Liquid Crystals* **2003**, *396*, 73–90.
- [172] W. W. H. Wong, T. B. Singh, D. Vak, W. Pisula, C. Yan, X. Feng, E. L. Williams, K. L. Chan, Q. Mao, D. J. Jones, et al., *Advanced Functional Materials* **2010**, *20*, 927–938.
- [173] J. L. C. Rowsell, O. M. Yaghi, *Microporous and Mesoporous Materials* **2004**, *73*, 3–14.
- [174] X. Feng, X. Ding, D. Jiang, *Chem. Soc. Rev.* **2012**, *41*, 6010–6022.
- [175] C. Tan, X. Cao, X.-J. Wu, Q. He, J. Yang, X. Zhang, J. Chen, W. Zhao, S. Han, G.-H. Nam, et al., *Chem. Rev.* **2017**, *117*, 6225–6331.
- [176] H. Zhang, *ACS Nano* **2015**, *9*, 9451–9469.

- [177] K. S. Novoselov, D. Jiang, F. Schedin, T. J. Booth, V. V. Khotkevich, S. V. Morozov, A. K. Geim, T. M. Rice, *Proceedings of the National Academy of Sciences of the United States of America* **2005**, *102*, 10451–10453.
- [178] F. Xia, H. Wang, D. Xiao, M. Dubey, A. Ramasubramaniam, *Nature Photonics* **2014**, *8*, 899–907.
- [179] G. Fiori, F. Bonaccorso, G. Iannaccone, T. Palacios, D. Neumaier, A. Seabaugh, S. K. Banerjee, L. Colombo, *Nature Nanotechnology* **2014**, *9*, 768–779.
- [180] M. Gobbi, E. Orgiu, P. Samorì, *Advanced Materials* **2018**, *30*, 1706103.
- [181] F. Yang, S. Cheng, X. Zhang, X. Ren, R. Li, H. Dong, W. Hu, *Advanced Materials* **2018**, *30*, 1702415.
- [182] B. H. Hamadani, D. A. Corley, J. W. Ciszek, J. M. Tour, D. Natelson, *Nano Lett.* **2006**, *6*, 1303–1306.
- [183] A. S. Aricò, P. Bruce, B. Scrosati, J.-M. Tarascon, W. van Schalkwijk, *Nature Materials* **2005**, *4*, 366–377.
- [184] R. M. Metzger, *J. Mater. Chem.* **2008**, *18*, 4364–4396.
- [185] D. Bonifazi, S. Mohnani, A. Llanes-Pallas, *Chemistry – A European Journal* **2009**, *15*, 7004–7025.
- [186] K. Ariga, M. V. Lee, T. Mori, X.-Y. Yu, J. P. Hill, *Advances in Colloid and Interface Science* **2010**, *154*, 20–29.
- [187] J. D. van der Waals, **1910**.
- [188] J. P. Rabe, S. Buchholz, *Science* **1991**, *253*, 424–427.
- [189] J. Adisoejoso, K. Tahara, S. Okuhata, S. Lei, Y. Tobe, S. De Feyter, *Angewandte Chemie International Edition* **2009**, *48*, 7353–7357.
- [190] S. Grabowski, Ed., *Hydrogen Bonding - New Insights*, Springer Netherlands, **2006**.
- [191] G. A. Jeffrey, *An Introduction to Hydrogen Bonding*, Oxford University Press, **1997**.
- [192] C.-A. Palma, J. Bjork, M. Bonini, M. S. Dyer, A. Llanes-Pallas, D. Bonifazi, M. Persson, P. Samorì, *J. Am. Chem. Soc.* **2009**, *131*, 13062–13071.
- [193] O. Lukin, J. Leszczynski, *J. Phys. Chem. A* **2002**, *106*, 6775–6782.
- [194] D. C. Sherrington, K. A. Taskinen, *Chem. Soc. Rev.* **2001**, *30*, 83–93.
- [195] T. F. A. de Greef, E. W. Meijer, *Nature* **2008**, *453*, 171–173.
- [196] A. Ciesielski, M. El Garah, S. Masiero, P. Samorì, *Small* **2016**, *12*, 83–95.
- [197] M. Lackinger, W. M. Heckl, *Langmuir* **2009**, *25*, 11307–11321.
- [198] S. Griessl, M. Lackinger, M. Edelwirth, M. Hietschold, W. M. Heckl, *Single Molecules* **2002**, *3*, 25–31.
- [199] B. Moulton, M. J. Zaworotko, *Chem. Rev.* **2001**, *101*, 1629–1658.
- [200] S. Kitagawa, R. Kitaura, S. Noro, *Angewandte Chemie International Edition* **2004**, *43*, 2334–2375.
- [201] M. M. S. Abdel-Mottaleb, N. Schuurmans, S. D. Feyter, J. V. Esch, B. L. Feringa, F. C. D. Schryver, *Chem. Commun.* **2002**, *0*, 1894–1895.
- [202] S. M. Cohen, *Chem. Rev.* **2012**, *112*, 970–1000.
- [203] J. D. Evans, C. J. Sumby, C. J. Doonan, *Chem. Soc. Rev.* **2014**, *43*, 5933–5951.
- [204] P. Deria, J. E. Mondloch, O. Karagiari, W. Bury, J. T. Hupp, O. K. Farha, *Chem. Soc. Rev.* **2014**, *43*, 5896–5912.
- [205] M. Kondo, T. Yoshitomi, H. Matsuzaka, S. Kitagawa, K. Seki, *Angewandte Chemie International Edition in English* **1997**, *36*, 1725–1727.
- [206] H. Li, M. Eddaoudi, M. O’Keeffe, O. M. Yaghi, *Nature* **1999**, *402*, 276–279.
- [207] S. S.-Y. Chui, S. M.-F. Lo, J. P. H. Charmant, A. G. Orpen, I. D. Williams, *Science* **1999**, *283*, 1148–1150.
- [208] K. M. L. Taylor-Pashow, J. D. Rocca, R. C. Huxford, W. Lin, *Chem. Commun.* **2010**, *46*, 5832–5849.
- [209] A. K. Mandal, J. Mahmood, J.-B. Baek, *ChemNanoMat* **2017**, *3*, 373–391.
- [210] X. Zhan, Z. Chen, Q. Zhang, *J. Mater. Chem. A* **2017**, *5*, 14463–14479.
- [211] S. Kandambeth, K. Dey, R. Banerjee, *J. Am. Chem. Soc.* **2018**, DOI 10.1021/jacs.8b10334.

- [212] H. Furukawa, O. M. Yaghi, *J. Am. Chem. Soc.* **2009**, *131*, 8875–8883.
- [213] S.-Y. Ding, J. Gao, Q. Wang, Y. Zhang, W.-G. Song, C.-Y. Su, W. Wang, *J. Am. Chem. Soc.* **2011**, *133*, 19816–19822.
- [214] S. Wan, J. Guo, J. Kim, H. Ihee, D. Jiang, *Angewandte Chemie International Edition* **2008**, *47*, 8826–8830.
- [215] S. Wan, J. Guo, J. Kim, H. Ihee, D. Jiang, *Angewandte Chemie International Edition* **2009**, *48*, 5439–5442.
- [216] A. P. Côté, A. I. Benin, N. W. Ockwig, M. O’Keeffe, A. J. Matzger, O. M. Yaghi, *Science* **2005**, *310*, 1166–1170.
- [217] S. J. Rowan, S. J. Cantrill, G. R. L. Cousins, J. K. M. Sanders, J. F. Stoddart, *Angewandte Chemie International Edition* **2002**, *41*, 898–952.
- [218] Y. Jin, Q. Wang, P. Taynton, W. Zhang, *Acc. Chem. Res.* **2014**, *47*, 1575–1586.
- [219] S.-Y. Ding, W. Wang, *Chem. Soc. Rev.* **2012**, *42*, 548–568.
- [220] X. Feng, L. Chen, Y. Honsho, O. Saengsawang, L. Liu, L. Wang, A. Saeki, S. Irle, S. Seki, Y. Dong, et al., *Advanced Materials* **2012**, *24*, 3026–3031.
- [221] X. Chen, M. Addicoat, S. Irle, A. Nagai, D. Jiang, *J. Am. Chem. Soc.* **2013**, *135*, 546–549.
- [222] H. M. El-Kaderi, J. R. Hunt, J. L. Mendoza-Cortés, A. P. Côté, R. E. Taylor, M. O’Keeffe, O. M. Yaghi, *Science* **2007**, *316*, 268–272.
- [223] D. Beaudoin, T. Maris, J. D. Wuest, *Nature Chemistry* **2013**, *5*, 830–834.
- [224] M. J. Kory, M. Wörle, T. Weber, P. Payamyar, S. W. van de Poll, J. Dshemuchadse, N. Trapp, A. D. Schlüter, *Nature Chemistry* **2014**, *6*, 779–784.
- [225] S. S. Han, H. Furukawa, O. M. Yaghi, W. A. Goddard, *J. Am. Chem. Soc.* **2008**, *130*, 11580–11581.
- [226] F. J. Uribe-Romo, J. R. Hunt, H. Furukawa, C. Klöck, M. O’Keeffe, O. M. Yaghi, *J. Am. Chem. Soc.* **2009**, *131*, 4570–4571.
- [227] E. Jin, M. Asada, Q. Xu, S. Dalapati, M. A. Addicoat, M. A. Brady, H. Xu, T. Nakamura, T. Heine, Q. Chen, et al., *Science* **2017**, *357*, 673–676.
- [228] Q. Fang, J. Wang, S. Gu, R. B. Kaspar, Z. Zhuang, J. Zheng, H. Guo, S. Qiu, Y. Yan, *J. Am. Chem. Soc.* **2015**, *137*, 8352–8355.
- [229] Y. Du, H. Yang, J. M. Whiteley, S. Wan, Y. Jin, S.-H. Lee, W. Zhang, *Angewandte Chemie International Edition* **2016**, *55*, 1737–1741.
- [230] M. R. Rao, Y. Fang, S. De Feyter, D. F. Perepichka, *J. Am. Chem. Soc.* **2017**, *139*, 2421–2427.
- [231] J. Guo, Y. Xu, S. Jin, L. Chen, T. Kaji, Y. Honsho, M. A. Addicoat, J. Kim, A. Saeki, H. Ihee, et al., *Nature Communications* **2013**, *4*, 2736.
- [232] P. Kuhn, M. Antonietti, A. Thomas, *Angewandte Chemie International Edition* **2008**, *47*, 3450–3453.
- [233] K. T. Jackson, T. E. Reich, H. M. El-Kaderi, *Chem. Commun.* **2012**, *48*, 8823–8825.
- [234] A. Nagai, X. Chen, X. Feng, X. Ding, Z. Guo, D. Jiang, *Angewandte Chemie International Edition* **2013**, *52*, 3770–3774.
- [235] P.-F. Wei, M.-Z. Qi, Z.-P. Wang, S.-Y. Ding, W. Yu, Q. Liu, L.-K. Wang, H.-Z. Wang, W.-K. An, W. Wang, *J. Am. Chem. Soc.* **2018**, *140*, 4623–4631.
- [236] A. Galanti, V. Diez-Cabanes, J. Santoro, M. Valášek, A. Minoia, M. Mayor, J. Cornil, P. Samorì, *J. Am. Chem. Soc.* **2018**, DOI 10.1021/jacs.8b06324.
- [237] A. Galanti, J. Santoro, R. Mannancherry, Q. Duez, V. Diez-Cabanes, M. Valášek, J. De Winter, J. Cornil, P. Gerbaux, M. Mayor, et al., *J. Am. Chem. Soc.* **2019**, *141*, 9273–9283.
- [238] D. Bléger, Z. Yu, S. Hecht, *Chem. Commun.* **2011**, *47*, 12260–12266.
- [239] D. Bléger, T. Liebig, R. Thiermann, M. Maskos, J. P. Rabe, S. Hecht, *Angewandte Chemie International Edition* **2011**, *50*, 12559–12563.
- [240] F. Cisnetti, R. Ballardini, A. Credi, M. T. Gandolfi, S. Masiero, F. Negri, S. Pieraccini, G. P. Spada, *Chemistry – A European Journal* **2004**, *10*, 2011–2021.
- [241] D. Bléger, J. Dokić, M. V. Peters, L. Grubert, P. Saalfrank, S. Hecht, *J. Phys. Chem. B* **2011**, *115*, 9930–9940.

- [242] S. Lee, S. Oh, J. Lee, Y. Malpani, Y.-S. Jung, B. Kang, J. Y. Lee, K. Ozasa, T. Isoshima, S. Y. Lee, et al., *Langmuir* **2013**, *29*, 5869–5877.
- [243] J. Kind, L. Kaltschnee, M. Leyendecker, C. M. Thiele, *Chem. Commun.* **2016**, *52*, 12506–12509.
- [244] M. Koch, M. Saphiannikova, S. Santer, O. Guskova, *J. Phys. Chem. B* **2017**, *121*, 8854–8867.
- [245] J. Bahrenburg, C. M. Sievers, J. B. Schönborn, B. Hartke, F. Renth, F. Temps, C. Näther, F. D. Sönnichsen, *Photochem. Photobiol. Sci.* **2013**, *12*, 511–518.
- [246] M. Lackinger, S. Griessl, W. M. Heckl, M. Hietschold, G. W. Flynn, *Langmuir* **2005**, *21*, 4984–4988.
- [247] M. Ruben, D. Payer, A. Landa, A. Comisso, C. Gattinoni, N. Lin, J.-P. Collin, J.-P. Sauvage, A. De Vita, K. Kern, *J. Am. Chem. Soc.* **2006**, *128*, 15644–15651.
- [248] J. F. Dienstmaier, K. Mahata, H. Walch, W. M. Heckl, M. Schmittl, M. Lackinger, *Langmuir* **2010**, *26*, 10708–10716.
- [249] T. C. Wang, W. Bury, D. A. Gómez-Gualdrón, N. A. Vermeulen, J. E. Mondloch, P. Deria, K. Zhang, P. Z. Moghadam, A. A. Sarjeant, R. Q. Snurr, et al., *J. Am. Chem. Soc.* **2015**, *137*, 3585–3591.
- [250] D. Ma, C. Xia, *Org. Lett.* **2001**, *3*, 2583–2586.
- [251] V. Kandathil, B. D. Fahlman, B. S. Sasidhar, S. A. Patil, S. A. Patil, *New J. Chem.* **2017**, *41*, 9531–9545.
- [252] A. Archut, F. Vögtle, L. D. Cola, G. C. Azzellini, V. Balzani, P. S. Ramanujam, R. H. Berg, *Chemistry – A European Journal* **1998**, *4*, 699–706.
- [253] H. J. Kuhn, S. E. Braslavsky, R. Schmidt, *Pure and Applied Chemistry* **2004**, *76*, 2105–2146.
- [254] G. Gauglitz, S. Hubig, *Journal of Photochemistry* **1985**, *30*, 121–125.
- [255] G. H. Aylward, J. L. Garnett, J. H. Sharp, *Anal. Chem.* **1967**, *39*, 457–460.
- [256] J. L. Sadler, A. J. Bard, *J. Am. Chem. Soc.* **1968**, *90*, 1979–1989.
- [257] S. S. Kurek, B. J. Laskowska, A. Stokłosa, *Electrochimica Acta* **2006**, *51*, 2306–2314.
- [258] K. A. Connors, *Chemical Kinetics : The Study of Reaction Rates in Solution* / VCH, New York ;, **c1990**.
- [259] J. Dokić, M. Gothe, J. Wirth, M. V. Peters, J. Schwarz, S. Hecht, P. Saalfrank, *J. Phys. Chem. A* **2009**, *113*, 6763–6773.
- [260] Á. Révész, D. Schröder, T. A. Rokob, M. Havlík, B. Dolenský, *Angewandte Chemie International Edition* **2011**, *50*, 2401–2404.
- [261] C. L. Feng, Y. Zhang, J. Jin, Y. Song, L. Xie, G. Qu, L. Jiang, D. Zhu, *Surface Science* **2002**, *513*, 111–118.
- [262] D. Bléger, A. Ciesielski, P. Samorì, S. Hecht, *Chemistry – A European Journal* **2010**, *16*, 14256–14260.
- [263] H. Furukawa, N. Ko, Y. B. Go, N. Aratani, S. B. Choi, E. Choi, A. Ö. Yazaydin, R. Q. Snurr, M. O’Keeffe, J. Kim, et al., *Science* **2010**, *329*, 424–428.
- [264] G. Férey, C. Mellot-Draznieks, C. Serre, F. Millange, J. Dutour, S. Surblé, I. Margiolaki, *Science* **2005**, *309*, 2040–2042.
- [265] A. Schaate, P. Roy, A. Godt, J. Lippke, F. Waltz, M. Wiebcke, P. Behrens, *Chemistry – A European Journal* **2011**, *17*, 6643–6651.
- [266] F. Gándara, H. Furukawa, S. Lee, O. M. Yaghi, *J. Am. Chem. Soc.* **2014**, *136*, 5271–5274.
- [267] J. Ren, N. M. Musyoka, H. W. Langmi, T. Segakweng, B. C. North, M. Mathe, X. Kang, *International Journal of Hydrogen Energy* **2014**, *39*, 12018–12023.
- [268] S. Ren, M. J. Bojdys, R. Dawson, A. Laybourn, Y. Z. Khimyak, D. J. Adams, A. I. Cooper, *Advanced Materials* **2012**, *24*, 2357–2361.
- [269] P. Puthiaraj, Y.-R. Lee, S. Zhang, W.-S. Ahn, *J. Mater. Chem. A* **2016**, *4*, 16288–16311.
- [270] M. J. Bojdys, J. Jeromenok, A. Thomas, M. Antonietti, *Advanced Materials* **2010**, *22*, 2202–2205.
- [271] S. Kuecken, J. Schmidt, L. Zhi, A. Thomas, *J. Mater. Chem. A* **2015**, *3*, 24422–24427.
- [272] S. Kuecken, A. Acharjya, L. Zhi, M. Schwarze, R. Schomäcker, A. Thomas, *Chem. Commun.* **2017**, *53*, 5854–5857.

- [273] S. Brunauer, P. H. Emmett, E. Teller, "Adsorption of Gases in Multimolecular Layers," DOI 10.1021/ja01269a023 can be found under <https://pubs.acs.org/doi/abs/10.1021/ja01269a023>, **2002**.
- [274] M. D. Donohue, G. L. Aranovich, *Advances in Colloid and Interface Science* **1998**, 76–77, 137–152.
- [275] G. Pohnert, *Journal für praktische Chemie* **2000**, 342, 731–734.
- [276] J. Wu, A. Fechtenkötter, J. Gauss, M. D. Watson, M. Kastler, C. Fechtenkötter, M. Wagner, K. Müllen, *J. Am. Chem. Soc.* **2004**, 126, 11311–11321.
- [277] L. F. Dössel, V. Kamm, I. A. Howard, F. Laquai, W. Pisula, X. Feng, C. Li, M. Takase, T. Kudernac, S. De Feyter, et al., *J. Am. Chem. Soc.* **2012**, 134, 5876–5886.
- [278] T. E. Barder, S. D. Walker, J. R. Martinelli, S. L. Buchwald, *J. Am. Chem. Soc.* **2005**, 127, 4685–4696.
- [279] R. A. Altman, S. L. Buchwald, *Nature Protocols* **2007**, 2, 3115–3121.
- [280] X. Cheng, A. Ver Heyen, W. Mamdouh, H. Uji-i, F. De Schryver, S. Höger, S. De Feyter, *Langmuir* **2007**, 23, 1281–1286.
- [281] J. Luo, Y. Zhou, Z.-Q. Niu, Q.-F. Zhou, Y. Ma, J. Pei, *J. Am. Chem. Soc.* **2007**, 129, 11314–11315.
- [282] T. M. Kosak, H. A. Conrad, A. L. Korich, R. L. Lord, *European Journal of Organic Chemistry* **2015**, 2015, 7460–7467.
- [283] B. Yang, H. Lin, K. Miao, P. Zhu, L. Liang, K. Sun, H. Zhang, J. Fan, V. Meunier, Y. Li, et al., *Angewandte Chemie International Edition* **2016**, 55, 9881–9885.
- [284] T. Wöhrle, S. J. Beardsworth, C. Schilling, A. Baro, F. Giesselmann, S. Laschat, *Soft Matter* **2016**, 12, 3730–3736.
- [285] T. Y. S. But, P. H. Toy, *Chemistry – An Asian Journal* **2007**, 2, 1340–1355.
- [286] Q. Yao, A. Bermejo Gómez, J. Su, V. Pascanu, Y. Yun, H. Zheng, H. Chen, L. Liu, H. N. Abdelhamid, B. Martín-Matute, et al., *Chem. Mater.* **2015**, 27, 5332–5339.
- [287] E. C. Taylor, G. S. K. Wong, *J. Org. Chem.* **1989**, 54, 3618–3624.
- [288] V. Kandathil, B. D. Fahlman, B. S. Sasidhar, S. A. Patil, S. A. Patil, *New J. Chem.* **2017**, 41, 9531–9545.
- [289] J. Mou, A. Park, Y. Cai, J. Yuan, C. Yuan, *Bioorganic & Medicinal Chemistry Letters* **2015**, 25, 3057–3061.
- [290] N. Wang, W. Chen, W. Shen, L. Duan, M. Qiu, J. Wang, C. Yang, Z. Du, R. Yang, *J. Mater. Chem. A* **2016**, 4, 10212–10222.
- [291] P. Wang, C. Yao, 王鹏, 姚朝阳, *Organic Dye as Well as Preparation Method and Application Thereof*, **2015**, CN104557971 (A).
- [292] D. Zhang, G. Wang, R. Li, X. Li, Y. Xiang, Z. Zhang, W. Jin, *RSC Adv.* **2015**, 5, 99688–99696.
- [293] S. Reimann, P. Ehlers, M. Sharif, A. Spannenberg, P. Langer, *Tetrahedron* **2016**, 72, 1083–1094.
- [294] J. Cao, Y.-M. Liu, X. Jing, J. Yin, J. Li, B. Xu, Y.-Z. Tan, N. Zheng, *J. Am. Chem. Soc.* **2015**, 137, 10914–10917.
- [295] B. Zhu, H. Chen, W. Lin, Y. Ye, J. Wu, S. Li, *J. Am. Chem. Soc.* **2014**, 136, 15126–15129.

7 Appendix

7.1 $Z \rightarrow E$ thermal isomerization studies on star-shaped azobenzene 3, 23 and 27

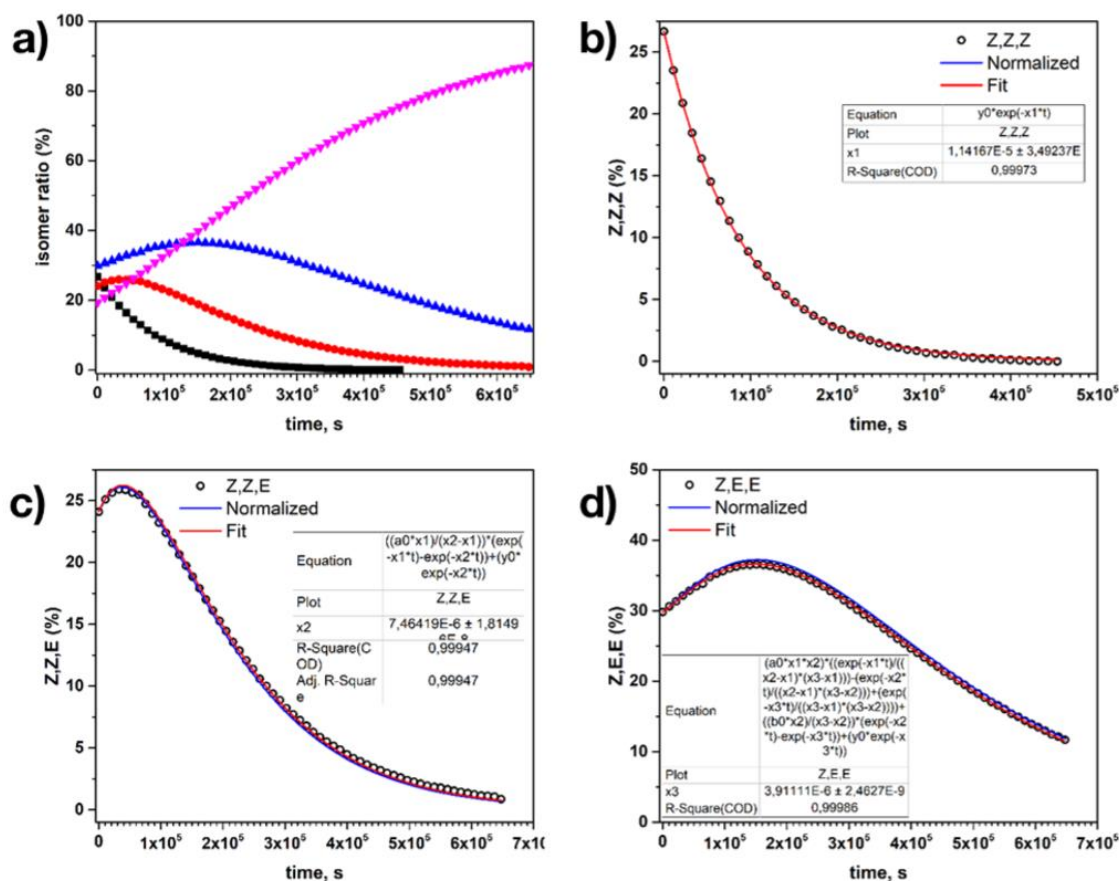


Figure 132. a) Thermal evolution of the isomers ratio of tris(azobenzene)-3: (E,E,E)-3 (pink triangles), (Z,E,E)-3 (blue triangles), (Z,Z,E)-3 (red dots), (Z,Z,Z)-3 (black squares) followed at 25 °C by HPLC. The empty dots show the amount of isomer (Z,Z,Z)-3, c) isomer (Z,Z,E)-3 and d) isomer (Z,E,E)-3 against the heating time. The red line is the fit of the temporal evolution yielding the rate constants k_1 , k_2 and k_3 for each isomer according to equations 2.2 and 2.3.

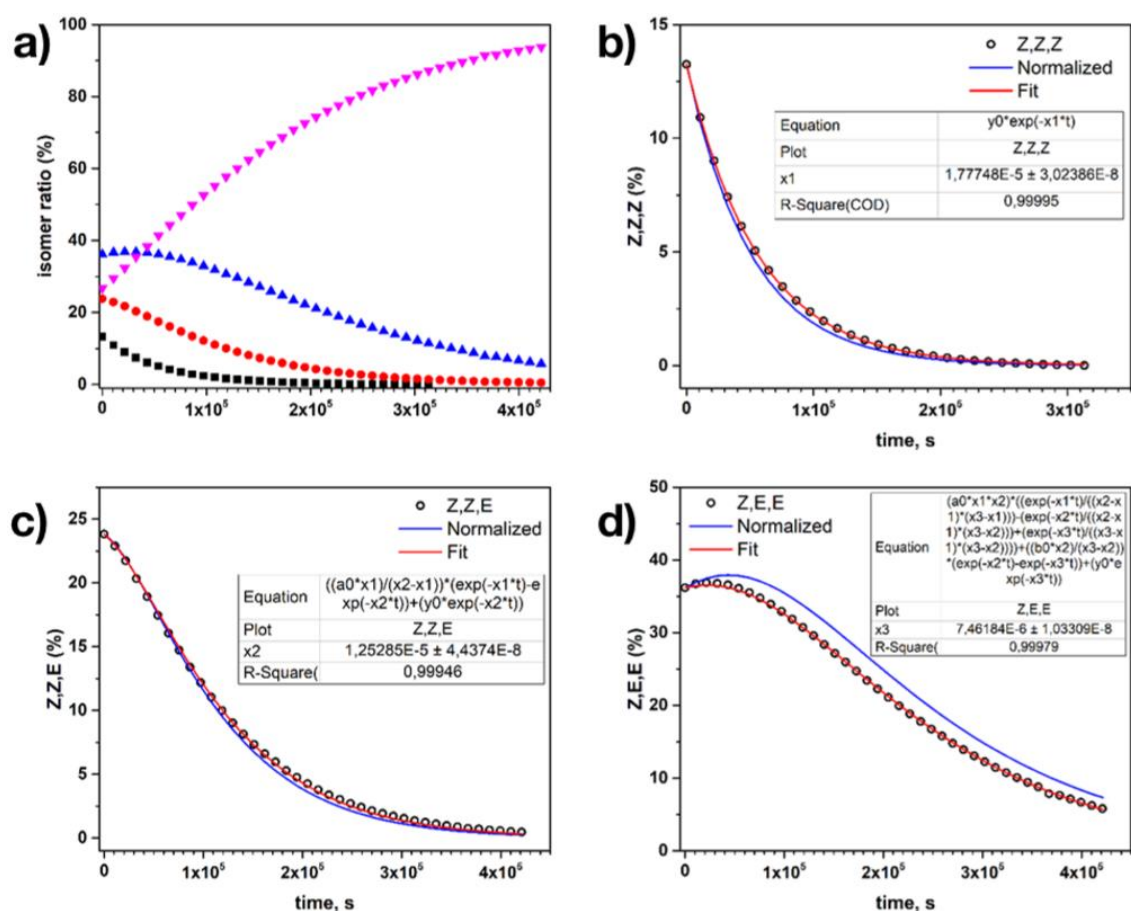
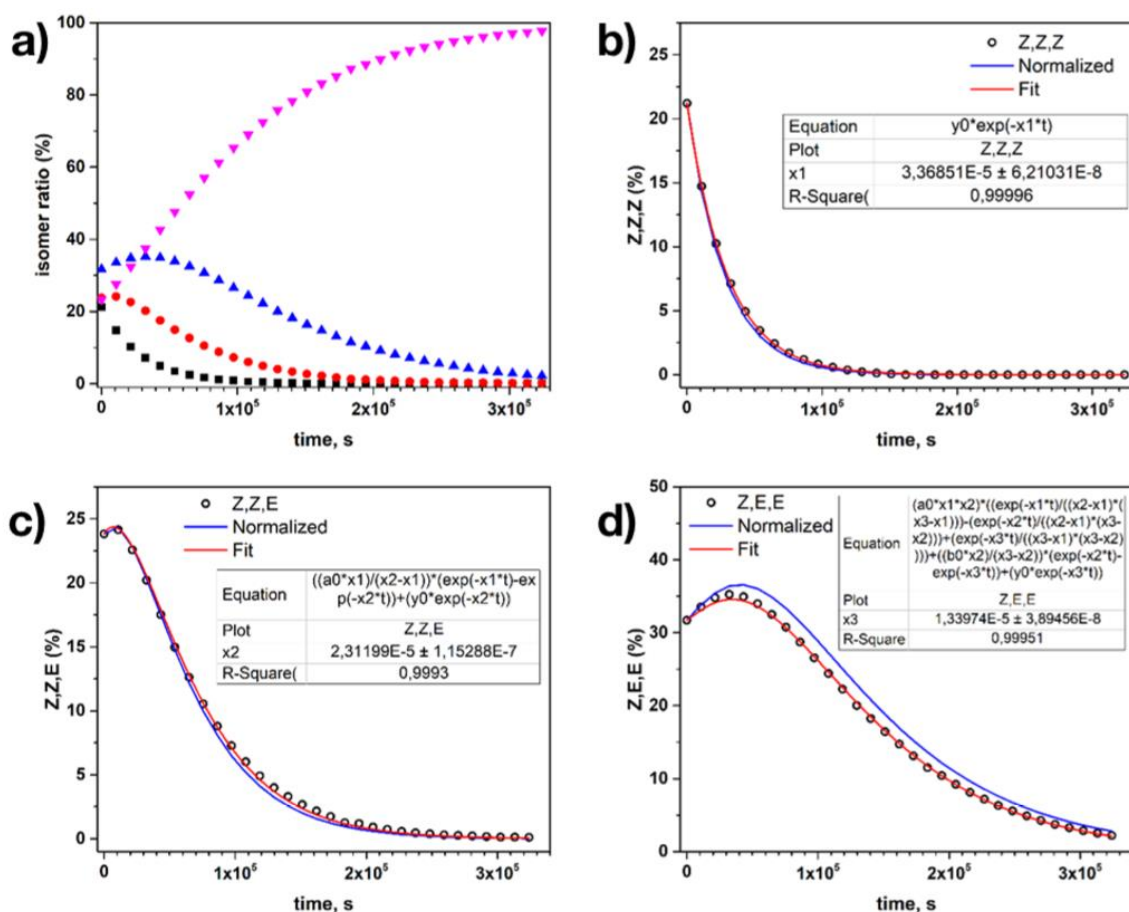


Figure 133. a) Thermal evolution of the isomers ratio of tris(azobenzene)-3: (E,E,E)-3 (pink triangles), (Z,E,E)-3 (blue triangles), (Z,Z,E)-3 (red dots), (Z,Z,Z)-3 (black squares) followed at 30 °C by HPLC. The empty dots show the amount of b) isomer (Z,Z,Z)-3, c) isomer (Z,Z,E)-3 and d) isomer (Z,E,E)-3 against the heating time. The red line is the fit of the temporal evolution yielding the rate constants k_1 , k_2 and k_3 for each isomer according to equations 2.2 and 2.3.



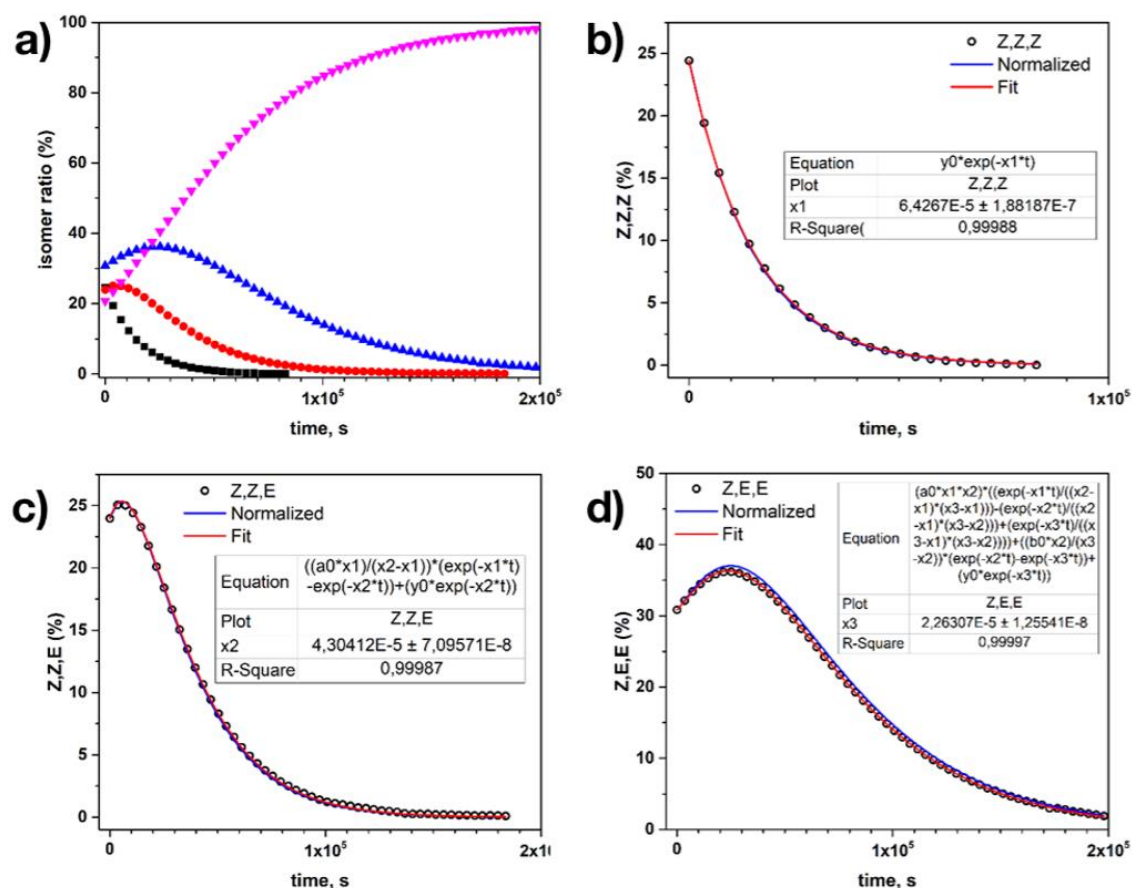


Figure 135. a) Thermal evolution of the isomers ratio of tris(azobenzene)-3: (E,E,E)-3 (pink triangles), (Z,E,E)-3 (blue triangles), (Z,Z,E)-3 (red dots), (Z,Z,Z)-3 (black squares) followed at 40 °C by HPLC. The empty dots show the amount of b) isomer (Z,Z,Z)-3, c) isomer (Z,Z,E)-3 and d) isomer (Z,E,E)-3 against the heating time. The red line is the fit of the temporal evolution yielding the rate constants k_1 , k_2 and k_3 for each isomer according to equations 2.2 and 2.3.

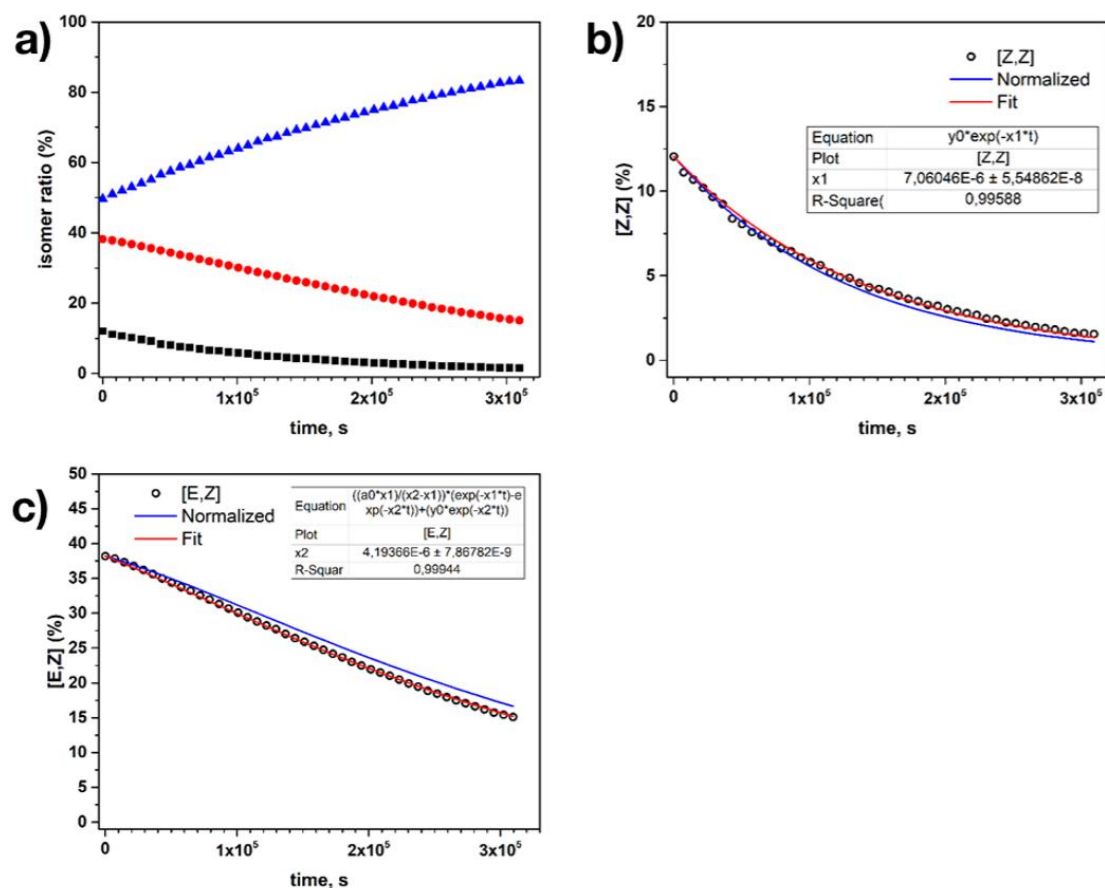


Figure 136. a) Thermal evolution of the isomers ratio of bis(azobenzene)-27: (Z,Z)-27 (black squares), (Z,E)-27 (red dots) and (E,E)-27 (blue triangles) followed at 25 °C by HPLC. The empty dots show the amount of b) isomer (Z,Z)-27, c) isomer (Z,E)-27 and d) isomer (E,E)-27 against the heating time. The red line is the fit of the temporal evolution yielding the rate constants k_1 and k_2 for each isomer according to equations 2.2 and 2.3.

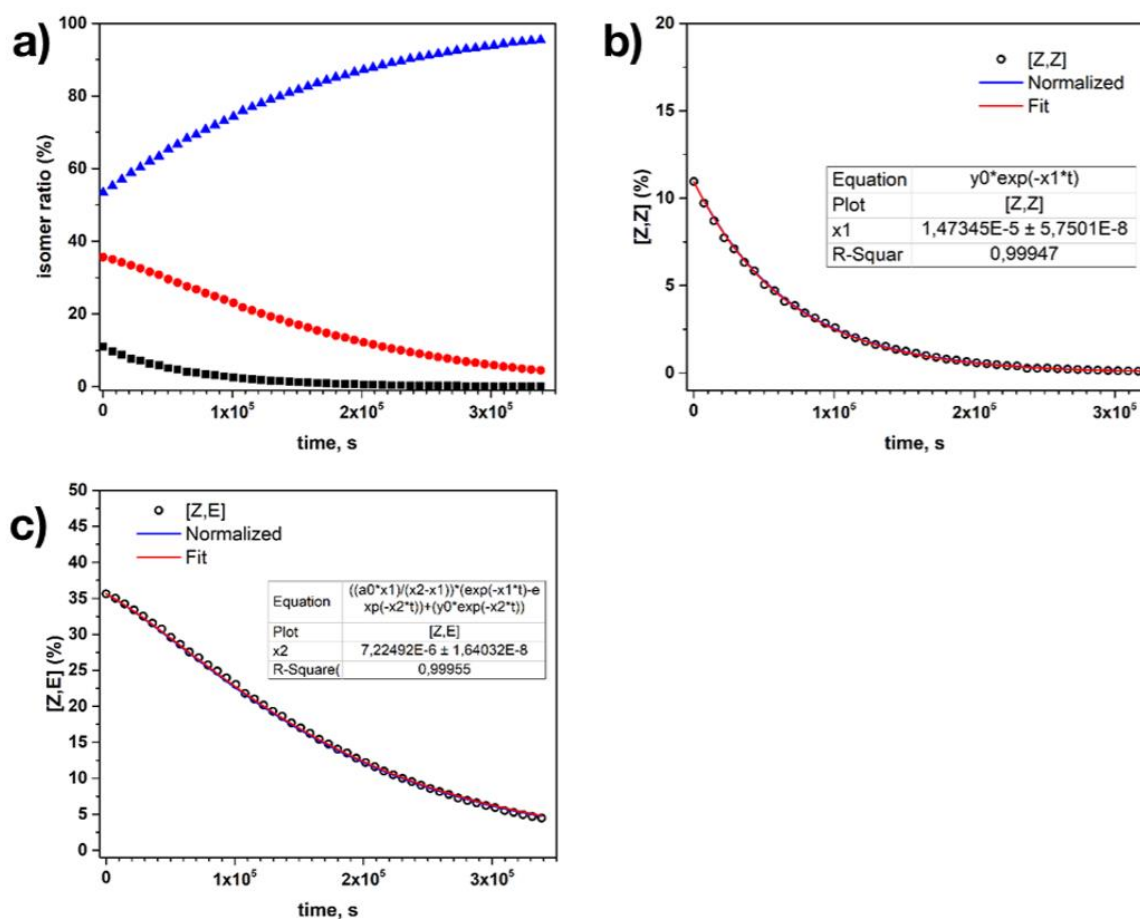


Figure 137. a) Thermal evolution of the isomers ratio of bis(azobenzene)-**27**: (Z,Z)-**27** (black squares), (Z,E)-**27** (red dots) and (E,E)-**27** (blue triangles) followed at 30 °C by HPLC. The empty dots show the amount of b) isomer (Z,Z)-**27**, c) isomer (Z,E)-**27** and d) isomer (E,E)-**27** against the heating time. The red line is the fit of the temporal evolution yielding the rate constants k_1 and k_2 for each isomer according to equations 2.2 and 2.3.

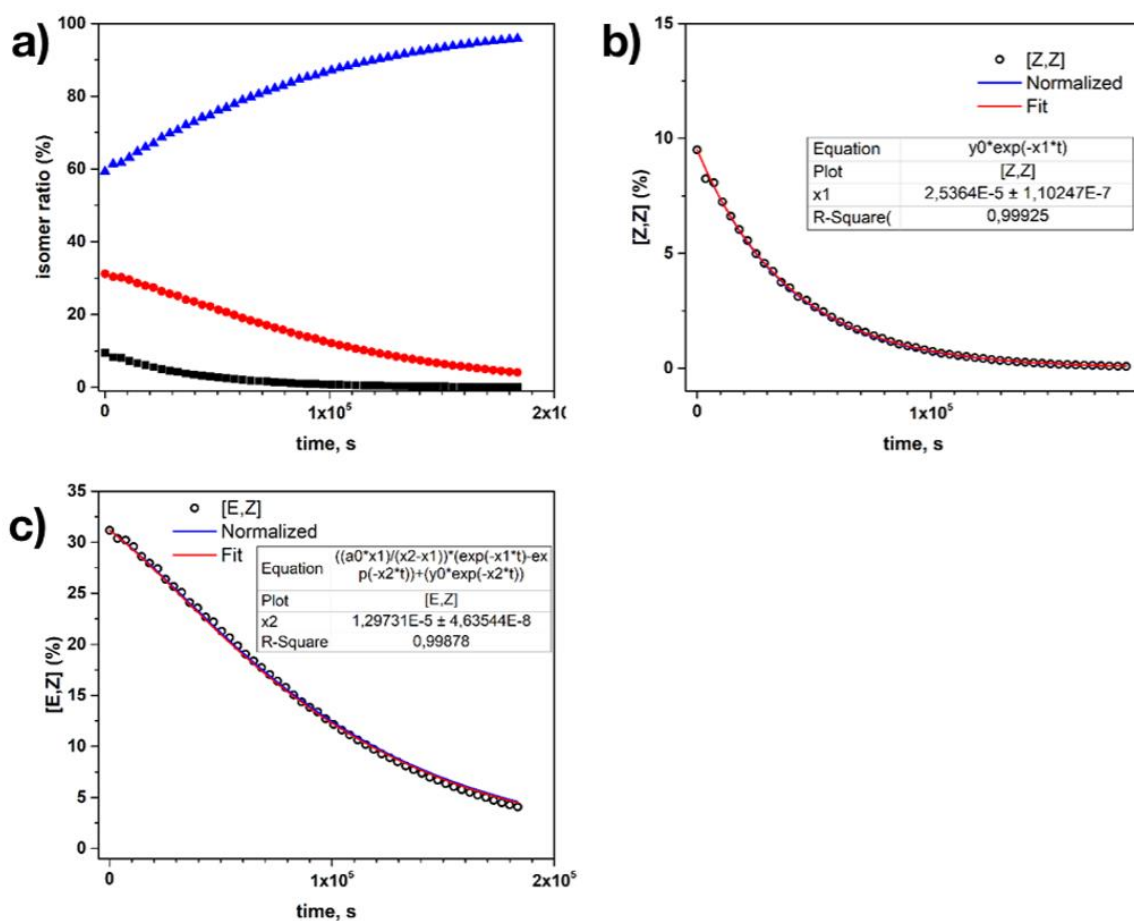


Figure 138. a) Thermal evolution of the isomers ratio of bis(azobenzene)-**27**: (Z,Z)-**27** (black squares), (Z,E)-**27** (red dots) and (E,E)-**27** (blue triangles) followed at 35 °C by HPLC. The empty dots show the amount of b) isomer (Z,Z)-**27**, c) isomer (Z,E)-**27** and d) isomer (E,E)-**27** against the heating time. The red line is the fit of the temporal evolution yielding the rate constants k_1 and k_2 for each isomer according to equations 2.2 and 2.3.

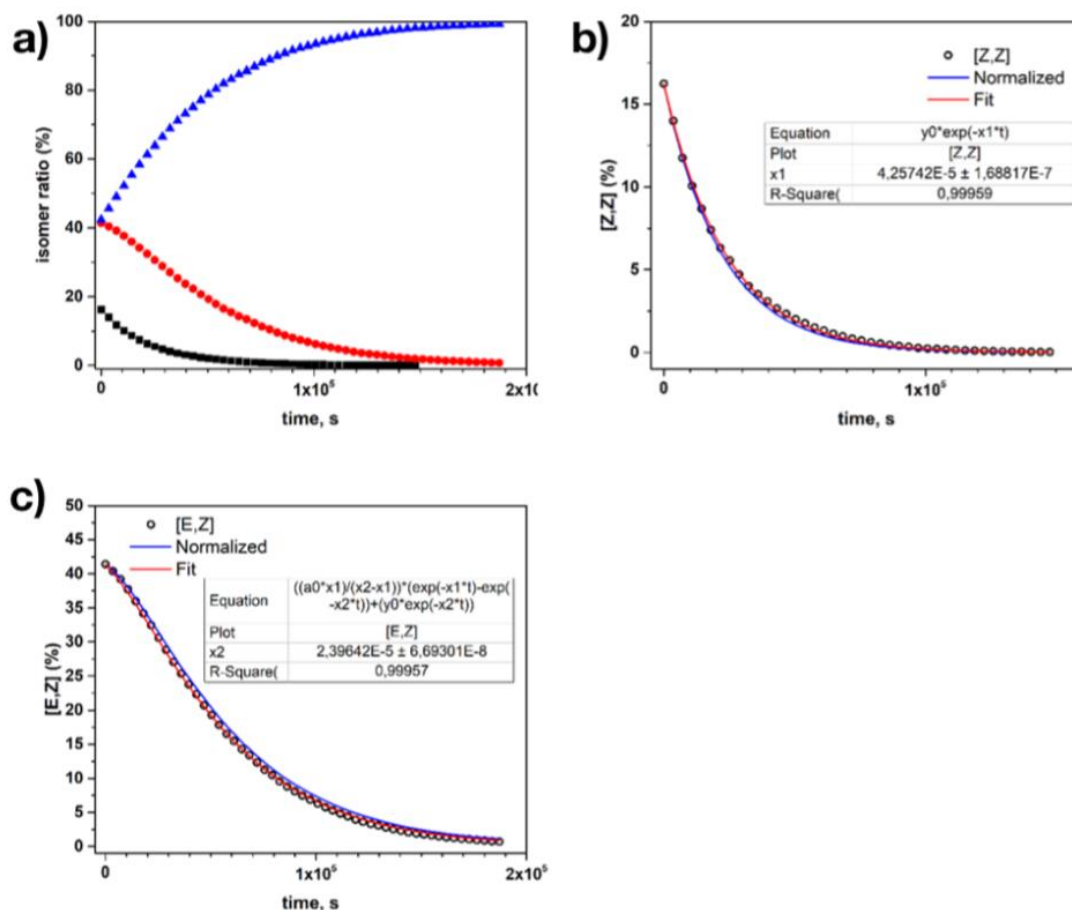


Figure 139. a) Thermal evolution of the isomers ratio of bis(azobenzene)-27: (Z,Z)-27 (black squares), (Z,E)-27 (red dots) and (E,E)-27 (blue triangles) followed at 40 °C by HPLC. The empty dots show the amount of b) isomer (Z,Z)-27, c) isomer (Z,E)-27 and d) isomer (E,E)-27 against the heating time. The red line is the fit of the temporal evolution yielding the rate constants k_1 , and k_2 for each isomer according to equations 2.2 and 2.3.

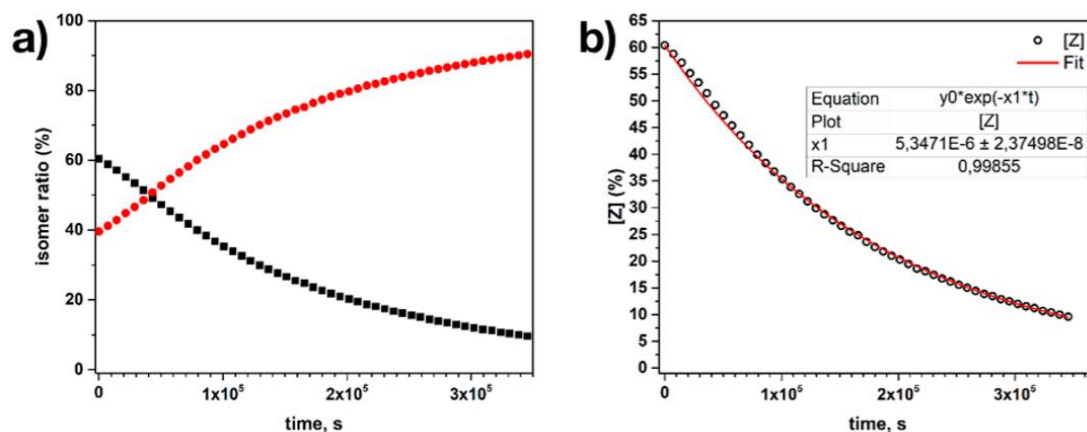


Figure 140. a) Thermal evolution of the isomers ratio of mono(azobenzene)-23: (Z)-23 (black squares) and (E)-23 (red dots) followed at 25 °C by HPLC. The empty dots show the amount of b) isomer (Z)-23 against the heating time. The red line is the fit of the temporal evolution yielding the rate constants k_1 for each isomer according to equation 2.2.

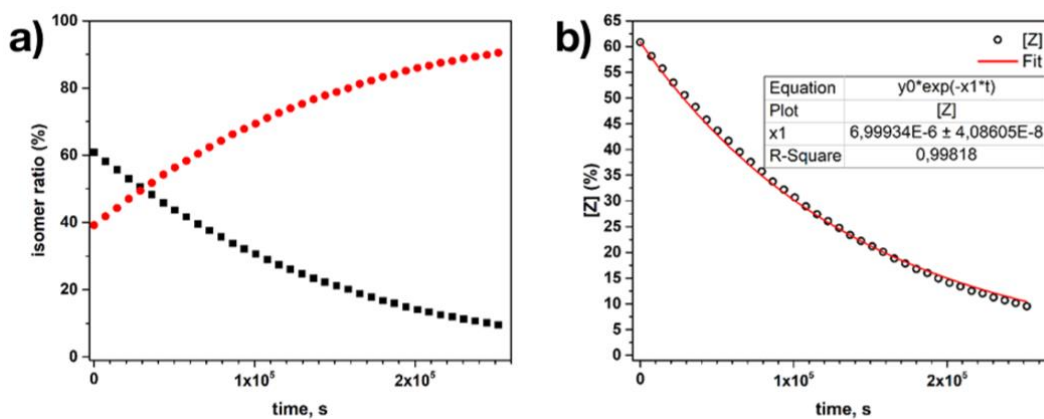


Figure 141. a) Thermal evolution of the isomers ratio of mono(azobenzene)-**23**: (Z)-**23** (black squares) and (E)-**23** (red dots) followed at 30 °C by HPLC. The empty dots show the amount of b) isomer (Z)-**23** against the heating time. The red line is the fit of the temporal evolution yielding the rate constants k_1 for each isomer according to equation 2.2.

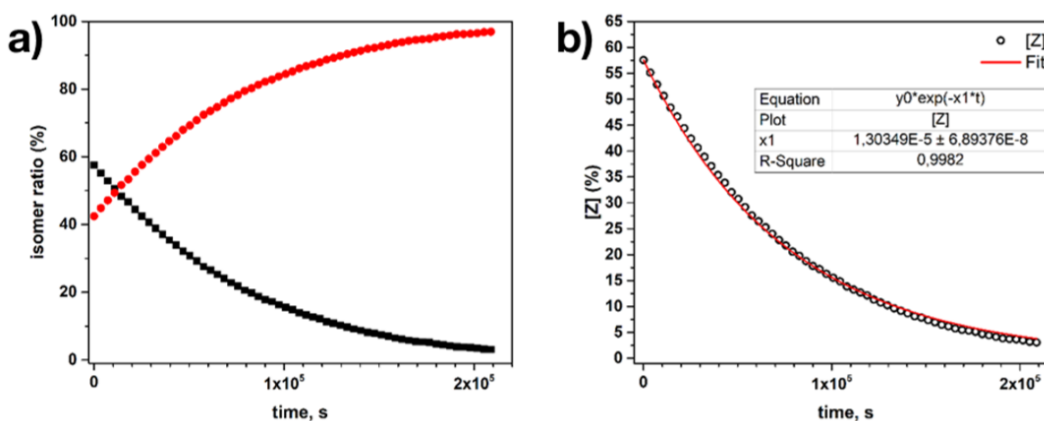


Figure 142. a) Thermal evolution of the isomers ratio of mono(azobenzene)-**23**: (Z)-**23** (black squares) and (E)-**23** (red dots) followed at 35 °C by HPLC. The empty dots show the amount of b) isomer (Z)-**23** against the heating time. The red line is the fit of the temporal evolution yielding the rate constants k_1 for each isomer according to equation 2.2.

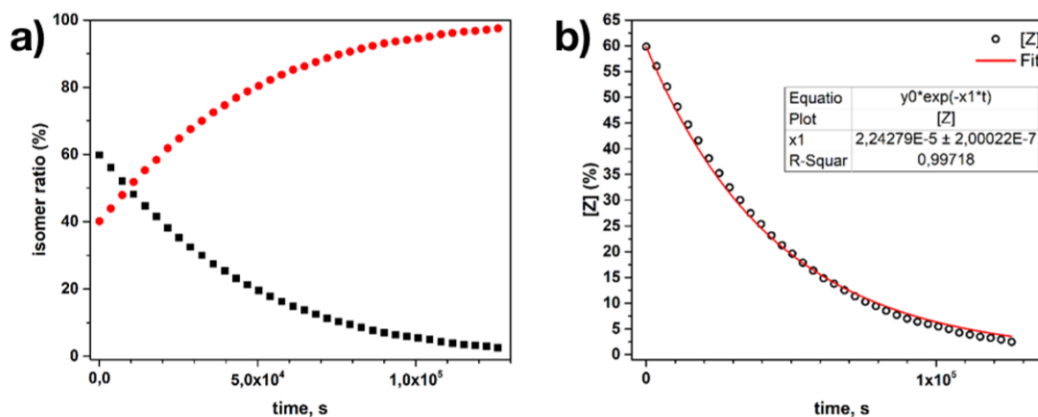


Figure 143. a) Thermal evolution of the isomers ratio of mono(azobenzene)-**23**: (Z)-**23** (black squares) and (E)-**23** (red dots) followed at 40 °C by HPLC. The empty dots show the amount of b) isomer (Z)-**23** against the heating time. The red line is the fit of the temporal evolution yielding the rate constants k_1 for each isomer according to equation 2.2.

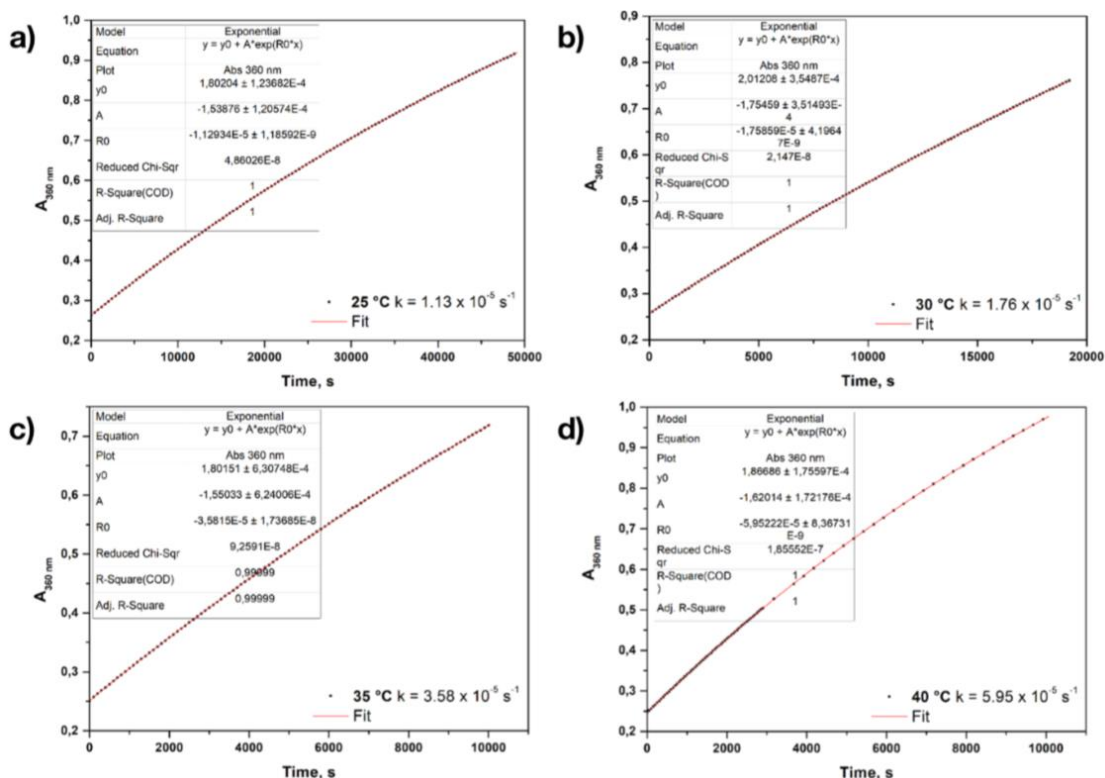


Figure 144. Thermal $Z \rightarrow E$ isomerization kinetics of azobenzene **35** followed by UV/Vis absorption spectroscopy. The solution containing azobenzene **35** ($c = 6.0 \times 10^{-5} \text{ M}$ in THF) was brought to the UV – PSS, then the absorption at $\lambda_{\text{max}} (\pi\text{-}\pi^*) = 360 \text{ nm}$ was monitored over time at constant temperature: a) 298 K, b) 303 K, c) 308 K, d) 313 K.

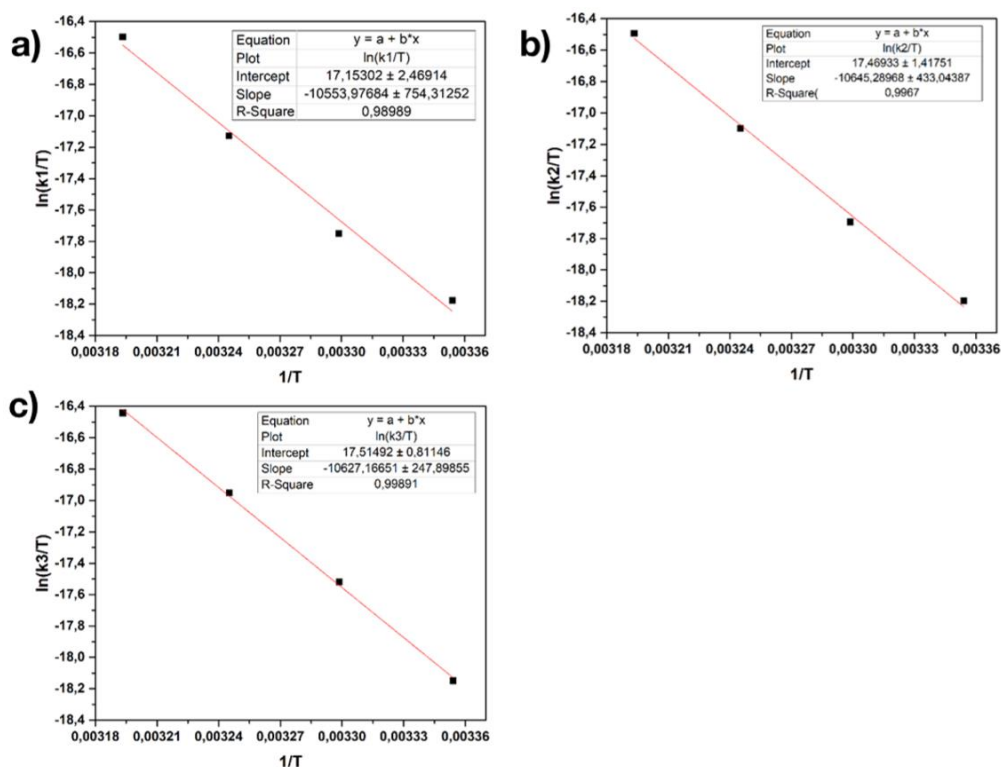


Figure 145. Eyring plots for thermal $Z \rightarrow E$ isomerization of a) (Z,Z,Z)-**3** → (Z,Z,E)-**3**, b) (Z,Z,E)-**3** → (Z,E,E)-**3** and c) (Z,E,E)-**3** → (E,E,E)-**3**.

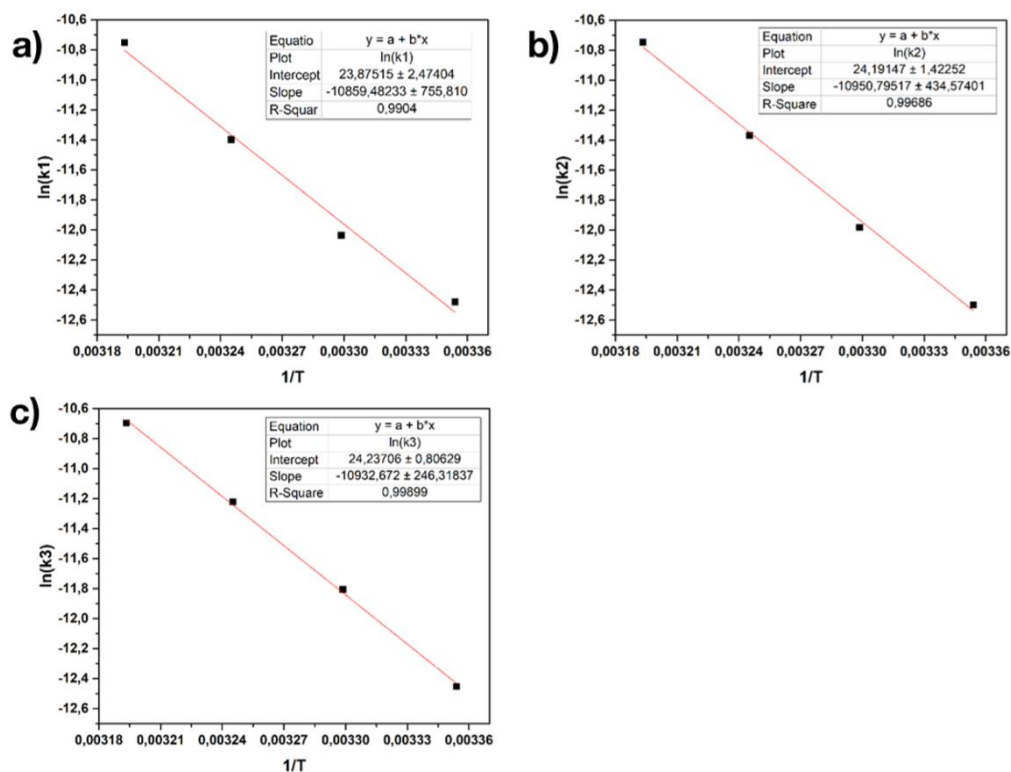


Figure 146. Arrhenius plots for thermal $Z \rightarrow E$ isomerization of: a) $(Z,Z,Z)\text{-3} \rightarrow (Z,Z,E)\text{-3}$, b) $(Z,Z,E)\text{-3} \rightarrow (Z,E,E)\text{-3}$ and c) $(Z,E,E)\text{-3} \rightarrow (E,E,E)\text{-3}$.

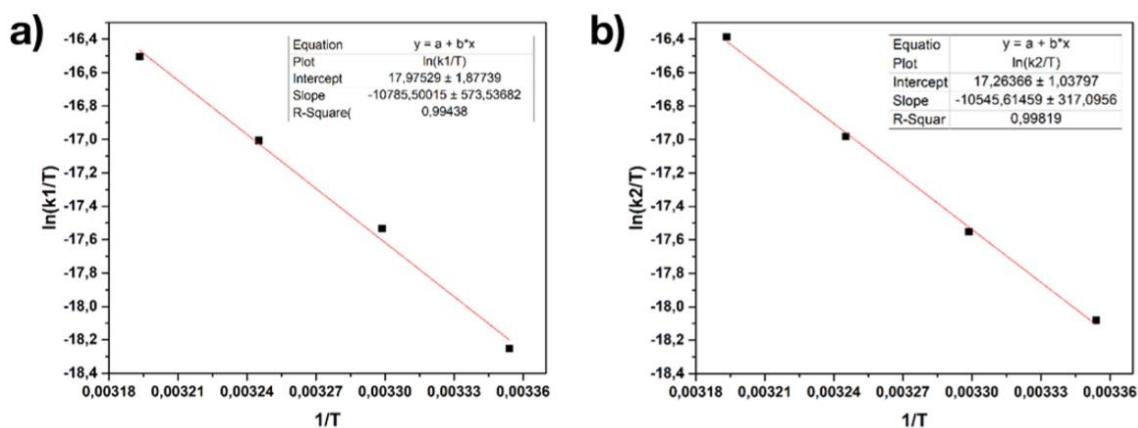


Figure 147. Eyring plots for thermal $Z \rightarrow E$ isomerization of a) $(Z,Z)\text{-27} \rightarrow (Z,E)\text{-27}$ and b) $(Z,E)\text{-27} \rightarrow (E,E)\text{-27}$.

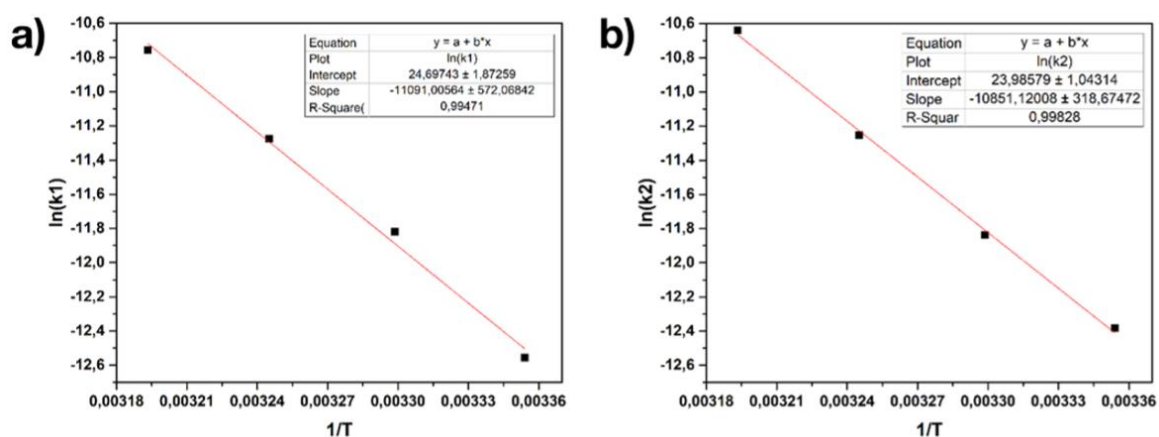


Figure 148. Arrhenius plots for thermal $Z \rightarrow E$ isomerization of: a) $(Z,Z)\text{-}27 \rightarrow (Z,E)\text{-}27$, b) $(Z,E)\text{-}27 \rightarrow (E,E)\text{-}27$.

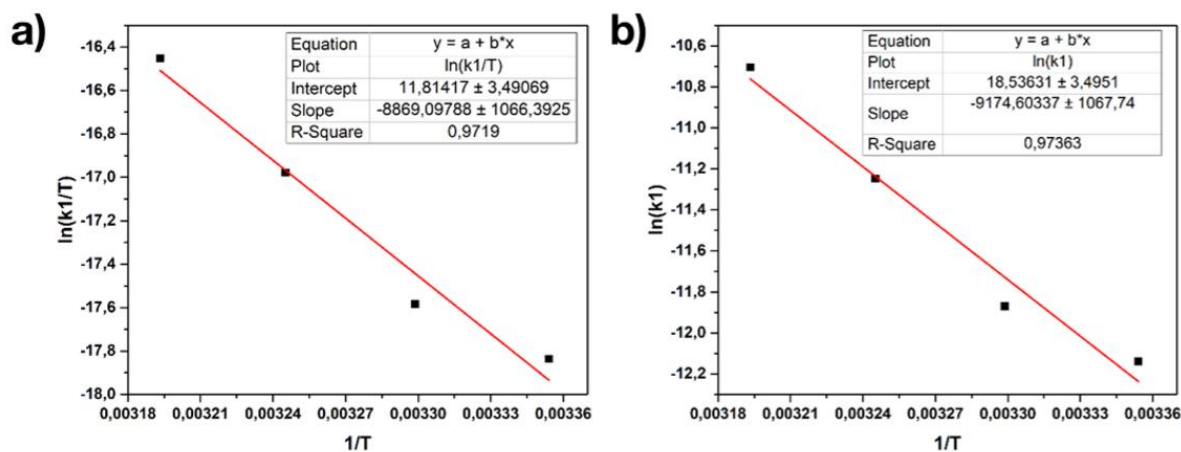


Figure 149. a) Eyring and b) Arrhenius plots for thermal $(Z)\text{-}23 \rightarrow (E)\text{-}23$ isomerization.

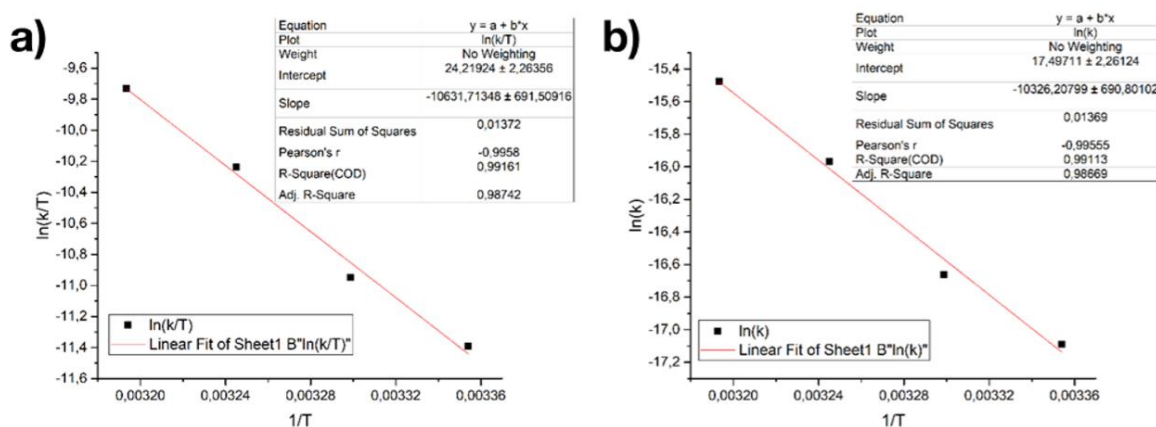


Figure 150. a) Eyring and b) Arrhenius plots for thermal $(Z)\text{-}35 \rightarrow (E)\text{-}35$ isomerization.

7.2 Curriculum Vitae

Jasmin Santoro

Date and place of birth: 20th February 1988 in S. Giovanni Rotondo (FG), Italy

Nationality: Italian

Addresse: Via G. Matteotti 52, 71011 Apricena (FG), Italy

Telephone: +39 3283398500

email: jasmin.santoro88@gmail.com

Experienced and trained with advances techniques in organic chemistry, including Schlenk-line techniques employed for the synthesis of moisture-sensitive compounds, reactions performed in microwave, multi-step reactions, solvothermal reactions carried out in oven, purification and characterization of organic compounds. Good knowledge of analytical techniques as NMR spectroscopy, mass spectrometry (ESI-MS, MALDI-TOF-MS), GC/MS, HPLC chromatography, IR spectroscopy, UV-Vis absorption spectroscopy, GPC. Good knowledge of scientific data bases as SciFinder and Reaxys. Experienced in team-work and scientific presentations.

Education

04/2019 – 09/2019:	Master's in Management and Marketing of Pharmaceutical Industry – Alma Laboris Business School, Bologna (Italy). Supervisor: Dr. Lorenza de Martinis Thesis: "Registration procedures of medicines: the centralized procedure".
10/2015 – 04/2019:	Ph.D. Chemistry – Universität Basel, Basel (Switzerland). Supervisor: Prof. Marcel Mayor Thesis: "Multi-photochromic systems based on azobenzene units towards 2D and 3D photo-responsive materials".
10/2007 – 10/2014:	Master of Science (M. Sc.) in Chemistry and Pharmaceutical Technologies – University of Bologna "Alma Mater Studiorum", Bologna (Italy). Supervisor: Prof. Stefano Masiero Thesis: "Complex systems <i>via</i> self-assembly of functionalized guanidines".
09/2002 – 07/2007:	Diploma High School Math and Science – Istituto Statale di Istruzione Secondaria Superiore "Federico II", Apricena (FG).

Professional Experiences and Trainings

10/2015 – 03/2019:	Early Stage Researcher (ESR) , Marie Skłodowska-Curie fellow of the INT "iSwitch" project funded by the EU framework Program for Research and Innovation <i>Horizon 2020</i> – Institute of Nanotechnology (INT) – Karlsruhe Institut für Technologie (KIT), Karlsruhe (Germany) and PhD candidate at the University of Basel, under the supervision of Prof. Marcel Mayor.
--------------------	--

Research activity: Design, synthesis, characterization and purification of organic compounds comprising azobenzene photoswitches for application in molecular electronics. The synthesized compounds were also employed as photoresponsive units in 3D metal-organic frameworks (MOFs) and covalent organic frameworks (COFs).

03/2017 – 06/2017:

Research internship

Max – Planck Institute for Polymer Research (MPIP), Mainz (Germany) under the supervision of Dr. Akimitsu Narita.

Research activity: design, synthesis, characterization and purification of disc-shape polycyclic aromatic hydrocarbons (PAHs), namely hexa(*peri*)hexabenzocoronene (HBC) bearing azobenzene photochromes for the study of the self-assembly and charge transport through the columnar aggregates.

05/2016 – 07/2016:

Research internship

SCRIBA Nanotecnologie Srl, Bologna (Italy) under the supervision of Dr. Pierpaolo Greco.

Research activity: synthesis and characterization of azobenzene self-assembled monolayers (SEMs) on gold and glass substrates. Investigations on the physical alteration of the functionalized surface upon UV/Vis light irradiation.

Training courses

01-03/03/2016:

Advanced optical materials and devices – University College London (UCL), London (UK)

06-10/06/2016:

Corso Nazionale di Introduzione alla Photochimica – University of Bologna “Alma Mater Studiorum”, Bologna (Italy)

12-16/09/2016:

Molecular Design and Synthesis – Summer School organized by the two European projects *MOLESCO* and *iSwitch* – Freiburg (Germany)

25/01/2017:

Entrepreneurship and Career Planning – SCRIBA Nanotecnologie Srl, Bologna (Italy)

07-08/11/2017:

Workshop on Presentation Skills – Institut de Science et d’Ingénierie Supramoléculaire (I.S.I.S.), Strasbourg (France)

16/03/2018:

Ethics in Research and Responsible Research and Innovation (RRI) – Institut de Ciència de Materials de Barcelona (ICMAB-CSIC), Barcelona (Spain)

14/09/2018:

Commercial Exploitation of Results and IPR – BASF, Ludwigshafen (Germany)

11-12/12/2018:

Prospectives on Switchable Systems and Materials for Smart Electronics – Humboldt-Universität zu Berlin, Berlin (Germany)

Publications

“Electronic Decoupling of C3-Symmetrical Light-Responsive Tris(Azobenzene) Scaffolds: Self-Assembly and Multi-Photochromism”, A. Galanti, V. Diez-Cabanes, J. Santoro, M. Valášek, A. Minoia, M. Mayor, J. Cornil, P. Samorì, *J. Am. Chem. Soc.* **2018**, 140(47), 16062-16070;

“A new class of rigid multi(azobenzene) switches featuring electronic decoupling: unravelling the isomerization in the individual photochrome”, A. Galanti, J. Santoro, R. Mannancherry, Q. Duez, V. Diez-Cabanes, M. Valášek, J. De Winter, J. Cornil, P. Gerbaux, M. Mayor, P. Samorì, *J. Am. Chem. Soc.* **2019**, 141(23), 9273-9283.

Languages

- Italian: mother tongue
- English: Fluent – C1
- Greek: good – B2
- German: Basic – A1

Additional Informations

- Deep interest in foreign cultures, travelling and photography.
- Sports e hobby: hiking, running, swimming, yoga and pilates.